SUDDEN FLOOD RELEASE DOWN A STEPPED CASCADE

Unsteady Air-Water Flow Measurements. Applications to Wave Run-up, Flash Flood and Dam Break Wave

by

Hubert CHANSON

M.E., ENSHM Grenoble, INSTN, PhD (Cant.), DEng (Qld)

Eur.Ing., MIEAust., MIAHR

Reader in Environmental Fluid Mechanics and Water Engineering

Dept of Civil Engineering, The University of Queensland, Brisbane QLD 4072, Australia

Email: mailto:h.chanson@mailbox.uq.edu.au

Url : http://www.uq.edu.au/~e2hchans/

REPORT No. CH 51/03

ISBN 1864996552

Department of Civil Engineering

The University of Queensland

January, 2003

Advancing flood wave down a stepped cascade (h = 0.0715 m, l = 1.2 m, Q(t=0+) = 0.055 m^3/s)

Synopsis :

Flood waves resulting from dam breaks have been responsible for numerous losses of life. Related situations include flash floods, debris flow surges, glacier lake outburst floods and natural dam overtopping. In the present study, flood releases down a flat stepped chute (θ = 3.4°) was investigated in a large size facility (L = 25 m) with two stepped geometries (h = 0.071 & 0.143 m). Measurements were conducted with high-shutter speed video-cameras and unsteady air-water flow properties were recorded with arrays of conductivity probes. Observations showed that the surge propagated as a succession of free-falling nappe, nappe impact and horizontal runoff on each step for all investigated flow conditions and step geometries. Visual observations highlighted further strong aeration of the leading edge. Wave front propagation data were successfully compared with HUNT's (1982,1984) theory. Best fit was achieved assuming a Darcy-Weisbach friction factor of f = 0.05 independently of flow rates and step heights. The result is very close to steady flow resistance measurements in the same facility.

Instantaneous distributions of void fractions were successfully compared with theoretical solutions of the air bubble diffusion equation. Void fraction distributions showed a marked change in shape for $(t - t_S)*\sqrt{g/d_o} \sim 1.3$. Possible explanations may include non-hydrostatic pressure field in the leading edge, some change in air-water flow structure associated with changes in rheological fluid properties, and changes in shear stress distributions and boundary friction. Experimental results showed that the strongly-aerated flow region, at the leading edge, was relatively small (i.e. typically 0.3 to 0.5 m long). Behind air-water flow properties tended rapidly towards steady flow characteristics. Specific interface area data highlighted large interfacial areas in the leading edge with depth-averaged specific interface areas of up to 400 m^{-1}. Such large interfacial areas enhance air-water mass transfer. This may reduce pollution induced by debris and hydrocarbons collected at the front of flash floods. Measurements of air and water chord sizes showed a wide range of bubble and droplet sizes. The median air chord sizes were typically between 1 and 10 mm, and the distributions were skewed with a preponderance of smaller bubbles compared to the mean. Time-variations of air-water flow structure was observed. At the leading edge (i.e. $(t - t_S)*\sqrt{g/d_o} < 0.5$), entrained bubbles and ejected droplets had similar sizes. Behind, however, the median water chord sizes increased with time, although the bubble sizes did not change.

Practically, the present study provides quantitative information on the propagation of surge waves down sloping waterways with large roughness. Although developed for smooth channels, HUNT's (1982,1984) theory may be applicable to flash floods. A related form of dam break wave is the wave runup in the swash zone. The large amount of air entrainment (i.e. 'white waters') in the wave front reduces buoyancy. In turn heavy sediment particles are more likely to be subjected to bed-load than to suspension.

Résumé :
Des ondes de submersion, similaires à celles causées par le lâcher instantané d'une retenue d'eau, sont aussi observées durant des orages intenses (ex. épisode cévenol), des débordements de barrages naturels ou des ouvertures accidentelles d'évacuateurs de crues. Dans chaque cas, ces ondes peuvent être très meurtrières.
Le rapport présent décrit une étude expérimentale de lâchers instantanés de grands volumes d'eau dans un canal à faible pente (3.4°), avec un coursier en marches d'escalier. Le canal est de grande taille (L = 25 m, h = 0.07 & 0.143 m) pour minimiser tout effet d'échelle. Des mesures instationnaires ont été conduites avec des caméras vidéo à ouverture très rapide, et avec des sondes de résistivité pour caractériser l'écoulement diphasique eau-air. Les résultats montrent que le front d'onde se propage comme une succession de jet libres, impactant sur la marche avale, et suivis d'ondes de submersion. La propagation du front a été prédite, avec succès, en utilisant la théorie élégante de Bruce HUNT (1982,1984).
Les mesures diphasiques instationnaires démontrent une aération conséquente du front. Les 0.3 à 0.5 mètres, qui suivent immédiatement le front, sont caractérisés par d'importants taux de vide moyens et surfaces interfacielles moyennes. Pratiquement, ces résultats suggèrent un potentiel important pour le transfert de gaz dissout, qui réduit la pollution induite par les débris et hydrocarbures entrainés par le front d'une onde d'orage. Mais aussi, on a démontré une poussée d'Archimède moindre dans le front de l'onde de submersion, qui réduit l'entrainment de sédiments par suspension, en particulier, dans les cas d'avances de vagues (*wave runup*) sur des plages.

TABLE OF CONTENTS

	Page
Synopsis	ii
Résumé	iii
Table of contents	iv
Notation	v
About the writer	ix
1. Introduction	1
2. Experimental configuration	10
3. Experimental results (1) Wave front propagation	19
4. Unsteady air-water flow properties (1) Void fractions, bubble count rates and specific interface areas	27
5. Unsteady air-water flow properties (2) Air and water chord sizes	45
6. Summary and discussion	51
Acknowledgments	54
APPENDICES	
Appendix I - Basic unsteady flow equations	A-1
Appendix II - A solution of the unsteady flow equations	A-2
Appendix III - Air bubble diffusion in self-aerated flows	A-3
Appendix IV - Wave front celerity data. (1) Channel data	A-6
Appendix V - Wave front celerity data. (2) Studies of individual steps	A-13
Appendix VI - Unsteady air-water flow measurements (1) Void fraction, Bubble count rate, specific interface area data	A-17
Appendix VII - Steady air-water flow measurements. Void fraction and Bubble count rate	A-51
Appendix VIII - Unsteady air-water flow measurements (2) Depth-averaged Void fraction, Bubble count rate, specific interface area data	A-55
Appendix IX - Unsteady air-water flow measurements (3) Distributions of air and water chord sizes	A-61
References	R-1
Internet reference	R-10
Bibliographic reference of the report CH51/03	R-11

NOTATION

The following symbols are used in this report :

A flow cross-section area (m^2);

a air-water specific area (1/m) defined as the air-water interface area per unit volume of air and water;

a_{mean} depth averaged specific interface area defined in terms of Y_{90} :

$$a_{mean} = \frac{1}{Y_{90}} * \int_{y=0}^{Y_{90}} a * dy$$

C 1- void fraction, or air concentration, defined as the volume of air per unit volume of air and water;

2- celerity of a small disturbance (m/s);

C_{gas} concentration of dissolved gas in water (kg/m^3);

C_{mean} depth averaged air content defined in terms of Y_{90} :

$$C_{mean} = \frac{1}{Y_{90}} * \int_{y=0}^{Y_{90}} C * dy$$

C_s wave front celerity (m/s);

C_{sat} gas saturation concentration in water (kg/m^3);

ch pseudo-chord size (m);

D_{gas} molecular diffusivity of gas in water (m^2/s);

D_t turbulent diffusivity (m^2/s) of air bubbles;

D_o dimensionless constant;

D' dimensionless turbulent diffusivity:

$$D' = \frac{D_t}{(u_r)_{Hyd} * \cos\theta * Y_{90}}$$

d water depth (m);

d_c critical flow depth (m); for a rectangular channel : $d_c = \sqrt[3]{\frac{Q^2}{g * W^2}}$;

d_o equivalent dam break reservoir depth (m) :

$$d_o = \frac{9}{4} * \sqrt[3]{\frac{Q^2}{g * W^2}}$$

Note : d_o is a function of flow rate and channel width only: $d_o = 9/4\ d_c$;

d_n water depth (m) at the nozzle : $d_n = 0.03$ m in the present study;

F bubble count rate (Hz) defined as the number of bubbles impacting the probe sensor per second;

F_{max} maximum bubble count rate (Hz) for $0 < y < Y_{90}$;

f Darcy-Weisbach friction factor;

f_e Darcy-Weisbach friction factor of air-water flows;

g gravity constant (m/s^2); g = 9.80 m/s^2 in Brisbane (Australia);

H 1- total head (m);

	2- dam height (m) (HUNT 1982,1984);
H_{res}	residual head (m);
h	step height (m);
h_s	wave front height (m) (HUNT 1982,1984);
I	integer;
K_L	liquid film coefficient (m/s);
Kurt	Fisher kurtosis (paragraph IX.3);
K'	dimensionless integration constant;
K"	dimensionless integration constant;
K^*	$K^* = \tanh^{-1}(\sqrt{0.1}) = 0.32745015...$
k_s	equivalent sand roughness height (m);
L	1- chute length (m);
	2- reservoir length (m) (HUNT 1982,1984);
L_r	geometric scaling ratio : i.e., ratio of prototype to model lengths;
l	step length (m);
M_{gas}	mass of dissolved gas (kg);
N_{ab}	number of air bubbles;
$n_{Manning}$	Gauckler-Manning coefficient ($s/m^{1/3}$)
P	pressure (Pa);
P_{hyd}	hydrostatic pressure (Pa);
Q	total volume discharge (m^3/s) of water;
Q(t=0+)	initial flow rate (m^3/s);
q	discharge per meter width (m^2/s) : at the orifice q = Q/W;
S_f	friction slope;
S_o	bed slope : $S_o = \sin\theta$;
Skew	Fisher skewness (paragraph IX.3);
Std	standard deviation of chord size (m) (paragraph IX.3);
s	longitudinal distance (m) measured from the upstream end of the channel;
t	time (s); usually t = 0 when $x_s = 0$;
t'	time (s) measured from nappe take-off;
t_{ch}	air/water chord time (s);
t_s	time (s) of passage of the wave front at the location x';
t_o	characteristic time (s);
U	uniform equilibrium flow velocity (m/s) at a depth H : $U = \sqrt{\frac{8*g}{f} * H * S_o}$
u_r	bubble rise velocity (m/s);
$(u_r)_{Hyd}$	bubble rise velocity (m/s) in hydrostatic pressure gradient;
V	velocity (m/s);
V_o	flow velocity (m/s) defined as : $V_o = Q/(W*d_o)$;

W	channel width (m);
X	dimensionless parameter;
X_r	ratio of prototype to model horizontal distances;
x	horizontal longitudinal Cartesian co-ordinate (m); x = 0 at the channel intake;
x'	horizontal distance (m) measured from the vertical step height;
x_s	wave front coordinate (m);
x'_s	wave front position (m) measured from the vertical step height;
Y_{90}	characteristic distance (m) where C = 0.9;
y	1- distance (m) normal to the invert;
	2- vertical distance positive upwards;
Z_r	ratio of prototype to model vertical distances;

Greek symbols

ΔH	head loss (m);
ΔT	integration time (s) corresponding to the control volume streamwise length ΔX: $\Delta T = \Delta X/C_s$;
ΔX	control volume streamwise length (m) : $\Delta X = I*\Delta x$ where I is an integer equal or larger than unity.
Δx	smallest control volume streamwise length (m) : Δx = 70 mm in the present study.
μ	water dynamic viscosity (Pa.s);
ν	water kinematic viscosity (m^2/s) : $\nu = \mu/\rho$;
π	π = 3.14159265358979323846264 3;
θ	1- invert slope with the horizontal;
	2- angle of the pseudo-bottom formed by the step edges with the horizontal;
ρ	water density (kg/m^3);
τ	integration time (s) corresponding to the smallest control volume streamwise length Δx : $\tau = \Delta x/C_s$;
$\varnothing$	diameter (m);

Subscript

c	critical flow conditions;
steady	steady flow conditions;
x	horizontal component;
z	vertical component;
1	initial flow conditions;
2	new flow conditions;

Abbreviations

D/S (or d/s)	downstream;
NA3	nappe flow regime without hydraulic jump;

SK1	skimming flow regime;
TRA	transition flow regime;
U/S (or u/s)	upstream.

ABOUT THE WRITER

Hubert Chanson received a degree of 'Ingénieur Hydraulicien' from the Ecole Nationale Supérieure d'Hydraulique et de Mécanique de Grenoble (France) in 1983 and a degree of 'Ingénieur Génie Atomique' from the 'Institut National des Sciences et Techniques Nucléaires' in 1984. He worked for the industry in France as a R&D engineer at the Atomic Energy Commission from 1984 to 1986, and as a computer professional in fluid mechanics for Thomson-CSF between 1989 and 1990. From 1986 to 1988, he studied at the University of Canterbury (New Zealand) as part of a Ph.D. project. He was awarded a Doctor of Engineering from the University of Queensland in 1999 for outstanding research achievements in gas-liquid bubbly flows.

Hubert Chanson is a Reader in environmental fluid mechanics and water engineering at the University of Queensland since 1990. His research interests include design of hydraulic structures, experimental investigations of two-phase flows, coastal hydrodynamics, water quality modelling, environmental management and natural resources. He is the author of four books : "Hydraulic Design of Stepped Cascades, Channels, Weirs and Spillways" (*Pergamon*, 1995), "Air Bubble Entrainment in Free-Surface Turbulent Shear Flows" (*Academic Press*, 1997), "The Hydraulics of Open Channel Flows : An Introduction" (*Butterworth-Heinemann*, 1999) and "The Hydraulics of Stepped Chutes and Spillways" (*Balkema*, 2001). He co-authored a fifth book "Fluid Mechanics for Ecologists" (*IPC Press*, 2002), while his textbook "The Hydraulics of Open Channel Flows : An Introduction" has already been translated into Spanish (*McGraw Hill Interamericana*, 2002) and Chinese (*Hydrology Bureau of Yellow River Conservancy Committee*, 2003). His publication record includes over 200 international refereed papers and his work was cited over 700 times since 1990. Hubert Chanson has been active also as consultant for both governmental agencies and private organisations.

He has been awarded five fellowships from the Australian Academy of Science. In 1995 he was a Visiting Associate Professor at National Cheng Kung University (Taiwan R.O.C.) and he was Visiting Research Fellow at Toyohashi University of Technology (Japan) in 1999 and 2001.

Hubert Chanson was the keynote lecturer at the 1998 ASME Fluids Engineering Symposium on Flow Aeration (Washington DC), at the Workshop on Flow Characteristics around Hydraulic Structures (Nihon University, Japan 1998), at the first International Conference of the International Federation for Environmental Management System IFEMS'01 (Tsurugi, Japan 2001) and at the 6th International Conference on Civil Engineering (Isfahan, Iran 2003). He gave an invited lecture at the International Workshop on Hydraulics of Stepped Spillways (ETH-Zürich, 2000). He lectured several short courses in Australia and overseas (e.g. Taiwan, Japan).

His Internet home page is http://www.uq.edu.au/~e2hchans. He also developed a gallery of photographs website {http://www.uq.edu.au/~e2hchans/photo.html} that received more than 2,000 hits per month since inception.

1. INTRODUCTION

1.1 Presentation

Flood waves resulting from dam breaks have been responsible for numerous losses of life. A related case is a flood wave down a spillway in which some energy dissipation takes place down the chute. Such a flood wave may result from some gate malfunction or the failure of an upstream reservoir as for the Silverleaf stepped weir which was overtopped for two days when an upstream cofferdam was breached (CHANSON 2000). A dominant characteristics of the process is the advancing bore down the dry chute. Although the wave front travels fast and the warning time is short, it is critical for spillway operators to estimate accurately the arrival time of the sudden water release downstream of the chute and in the downstream valley. Figure 1-1 illustrates a series of field tests conducted at Brushes Clough dam spillway (BAKER 1994,2000). A gate was located at the upstream end of quasi-horizontal, trapezoidal channel followed by a stepped chute. Movies and photographs highlighted the aerated nature of the advancing front, especially down the stepped chute.

A related situation is the flash floods down stormwater systems (e.g. Fig. 1-2). Figure 1-2A shows the outcome of an intense rainfall in Queensland on 9 March 2001 : severe flash flooding caused up to $20 millions of damage in the Brisbane area and two people drowned in separate incidents in floodwaters. The highest 24 hour rainfall totals were at Beenleigh (317 mm) and Logan City (284 mm) (source: Bureau of Meteorology), although most rainfall occurred in few hours. Figure 1-2B illustrates a flash flood event in the Gard Department, France ("épisode cévenol"). The hydrological event was not considered extreme : i.e., only 650 mm in 24 hours. However more than 37 people were killed or missing. The most devastated area included the villages of Saint-Christol-d'Alès, Saint-Martin-de-Valgalques, Aramon (11 dead, 4 missing), Sommières, and Chusclan.

Debris flow surges have been responsible for significant damages. Well-documented field studies were conducted in particular in China, Japan, and Taiwan. In debris flow surges, large debris and big rocks are often observed "rolling" and "floating" at the wave front (e.g. ANCEY 2000). CAPART and YOUNG (1998) discussed specifically the wave propagation associated with sediment motion. They observed intense scouring of the bed at the leading edge of the bore. KHAN et al. (2000) studied the effects of floating debris on dam break waves. The results showed an accumulation of debris near the wave front and a reduction of the front celerity both with and without initial water levels. NSOM et al. (2000) investigated dam break waves downstream of a finite reservoir in horizontal and sloping channels with very-viscous fluids. The dam break wave propagation was first dominated by inertial forces and then by viscous processes. In the viscous regime, the wave front location followed :

$$x_S \propto \sqrt{\frac{\cos\theta * t}{\mu}} \qquad (1\text{-}1)$$

where t is the time, θ is the bed slope and μ is the fluid viscosity.

Another related debris flow is the rockslide. Famous examples include the disastrous Vajont slide on 9 October 1963. Designed by Carlo SEMENZA (1893-1961), the Vajont dam (Italy) is a double-curvature arch structure, built between 1956 and 1960. The 262-m high reinforced-concrete dam created a 169 E+6 m^3

reservoir which was filled up by a major landslide on 9 October 1963. The reservoir waters overtopped the dam and the flood wave devastated the downstream valley. More than 2,000 people died in the catastrophe. Little damage was done however to the dam itself which is still standing and used despite a drastically-reduced storage capacity. Another major rockslide was the Mont Granier Cliff rockslide near Chambéry (France) in AD 1248. For both rockslides, it was proposed that mechanical energy dissipated in heat inside the slip zone led to vaporisation of pore pressure, thus creating a cushion of zero or negligible friction (e.g. VARDOULAKIS 2000).

Fig. 1-1 - Flood wave propagating down Brushes Clough dam spillway during field tests in 1994 (Courtesy of Dr R. BAKER).

(A) Gate opening (note gate in background)

(B) Runoff into the stepped chute ($t = t_o$)

(C) Runoff down the stepped chute ($t = t_o + 1.2$ s)

(D) Runoff down the chute ($t = t_o + 2.68$ s)

Fig. 1-2 - Photographs of flash floods

(A) After the flash flood on 9 March 2001 in Norman Creek, Brisbane QLD (Australia) (Courtesy of Anthony CORNELIUS)

(B) Mud flows from the Gardon d'Anduze and Gardon d'Alès, Alès (France) on 8-9 Sept. 2002 (after *Le Figaro Magazine*, Sat. 14 Sept. 2002)

In some cases, "natural" lakes and reservoirs may be formed by landslides and rockslides. For example, during the Chi-chi earthquake in Taiwan on 21 September 1999, the Chin-Shui and Ta-Chia rivers, and the Tzao-Ling valley were dammed by massive landslides (HWANG 1999). The Tzao-Ling valley was previously dammed by record landslides in 1943 and 1974. In Tajikistan, Lake Sarez was formed by a massive rockslide (called Usoy dam) which dammed the Murgab river valley during a severe earthquake in 1911. The reservoir contains today 17 E+9 m^3 of water. These landslide dams might become a hazard. In August 1191, a natural dam formed at Vaudaine (France) across the Romanche river as the result of massive landslides from the Belledonne range. The reservoir, called Lac Saint-Laurent or Lac de l'Oisans, was located upstream of Bourg-d'Oisans. The dam failed during the night of the 14 to 15 September 1219, the city of

Grenoble suffered massive flooding and several thousand people were killed in the floods. In Taiwan, a 217-m high natural dam in the Tzao-Ling valley was overtopped and failed in May 1951, and 154 people were killed in the subsequent floods. In Tajikistan, the 550-m high Usoy dam is recognised as a potential hazard The failure of the Usoy dam would raise the level of the large Aral Sea by one metre if all the water reached the Aral Sea (after causing massive destruction) (WALTHAM and SHOLJI 2001).

GALAY (1987) described several glacier lake outburst floods (GLOF) in Nepal. The event shown in Figure 1-3 took place on 4 Aug. 1985. The Dig Cho glacier lake outbursted and the subsequent flood wave lasted for about 4 hours. A volume of 6 to 10 Mm^3 of water was drained : "*Local witnesses reported that the surge front advanced rather slowly down-valley as a huge 'black' mass of water full of debris. Trees and large boulders were dragged along and bounced around. The surge emitted a loud noise 'like many helicopters' and a foul mud-smell. The valley bottom was wreathed in misty clouds of water vapour; the river banks were trembling; houses were shaking; the sky was cloudless*" (GALAY 1987, p. 2.36).

Fig. 1-3 - Surge wave from outburst flood eroding the right bank of Bhote Kosi at Namche, Nepal (from GALAY 1987) - Flow from right to left - Note the building near the centre-right of the photograph

Discussion

A related case of dam break waves and flash floods is the flooding of valley and cities during armed conflicts around and near freshwater systems. In the Bible, a wind-setup effect allowed Moses and the Hebrews to cross shallow water lakes and marshes during their exodus, while the returning waters at the end of the storm crushed the Egyptian army. Man-made flooding ([1]) of an army or a city was carried out by the Assyrians (Babylon, Iraq BC 689), the Spartans (Mantinea, Greece BC 385-84), the Chinese (Huai river, AD 514-15),

[1] by building an upstream dam and destroying it.

the Russian army (Dnieprostroy dam, 1941) (RÉ 1946, DRESSLER 1952, SMITH 1971, SCHNITTER 1994). It may be added the aborted attempt to blow up Ordunte dam, during the Spanish civil war, by the troops of General Franco, and the anticipation of German dam destruction at the German-Swiss border to stop the crossing of the Rhine river by the Allied Forces in 1945 (RÉ 1946) ([2]). A related case was the air raid on the Möhne dam conducted by the British, in 1943, during the dam buster campaign (Fig. 1-4). Dyke destruction and associated flooding played also a role in several wars. For example, the war between the cities of Lagash and Umma (Assyria) around BC 2,500 was fought for the control of irrigation systems and dykes; the Dutch broke dykes near Amsterdam to stop the French army in 1672; in 1938, the Chinese army destroyed dykes along the Huang Ho River (Yellow River) to slow down the Japanese army.

Fig. 1-4 - Möhne dam shortly after the R.A.F. raid on 16-17 May 1943 - Almost 1,300 people died in the floods following the dam buster campaign, mostly inmates of a Prisoner of War (POW) camp just below the dam.

1.2 Basic theory of dam break wave

In unsteady open channel flows, the continuity and momentum principles may provide a system of two equations with two unknowns (velocity and depth) within a framework of very strict assumptions : i.e., the Saint-Venant equations (e.g. LIGGETT 1994, MONTES 1998, CHANSON 2002a)

Considering an ideal dam break surging over a **dry horizontal channel**, the method of characteristics may be applied to solve the wave profile as first proposed by RITTER in 1892 (Fig. 1-5A). The celerity of the wave front equals :

$$C_S = 2 * \sqrt{g * d_o} \qquad (1\text{-}2)$$

where d_o is the initial reservoir water depth (e.g. HENDERSON 1966, MONTES 1998). After dam break, critical flow conditions take place at the origin x = 0. The flow depth and discharge at the origin are two constants independent of time :

[2]The hypothetical destruction of the Ataturk dam, Turkey, on the Euphrates river by terrorists and the subsequent downstream flooding of Southern Anatolia and Syria was the topic of a recent novel ("Acts of War", Tom Clancy's Op-centre, 1997).

Fig. 1-6 - Definition sketch of dam break wave in a horizontal channel

(A) Dry horizontal channel

(B) Horizontal channel initially filled with water

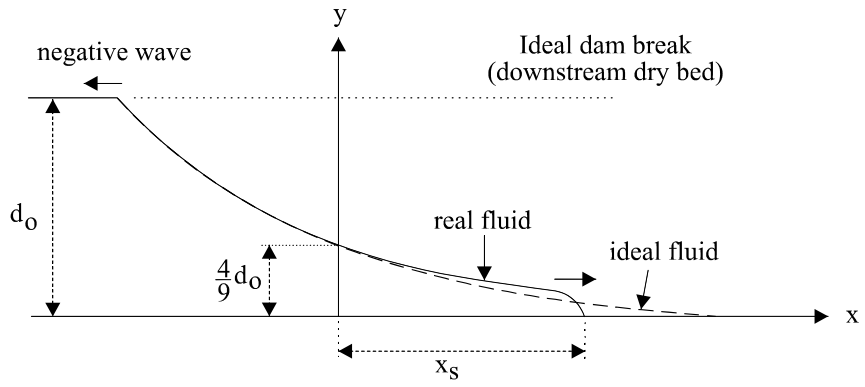

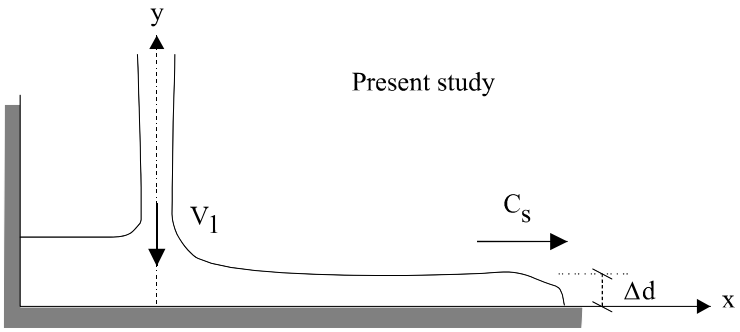

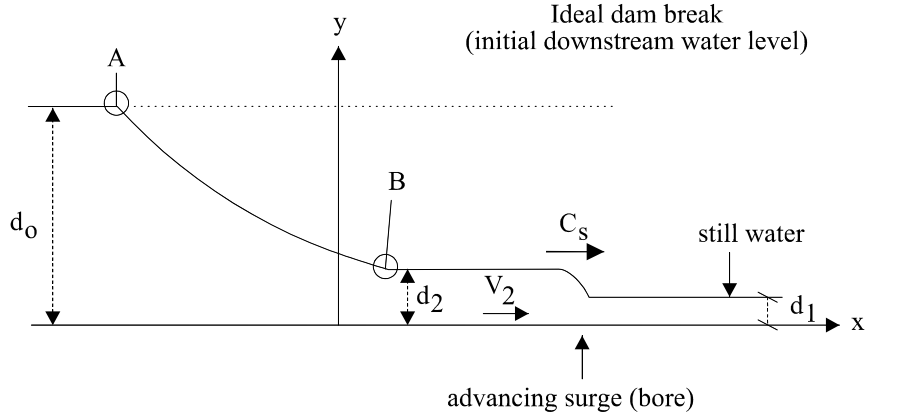

Quasi-steady flow analogy at the surge front
(as seen by an observer travelling at the surge velocity)

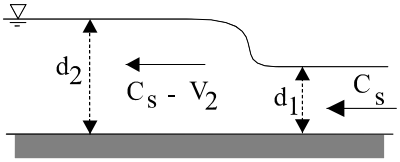

$$d_{(x=0)} = \frac{4}{9} * d_o \qquad (1\text{-}3)$$

$$Q_{(x=0)} = \frac{8}{27} * d_o * \sqrt{g * d_o} * W \quad (1\text{-}4)$$

where the longitudinal origin (x = 0) is the dam location, the time origin (t = 0) is the instantaneous dam break and W is the channel width. Basically critical flow conditions occur at the dam site (x=0). The water depth and flow velocity there are functions of the flow rate only (HENDERSON 1966, CHANSON 1999) and $d(x=0) = d_c$. Between the leading edge of the negative wave and of the wave front, the water surface profile is given by:

$$\frac{x}{t} = 2 * \sqrt{g * d_o} - 3 * \sqrt{g * d} \quad (1\text{-}5)$$

At a given time, Equation (1-5) is a parabola.

Bottom friction affects significantly the propagation of the leading tip. DRESSLER (1952) and WHITHAM (1955) proposed analytical solutions of the wave front celerity (e.g. CHANSON 2002a). Experimental data showed that the wave front has a rounded shape and that its celerity C_S is less than $2*\sqrt{g*d_o}$ (e.g. SCHOKLITSCH 1917, DRESSLER 1954, FAURE and NAHAS 1961). ESCANDE et al. (1961) investigated specifically the effects of bottom roughness on dam break wave in a natural valley. They showed that, with a very-rough bottom, the wave celerity could be about 20 to 30% lower than for a smooth bed. FAURE and NAHAS (1965) conducted both physical and numerical modelling of the catastrophe of the Malpasset dam. They conducted physical model tests based upon a Froude similitude with distorted (X_r = 1600:1, Z_r = 400:1) and undistorted (L_r = 400:1) models. Field data ([3]) were best reproduced in the undistorted physical model with a Gauckler-Manning coefficient $n_{Manning}$ = 0.025 to 0.033 $s/m^{1/3}$. Both numerical results and distorted model data were less accurate.

The propagation of a **dam break wave over still water** with an initial depth $d_1 > 0$ is a different situation because the dam break wave is lead by a positive surge (Fig. 1-5B) (HENDERSON 1966, CHANSON 2002a). The basic flow equations are the continuity and momentum equations across the positive surge front, and the condition along the C_1 forward characteristics :

$$d_1 * C_s = d_2 * (C_s - V_2) \quad \text{Continuity} \quad (1\text{-}6)$$

$$d_2 * (C_s - V_2)^2 - d_1 * C_s^2 = \frac{1}{2} * g * d_1^2 - \frac{1}{2} * g * d_2^2 \quad \text{Momentum} \quad (1\text{-}7)$$

$$V_2 + 2 * \sqrt{g * d_2} = 2 * \sqrt{g * d_o} \quad \text{Forward characteristics A-B} \quad (1\text{-}8)$$

where the subscripts 1 and 2 refer respectively to the initial flow conditions and the new flow conditions (i.e. upstream and downstream of the wave front). The system of equation may be solved graphically as (MONTES 1998) :

$$\sqrt{\frac{d_o}{d_1}} = \frac{1}{2} * \frac{C_s}{\sqrt{g * d_1}} * \left(1 - \frac{1}{X}\right) + \sqrt{X} \quad (1\text{-}9)$$

---

[3]Field observations showed that the catastrophe induced a surging wave of 40 m height at 340 m downstream of the dam site and the wave height was still about 7 m at 9 km downstream. Relatively accurate time records of the dam break and wave propagation were obtained from the destruction of a series of electrical stations located in the downstream valley.

where

$$X = \frac{1}{2} * \left(\sqrt{1 + 8 * \frac{C_s^2}{g * d_1}} - 1 \right) \quad (1\text{-}10)$$

Equation (1-9) may be *correlated* by :

$$\frac{C_s}{\sqrt{g*d_1}} = \frac{0.63545 + 0.3286*\left(\frac{d_1}{d_o}\right)^{0.65167}}{0.00251 + \left(\frac{d_1}{d_o}\right)^{0.65167}} \quad (1\text{-}11)$$

with a normalised coefficient of correlation of 0.9999996. The flow depth downstream of (behind) the positive surge is deduced from the continuity and momentum equations. It is independent of the time t and distance x, being *correlated* by :

$$\frac{d_2}{d_o} = 0.9319671 * \left(\frac{d_1}{d_o}\right)^{0.371396} \quad (1\text{-}12)$$

with a normalised coefficient of correlation of 0.99983. CHANSON et al. (2000) showed some good agreement between Equation (1-12) and large-size experimental data.

HUNT (1982) gave a kinematic wave solution ([4]) down a **sloping channel** that is valid after the flood wave has covered approximately four lengths of the reservoir downstream of the dam site :

$$\frac{U * t}{L} = \frac{1 - \left(\frac{h_s}{H}\right)^2}{\left(\frac{h_s}{H}\right)^{3/2}} \quad (1\text{-}13)$$

$$\frac{x_s}{L} = \frac{\frac{3}{2}}{\frac{h_s}{H}} - \frac{1}{2} * \frac{h_s}{H} - 1 \quad (1\text{-}14)$$

$$\frac{C_s}{U} = -\frac{3}{4} * \frac{U * t}{L} + \sqrt{\frac{x_s + L}{L} + \left(\frac{3}{4} * \frac{U * t}{L}\right)^2} \quad (1\text{-}15)$$

where t is the time with t = 0 at dam break, h_s is the dam break wave front thickness, x_s is the dam break wave front position measured from the dam site, H is the reservoir height at dam site, L is the reservoir length (Fig. 1-6), U is the uniform equilibrium flow velocity at a depth H :

$$U = \sqrt{\frac{8*g}{f} * H * S_o} \quad (1\text{-}16)$$

where f is the Darcy friction factor (assumed constant in HUNT's development) and S_o is the bed slope. Note that S_o = H/L (Fig. 1-6). Equations (1-13), (1-14) and (1-15) are valid for $S_o = S_f$ where S_f is the friction slope, and when the free-surface is parallel to the bottom of the sloping channel. HUNT (1984) showed that Equation (1-14) yields :

---

[4]That is, the kinematic wave approximation of the Saint-Venant equations (App. I).

$$\frac{h_S}{H} = \frac{3}{2} * \frac{L}{x_S - L} \qquad \text{for } x_S/L > 5 \quad (1\text{-}14b)$$

HUNT (1984, 1988) developed an analytical expression of the shock front shape (called inner solution) :

$$\frac{x - x_S}{L} = \frac{h_S}{H} * \left(\frac{y}{h_S} + Ln\left(1 - \frac{y}{h_S}\right) + \frac{1}{2} \right) \qquad (1\text{-}17)$$

where y is the distance measured normal to the bottom, and h_S and x_S are functions of time which may be calculated using Equations (1-13) and (1-14) respectively.

Fig. 1-6 - Definition sketch of dam break wave on a sloping channel

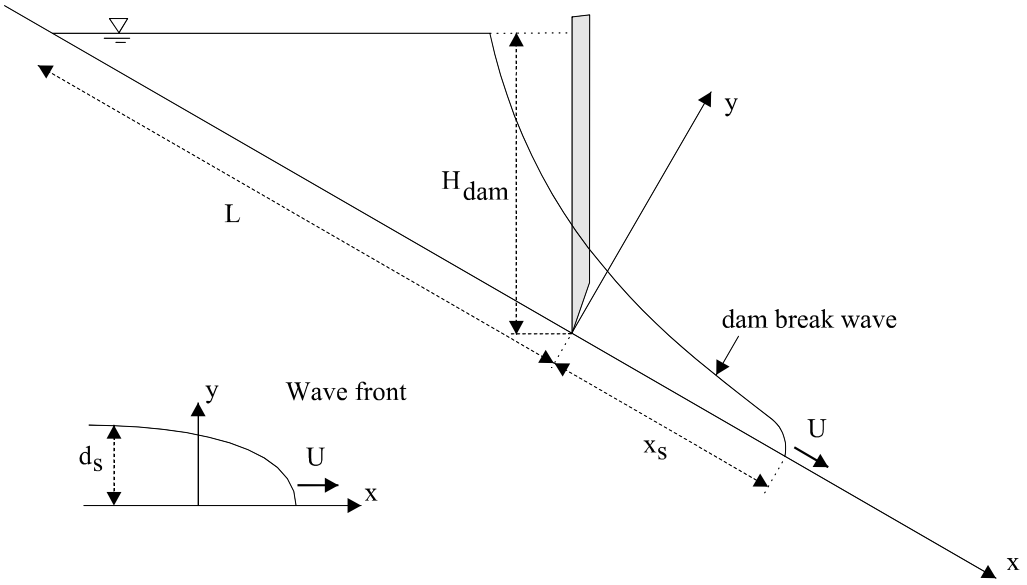

1.3 Structure of the report

During the present work, flood releases down a flat stepped chute ($\theta = 3.4°$) were investigated in a large size facility with two stepped geometries (h = 0.071 & 0.143 m). The results provide new information on the rate of energy dissipation and on the downstream wave celerity, which are compared with 'classical' dam break wave results. Wave propagation along a single step was also investigated. Unsteady two-phase flow measurements were conducted in the wave front to comprehend the wave front dynamics, its air-water flow structure and possible drag reduction effects induced by aeration.

2. EXPERIMENTAL CONFIGURATION

2.1 Experimental flume

Experiments were performed in a 25-m long 0.5-m wide flume (Fig. 2-1, 2-2 and 2-3). The channel was a flat waterway ($S_o \approx 0.065$, $\theta = 3.4°$). The flow rate was delivered by a pump controlled with an adjustable frequency AC motor drive Taian T-Verter K1/N1 (Pulse Width Modulated design), enabling an accurate discharge adjustment in a closed-circuit system. The flow was fed through a smooth convergent nozzle (1.7-m long), and the nozzle exit was 30-mm high and 0.5-m wide. The measured contraction ratio was about unity (i.e. $d_n = 30$ mm for all experiments). Earlier experiments (CHANSON 1995) showed that steady flows downstream of the nozzle were two-dimensional and became fully-developed upstream of the first drop.

Two stepped configurations were used (Table 2-1). The first geometry was equipped with ten identical steps (0.143-m high 2.4-m long) (Fig. 2-2). In the second configuration, the nozzle was followed by a 2.4 m long horizontal invert and by 18 steps (h = 0.0715 m, l = 1.2 m) (Fig. 2-3).

Further a sudden discharge release was videotaped at Brushes Clough dam spillway in 1994 (BAKER 1994). The video footage was analysed by the writer (CHANSON 2001, pp. 295-297).

Table 2-1 - Summary of unsteady flow experiments

Experiment	θ (deg.)	h m	Run	Q(t=0+) (m^3/s)	Initial channel condition	Steady flow regime	Remarks
(1)	(2)	(3)	(4)	(5)	(6)	(7)	(8)
Series 1	3.4	0.143					10 horizontal steps (l = 2.4 m). W = 0.5 m. Nozzle depth : d_n = 0.030 m.
			CT15	0.019	Wet	Nappe NA3	
			CT26	0.030	Wet	Nappe NA3	
			CT37	0.040	Wet	Nappe NA3	
			CT48	0.075	Dry/Wet	Nappe NA3	
Series 2	3.4	0.0715					18 horizontal steps (l = 1.2 m). W = 0.5 m. Nozzle depth : d_n = 0.030 m.
			TL1	0.040	Wet	Transition	Air-water flow measurements on Step 16.
			TL2	0.0475	Wet	Trans./Skim.	
			TL3	0.055	Wet	Skimming	Air-water flow measurements on Step 16.
			TL4	0.065	Wet	Skimming	
			TL5	0.075	Wet	Skimming	Air-water flow measurements on Steps 10 and 16.
Brushes Clough dam	18.4						Inclined downward steps, trapezoidal channel (2 m bottom width)
			BC1	0.5	Empty	Skimming	Data analysis by the writer.

Notes : Q(t=0+) : initial flow rate; d_n : approach flow depth (nozzle depth); h : step height; l : step length.

2.2 Instrumentation

The flow rates in steady flow conditions were measured with a Dall™ tube flowmeter, calibrated on site with a sharp-crested weir. The accuracy on the discharge measurement was about 2%.

The surging flow was studied with two video-cameras : i.e., a VHS video-camera Panasonic™ NV-RX10A (speed: 25 frames/sec., shutter: sport mode, zoom: 1 to 14) and a digital video-camera handycam Sony™ DV-CCD DCR-TRV900 (speed: 25 fr/s ([5]), shutter: 1/4 to 1/10,000 sec., zoom: 1 to 48). The cameras were installed above and along the axis of the channel. Studies of individual steps were further conducted by mounting the camera vertically above the step. Additional observations were obtained using a digital camera Olympus™ Camedia C-700 (shutter: 1/2 to 1/1,000 sec., zoom: 1 to 27).

Fig. 2-1 - Definition sketch of the experiments Series 1 and 2

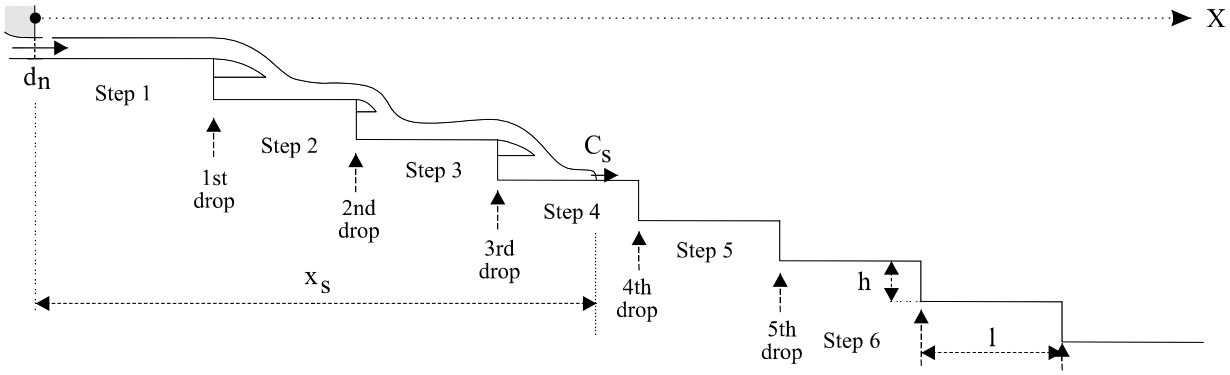

Fig. 2-2 - Photographs of the experimental facility Series 1 (h = 0.143 m, l = 2.4 m)

(A) Experiments Series 1 - Q(t=0+) = 0.030 m^3/s, t = 5.96 s - Looking upstream

[5]In PAL, 25 frames per seconds.

(B) Experiments Series 1 - Q(t=0+) = 0.075 m^3/s, t = 4.72 s

Fig. 2-3 - Photographs of the experimental facility Series 2 (h = 0.0715 m, l = 1.2 m)

(A) Experiments Series 2 - Q(t=0+) = 0.040 m^3/s

(B) Experiments Series 2 - Conductivity probes on step 16 (x' = 1m) with the reference probe (touching the invert) underneath the group of 3 single-tip probes - Flow direction from top left to bottom right

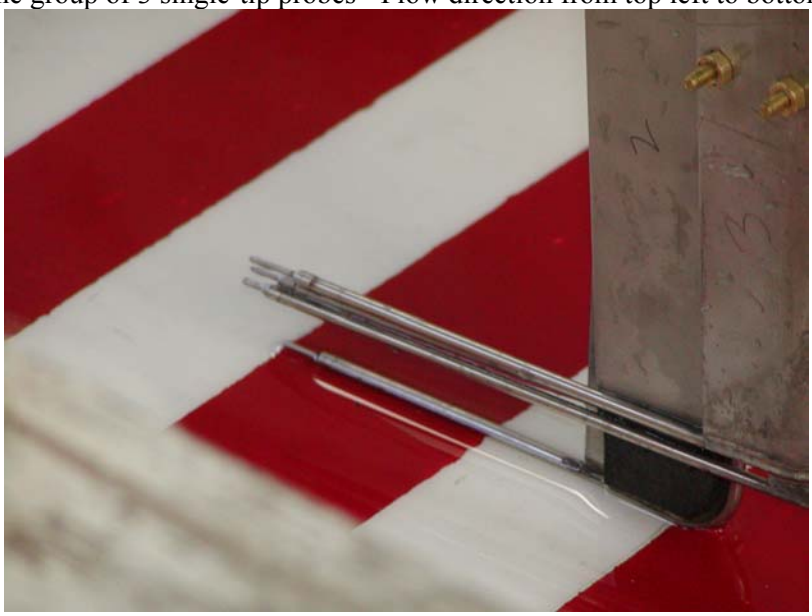

(C) Experiment Series 2 : Q(t=0+) = 0.055 m^3/s, step 16 - Wave front immediately upstream of the probes - Flow direction from top left to bottom right

(D) Experiment Series 2 : Q(t=0+) = 0.055 m^3/s, step 16 - Wave front immediately after wetting the conductivity probes - Flow direction from top left to bottom right

Air-water flow properties were measured with a series of single-tip conductivity probes (needle probe design). Each probe consisted of a sharpened rod (platinum wire ∅ = 0.35 mm) which was insulated except for its tip and set into a metal supporting tube (stainless steel surgical needle ∅ = 1.42 mm) acting as the second electrode. The probes were excited by an electronics designed with a response time less than 10 μs and calibrated with a square wave generator. Further details on the probe system and electronics were reported in CHANSON (1995) and CUMMINGS (1996). The probe output signals were scanned at 10 kHz per channel for six seconds. Data acquisition was triggered manually immediately prior to the flow arrival.

Visual and video observations showed that the wave front was roughly two-dimensional. Hence conductivity probe measurements were taken on the centreline at several distances x' from the step vertical face. At each location x', one probe (i.e. reference probe) was set on the invert, acting as a time reference, while three other probes were set at different elevations (Fig. 2-3B, C & D). Each experiment was repeated until sufficient data were obtained at each profile. The displacement of the probes in the direction normal to the invert was controlled by a fine adjustment travelling mechanism. The error in the probe position was less than 0.2 mm and 2 mm in the vertical and horizontal directions respectively.

2.3 Data processing

Each step was painted with red and white stripes spaced 50 mm apart (Fig. 2-3). Video-taped movies were analysed frame-by-frame. The error on the time was less than 1/250 s, and the error on the longitudinal position of the wave front was +/- 1 cm. In experiments Series 1, two video footages were taken for each experiment and subsequently analysed. The results are presented in terms of the average over two runs. In experiments Series 2, and for each experiment, three video recordings were taken at each location and subsequently analysed. The results are presented in terms of the average over three recordings.

Conductivity probe signal processing

In steady flows, the void fraction C is the proportion of time that the probe tip is in the air while the bubble count rate F is the number of bubbles impacting the probe tip (e.g. CHANSON 2002b). In unsteady gas-liquid flows, the processing technique must be adapted. Few studies considered highly unsteady gas-liquid flows : e.g., STUTZ and REBOUD (1997, 2000) ([6]).

Typical conductivity probe signal outputs are presented in Figure 2-4 for one flow rate at one cross-section and at several vertical elevations y above the step invert. Figure 2-4A shows voltage outputs for 10 probe positions, while Figure 2-4B details three signal outputs next to the leading edge of the wave front.

In the present study, the void fractions and bubble count rates were calculated during a short time interval τ such as $\tau = \Delta x/C_s$ where C_s is the surge front celerity measured with the video-cameras and Δx is the control volume streamwise length. A difficulty consisted in determining an optimum control volume size Δx for the moving averaging process. After preliminary tests conducted with 10 mm $\leq \Delta x \leq$ 100 mm ([7]), the basic control volume size was set at 70 mm ([8]). Such a size would contain typically 5 to 20 bubbles, and the selection was consistent with the processing technique of STUTZ and REBOUD (2000) who set τ to encompass at least 5 bubbles. In the present study, the voltage signal was processed using a single threshold technique. The threshold was set at about 50% of the air-water voltage range. For the data shown in Figure 2-4, the short time interval τ equals : $\tau = 0.0327$ s.

Bubble and water chord times were measured where the bubble chord time t_{ch} is defined as the time spent by the bubble on the probe tip. The results are presented in terms of pseudo-chord length ch defined as :

$$ch = C_s * t_{ch} \quad (2\text{-}1)$$

where C_s is the wave front celerity. Equation (2-1) predicts accurately chord lengths near the front where the flow velocity is about the wave front speed. Note that the chord time data analysis was independent of the selection of the integration time interval τ.

The bubble count rate measurement is sensitive to the probe tip size, bubble sizes, velocity and scanning rate, particularly when the sensor size is larger than the smallest bubble sizes (e.g. CHANSON and TOOMBES 2002b). During the present study, the bubble count rate was calculated as :

$$F = \frac{N_{ab}}{\tau} \quad (2\text{-}2)$$

where N_{ab} is the number of bubbles detected during the time interval τ.

---

[6]Some void fraction measurements were performed in breaking waves (e.g. HWUNG et al. 1992, WALKDEN 1999, HOQUE 2002). Such studies often averaged the void fractions over half or quarter wave periods for several wave breaking events, and the results provided very coarse informations on the air-water flow structure.

[7]For $\Delta x < 10$ mm, the control volume size was smaller than a fair proportion of detected bubbles. For $\Delta x >$ 100 mm, the averaging process did not always reflect the flow unsteadiness, especially next to the leading edge of the surging waters.

[8]Preliminary results with $\Delta x = 50$, 70 and 80 mm showed little differences between the three control volume lengths.

Fig. 2-4 - Typical conductivity probe output signal

(A) Experiments Series 2 - Q(t=0+) = 0.055 m^3/s, Step No. 16, x' = 1.0 m, C_S = 2.14 m/s

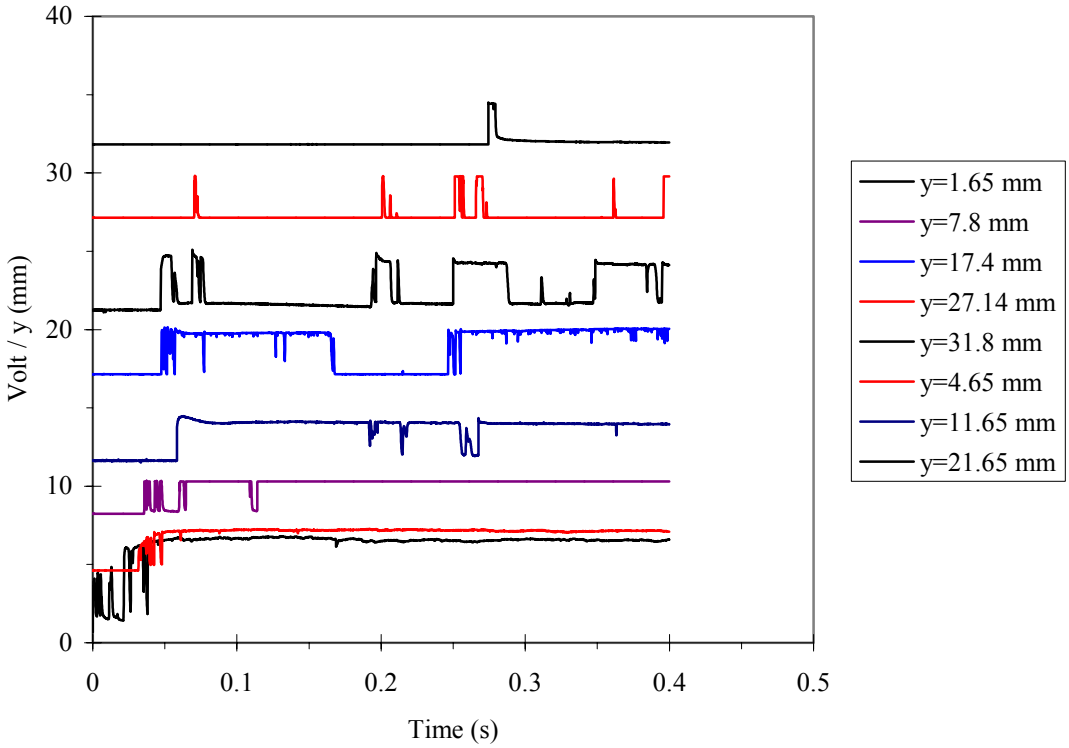

(B) Details of three signal outputs

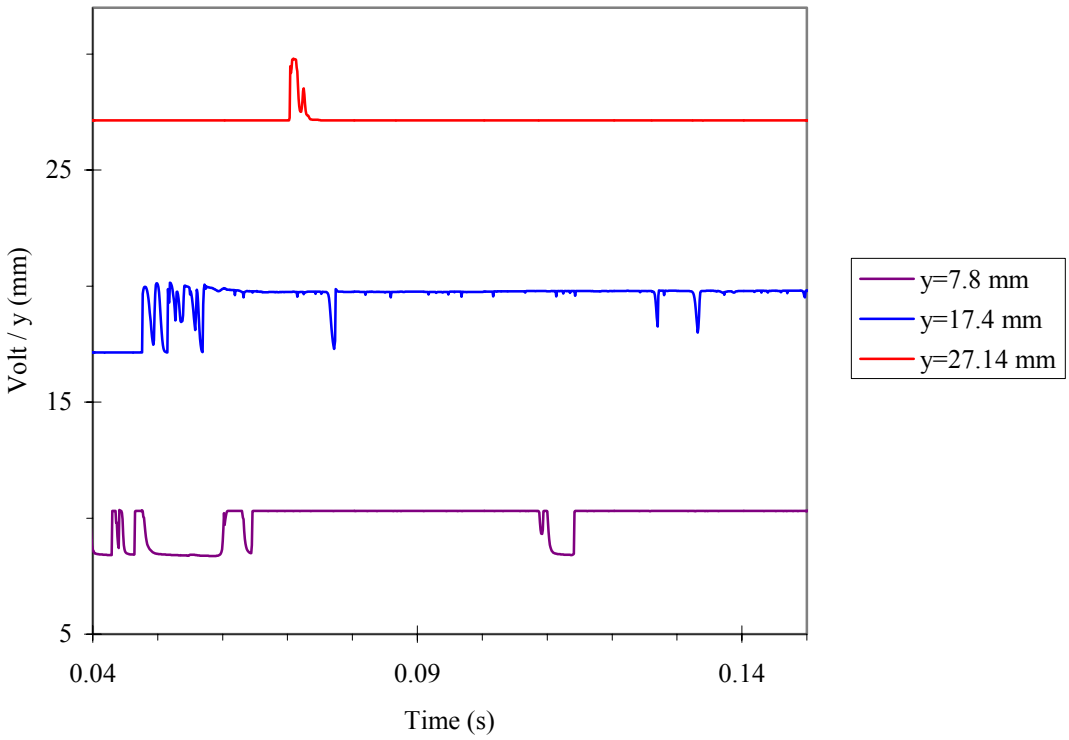

The measurement of air-water interface area is a function of the void fraction, velocity, bubble size and bubble count. For any bubble shape, bubble size distribution and chord length distribution, the specific air-water interface area may be estimated as:

$$a = \frac{4 * F}{C_s} \quad (2\text{-}3)$$

Equation (2-3) is valid in bubbly flows. In high air content regions (C > 0.3 to 0.5), the flow structure is more complex and the result is not exactly the true specific interface area. a becomes simply proportional to the number of air-water interfaces per unit length of air-water mixture : i.e., $a \propto 2*F/C_s$ (CHANSON 2002b).

2.4 Initial flow conditions

Prior to the start of each experiment, the recirculation pipe system and convergent intake were emptied. The channel was initially dry ([9]). The pump was rapidly started. The electronic controller had a 5 seconds ramp. The pump reached its nominal power (i.e. flow rate) at least 10 seconds prior to the water entering the channel. The flow rate Q(t=0+) was maintained constant until at least 10 seconds after the wave front reached the downstream end of the flume.

The time origin (t=0) was taken as the instant when the water entered the flume. The longitudinal origin (x=0) was the upstream end of the chute (i.e. nozzle).

2.5 Discussion

Previously, steady flow experiments were conducted in the same channel with a smooth invert and both stepped configurations (Table 2-2). Results were reported in CHANSON (1995,1997b), and CHANSON and TOOMBES (1997,2002a). CHANSON and TOOMBES (1997) presented flow pattern and energy dissipation results with the 0.143 m high steps. CHANSON and TOOMBES (2002a) detailed air-water flow properties down both stepped configurations.

The steady air-water flow results provide the limiting conditions of the present study of unsteady flows.

[9]although the step invert was wet.

Table 2-2 - Summary of steady flow experiments at the University of Queensland

Ref.	θ	h	l	q	d_n	Comments
	deg.	m	m	m^2/s	m	
(1)	(2)	(3)	(4)	(5)	(6)	(7)
Smooth chute	4.0	N/A	N/A	0.142 to 0.164	0.03	L = 25 m. W = 0.5 m. Painted timber (k_S = 1 mm). Ref.: CHANSON (1995,1997b).
Stepped chute						
Series S1a	3.4 ([a])	0.143	2.4	0.04 to 0.150	0.03	L = 25 m, W = 0.5 m. Horizontal timber steps. (No sidewall offset at 1st drop) Ref.: CHANSON and TOOMBES (1997).
Series S1b	3.4 ([a])	0.143	2.4	0.080 to 0.150	0.03	L = 25 m, W = 0.5 m. Horizontal timber steps. Sidewall offset for nappe ventilation at 1st drop (only). Ref.: CHANSON and TOOMBES (2002a).
Series S2	3.4 ([a])	0.071	1.2	0.080 to 0.150	0.03	L = 25 m, W = 0.5 m. Horizontal timber steps. Sidewall offset for nappe ventilation at 1st drop (only). First drop located 2.4-m downstream of intake. Ref.: CHANSON and TOOMBES (2002a).

Notes : d_n : approach flow depth (nozzle depth); h : step height; k_S : equivalent roughness height; L : channel length; l : step length; q : water discharge per unit width; ([a]) : longitudinal slope of pseudo-bottom formed by step edges.

3. EXPERIMENTAL RESULTS (1) WAVE FRONT PROPAGATION

3.1 Basic flow patterns

In experiments Series 1 and 2, visual observations showed that the wave front propagated basically as a nappe flow: i.e., as a succession of free-falling nappe and horizontal runoff. For comparison, the flow regime observations in steady flows are summarised in Table 2-1 (column 7). Basically the wave front exhibited a nappe flow behaviour for all flow rates and geometries, although steady flow conditions could correspond to transition or skimming flow regimes, as defined by CHANSON (2001).

The wave front was highly aerated, in particular for the larger flow rates (Fig. 2-2, 2-3 & 3-1). Figure 3-1 shows three flow conditions ([1]). The photographs highlight the chaotic nature of wave front, with strong spray, splashing and wavelets. Visually the wave leading edge had a similar appearance to that observed during the Brushes Clough dam spillway tests (Fig. 1-1).

3.2 Wave front propagation down the chute

The propagation of the wave leading edge was recorded for a range of unsteady flow conditions (Table 3-1). The full data set is reported in Appendix IV. Dimensionless locations of wave front x_S/d_O are presented in Figure 3-2 as a function of the dimensionless time $t^*\sqrt{g/d_O}$, where x_S is the distance along the pseudo-bottom formed by the step edges measured from the upstream end and d_O is a measure of the initial flow rate:

Fig. 3-1 - Photographs of wave front propagation
(A) Experiment Series 2 : Q(t=0+) = 0.065 m^3/s, h = 0.07 m, Step 10 - Note the chaotic nature of the "white waters" next to the leading edge

[1]Each photograph was taken with high shutter speed (Sport mode).

(B) Experiment Series 2 : Q(t=0+) = 0.055 m^3/s, h = 0.07 m, Step 16 - Looking at the advancing wave, with the conductivity probes on the channel centreline

(C) Experiment Series 2 : Q(t=0+) = 0.075 m^3/s, h = 0.07 m, Step 16 - Wave front advancing from the top left to the bottom right - The wave front has not yet reached the probe sensors

$$d_o = \frac{9}{4} * \sqrt[3]{\frac{Q(t=0+)^2}{g * W^2}} \qquad (3\text{-}1)$$

where Q(t=0+) is the initial flow rate and W is the channel width (paragraph 1.2). The experimental data suggest an almost linear relationship between the wave front location and time (Fig. 3-2).
On the same graphs, dimensionless wave front celerity data $C_s/\sqrt{g*d_o}$ are presented (Fig. 3-2). The wave front celerity was measured over one step length : i.e., the velocity was averaged between one step edge and the next one. For small flow rates ($Q(t=0+) \leq 0.04$ m^3/s), the wave front celerity C_s was relatively uniform along the 24-m long chute. For larger discharges, the flow accelerated in the first 4 to 6 steps. Further

downstream, a gradual exponential decay was observed. In average, the dimensionless wave front celerity at the end of the chute was about for all flow rates and stepped geometries:

$$\frac{C_s}{\sqrt{g * d_o}} \approx 1.5 \qquad \text{end of stepped chute} \quad (3\text{-}2)$$

The experimental data were compared successfully with HUNT's (1982) theory (paragraph 1.2). The latter is valid only after the wave front travels more than 4 times the reservoir length, which would correspond to about $t^*\sqrt{g/d_o} \geq 35$ for the present study (Eq. (1-13) to (1-17)). A fair agreement between HUNT's theory and wave front celerity data was achieved assuming an equivalent Darcy-Weisbach friction factor f = 0.05, irrespective of the flow rate and chute configuration (Fig. 3-2). Calculated wave celerity are reported in Figure 3-2 (dashed line) for $t^*\sqrt{g/d_o} \geq 35$. The predicted wave front locations are also reported (Fig. 3-2, solid line).

3.3 Wave front propagation along a single step

Although Figure 3-2 suggests an almost linear relationship between wave front location and time, the wave propagation along each step was not smooth. It consisted of nappe take-off at the upstream step edge, free-falling jet, nappe impact and horizontal runoff toward the downstream end of the step.

Fig. 3-2 - Propagation of the wave front - Dimensionless wave front location x_s/d_o and wave front celerity $C_s/\sqrt{g*d_o}$ - Comparison with HUNT's (1982) theory

(A) Q(t=0+) = 0.040 m^3/s, h = 0.07 & 0.143 m

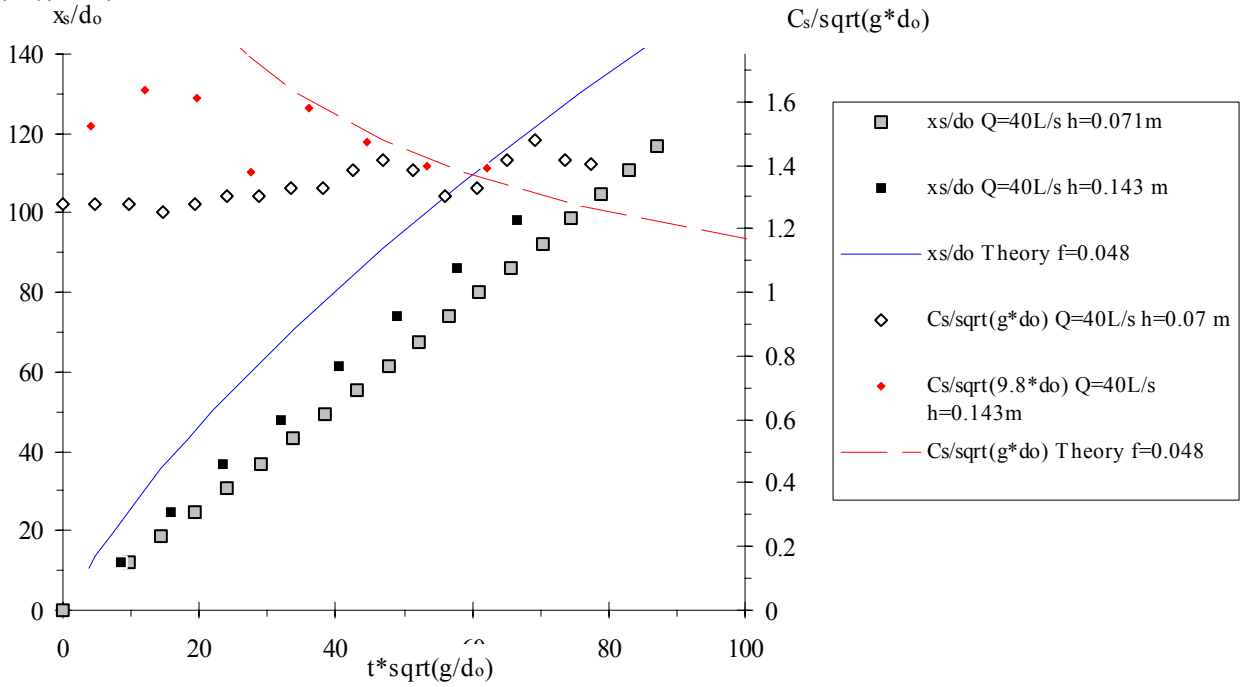

(B) Q(t=0+) = 0.055 m^3/s, h = 0.07 m

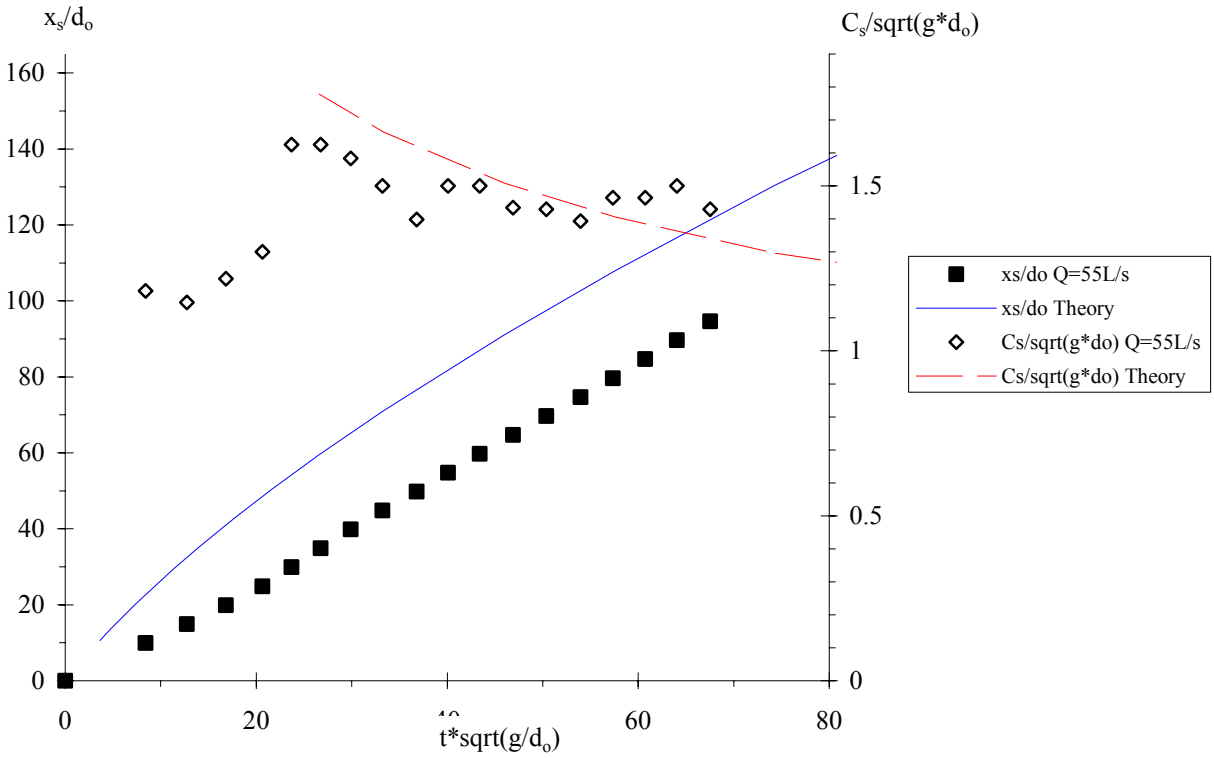

(C) Q(t=0+) = 0.075 m^3/s, h = 0.07 & 0.143 m

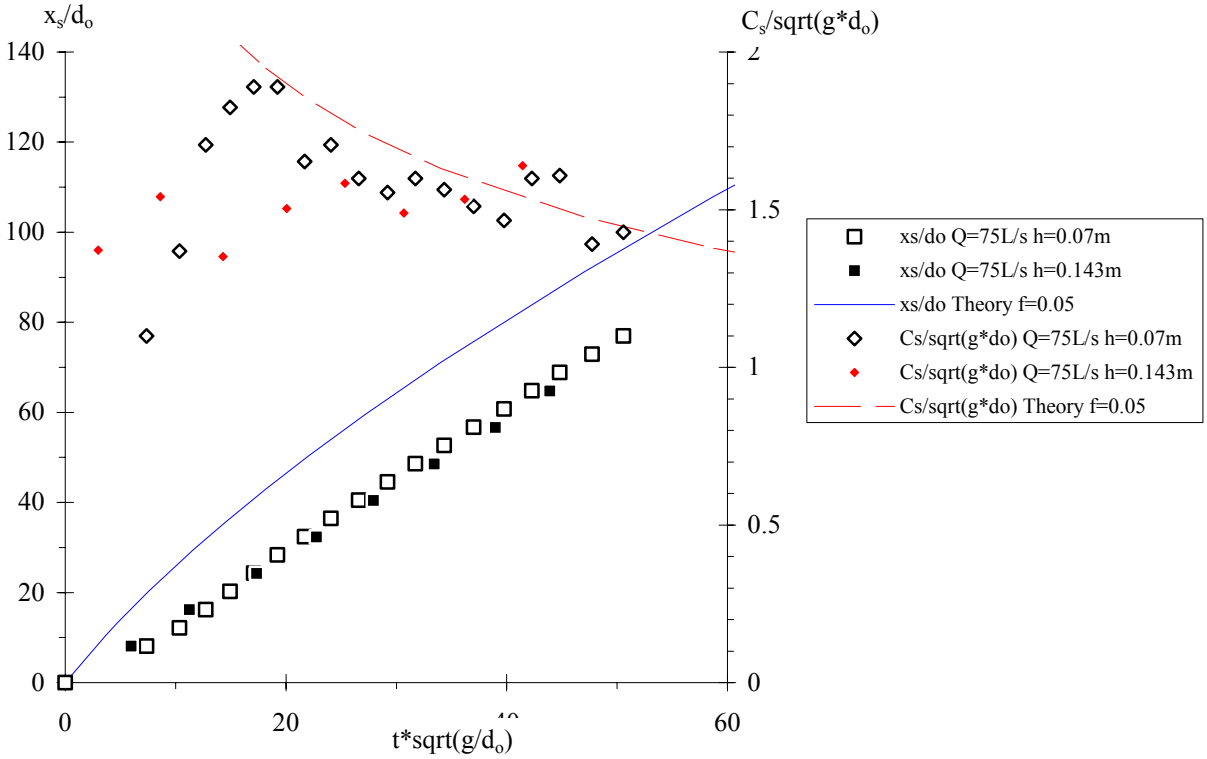

Table 3-1 - Summary of video observations of unsteady flow experiments

Ref.	θ (deg.)	h m	Run	Q(t=0+) (m^3/s)	Overall chute study	Individual step study	Remarks
(1)	(2)	(3)	(4)	(5)	(6)	(7)	(8)
Series 1	3.4	0.143					10 horizontal steps (l = 2.4 m). W = 0.5 m. Nozzle depth : d_n = 0.030 m.
			CT15	0.019	YES	NO	Runs CT1 and CT5.
			CT26	0.030	YES	NO	Runs CT2 and CT6.
			CT37	0.040	YES	NO	Runs CT3 and CT7.
			CT48	0.075	YES	NO	Runs CT4 and CT8.
Series 2	3.4	0.0715					18 horizontal steps (l = 1.2 m). W = 0.5 m. Nozzle depth : d_n = 0.030 m.
			TL1	0.040	YES	Step 3: $(C_S)_X$ & $(C_S)_Z$ Step 9: $(C_S)_X$ Step 10: $(C_S)_X$ & $(C_S)_Z$ Step 16: $(C_S)_X$ Step 17: $(C_S)_X$	Air-water flow measurements (step 17).
			TL2	0.0475	YES	Step 3: $(C_S)_X$ & $(C_S)_Z$ Step 9: $(C_S)_X$ Step 10: $(C_S)_X$ & $(C_S)_Z$ Step 16: $(C_S)_X$ Step 17: $(C_S)_X$	
			TL3	0.055	YES	Step 3: $(C_S)_X$ & $(C_S)_Z$ Step 9: $(C_S)_X$ Step 10: $(C_S)_X$ & $(C_S)_Z$ Step 16: $(C_S)_X$ Step 17: $(C_S)_X$	Air-water flow measurements (step 17).
			TL4	0.065	YES	Step 3: $(C_S)_X$ & $(C_S)_Z$ Step 9: $(C_S)_X$ Step 10: $(C_S)_X$ & $(C_S)_Z$ Step 16: $(C_S)_X$ Step 17: $(C_S)_X$	
			TL5	0.075	YES	Step 3: $(C_S)_X$ & $(C_S)_Z$ Step 9: $(C_S)_X$ Step 10: $(C_S)_X$ & $(C_S)_Z$ Step 16: $(C_S)_X$ Step 17: $(C_S)_X$	Air-water flow measurements (steps 10 and 17).
Brushes Clough dam	18.4						Inclined downward steps, trapezoidal channel (2 m bottom width)
			BC1	0.5	YES	NO	

Notes : Q(t=0+) : initial flow rate; d_n : approach flow depth (nozzle depth); h : step height; l : step length.

Dimensionless wave front celerity data $C_S/\sqrt{g*d_o}$ measured on a single step are presented in Figures 3-3 and 3-4. The full data set is presented in Appendix V. Figure 3-3 shows experimental results at one step for three

flow rates, while Figure 3-4 presents experimental data at several steps for one flow rate. In Figures 3-3 and 3-4, C_S is the magnitude of the wave celerity : $C_S = \sqrt{(C_S)_X^2 + (C_S)_Z^2}$, where the subscripts x and z refer to the measured horizontal and vertical celerity component respectively. Although $C_S = (C_S)_X$ downstream of nappe impact, the vertical celerity component must be accounted for in the free-falling nappe. Experiments at two steps for five flow rates (Table 3-1, column 7) demonstrated that the vertical component of wave front celerity $(C_S)_Z$ satisfied the motion equation and hence basic trajectory equation: i.e., $(C_S)_Z \propto t' \propto x'$, where t' is the time from take-off and x' is the horizontal distance from the step vertical face. Experimental data (Fig. 3-3 and 3-4) highlighted nappe acceleration in the free-jet followed by a gradual flow deceleration downstream of nappe impact.

3.4 Discussion

In smooth concrete chutes, steady flow Darcy-Weisbach friction factors f range typically between 0.01 and 0.03 (e.g. HENDERSON 1966, CHANSON 1999). In skimming flows down stepped chutes, the equivalent Darcy friction factor is about $f_e = 0.2$, where f_e is the friction factor of air-water flows (CHANSON 2001, CHANSON et al. 2002). The analysis of steady air-water flow experiments in the same chute as the present study showed that the smooth chute flow resistance yielded $f_e = 0.015$, while the equivalent friction factor of stepped chute flows was about $f_e = 0.047$ in average ([2]) (Table 3-2, column 9).

Fig. 3-3 - Dimensionless wave front celerity $C_S/\sqrt{g*d_o}$ along a single step (Series 2, h = 0.07 m)

(A) Step 3

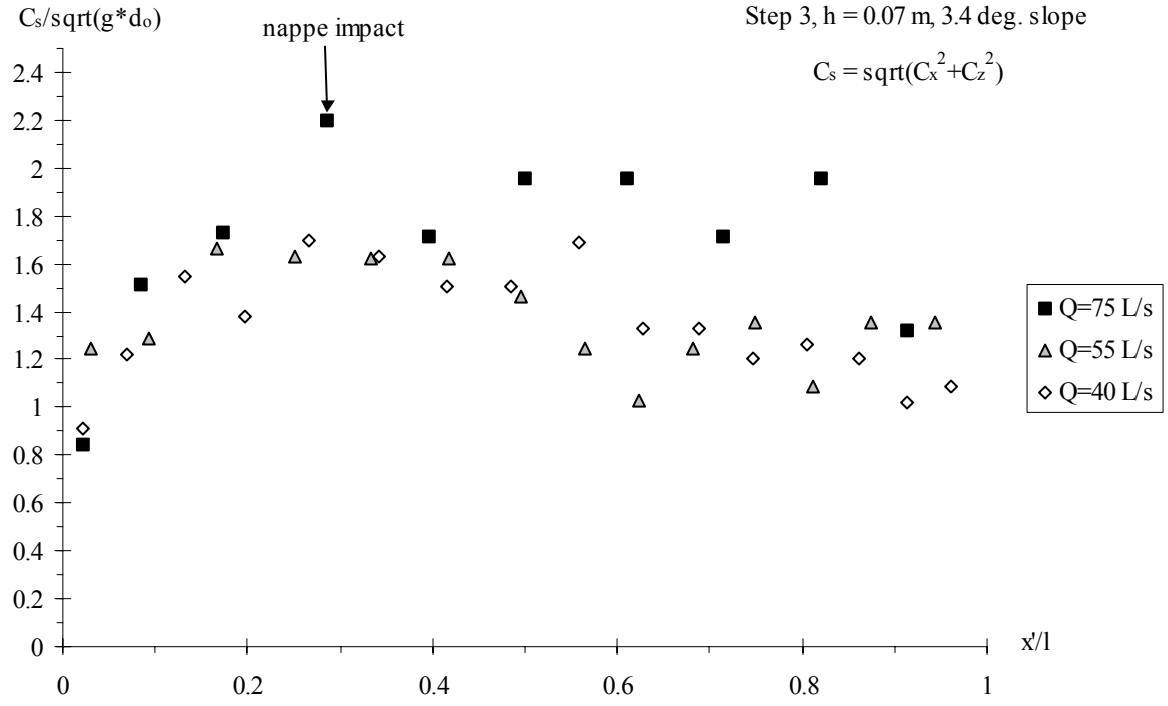

[2]Note the range of flow regimes (nappe flows, transition flow, skimming flows) investigated by CHANSON and TOOMBES (2002a) (Table 3-2, column 3). Flow resistance comparison between such different regimes is not strictly correct.

(B) Step 10

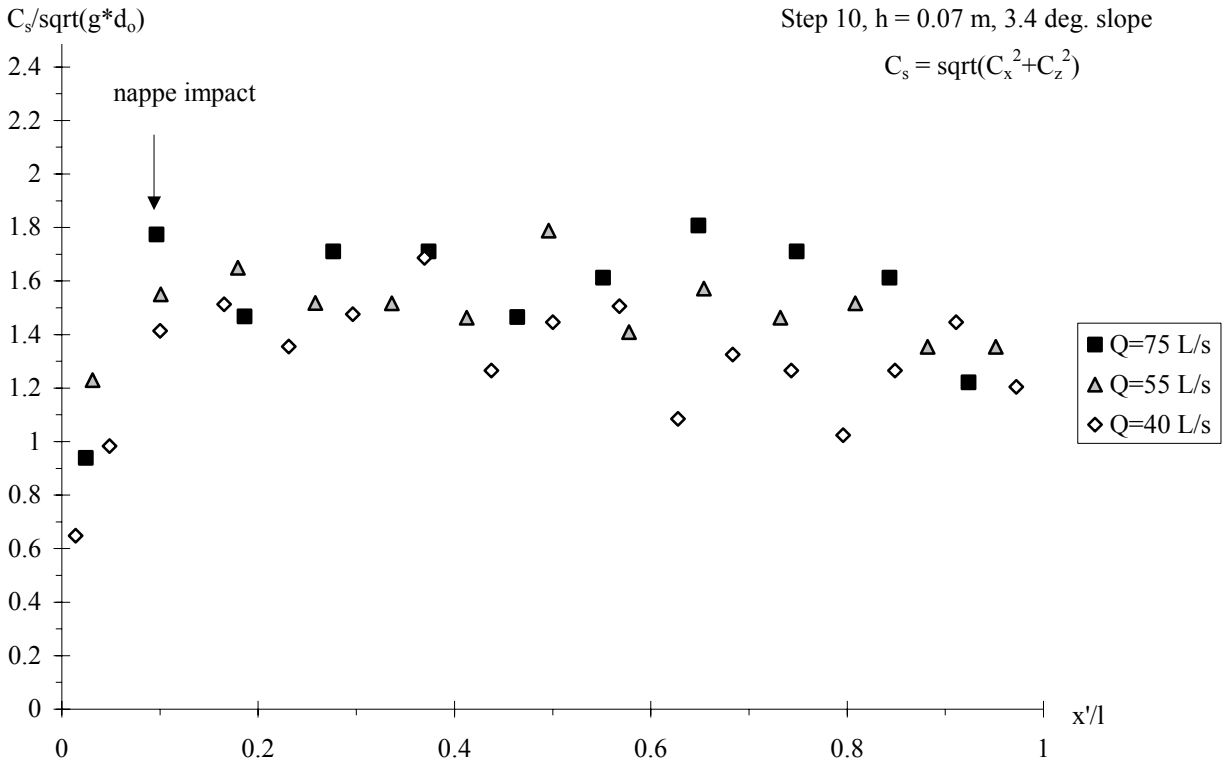

Fig. 3-4 - Dimensionless wave front celerity $C_S/\sqrt{g*d_o}$ along a single step - Series 2, h = 0.07 m, Q(t=0+) = 0.075 m^3/s

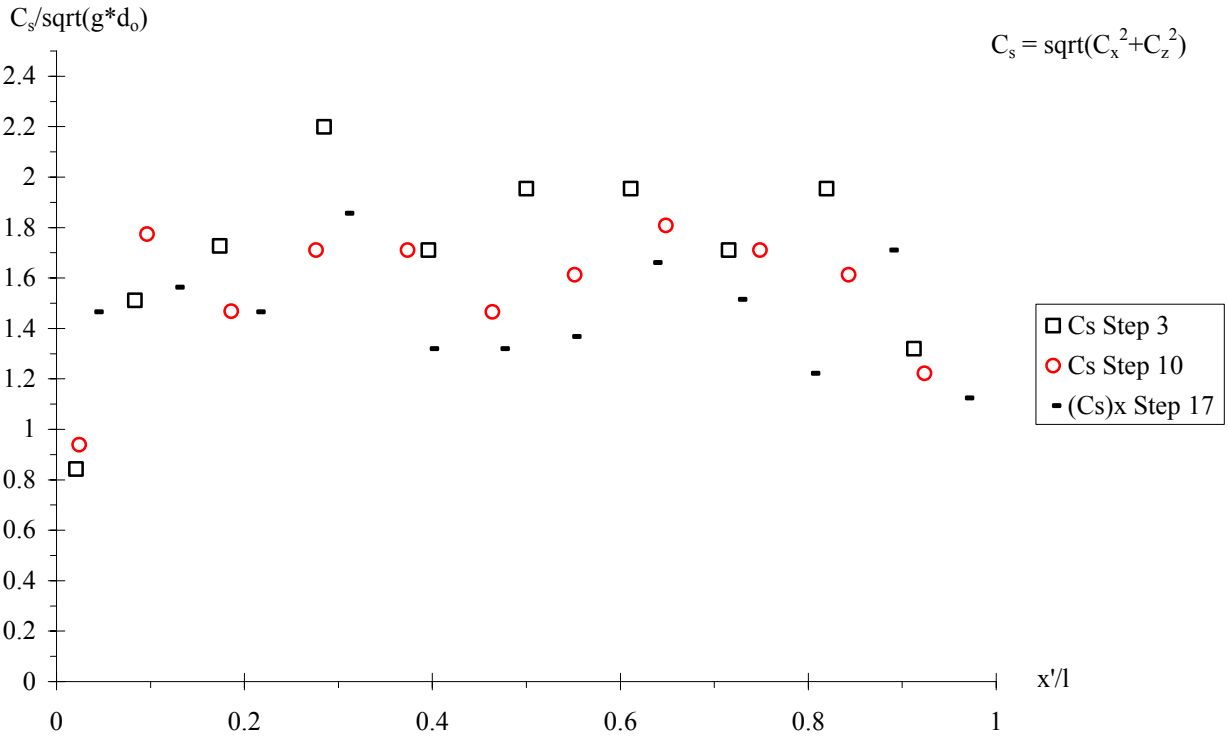

The unsteady flow results show a fair agreement between present data and HUNT's (1982) theory assuming f = 0.05 (paragraph 3.2). Such a flow resistance is very close to steady flow experiments in the same facility. This suggests that flow resistance in unsteady dam break wave flows is comparable to steady flow resistance. The result refutes any suggestion that air entrainment at the wave front would create an air cushion, inducing some drag reduction. Further the flow resistance estimate f ~ 0.05 was found to be independent of the step height (h = 0.07 & 0.143 m) and flow rate for Q(t=0+) = 0.019 to 0.075 m^3/s.

Table 3-2 - Steady flow experiments : flow regimes and experimental observations at the downstream end of the chute (after CHANSON and TOOMBES 2002a)

Ref.	q	Flow	End chute data (1)						Remarks
	m^2/s	regime	C_{mean}	$\frac{Y_{90}}{d_c}$	$\frac{\Delta H}{H_1}$	$\frac{H_{res}}{d_c}$	S_f	f_e	
(1)	(2)	(3)	(4)	(5)	(6)	(7)	(8)	(9)	(10)
Smooth chute	0.150	Smooth -invert	0.09	0.365	0.76	4.84	0.0419	0.0154	Smooth-invert.
Series S1a									h = 0.143 m
	0.130	NA3	0.19	0.501	0.81	3.41	0.1116	0.0596	
	0.150	NA3	0.18	0.478	0.80	3.62	0.150	0.080	
Series S1b									h = 0.143 m
	0.080	NA3	0.20	0.544	0.83	3.05	0.0655	0.0287	Run CR1.
	0.110	NA3	0.18	0.510	0.81	3.31	0.0297	0.0153	Run CR2.
	0.150	NA3	0.20	0.501	0.81	3.53	0.1812	0.0956	Run CR2.
Series S2									h = 0.071 m
	0.080	TRA	0.22	0.515	0.79	3.49	0.0726	0.038	Run ES1.
	0.110	SK1	0.24	0.547	0.79	3.51	0.0373	0.0199	Run ES2.
	0.150	SK1	0.24	0.429	0.72	5.03	0.084	0.0375	Run ES3.

Notes : NA2 = nappe flow with hydraulic jumps; NA3 = nappe flow without hydraulic jump; TRA = transition flow; SK1 = skimming flow; End chute data : calculated based upon air-water flow properties; (1) : end chute flow conditions measured at downstream end of steps 9 (Series S1) and 16 (Series S2); f_e : air-water flow Darcy-Weisbach friction factor.

4. UNSTEADY AIR-WATER FLOW PROPERTIES (1) VOID FRACTIONS, BUBBLE COUNT RATES AND SPECIFIC INTERFACE AREAS

Air concentrations and bubble count rates were measured for three flow rates at two steps (Table 4-1). On each step, void fraction and bubble count distributions were recorded at five locations x' = 0.2, 0.4, 0.6, 0.8 and 1.0 m where x' is the horizontal distance from the vertical step edge (Fig. 4-1). The full data set is reported in Appendices VI to VIII.

Table 4-1 - Summary of unsteady air-water flow measurements in dam break wave flow

Run	θ (deg.)	h m	Q(t=0+) (m^3/s)	Air-water flow measurements	Remarks
(1)	(2)	(3)	(4)	(5)	(6)
Series 2	3.4	0.071			18 horizontal steps (l = 1.2 m, W = 0.5 m).
			0.040	Step 16	
			0.055	Step 16	
			0.075	Steps 10 & 16	

Notes : h : step height; l : step length; Q(t=0+) : initial flow rate; W : chute width.

Fig. 4-1 - Void fraction C behind the leading edge of wave front - Definition sketch

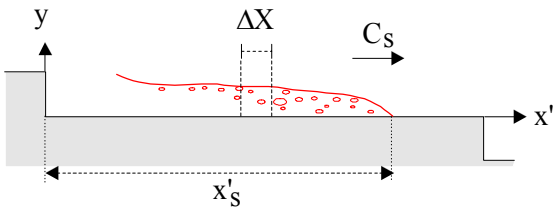

4.1 Void fraction distributions

Typical void fraction distributions are presented in Figure 4-2 and 4-3 where void fractions were calculated during a short time interval ΔT such as $\Delta T = \Delta X/C_S$ where C_S is the measured surge front celerity and ΔX is the control volume streamwise length. (ΔX was selected to be a multiple of Δx : i.e., $\Delta X = I*\Delta x$ where I is an integer equal or larger than unity and Δx is the smallest control volume streamwise length (70 mm).) In Figures 4-2 and 4-3, the legend indicates the location and size of the control volume behind the leading edge of wave front: e.g., 350-735 mm means the 385 mm long control volume located between 350 mm and 735 mm behind the leading edge. In each case, the data are compared with the corresponding steady flow data of CHANSON and TOOMBES (2002a).

Figure 4-2 presents data for one flow rate at five locations x' along a single step. At x' = 0.2 m (Fig. 4-2A), a free-falling nappe was observed in the unsteady flow, although the steady flow data did not show such a free-jet. The finding is typical : i.e., a free-falling nappe was always observed at x' = 0.2 m for all flow conditions (Table 4-1). For x' = 0.4 to 1.0 m, the air concentration distributions exhibited a shape somehow close to self-aerated open channel flows (Fig. 4-2B to 4-2E). The data suggested consistently maximum flow aeration between x' = 0.4 and 0.6 m, followed by some flow de-aeration further downstream up to x' = 1.0 m. The trend is illustrated by the shape of the void fraction curves. The result is confirmed by depth-averaged

void fraction data for all flow conditions (section 4.4, App. VIII).

Figure 4-3 shows data at one location at the end of a step (x' = 1.0 m, Step 16) for two flow rates. The data were measured at the same location as the data presented in Figure 4-2E. Overall the data suggested increasing flow aeration and increasing mean air content with increasing flow rate Q(t=0+). The same trend was observed in steady flows (CHANSON and TOOMBES 2002a).

Further the distributions of void fractions (Fig. 4-2 & 4-3) demonstrated consistently a very strong aeration of the leading edge, especially the first 0.3 to 0.7 m of the wave front flow : i.e., $(t - t_s)*\sqrt{g/d_o} < 1.0$ to 1.2 where t is the time and where t_s is the time of passage of wave front at x'. The finding was clearly seen for all flow rates and steps for x' ≥ 0.4 m. For example, in Figure 4-2E, the depth-average void fractions defined between 0 and 90% were C_{mean} = 0.86, 0.56, 0.42 and 0.21 for 0-70 mm, 0-210 mm, 0-385 mm and 700-1085 mm respectively. In steady flow, the mean air content was C_{mean} = 0.21 (for Q = 0.075 m^3/s, step 16 and x' = 1.0 m). Another example : in Figure 4-2D, the depth-average void fractions defined between 0 and 90% were C_{mean} = 0.90, 0.54, 0.48 and 0.31 for ΔX = 0-70 mm, 0-210 mm, 0-385 mm and 700-1085 mm respectively. In steady flow, the mean air content was C_{mean} = 0.24 at that location for that flow rate.

In addition, the data highlighted a distinctive spray region (C > 0.7) extending up to y = 1.5 to 2 * Y_{90}, where Y_{90} is the location where C = 90%.

Fig. 4-2 - Void fraction distributions behind the leading edge of wave front on Step 16 for Q(t=0+) = 0.075 m^3/s (C_S = 2.43 m/s, h = 0.07 m) - Comparison with steady flow data (CHANSON and TOOMBES 2002a)

	0-70 mm	0-210 mm	0-385 mm	350-735 mm	700-1085 mm	2100-2485 mm	4200-4585 mm
ΔX (m) =	0.070	0.210	0.385	0.385	0.385	0.385	0.385
$(t - t_s)*\sqrt{g/d_o}$ =	0.0828	0.248	0.455	1.283	2.110	5.421	10.39

(A) x' = 0.2 m

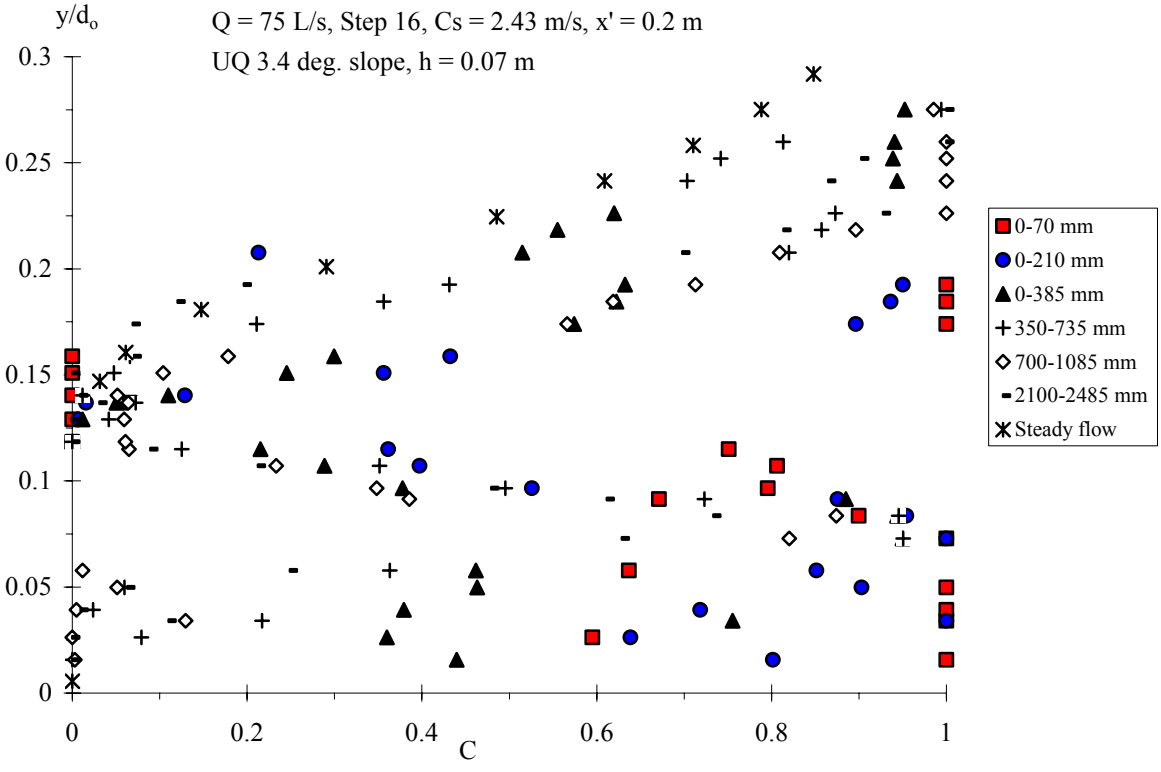

(B) x' = 0.4 m

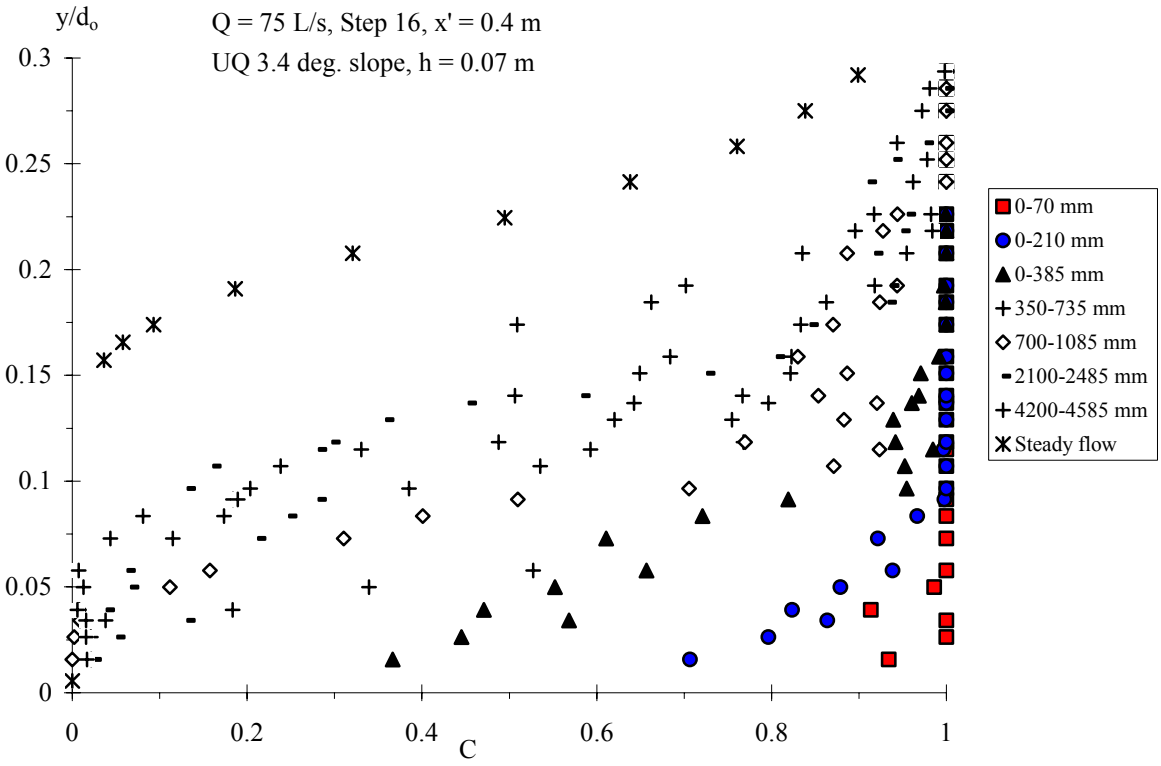
y/do
Q = 75 L/s, Step 16, x' = 0.4 m
UQ 3.4 deg. slope, h = 0.07 m
0.3
0.25
0.2
0.15
0.1
0.05
0
0
0.2
0.4
0.6
0.8
1
C
0-70 mm
0-210 mm
0-385 mm
350-735 mm
700-1085 mm
2100-2485 mm
4200-4585 mm
Steady flow

(C) x' = 0.6 m

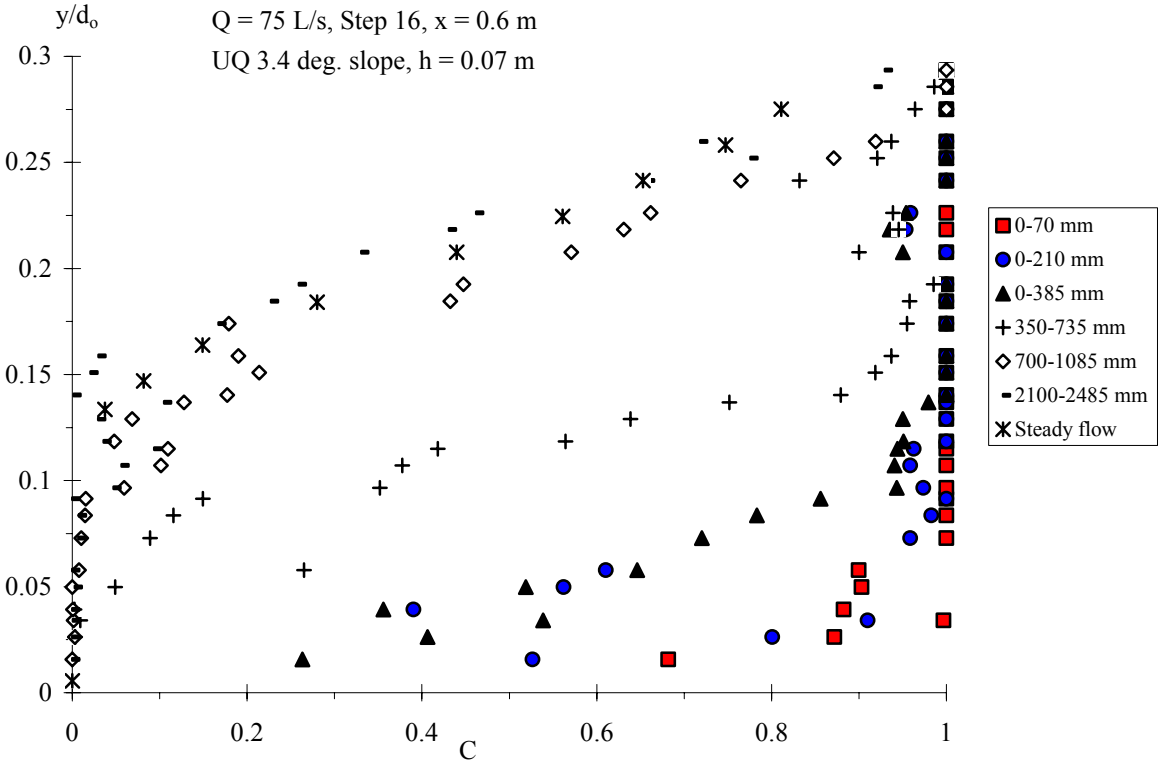
y/do
Q = 75 L/s, Step 16, x = 0.6 m
UQ 3.4 deg. slope, h = 0.07 m
0.3
0.25
0.2
0.15
0.1
0.05
0
0
0.2
0.4
0.6
0.8
1
C
0-70 mm
0-210 mm
0-385 mm
350-735 mm
700-1085 mm
2100-2485 mm
Steady flow

(D) x' = 0.8 m - Comparison with Equations (4-1) and (4-2)

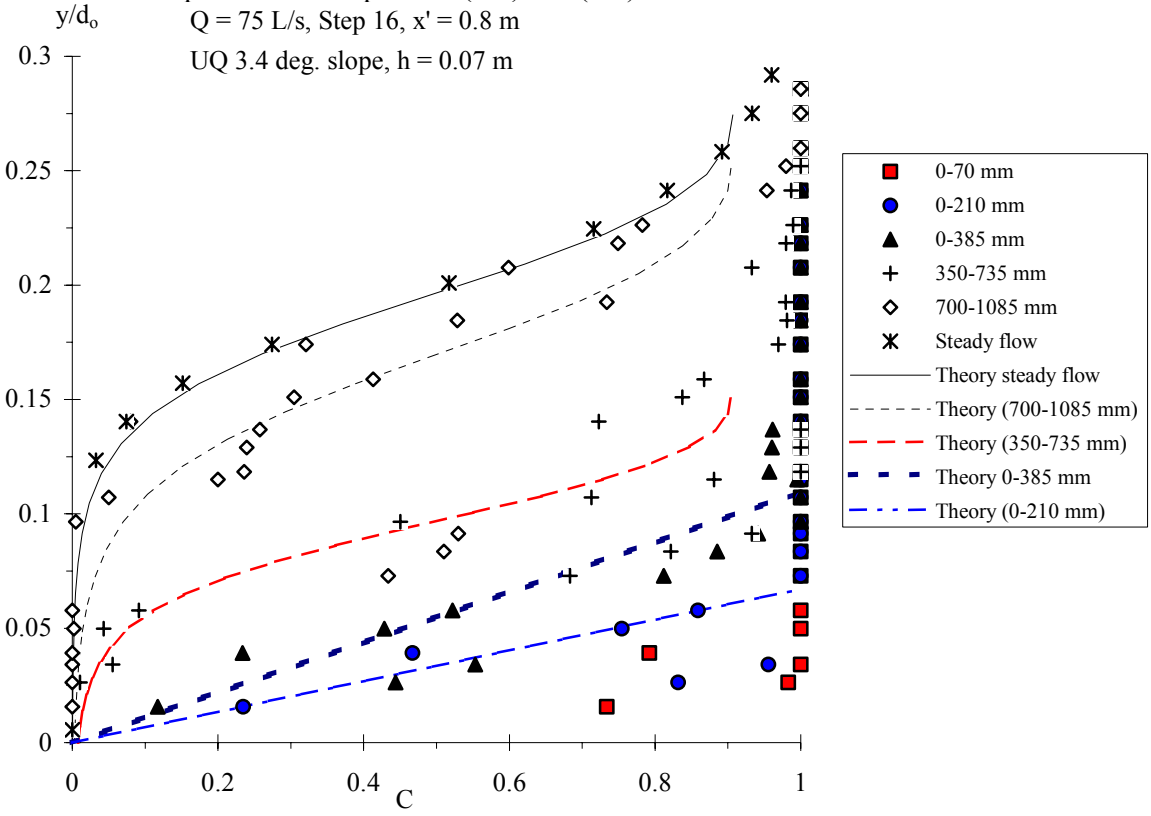

(E) x' = 1.0 m

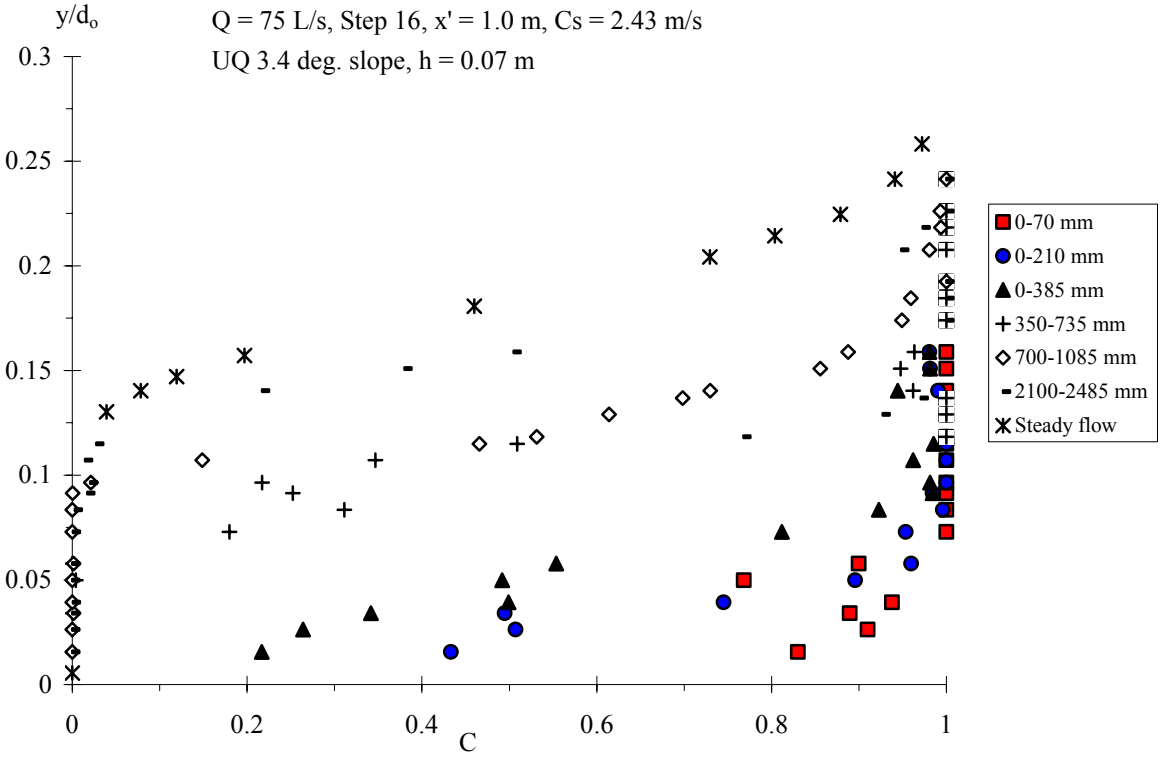

Fig. 4-3 - Void fraction distributions behind the leading edge of wave front at the end of a step (x' =1.0 m, Step 16) - Comparison with steady flow data (CHANSON and TOOMBES 2002a)

(A) Q(t=0+) = 0.040 m^3/s, Step 16 (C_S = 1.97 m/s, h = 0.07 m)

	0-70 mm	0-210 mm	0-385 mm	350-735 mm	700-1085 mm	2100-2485 mm	4200-4585 mm
ΔX (m) =	0.070	0.210	0.385	0.385	0.385	0.385	0.385
$(t - t_S)*\sqrt{g/d_o}$ =	0.26	0.378	0.692	1.951	3.21	8.245	15.8

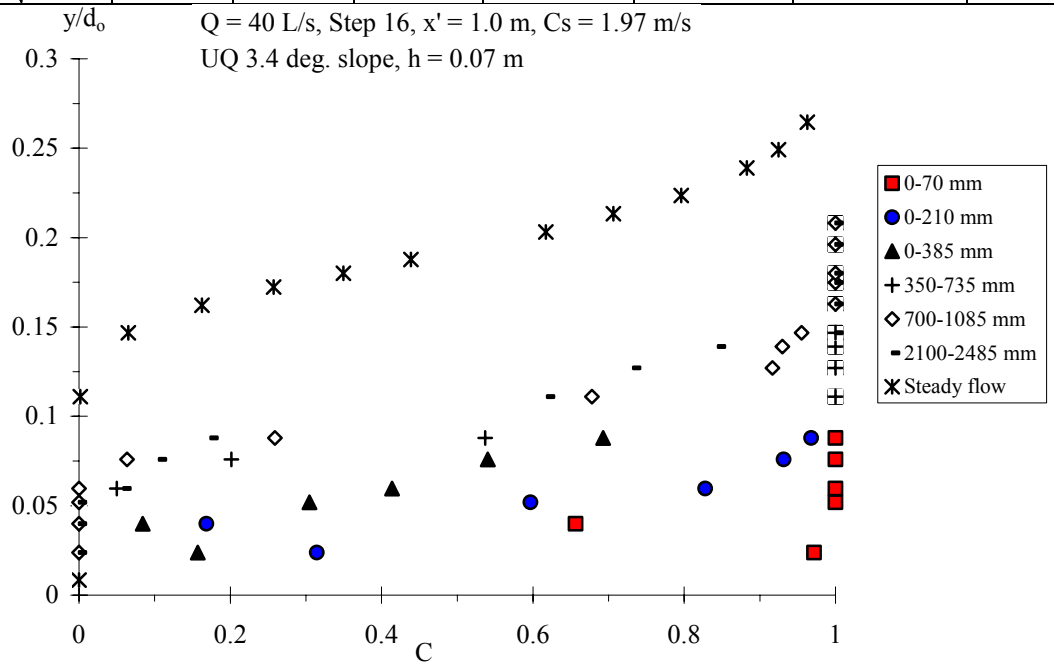

(B) Q(t=0+) = 0.055 m^3/s, Step 16 (C_S = 2.14 m/s, h = 0.07 m)

	0-70 mm	0-210 mm	0-385 mm	350-735 mm	700-1085 mm	2100-2485 mm	4200-4585 mm
ΔX (m) =	0.070	0.210	0.385	0.385	0.385	0.385	0.385
$(t - t_S)*\sqrt{g/d_o}$ =	0.104	0.313	0.573	1.615	2.657	6.826	13.08

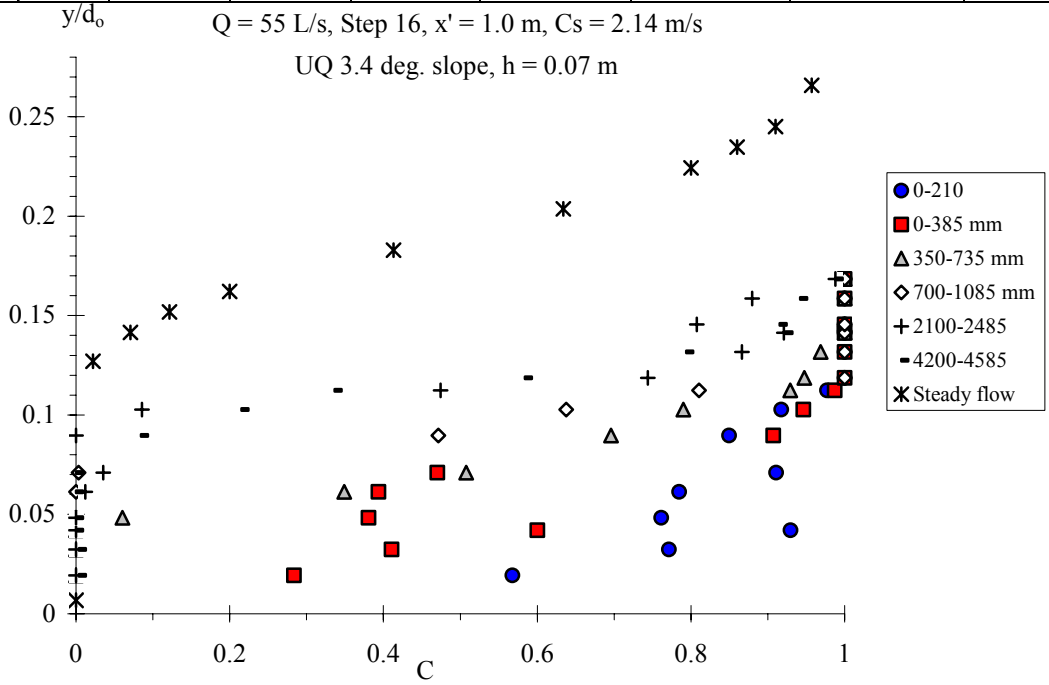

Discussion

Figure 4-4 presents further void fraction data for Q(t=0+) = 0.075 m^3/s on Step 10. For 0-70 mm, 0-210 mm, 0-385 mm and 350-735 mm, the dimensionless times $(t - t_s)*\sqrt{g/d_o}$ was 0.077, 0.231, 0.424 and 1.2. For 0-210 mm, 0-385 mm and 350-735 mm, the data yielded C_{mean} = 0.40, 0.54, and 0.22, compared to C_{mean} = 0.20 in steady flow.

At the front of the wave, the void fraction distributions had roughly a linear shape :

$$C = 0.9 * \frac{y}{Y_{90}} \qquad 0.1 < (t - t_s)*\sqrt{g/d_o} < 1.3 \quad (4\text{-}1)$$

Equation (4-1) is a limiting case of the analytical solution of air bubble diffusion equation for steady transition flows down stepped chute (App. III). For larger times $(t - t_s)$, the distribution of air concentration may be described by a diffusion model developed for steady flows :

$$C = 1 - \tanh^2\left(K' - \frac{\frac{y}{Y_{90}}}{2 * D_o} + \frac{\left(\frac{y}{Y_{90}} - \frac{1}{3}\right)^3}{3 * D_o}\right) \qquad (t - t_s)*\sqrt{g/d_o} > 1.3 \quad (4\text{-}2)$$

where K' and D_o are functions of the mean air content only (App. III). Equations (4-1) and (4-2) are plotted for unsteady and steady flow conditions in Figures 4-2D and 4-4. The analytical models compare favourably with the data.

Fig. 4-4 - Void fraction distributions behind the leading edge of wave front

(A) Comparison between unsteady data, steady flow data (CHANSON and TOOMBES 2002a), and Equations (4-1) and (4-2)

Q(t=0+) = 0.075 m^3/s, h = 0.07 m, Step 10, C_S = 2.61 m/s, x' = 1.0 m

	0-70 mm	0-210 mm	0-385 mm	350-735 mm	700-1085 mm	2100-2485 mm	4200-4585 mm
ΔX (m) =	0.070	0.210	0.385	0.385	0.385	0.385	0.385
$(t - t_s)*\sqrt{g/d_o}$ =	0.077	0.231	0.424	1.194	1.965	5.047	9.67

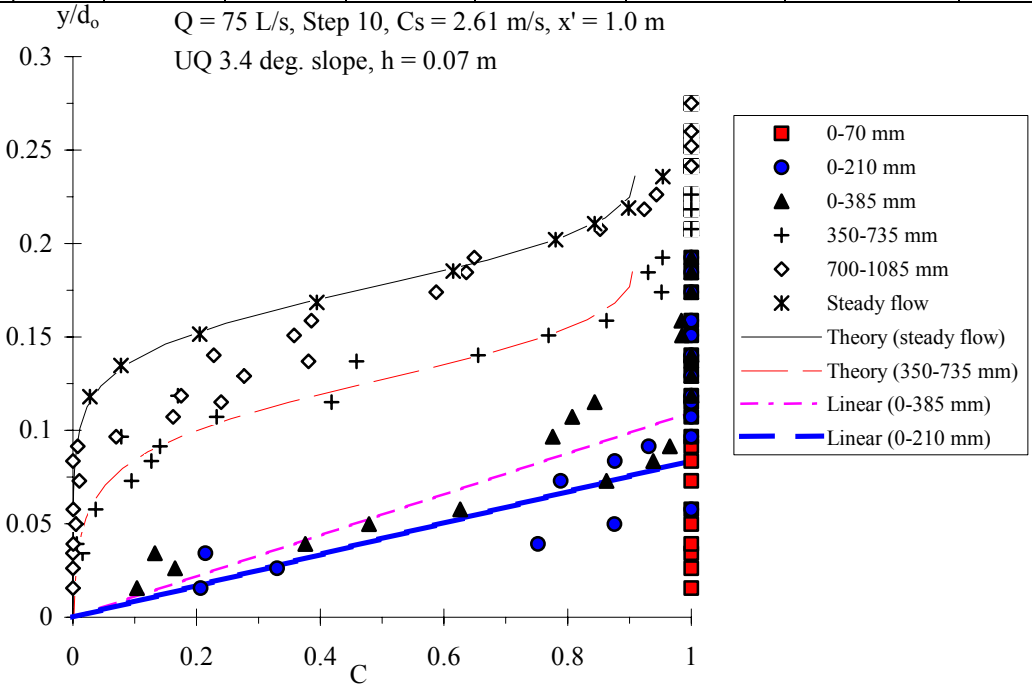

(B) Sketch of the air-water flow region at the leading edge

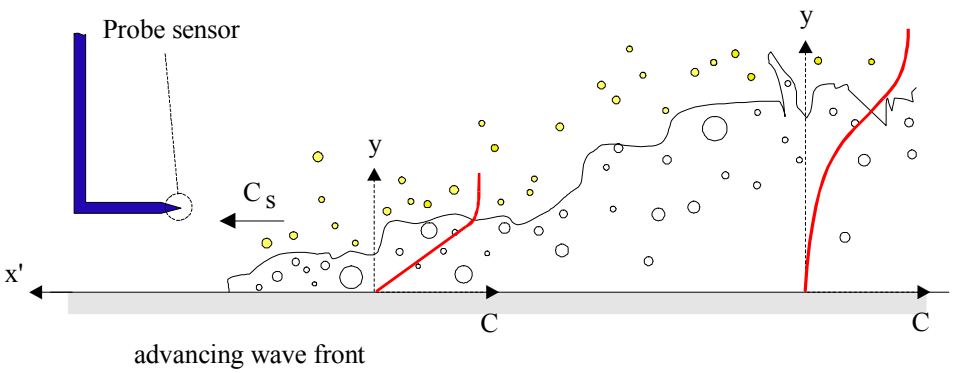

Figures 4-2 to 4-4 highlight a major change in void fraction distribution shape which took place for $(t - t_s)*\sqrt{g/d_o} \sim 1.2$ to 1.5. Possible explanations may include a non-hydrostatic pressure field in the leading front of the wave. Further there might be a change in air-water flow structure between the leading edge and the main flow, associated with a change in rheological fluid properties. More a change in gas-liquid flow regime might take place, with a plug/slug flow regime in front and a homogenous bubbly flow region behind. This would be consistent with high-shutter speed movies of the leading edge highlighting very dynamic processes. Another explanation might be a change in shear stress distributions and boundary friction between the leading edge and the main flow behind.

4.2 Bubble count rate distributions

Typical distributions of dimensionless bubble count rates are presented in Figure 4-5. The dimensionless bubble count rate is defined as $F*d_o/V_o$ where d_o is a measure of the flow rate (Eq. (3-1)) ([3]) and V_o is the corresponding flow velocity (i.e. $V_o = Q(t=0+)/(W*d_o)$). Figure 4-5 presents data for one flow rate at five locations x' along a single step. The unsteady flow data are compared with steady flow conditions. Note that the scale of the horizontal axis differs between each figure.

The experimental data highlighted consistently large bubble count rates in the leading edge of the wave front (i.e. the first 0.2 to 0.3 m) for all flow rates and step locations. Measurements showed maximum bubble count rates of up to 500 bubbles per second (Table 4-2, App. VIII). A summary is given in Table 4-2 for the data presented in Figure 4-5. The full analysis is reported in Appendix VIII. Further away from the leading edge, the observed count rates were lower : i.e., the measured values were of the same order of magnitude as steady flow observations. The finding may support the hypothesis of differences in air-water flow structure between the leading edge and the rest of the flow.

[3]Note that $d_o = 9/4*d_c$ where d_c is the critical depth associated with the flow rate Q(t=0+) (paragraph 1.2).

Table 4-2 - Maximum bubble count rates behind the leading edge of wave front on Step 16 for Q(t=0+) = 0.075 m^3/s (C_S = 2.43 m/s, h = 0.07 m) - Comparison with steady flow data (CHANSON and TOOMBES 2002a)

x' m	F_{max} Hz										
	0-70 mm	0-210 mm	140-210 mm	0-385 mm	175-385 mm	350-735 mm	525-595 mm	700-1085 mm	2100-2485 mm	4200-4585 mm	Steady flow
$t-t_S$ (s)	0.0144	0.0432	0.0720	0.07922	0.11523	0.2233	0.2305	0.3673	0.9434	1.808	$+\infty$
(1)	(2)	(3)	(4)	(5)	(6)	(7)	(8)	(9)	(10)	(11)	(12)
1.0	173.6	300.9	--	82.5	5.9	79.3	69.4	57.1	126.2	97.8	39.23
0.8	208.3	335.6	173.6	92.0	11.6	76.1	104.1	98.3	88.4	82.1	38.65
0.6	104.1	497.6	208.3	136.4	6.5	79.3	138.9	88.8	123.1	116.8	38.9
0.4	104.1	324.0	208.3	88.8	8.89	123.7	243.0	136.4	82.1	126.2	56.3
0.2	--	266.1	--	--	--	--	--	--	--	--	33.8

Fig. 4-5 - Dimensionless distributions of bubble count rates behind the leading edge of wave front on Step 16 for Q(t=0+) = 0.075 m^3/s (C_S = 2.43 m/s, h = 0.07 m) - Comparison with steady flow data (CHANSON and TOOMBES 2002a)

	0-70 mm	0-210 mm	0-385 mm	350-735 mm	700-1085 mm	2100-2485 mm	4200-4585 mm
ΔX (m) =	0.070	0.210	0.385	0.385	0.385	0.385	0.385
$(t - t_S)*\sqrt{g/d_o}$ =	0.0828	0.248	0.455	1.283	2.110	5.421	10.39

(A) x' = 0.2 m

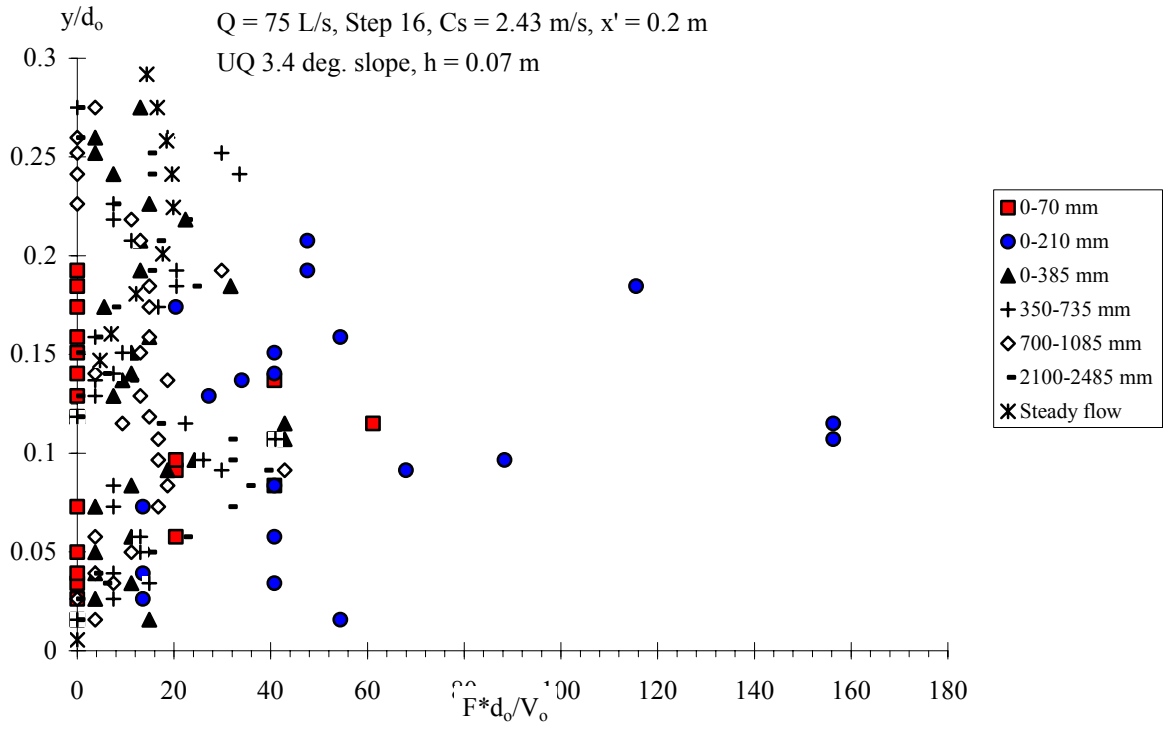

(B) x' = 0.4 m

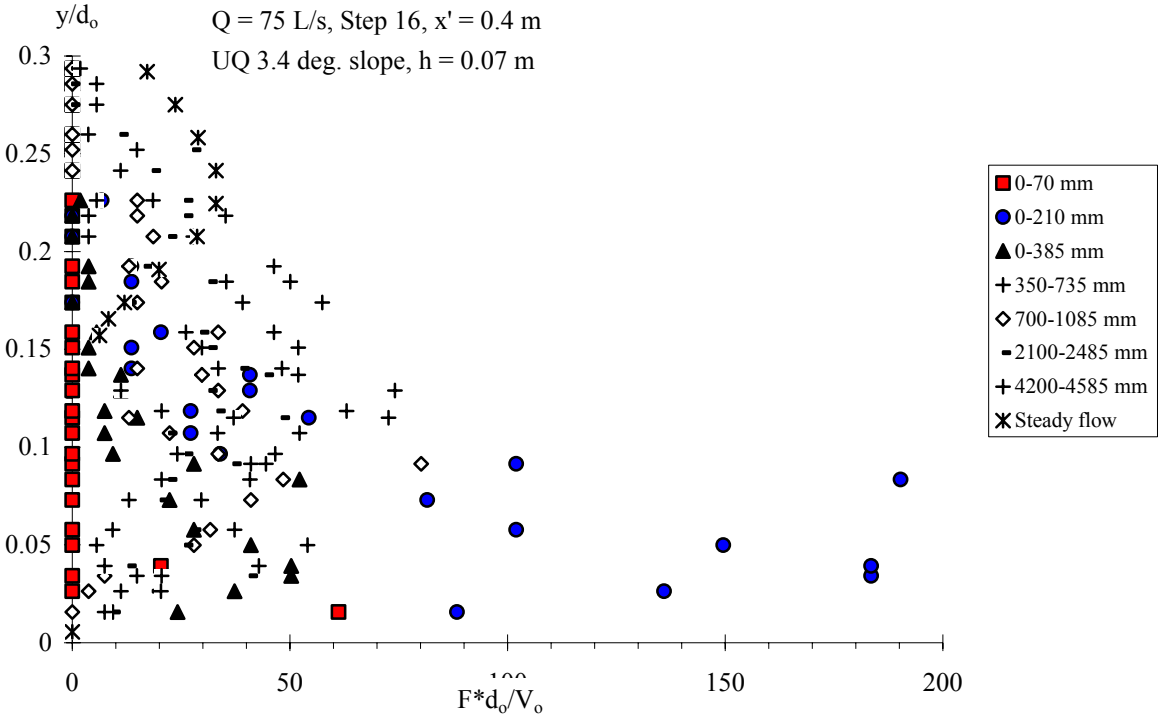
y/do
Q = 75 L/s, Step 16, x' = 0.4 m
UQ 3.4 deg. slope, h = 0.07 m
0.3
0.25
0.2
0.15
0.1
0.05
0
0
50
150
200
F*do/Vo
0-70 mm
0-210 mm
0-385 mm
350-735 mm
700-1085 mm
2100-2485 mm
4200-4585 mm
Steady flow

(C) x' = 0.6 m

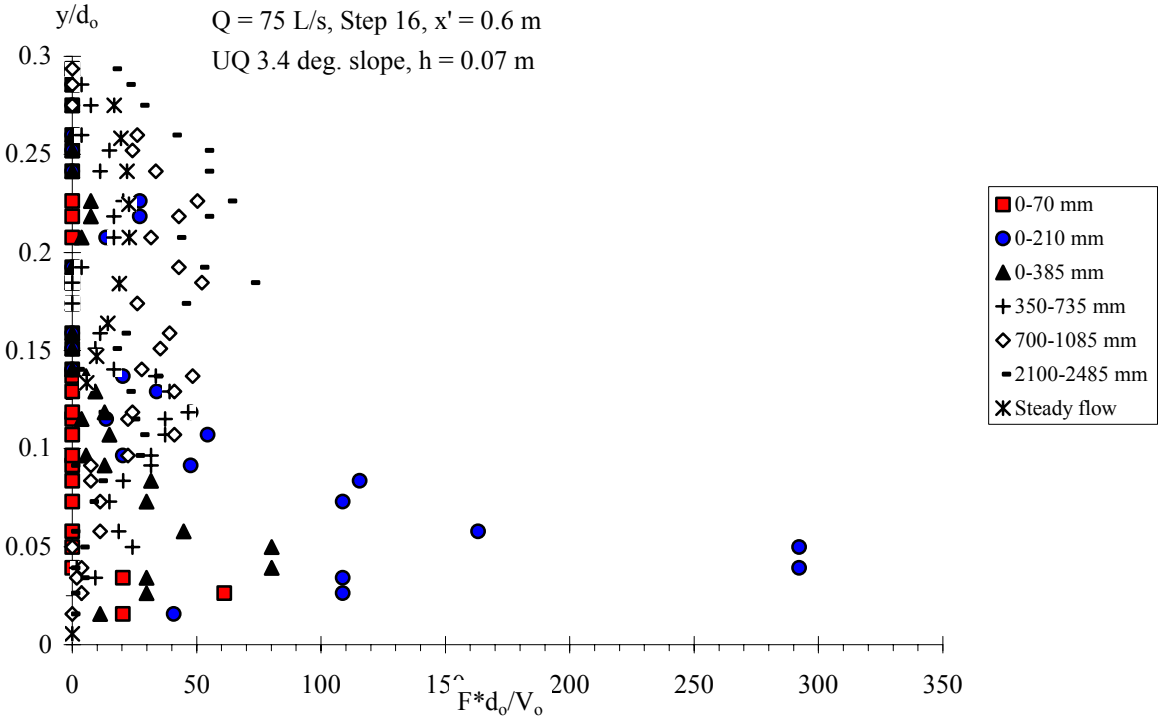
y/do
Q = 75 L/s, Step 16, x' = 0.6 m
UQ 3.4 deg. slope, h = 0.07 m
0.3
0.25
0.2
0.15
0.1
0.05
0
0
50
100
200
250
300
350
F*do/Vo
0-70 mm
0-210 mm
0-385 mm
350-735 mm
700-1085 mm
2100-2485 mm
Steady flow

(D) x' = 0.8 m

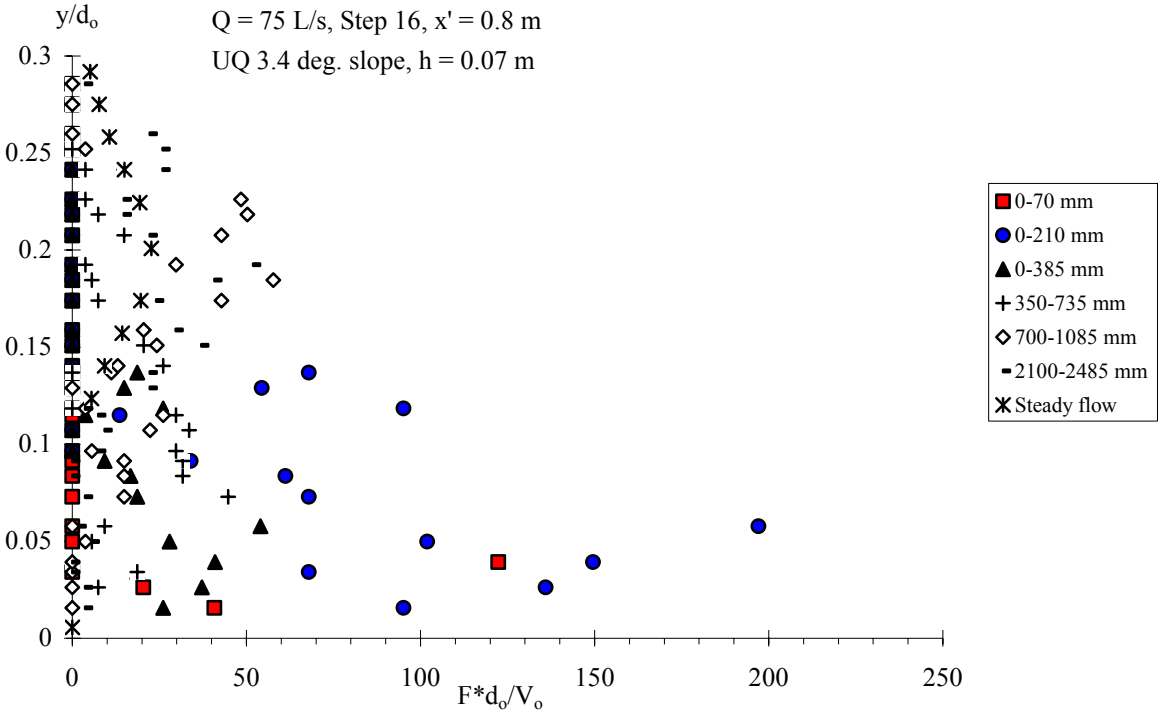
y/do
Q = 75 L/s, Step 16, x' = 0.8 m
UQ 3.4 deg. slope, h = 0.07 m
0.3
0.25
0.2
0.15
0.1
0.05
0
0
50
100
150
200
250
F*do/Vo
0-70 mm
0-210 mm
0-385 mm
350-735 mm
700-1085 mm
2100-2485 mm
Steady flow

(E) x' = 1.0 m

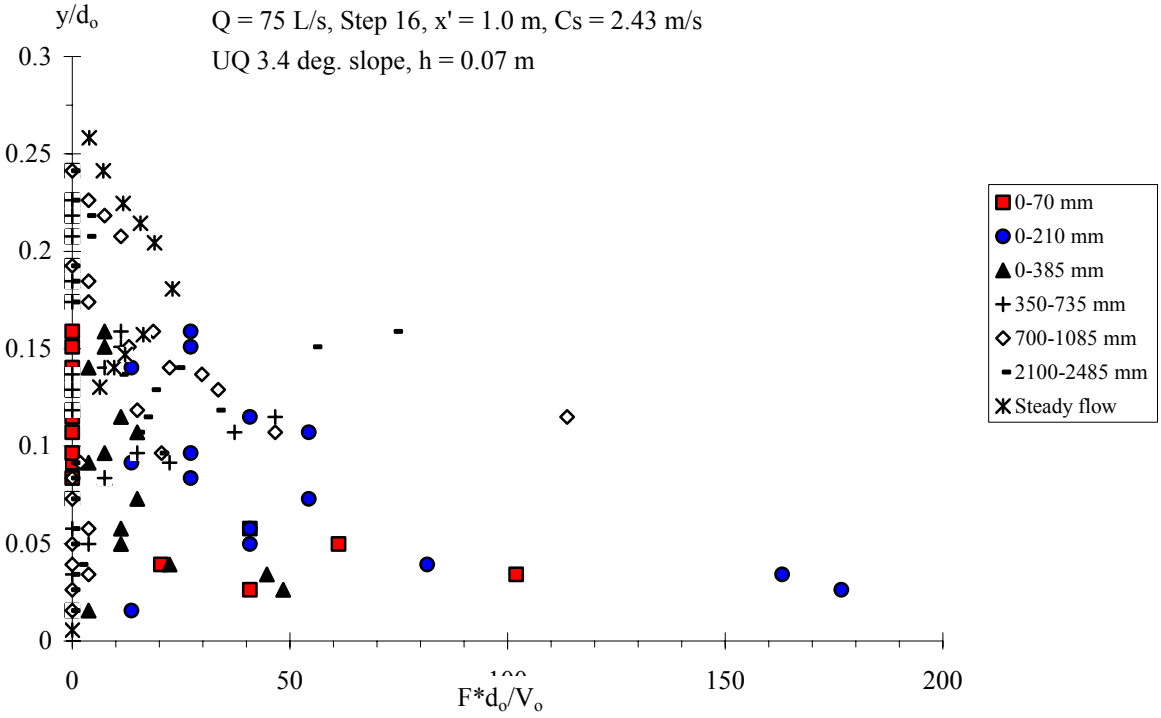
y/do
Q = 75 L/s, Step 16, x' = 1.0 m, Cs = 2.43 m/s
UQ 3.4 deg. slope, h = 0.07 m
0.3
0.25
0.2
0.15
0.1
0.05
0
0
50
150
200
F*do/Vo
0-70 mm
0-210 mm
0-385 mm
350-735 mm
700-1085 mm
2100-2485 mm
Steady flow

Fig. 4-6 - Relationship between bubble count rates and void fractions behind the leading edge of wave front
$Q(t=0+) = 0.075\ m^3/s$, h = 0.07 m, Step 16, $C_S = 2.43$ m/s, x' = 1.0 m

	0-70 mm	0-210 mm	0-385 mm	350-735 mm	700-1085 mm	2100-2485 mm	4200-4585 mm
ΔX (m) =	0.070	0.210	0.385	0.385	0.385	0.385	0.385
$(t - t_S)*\sqrt{g/d_o}$ =	0.0828	0.248	0.455	1.283	2.110	5.421	10.39

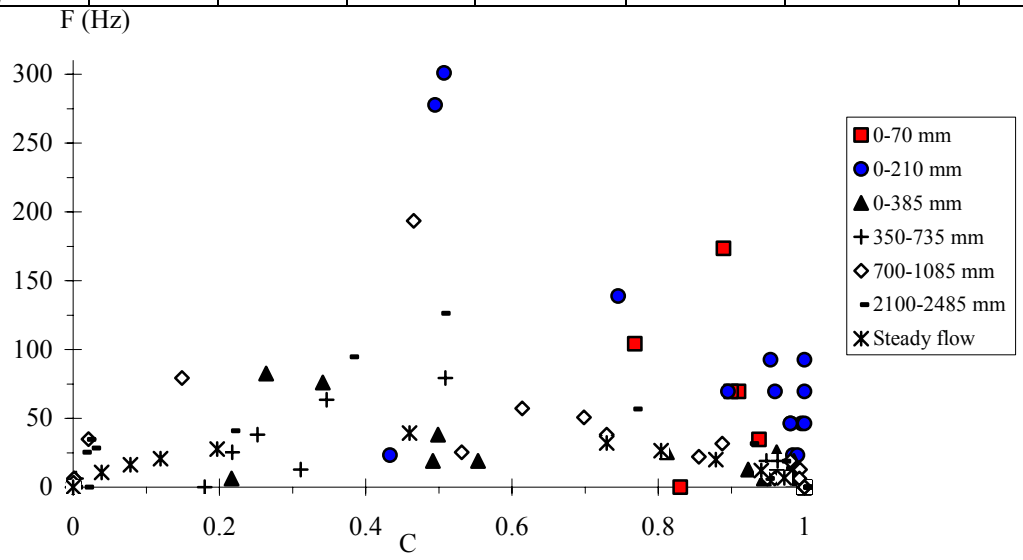

Fig. 4-7 - Air-water specific interface area distributions behind the leading edge of wave front
$Q(t=0+) = 0.075\ m^3/s$, h = 0.07 m, Step 16, $C_S = 2.43$ m/s, x' = 1.0 m

	0-70 mm	0-210 mm	0-385 mm	350-735 mm	700-1085 mm	2100-2485 mm	4200-4585 mm
ΔX (m) =	0.070	0.210	0.385	0.385	0.385	0.385	0.385
$(t - t_S)*\sqrt{g/d_o}$ =	0.0828	0.248	0.455	1.283	2.110	5.421	10.39

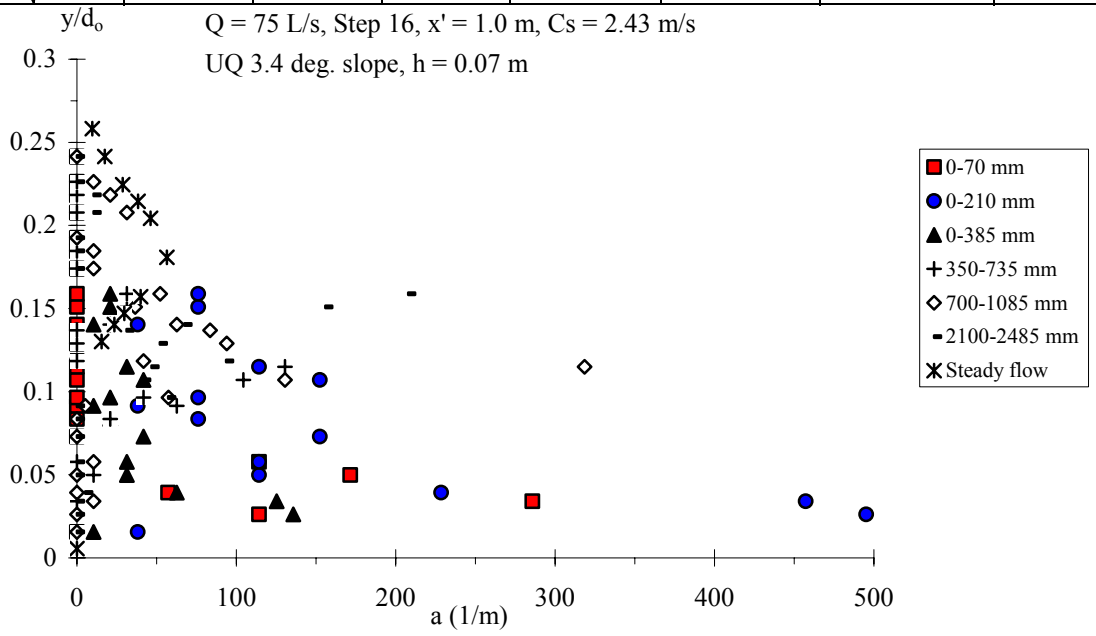

Discussion

Figure 4-6 shows a typical relationship between bubble count rate and void fraction at one cross-section (x' = 1.0 m). Despite some scatter, the data suggest a parabolic relationship such as :

$$\frac{F}{F_{max}} = 4 * C * (1 - C) \quad (4\text{-}3)$$

where F_{max} is the maximum bubble count rate between 0 and Y_{90}. Such a parabolic relationship was observed in self-aerated open channel flows and in free-falling nappe interfaces (CHANSON 1997b, TOOMBES 2002, CHANSON and TOOMBES 2002c). TOOMBES (2002) demonstrated the unicity of the relationship between bubble frequency and void fraction, and he derived Equation (4-3) for an air-water structure with constant, equal minimum bubble and droplet sizes in a cross-section.

4.3. Air-water specific interface area results

Figure 4-7 shows distributions of specific interface area for one flow rate at one location x'. The horizontal axis is the specific interface area in square metres per cubic metres. Figure 4-8 presents typical distributions of dimensionless specific interface area $a*d_o$, where d_o is a measure of the flow rate (Eq. (3-1)). Figure 4-8 presents data at five locations x' along a single step for the same flow conditions as in Figures 4-2 and 4-5. Note that the scale of the horizontal axis differs between each figure.

For all flow rates and step locations, the data demonstrated consistently very-significant interfacial areas in the leading edge of the wave front (i.e. the first 0.2 to 0.3 m) (Fig. 4-7 and 4-8). The results were basically one order of magnitude greater than steady flow interface area data (CHANSON and TOOMBES 2002a). Depth-averaged air-water specific interface areas were calculated for all the data set, where the mean specific interface area was defined between 0 and Y_{90} :

$$a_{mean} = \frac{1}{Y_{90}} * \int_{y=0}^{Y_{90}} a * dy \quad (4\text{-}4)$$

and a is the air-water specific interface area, y is the distance normal to the invert and Y_{90} is the distance where C = 0.9. The entire results are reported in Appendix VIII. For the data shown in Figure 4-8, depth-averaged specific interface areas are presented in Table 4-3. In Table 4-3, the results are presented with increasing times ($t - t_s$) from left to right. Note that different control volumes ΔX were used, while maximum depth-averaged specific interface areas were achieved for x' = 0.4 to 0.6 m at $t - t_s$ = 0.043 s.

Table 4-3 - Depth averaged air-water specific interface area behind the leading edge of wave front on Step 16 for Q(t=0+) = 0.075 m^3/s (C_s = 2.43 m/s, h = 0.07 m) - Comparison with steady flow data

x	a_{mean}										
m	1/m										
	0-70 mm	0-210 mm	140-210 mm	0-385 mm	175-385 mm	350-735 mm	525-595 mm	700-1085 mm	2100-2485 mm	4200-4585 mm	Steady flow
$t-t_s$ (s)	0.0144	0.0432	0.0720	0.0792	0.1152	0.2233	0.2305	0.3673	0.9434	1.8076	$+\infty$
(1)	(2)	(3)	(4)	(5)	(6)	(7)	(8)	(9)	(10)	(11)	(12)
1.0	93.4	214.4	0.0	47.5	1.1	22.3	26.2	20.4	39.2	26.6	21.6
0.8	102.7	295.2	122.1	84.4	4.7	50.6	48.8	53.6	43.4	40.7	25.9
0.6	88.6	397.5	135.3	99.8	1.5	56.2	53.9	69.0	73.5	71.6	32.4
0.4	--	368.8	147.2	95.7	3.0	83.3	105.5	71.3	71.2	95.9	38.4
0.2	--	108.0	--	--	--	--	--	--	--	--	28.1

Notes : (--) data not available; steady flow data : CHANSON and (TOOMBES 2002a).

Fig. 4-8 - Dimensionless distributions of specific interface area behind the leading edge of wave front on Step 16 for Q(t=0+) = 0.075 m^3/s (C_S = 2.43 m/s, h = 0.07 m) - Comparison with steady flow data (CHANSON and TOOMBES 2002a)

	0-70 mm	0-210 mm	0-385 mm	350-735 mm	700-1085 mm	2100-2485 mm	4200-4585 mm
ΔX (m) =	0.070	0.210	0.385	0.385	0.385	0.385	0.385
$(t - t_S)*\sqrt{g/d_o}$ =	0.0828	0.248	0.455	1.283	2.110	5.421	10.39

(A) x' = 0.2 m

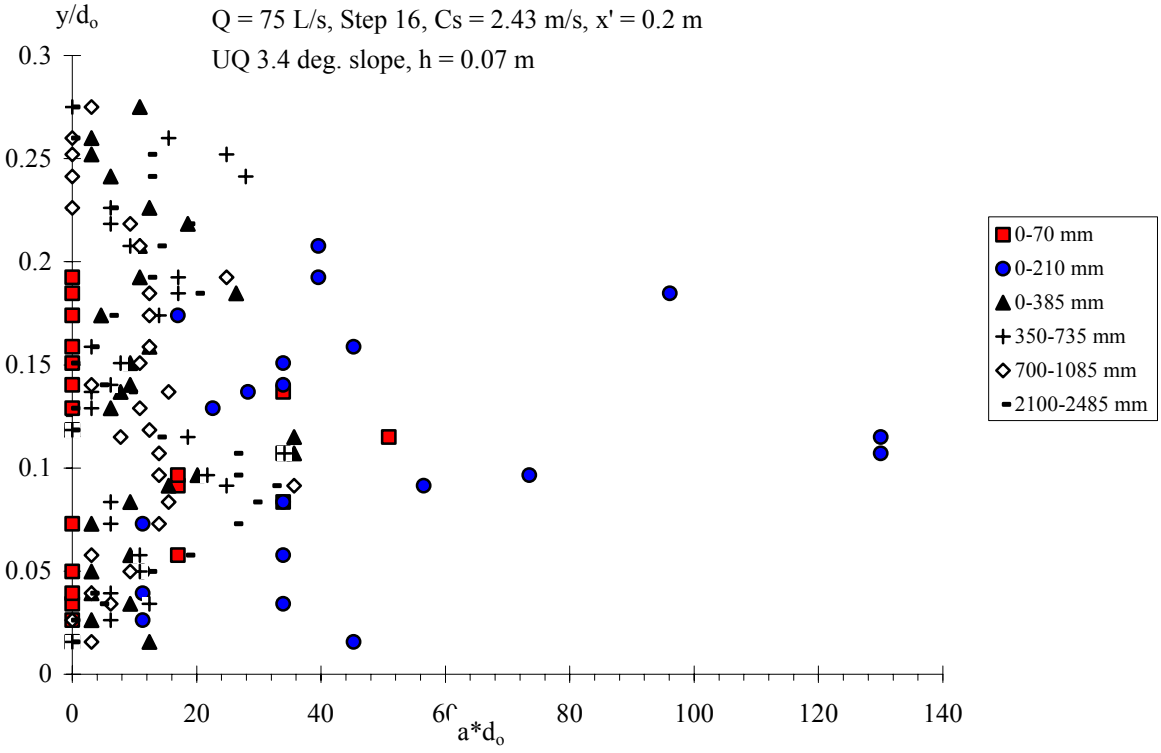

(B) x' = 0.4 m

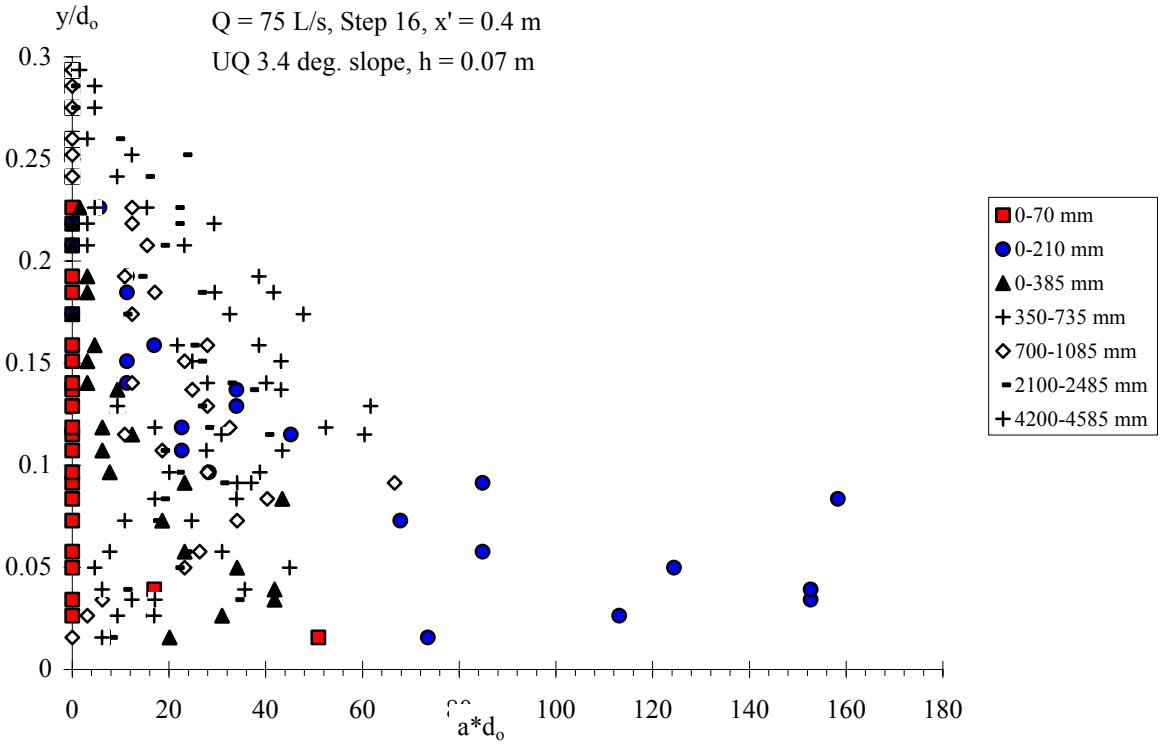

(C) x' = 0.6 m

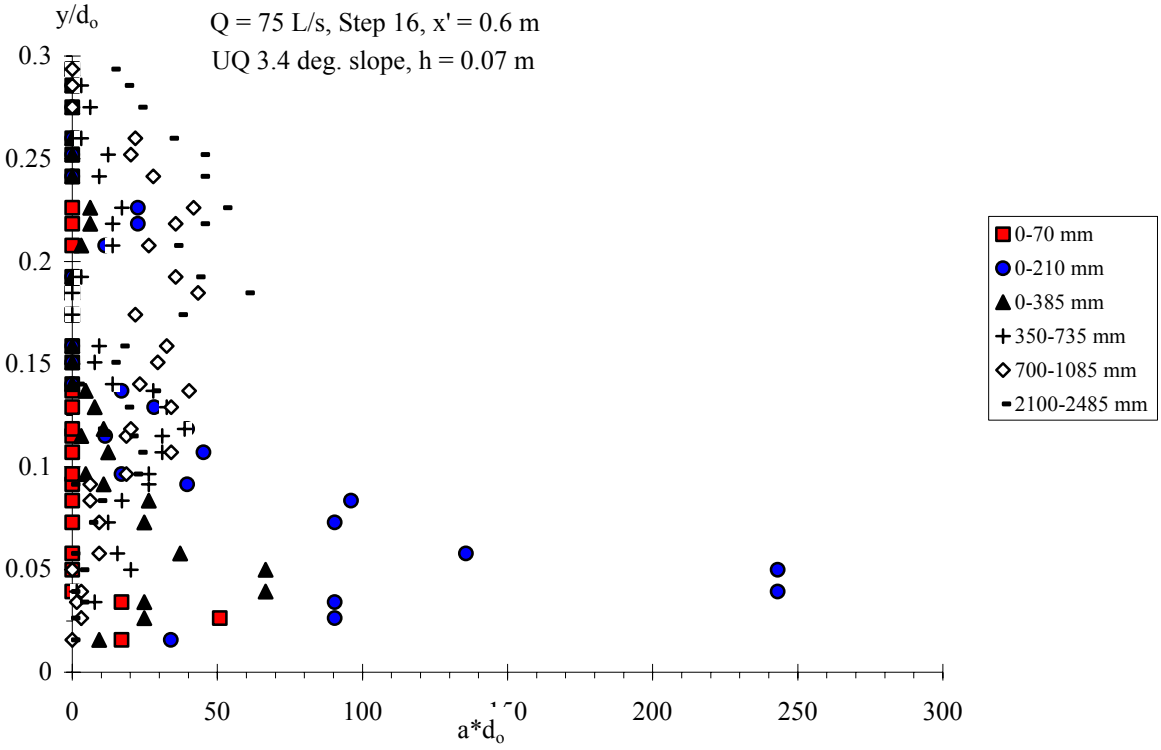
y/do
Q = 75 L/s, Step 16, x' = 0.6 m
UQ 3.4 deg. slope, h = 0.07 m
0.3
0.25
0.2
0.15
0.1
0.05
0
0
50
100
200
250
300
a*do
0-70 mm
0-210 mm
0-385 mm
350-735 mm
700-1085 mm
2100-2485 mm

(D) x' = 0.8 m

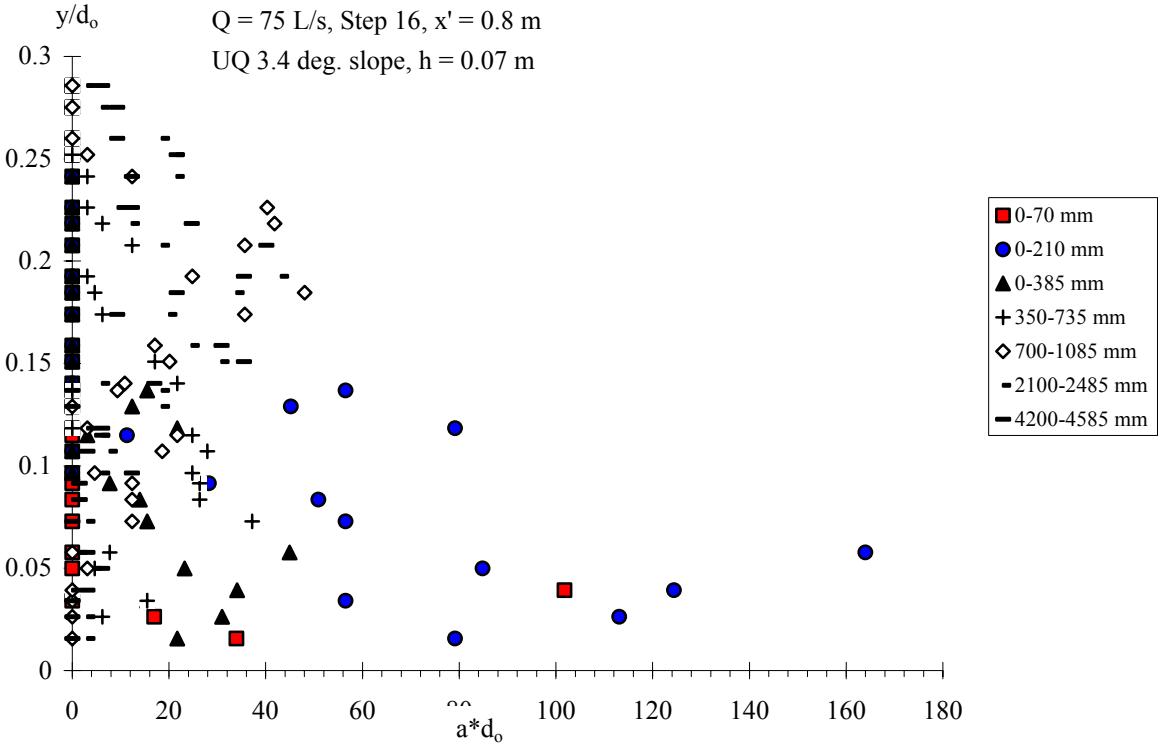
y/do
Q = 75 L/s, Step 16, x' = 0.8 m
UQ 3.4 deg. slope, h = 0.07 m
0.3
0.25
0.2
0.15
0.1
0.05
0
0
20
40
60
100
120
140
160
180
a*do
0-70 mm
0-210 mm
0-385 mm
350-735 mm
700-1085 mm
2100-2485 mm
4200-4585 mm

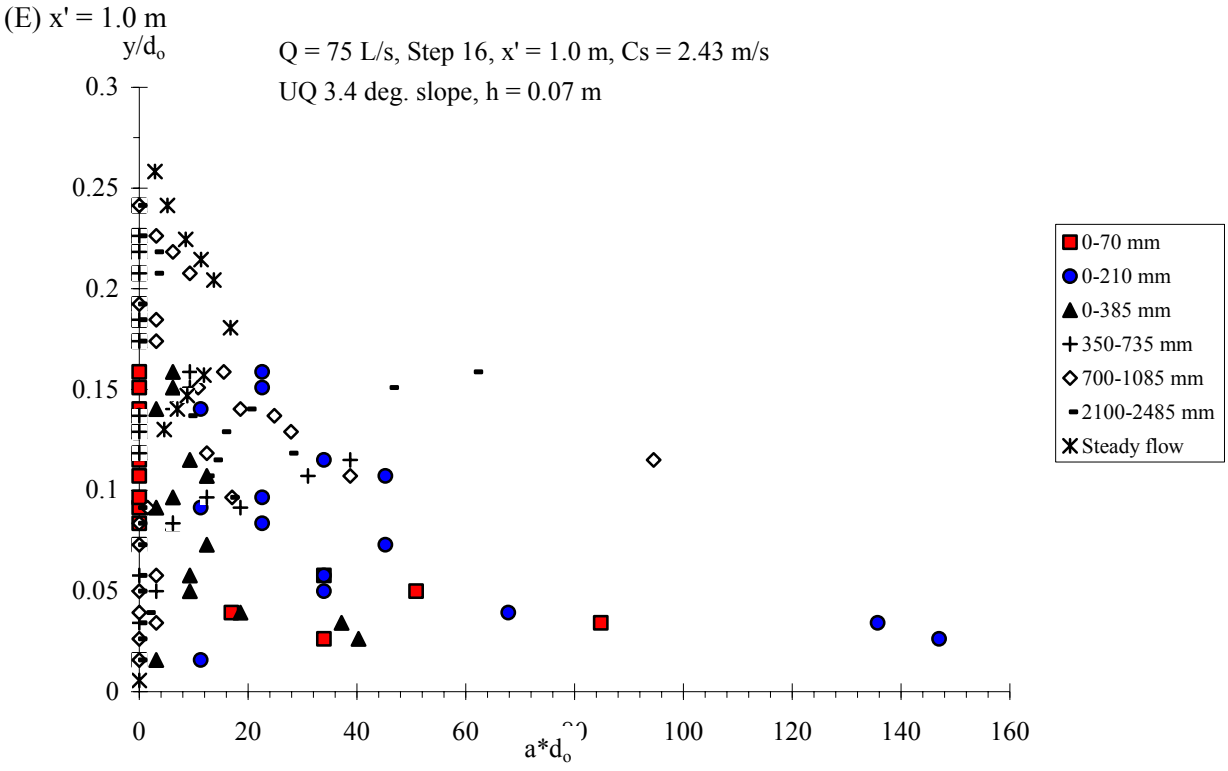

Discussion

Experimental results emphasised a very-strong aeration of the wave front (Fig. 4-7 and 4-8, Table 4-3). The finding is significant because the strong flow aeration will contribute to oxidation of debris, pollutants and hydrocarbons collected at the leading edge of flash floods and dam break waves.

For volatile gases in liquids, Fick's law states that the mass transfer rate of a chemical across an interface normal to the x-direction and in a quiescent fluid varies directly as the coefficient of molecular diffusion D_{gas} and the negative gradient of gas concentration :

$$\frac{\partial}{\partial t} M_{gas} \propto - D_{gas} * \left(\frac{\partial}{\partial x} C_{gas} \right) \qquad (4\text{-}5)$$

where C_{gas} is the concentration of the dissolved chemical in liquid and t is the time. The analysis of the fluid layers surrounding a gas bubble is very complicated because of the bubble shape, the presence of laminar or turbulent flow, a mobile interface in the case of large air bubbles and the interactions between concentration boundary layers from adjacent bubbles. When the particular chemical is volatile (e.g. oxygen, methane), the transfer is controlled by the liquid phase and the coefficient of transfer is almost equal to the liquid film coefficient which is a function of the salinity, temperature, surfactants and to a lesser extent the pressure. The mass transfer equation for volatile gas in a liquid becomes :

$$\frac{\partial}{\partial t} C_{gas} = K_L * a * (C_{sat} - C_{gas}) \qquad (4\text{-}6)$$

where a is the specific surface area defined as the air-water interface area per unit volume of air and water, C_{sat} is the concentration of dissolved gas in water at equilibrium and K_L is the liquid film coefficient (GULLIVER 1990, JIRKA 1991). Although some studies implied that the term (K_L*a) was constant, this assumption is incorrect. Detailed studies showed that the mass transfer coefficient K_L in turbulent gas-liquid

flows is almost constant regardless of bubble sizes and flow situations (KAWASE and MOO-YOUNG 1992), but the interface area varies greatly along a hydraulic structure as a function of the air-water flow properties (e.g. Fig. 4-8 and Table 4-3).

Equation (4-6) demonstrates that the rate of mass transfer is proportional to the residence time and air-water interfacial area. In a flash flood, the interfacial area is important in the leading edge and the mass transfer of chemicals is significant. That is, the effects of pollution induced by flash flooding might not be as important as initially foreseen (neglecting flow aeration).

Fig. 4-9 - Dimensionless air-water characteristic depth $Y_{90}/(Y90)_{steady}$ as functions of the dimensionless time $(t - t_s)/\sqrt{g/d_o}$ (h = 0.07 m, Step 16, x' = 1.0 m) - Comparison with Equation (4-7)

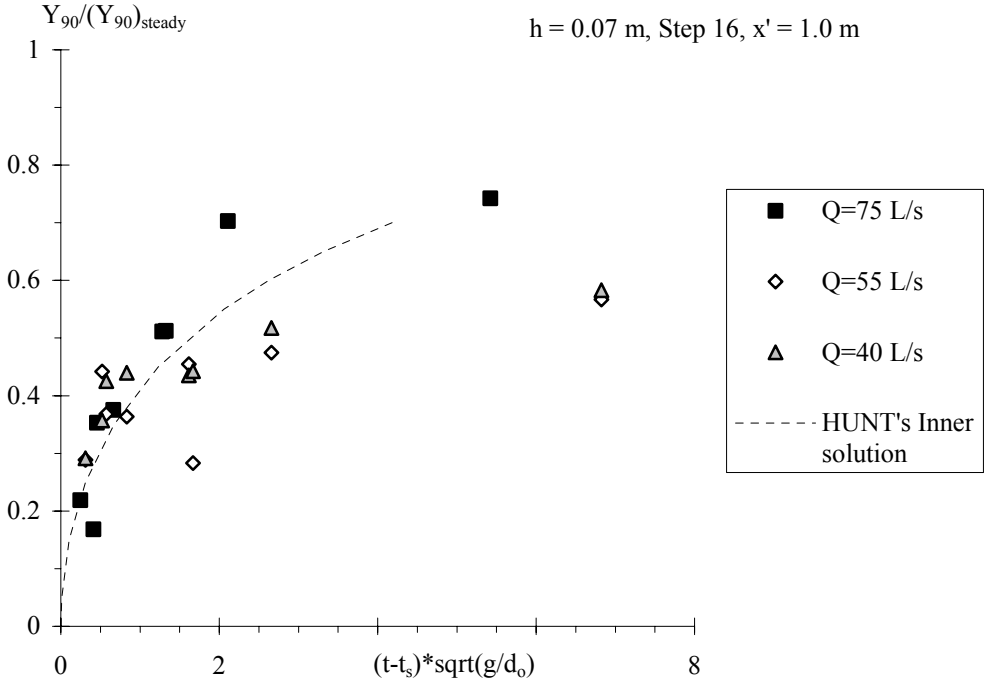

4.4 Comments

The shape of the propagating wave followed the wave shape predicted by HUNT's (1984) theory (i.e. inner solution). The characteristic air-water depth Y_{90} satisfied consistently :

$$(t - t_s) * \sqrt{\frac{g}{d_o}} \propto \frac{Y_{90}}{(Y90)_{steady}} + Ln\left(1 + \frac{Y_{90}}{(Y90)_{steady}}\right) \quad (4\text{-}7)$$

where $(Y90)_{steady}$ is the steady flow characteristic depth where C = 90%. A typical data set is shown in Figure 4-9 and compared with Equation (4-7).

All unsteady flow data demonstrated strong aeration of wave front leading edge. Results in terms of depth-averaged void fractions, maximum bubble count rates and depth-averaged specific interface area are detailed in Appendix VIII, where the depth-averaged void fraction C_{mean}, the maximum bubble count rate F_{max} and the depth-averaged air-water specific interface area a_{mean} are defined as :

$$C_{mean} = \frac{1}{Y_{90}} * \int_{y=0}^{Y_{90}} C * dy \quad (4\text{-}8)$$

$$F_{max} = Max(F, \text{ for } 0 \leq y \leq Y_{90}) \quad (4\text{-}9)$$

$$a_{mean} = \frac{1}{Y_{90}} * \int_{y=0}^{Y_{90}} a * dy \quad (4\text{-}4)$$

and C is the void fraction, F is the bubble count rate, a is the air-water specific interface area, y is the distance normal to the invert and Y_{90} is the distance where C = 0.9.

Figure 4-10 illustrates typical results. In Figure 4-10, the horizontal axis is the time ($t - t_s$) where t_s is the time of passage of the wave front. The axis has a logarithmic scale with dimensional units to emphasise the relevant time scales. Note that, in Figure 4-10, the last data ($t - t_s$ = 10 s) are the steady flow data (CHANSON and TOOMBES 2002a). The results highlight a rapid decrease in depth-averaged void fraction, mean specific interface area and maximum bubble count rate with increasing time ($t - t_s$), especially within the first 0.3 to 0.7 seconds (Fig. 4-10). For longer times ($t - t_s$), the depth-averaged properties were equal basically the corresponding steady flow conditions.

Note that, for the smallest flow rates (Q(t=0+) = 0.040 and 0.055 m^3/s), experimental results might suggest a lesser flow aeration for $1 < (t - t_s) < 6$ seconds than that in steady flow conditions (e.g. Fig. 4-10A).

Fig. 4-10 - Depth-averaged void fraction C_{mean}, maximum bubble count rate F_{max} and depth-averaged specific interface area a_{mean} behind the wave front as functions of the time ($t - t_s$)
(A) Q(t=0+) = 0.055 m^3/s, h = 0.07 m, Step 16, C_s = 2.14 m/s, x' = 0.8 m

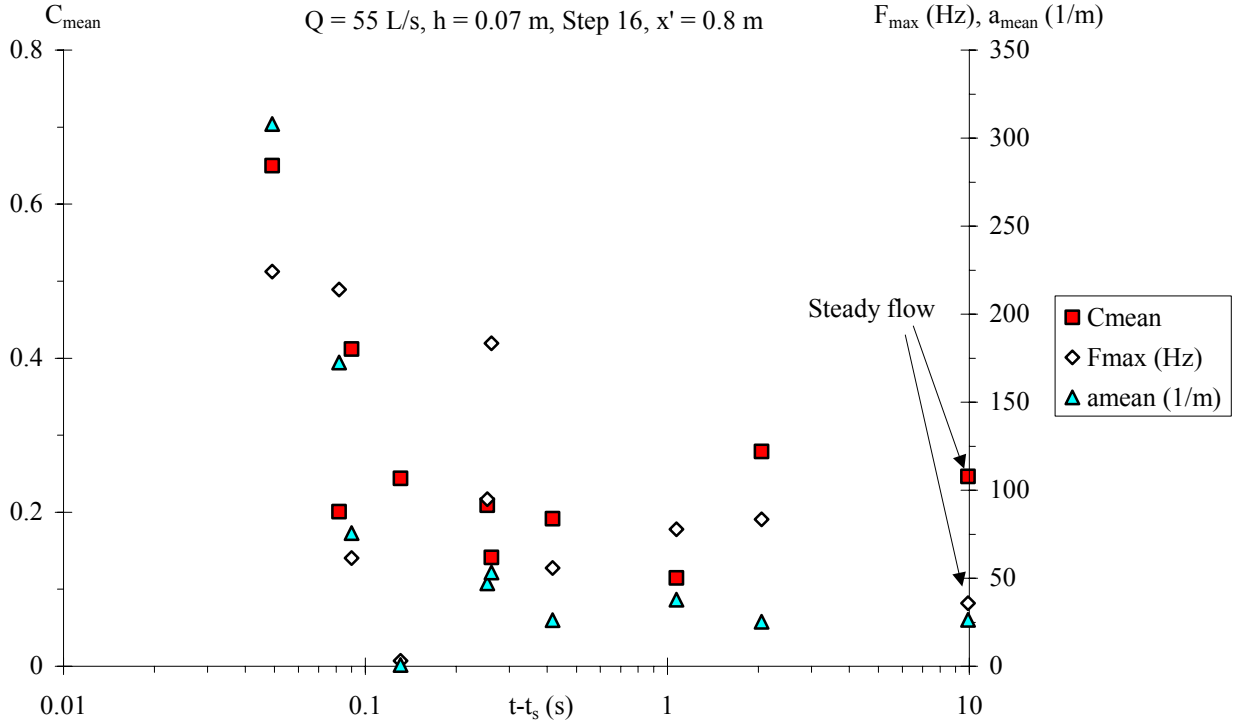

(B) Q(t=0+) = 0.075 m^3/s, h = 0.07 m, Step 10, C_S = 2.61 m/s, x' = 0.8 m

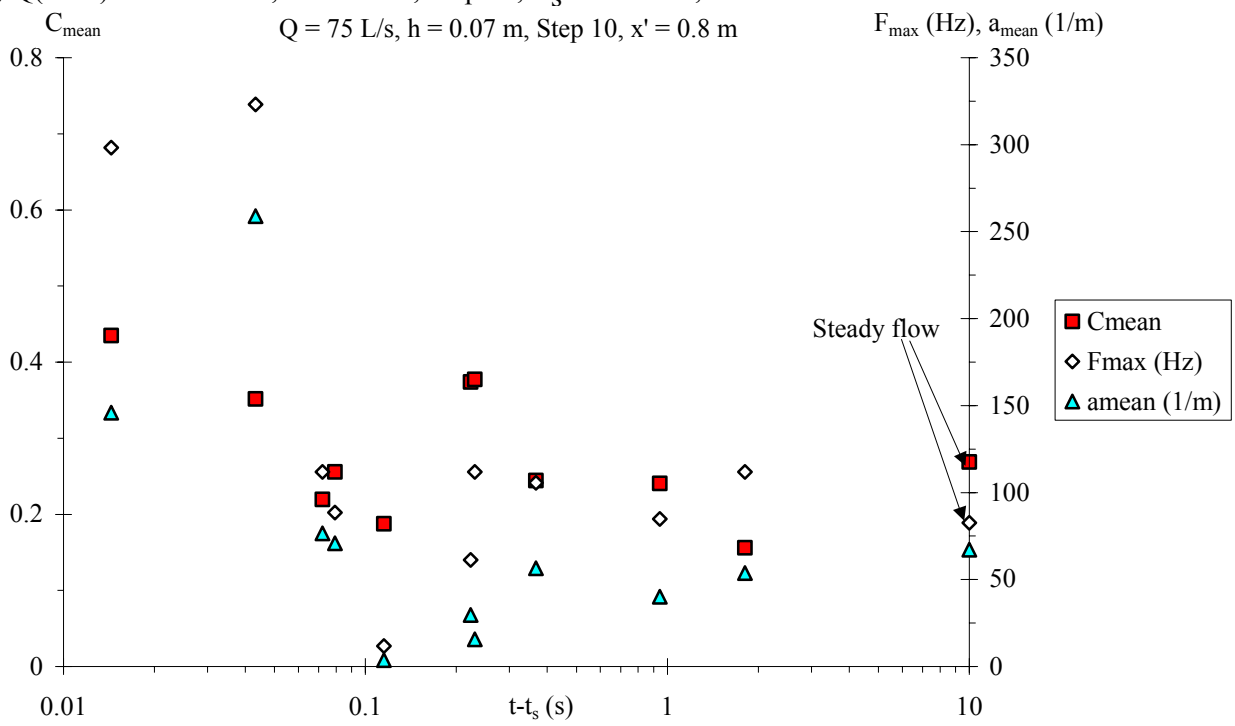

(C) Q(t=0+) = 0.075 m^3/s, h = 0.07 m, Step 16, C_S = 2.43 m/s, x' = 0.8 m

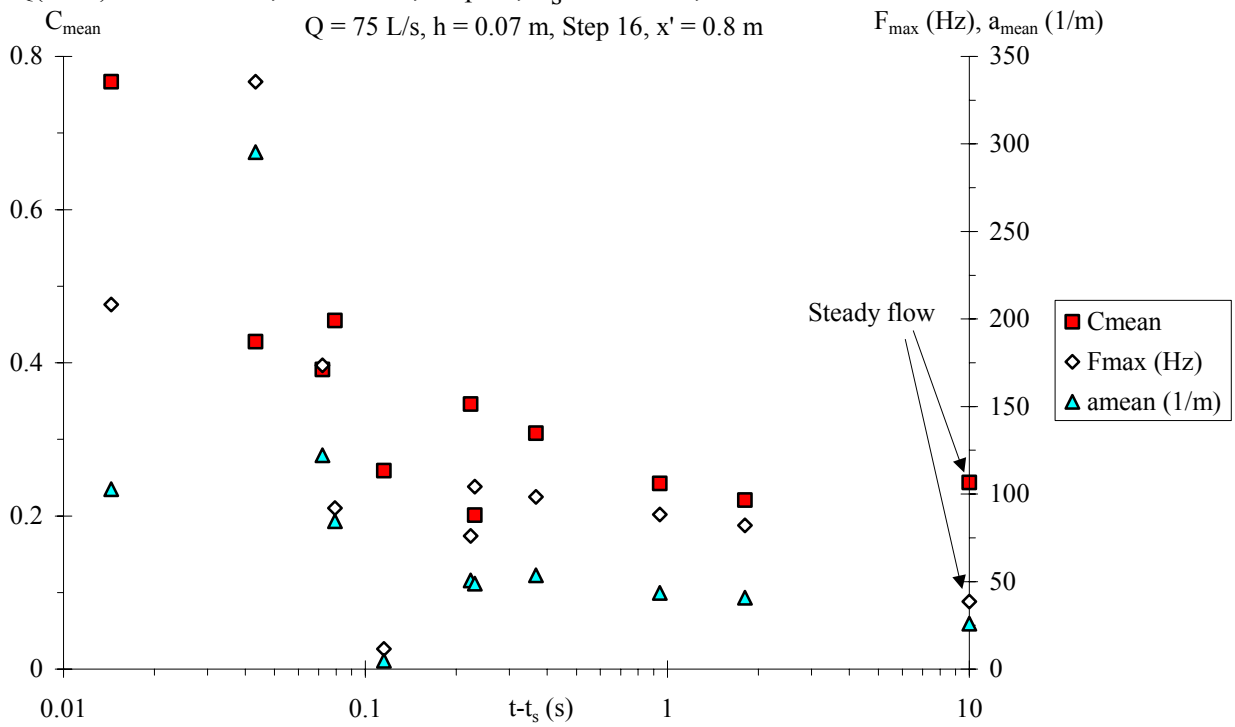

5. UNSTEADY AIR-WATER FLOW PROPERTIES (2) AIR AND WATER CHORD SIZES

5.1 Introduction

The bubble chord time t_{ch} is defined as the time spent by the bubble on the probe tip (Fig. 5-1). Figure 5-1 illustrates a sequence of two bubbles impacting successively the probe sensor. Figure 5-1 provides further the definition of air and water chord lengths. Bubble and water chord times were measured for three flow rates at two steps (Table 4-1). The results are presented in terms of pseudo-chord length ch defined as :

$$ch = C_s * t_{ch} \quad (5\text{-}1)$$

where C_s is the wave front celerity. Equation (5-1) predicts accurately chord lengths near the front where the flow velocity is about the wave front speed.

The chord time data analysis was conducted for all the flow conditions. In section 5.2, statistical results are presented for entire recordings (i.e. $0 \leq t - t_s < 6$ s). Such results are basically independent of the selection of an integration time interval ΔT. In section 5.3, chord sizes were calculated for small control volumes to assess time variations of the air-water flow structure.

Figure 5-1 - Sketch of two air bubble impacting a single-tip probe

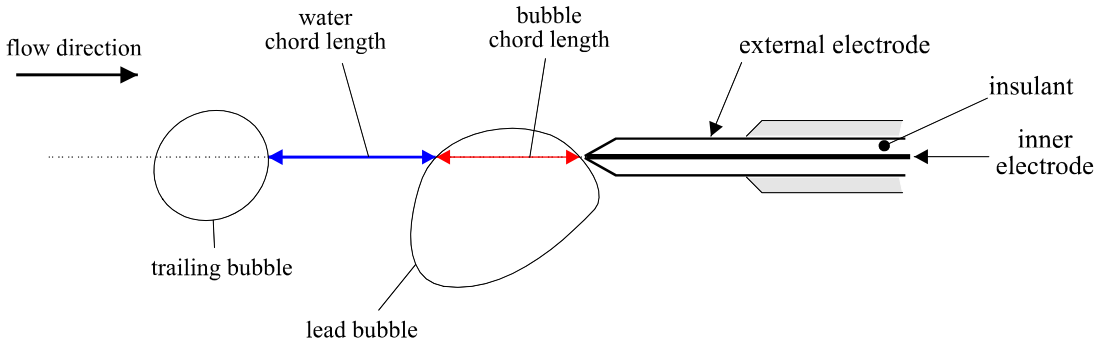

5.2 Experimental results

Pseudo-bubble chord length distributions are shown in Figure 5-2 for one flow rate at one location for several vertical positions. Each histogram is the probability distribution function of an entire recording (i.e. $0 \leq t - t_s < 6$ s) at a fixed location in space (x', y) and the histogram columns represent the probability of chord length in 0.5 mm intervals : e.g., the probability of a chord length from 2.0 to 2.5 mm is represented by the column labelled 2.0. The last column (i.e. > 15) indicates the probability of chord lengths exceeding 15 mm. Statistical properties of the pseudo-chord size distributions are summarised in Appendix IX : i.e., means, medians ([1]), standard deviations, skewness and kurtosis of air and water chord sizes.

Typical distributions of air and water median chord sizes are presented in Figure 5-3. Each data point represents the median air/water chord size at a location (x', y) during the entire study period $0 \leq t - t_s < 6$ s where t is the time and t_s is the time of passage of wave front. Note that the horizontal axis has a logarithmic

[1]The median size is defined as the size for which 50% of all the data are smaller.

scale and that the units are millimetre. Further experimental results in terms of median air chord sizes are shown in Figure 5-4.

For all investigated flow conditions, the results demonstrated consistently similar trends, although to a lesser extent in the free-falling nappe (x' = 0.2 m). First, the median air chord size was typically millimetric : i.e., between 1 and 10 mm (Fig. 5-2). This is illustrated in Figure 5-4. Second, a broad range of measured chord sizes was detected, from less than 0. 5 mm to more than 25 mm. This is clearly demonstrated by large standard deviations of chord size distributions (App. IX). Third, for all flow conditions, the air chord size distributions were skewed with a preponderance of small bubble sizes relative to the mean in the bubbly flow region (i.e. C < 0.3) ([2]). The probability of bubble chord length was the largest for bubble sizes between 0 and 3 mm although the mean/median pseudo-chord size was much larger (e.g. Fig. 5-2). The trends were emphasised by positive skewness and large kurtosis (App. IX).

Remarks

At the leading edge of the wave front, some splashing was observed (Fig. 5-5). Sometimes the probe sensor was wetted by water droplets and spray although the event was followed by a significant air chord time (e.g. Fig. 5-5). That is, the splashing biased the arithmetic mean of air chord size. Therefore the median chord sizes results were presented. For all air chord size distributions, the writer believes that the median chord size was a more representative indicator of typical bubble chord sizes. Similarly the water chord median size is believed to be more meaningful.

Fig. 5-2 - Bubble chord size distributions at the leading edge of wave front
Q(t=0+) = 0.075 m^3/s, h = 0.07 m, Step 16, C_S = 2.43 m/s, x' = 1.0 m

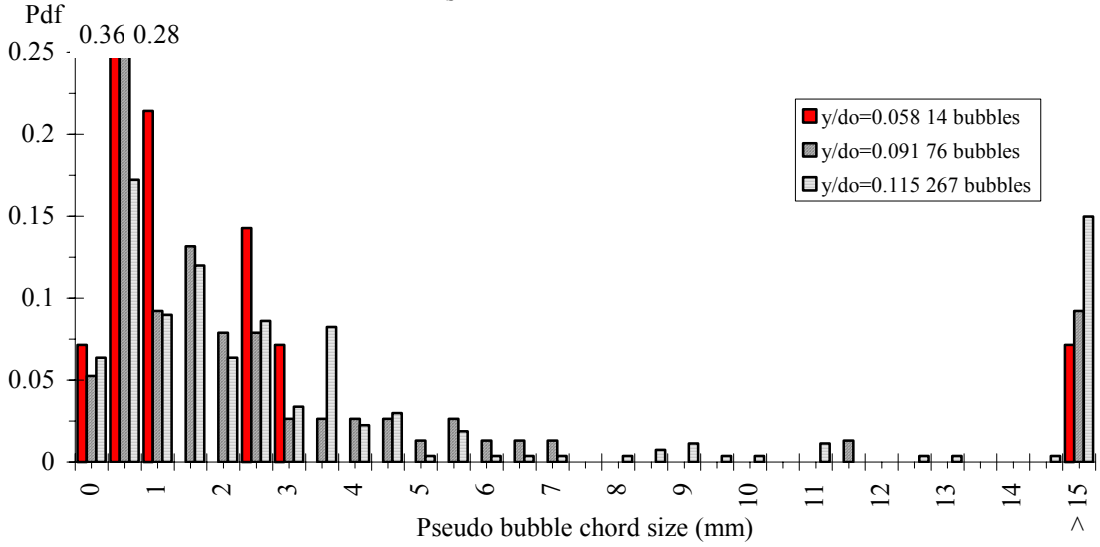

[2]In self-aerated open channel flows, it is commonly accepted the flow structure is a dispersed bubbly flow region for C > 0.3 while the spray region extends for C > 0.7 (WOOD 1991, CHANSON 1997a). In between (0.3 < C < 0.7), the air-water flow structure is complicated and this is the topic of discussions among researchers.

Figure 5-3 - Vertical distributions of median chord sizes at x' = 0.4 m

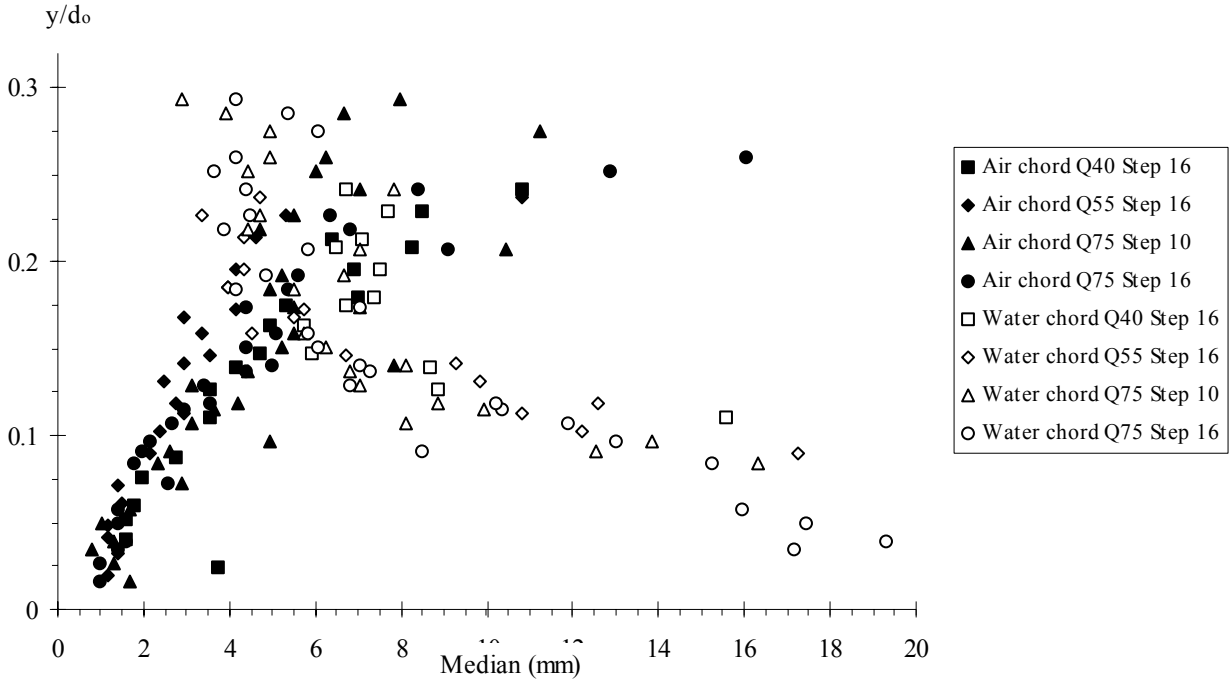

Figure 5-4 - Vertical distributions of median air chord sizes

(A) x' = 0.4 m

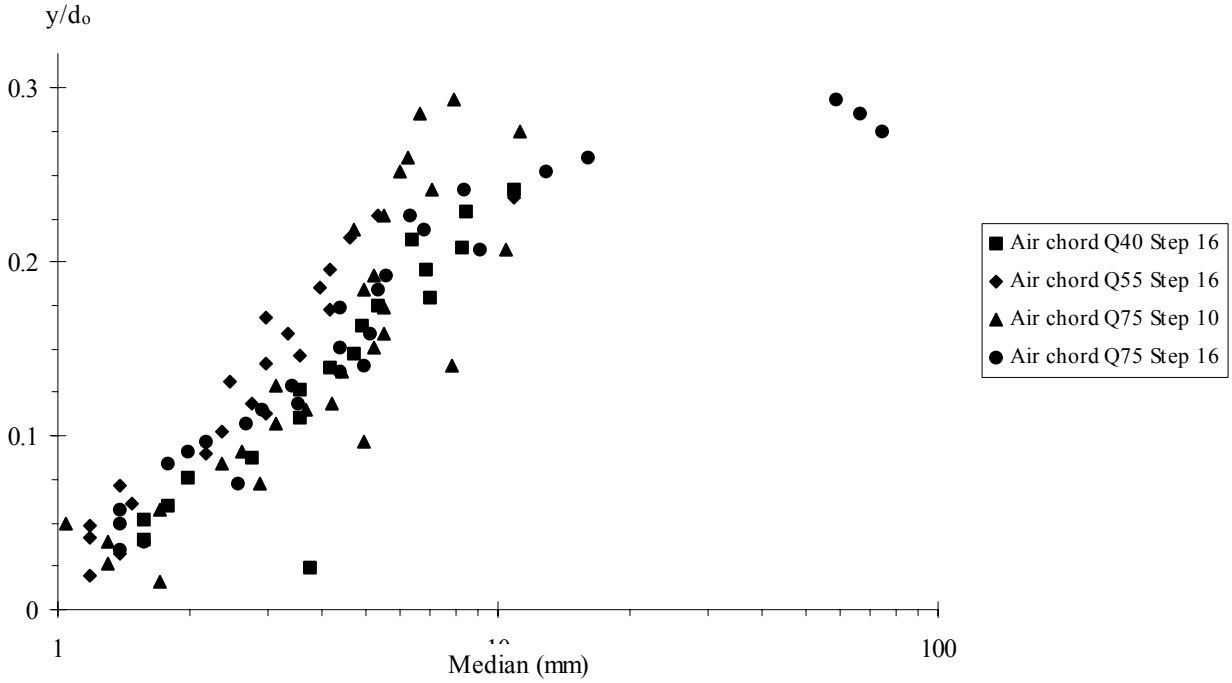

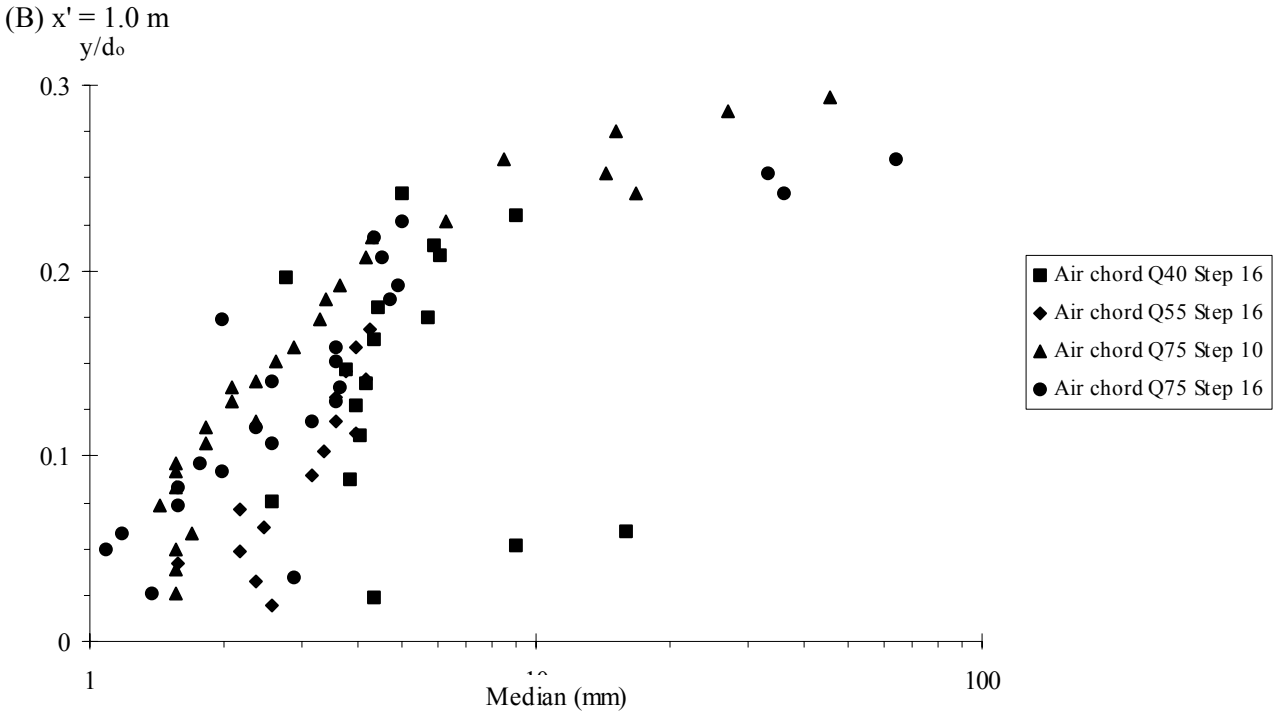

Figure 5-5 - Sketch of the advancing wave front

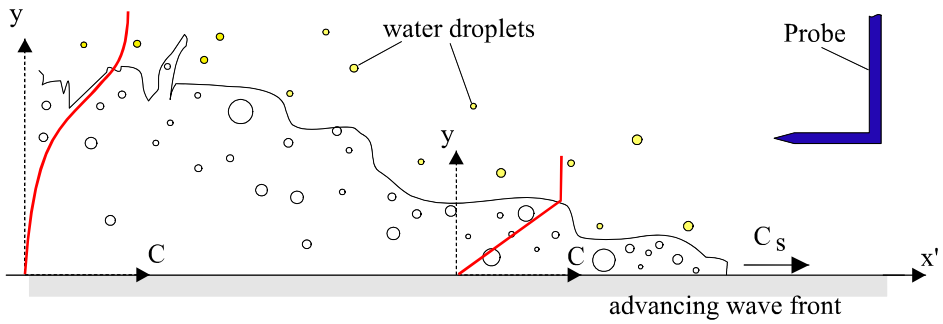

5.3 Discussion

For the largest flow rate (Q(t=0+) = 0.075 m^3/s), a detailed analysis of the variations in air-water flow structure with time was conducted at several cross-sections for x' ≥ 0.4 m. A typical example is shown in Figure 5-6 in terms of median air/water chord sizes calculated for relatively small control volumes (ΔT = 0.158 s, ΔX = 0.385 m). In Figure 5-6, the median chord size (in mm) is plotted as a function of the relative depth y/Y_{90} where Y_{90} is the instantaneous location where C = 0.9. Note that the horizontal scale differs between Figures 5-6A and 5-6B.

At the wave leading edge (0-385 mm), air and water chord sizes are comparable with median sizes of about 3-6 mm. This might suggest that individual bubble entrainment is associated with the ejection of water droplet of similar size. For larger times (i.e. $(t - t_S)*\sqrt{g/d_o} > 0.5$), the order of magnitude of median air chord sizes remains basically constant and independent of time. while water chord sizes tend to increase with time, especially for $y/Y_{90} < 0.7$. Such a different behaviour might be related to fundamental differences between air bubbles and water droplets.

Water droplets have a momentum response time about 46,000 times larger than that of an air bubble of identical diameter (e.g. CROWE et al. 1998). As the bubble response time is significantly smaller than the characteristic time of the flow, bubble trapping in large-scale turbulent structures is a dominant mechanism in the bubbly flow region. Bubbles may remain trapped for very long times, the bubbly flow structure has some memory of its past, and it is affected by its previous structure. In the spray region, drop formation results from surface distortion, tip-streaming of ligaments and interactions between eddies and free-surface (e.g. HOYT and TAYLOR 1977, REIN 1998). Once ejected, the droplet response time is nearly two orders of magnitude larger the air flow response time. Most droplets have a short life and the spray region has little memory of its past. The spray structure may then change very rapidly in response to changes in flow conditions, while the bubbly flow region is deeply affected by its earlier structure.

Fig. 5-6 - Vertical distributions of median chord sizes in small streamwise control volumes (ΔX = 385 mm) at several dimensionless time $(t - t_s)*\sqrt{g/d_o}$ - Q(t=0+) = 0.075 m^3/s, h = 0.07 m, Step 16, C_s = 2.43 m/s, x' = 0.8 m

	0-385 mm	350-735 mm	700-1085 mm	2100-2485 mm	4200-4585 mm
ΔX (m) =	0.385	0.385	0.385	0.385	0.385
$(t - t_s)*\sqrt{g/d_o}$ =	0.455	1.283	2.110	5.421	10.39

(A) Median air chord sizes

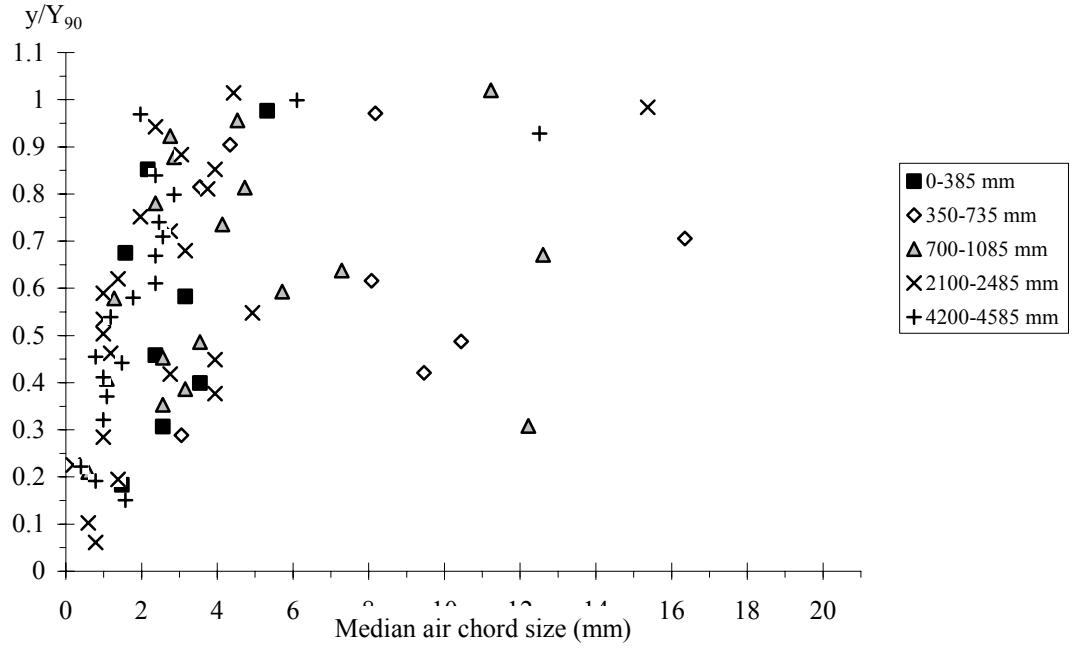

(B) Median water chord sizes

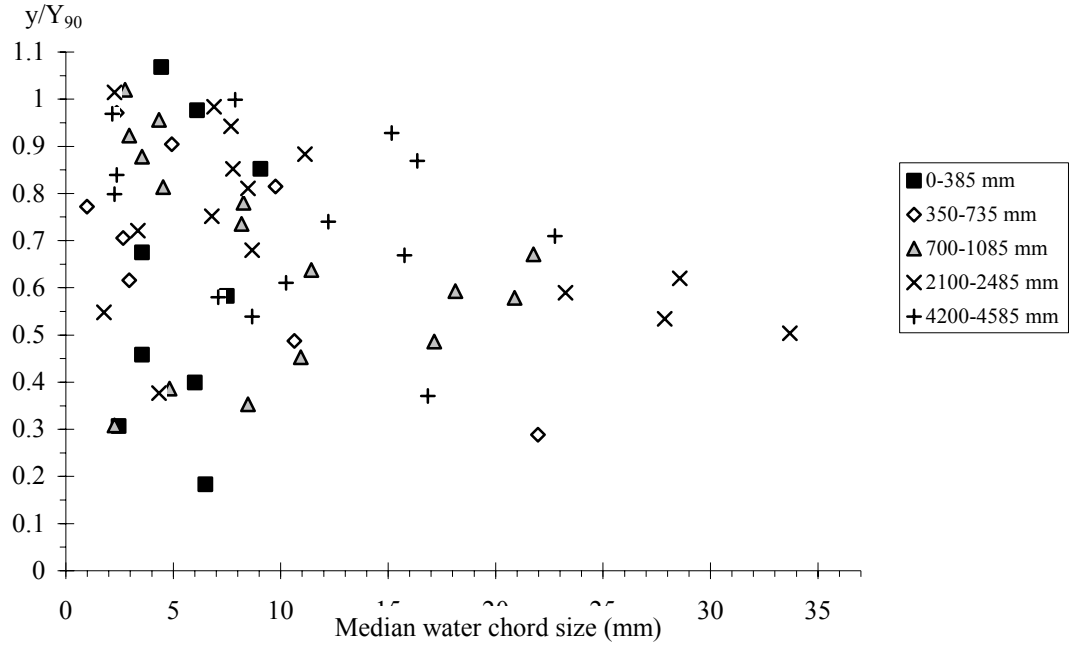

6. SUMMARY AND DISCUSSION

New dam break wave experiments were conducted systematically down a 25-m long flat waterway with two stepped geometries (e.g. Fig. 6-1). Experimental results (photographs and conductivity probe data) demonstrated that the wave propagated as a succession of free-falling nappe, nappe impact and horizontal runoff on each step for all investigated flow conditions and step geometries. Visual observations highlighted the chaotic nature of the advancing flow with strong aeration of the leading edge.

Observations of wave front propagation showed some flow deceleration in the downstream half of the channel. The wave celerity data were successfully compared with HUNT's (1982,1984) dam break wave theory. The comparison was best achieved assuming a Darcy-Weisbach friction factor f = 0.05 independently of flow rates and step heights. The result is very close to steady flow resistance measurements in the same facility by CHANSON and TOOMBES (2002a) (i.e. $f_e = 0.047$).

Studies of wave propagation on individual steps highlighted some flow acceleration in the free-jet, followed by energy dissipation and flow deceleration downstream of nappe impact. In the free-jet, both horizontal and vertical celerity components were recorded. The data satisfied the motion equation for free-jets.

Unsteady air-water flow measurements were performed in the wave front. The results demonstrated quantitatively strong aeration of the leading edge. Void fraction distributions showed a marked change in shape for $(t - t_s)*\sqrt{g/d_o} \sim 1.3$. Possible explanations may include non-hydrostatic pressure field in the leading edge, some change in air-water flow structure associated with a change in rheological fluid properties, and changes in shear stress distributions and boundary friction. In any case, the instantaneous distributions of void fractions were successfully compared with theoretical solutions of air bubble diffusion equation.

Bubble count rate and specific interface area data highlighted large interfacial areas in the wave front, with depth-averaged specific interface areas of up to 400 m^{-1}. Such large interfacial areas enhance air-water mass transfer at the wave front. This may possibly reduce pollution induced by debris and hydrocarbons collected at the leading edge of flash floods.

Experimental results showed that the strongly-aerated flow region at the leading edge was relatively short : i.e. typically 0.3 to 0.5 m long corresponding to $(t - t_s)*\sqrt{g/d_o} < 0.5$. Behind the flow properties tended rapidly towards steady flow characteristics.

Measurements of air and water chord sizes highlighted a wide range of bubble and droplet sizes. The median air chord sizes were typically between 1 and 10 mm, and the distributions were skewed with a preponderance of smaller bubbles compared to the mean. Time-variations of the air-water flow structure were observed. At the leading edge (i.e. $(t - t_s)*\sqrt{g/d_o} < 0.5$), entrained bubbles and ejected droplets had similar sizes. Behind, however, the median water chord sizes increased with time, although the bubble sizes did not change.

Fig. 6-1 - Advancing flood wave down a stepped cascade (h = 0.0715 m, l = 1.2 m, Q(t=0+) = 0.055 m^3/s)

Discussion : applications

The present study provides quantitative information on the propagation of surge waves and flash floods down sloping waterways with large roughness. Although developed for smooth channels, HUNT's (1982,1984) theory may be applicable and a typical Darcy friction factor of f = 0.05 is appropriate for flat stepped geometries. The model may be used to estimate warning times of downstream populations during intense rainstorm events (e.g. Fig. 6-2).

Fig. 6-2 - Thunderstorm on 1 May 1999 in South-East Queensland (Australia) (Courtesy of Anthony CORNELIUS) - The storm produced a heavy rain shaft with hail

Laboratory and field observations demonstrated an accumulation of debris near the front of flash floods and dam break waves. Present results provide new information on air-water interface areas which may yield to better estimates of mass transfer at wave leading edge. It is believed that the significant interface areas

enhance the oxidation of pollutants and hydrocarbons. In turn, the 'white waters' may dampen the impact of debris pollution.

A related form of dam break wave is the wave runup in the swash zone ([3]). On beach slopes, waves run up downstream of the breaking point like positive surge (Fig. 6-3). The swash zone wave runup is believed to be a significant factor in sediment processes in coastal zones. The large amount of air bubble entrainment in the wave front (i.e. 'white waters') reduces buoyancy. In turn heavy sediment particles will be subjected to bed-load rather than suspension. Note however that surge propagation in the swash zone takes often place over retreating waters (i.e. against water run down) and on dry sloping upwards slopes.

Fig. 6-3 - Swash zones at Main Beach, North Stradbroke Island Qld, Australia
(Left) Surging waters on the sandy beach on 22 Dec.. 2002 - After wave breaking, the wave runup forms a series of positive surges at the upper end of the swash zone
(Right) Details of a wave runup down the glassy beach face on 21 Dec. 2002 (runup from right to left)

[3]In coastal engineering, the *swash* is the rush of water up a beach from the breaking waves.

ACKNOWLEDGMENTS

The writer thanks his students Chung Hwee "Jerry" LIM and York-wee TAN for their help and assistance. He acknowledges the assistance of Dr L. TOOMBES (Australia). He thanks Dr R. BAKER for providing information on the Brushes Clough dam spillway.

Further the writer thanks Dr T. BALDOCK, The University of Queensland for his helpful review.

APPENDIX I - BASIC UNSTEADY FLOW EQUATIONS

In unsteady open channel flows, the velocities and water depths change with time and longitudinal position. For one-dimensional applications, basic unsteady open channel flow equations, called Saint-Venant equations, may be developed. The basic assumptions of the development are : [H1] the flow is on-dimensional, [H2] the streamline curvature is very small and the pressure distributions are hydrostatic, [H3] the flow resistance are the same as for a steady uniform flow for the same depth and velocity, [H4] the bed slope is small enough to satisfy : $\cos\theta \approx 1$ and $\sin\theta \approx \tan\theta$; and [H5] the water density is a constant. Sediment transport is further neglected. With these basic hypotheses, the flow can be characterised at any point and any time by two variables: e.g., Q and d where Q is the flow rate and d is the flow depth.

The unsteady flow properties are described by a system of two partial differential equations :

$$\frac{\partial A}{\partial t} + \frac{\partial Q}{\partial x} = 0 \qquad \text{Continuity equation (I-1)}$$

$$\frac{1}{g} * \left(\frac{\partial V}{\partial t} + V * \frac{\partial V}{\partial x} \right) + \frac{\partial d}{\partial x} + S_f - S_o = 0 \qquad \text{Dynamic equation (I-2)}$$

where A is the cross-section area, t is the time, V is the flow velocity, S_o is the bed slope ($S_o = \sin\theta$), S_f is the friction slope and x is the longitudinal distance.

Simplification of the dynamic wave equation

In the general case of unsteady flows, the dynamic equation (Eq. (I-2)) may be simplified under some conditions, if the acceleration term $\partial V/\partial t$ and the inertial term $V*\partial V/\partial x$ become small. For example, when the flood flow velocity increases from 1 to 2 m/s in three hours (i.e. rapid variation), the dimensionless acceleration term $1/g*\partial V/\partial x$ equals 9.4 E-6; when the velocity increases from 1.0 m/s to 1.4 m/s along a 10 km reach (e.g. reduction in channel width), the longitudinal slope of the kinetic energy line $1/g*V*\partial V/\partial x$ is equals to 4.9 E-6. For comparison, the average bed slope S_o of the Rhône river between Lyon and Avignon is about 0.7 E-3 and the friction slope is of the same order of magnitude.

The dynamic equation may be simplified when one or more terms become negligible. Table I-1 summarises various forms of the dynamic wave equation which may be solved in combination with the unsteady flow continuity equation (Eq. (I-1)).

Table I-1 - Simplification of the dynamic wave equation

Equation (1)	Dimensionless expression (2)	Remarks (3)
Dynamic wave equation	$\frac{1}{g} * \left(\frac{\partial V}{\partial t} + V * \frac{\partial V}{\partial x} \right) + \frac{\partial d}{\partial x} + S_f - S_o = 0$	Saint-Venant equation.
Diffusive wave equation	$\frac{\partial d}{\partial x} + S_f - S_o = 0$	
Kinematic wave equation	$S_f - S_o = 0$	
Simple wave	$S_f = S_o = 0$	

APPENDIX II - A SOLUTION OF THE UNSTEADY FLOW EQUATIONS

During the present study, the boundary conditions are an initially dry channel (t = 0, x > 0), and Q(x = 0) and d(x = 0) fixed for t > 0. That is, d(x = 0) = 0.03 m for all the experiments.

Considering a simple wave problem in a horizontal channel, the characteristic system of equations is :

$$\frac{D}{Dt}(V + 2 * C) = 0 \qquad \text{forward characteristics}$$

$$\frac{D}{Dt}(V - 2 * C) = 0 \qquad \text{backward characteristics}$$

along :

$$\frac{dx}{dt} = V + C \qquad \text{forward characteristics C1}$$

$$\frac{dx}{dt} = V - C \qquad \text{backward characteristics C2}$$

where C is the celerity of a small disturbance : i.e., $C = \sqrt{g*d}$ in a rectangular channel.

A forward characteristics issuing from the origin for t > 0 intersecting the trajectory of the leading edge of the wave front and satisfies :

$$V + 2 * C = V(x = 0) + 2 * C(x = 0) \qquad \text{(II-1)}$$

where V(x=0) = Q(t=0+)/(W*d(x = 0)) and $C(x=0) = \sqrt{g*d(x = 0)}$. At the leading edge of the ideal dam break wave front, the water depth is zero, hence C = 0, and the propagation speed of the dam break wave front equals :

$$C_S = V(x = 0) + 2 * \sqrt{g * d(x = 0)} \qquad \text{(II-2)}$$

Remark

Considering any backward characteristics issuing from the dam break wave front, the C2 characteristics satisfies everywhere :

$$V - 2 * C = V(x = 0) - 2 * \sqrt{g * d(x = 0)}$$

APPENDIX III - AIR BUBBLE DIFFUSION IN SELF-AERATED FLOWS

In supercritical flows, 'white waters' are often observed. The phenomenon occurs when turbulence acting next to the free-surface is large enough to overcome both surface tension for the entrainment of air bubbles and buoyancy to carry downwards the bubbles. Assuming a homogeneous air-water mixture for $0 < y < Y_{90}$, the advective diffusion of air bubbles may be analytically predicted (CHANSON 1995,1997). At uniform equilibrium, the air concentration distribution is a constant with respect to the distance x in the flow direction. The continuity equation for air in the air-water flow yields :

$$\frac{\partial}{\partial y}\left(D_t * \frac{\partial C}{\partial y}\right) = \cos\theta * \frac{\partial}{\partial y}(u_r * C) \quad \text{(III-1)}$$

where C is the air concentration or void fraction, D_t is the turbulent diffusivity, u_r is the bubble rise velocity, θ is the channel slope and y is measured perpendicular to the mean flow direction. The bubble rise velocity in a fluid of density $\rho_w*(1-C)$ equals :

$$u_r^2 = [(u_r)_{Hyd}]^2 * (1 - C) \quad \text{(III-2)}$$

where $(u_r)_{Hyd}$ is the rise velocity in hydrostatic pressure gradient. A first integration of the continuity equation for air in the equilibrium flow region leads to :

$$\frac{\partial C}{\partial y'} = \frac{1}{D'} * C * \sqrt{1 - C} \quad \text{(III-3)}$$

where $y' = y/Y_{90}$, Y_{90} is the depth where C = 0.90 and D' is a dimensionless turbulent diffusivity:

$$D' = \frac{D_t}{(u_r)_{Hyd} * \cos\theta * Y_{90}}$$

D' is the ratio of the air bubble diffusion coefficient to the rise velocity component normal to the flow direction times the characteristic transverse dimension of the shear flow.

Analytical solution for D' = constant

Assuming a homogeneous turbulence across the flow (i.e. D' constant), the solution of Equation (III-3) is:

$$C = 1 - \tanh^2\left(K' - \frac{y'}{2 * D'}\right) \quad \text{(III-4)}$$

where tanh is the hyperbolic tangent function and K' a dimensionless integration constant (CHANSON 1995,1997). A relationship between D' and K' is deduced for C = 0.9 for y' = 1 :

$$K' = K^* + \frac{1}{2 * D'} \quad \text{(III-5)}$$

where $K^* = \tanh^{-1}(\sqrt{0.1}) = 0.32745015...$ The diffusivity and the mean air content C_{mean} defined in terms of Y_{90} are related by :

$$C_{mean} = 2 * D' * \left(\tanh\left(K^* + \frac{1}{2 * D'}\right) - \tanh(K^*)\right) \quad \text{(III-6)}$$

Advanced void fraction distribution models may be developed assuming a non constant diffusivity.

Analytical solutions for non-constant dimensionless diffusivity

Assuming a bubble diffusivity distribution such as :

$$D' = \frac{D_o}{1 - 2 * \left(\frac{y}{Y_{90}} - \frac{1}{3}\right)^2} \quad \text{(III-7)}$$

The analytical solution of the advective diffusion equation yields :

$$C = 1 - \tanh^2\left(K'' - \frac{\frac{y}{Y_{90}}}{2 * D_o} + \frac{\left(\frac{y}{Y_{90}} - \frac{1}{3}\right)^3}{3 * D_o}\right) \quad \text{(III-8)}$$

where D_o and K" are functions of the depth-averaged air content only :

$$K'' = K^* + \frac{1}{2 * D_o} - \frac{8}{81 * D_o}$$

$$C_{mean} = 0.7622*(1.0434 - \exp(-3.614*D_o))$$

and $K^* = \tanh^{-1}(\sqrt{0.1}) = 0.32745015...$ (CHANSON and TOOMBES 2001,2002). Equations (III-7) and (III-8) are plotted in Figure III-1 and Equation (III-8) is compared with void fraction experiments in unsteady flows. The agreement is good but for C > 0.9.

Note that Equation (III-7) predicts a drastic increase in dimensionless diffusivity for C > 0.7 to 0.9. The result may be explained physically. In light spray, droplets are surrounded by air, the buoyancy force tends to zero and D' tends to infinite for $(u_r)_{Hyd} = 0$.

Assuming a bubble diffusivity distribution such as :

$$D' = \frac{C * \sqrt{1 - C}}{0.9} \quad \text{(III-9)}$$

the analytical solution of Equation (II-3) is:

$$C = 0.9 * \frac{y}{Y_{90}} \quad \text{(III-10)}$$

Equation (III-9) and (III-10) are a limiting case of the analytical solution of air bubble diffusion equation for steady transition flows down stepped chute (CHANSON and TOOMBES 2001,2002).

Equations (III-9) and (III-10) are plotted in Figure III-1 and Equation (III-10) is compared with void fraction experiments in unsteady flows. The agreement is good for C < 0.95.

Discussion

Figure III-1 suggests a major change in void fraction distributions at the leading edge of dam break wave flows. Possible explanations may include :

- non hydrostatic pressure distribution at the leading wave front,
- a change in air-water flow structure, associated with a change in rheological fluid properties
- a change in gas-liquid flow regime, with a plug/slug flow regime in front a homogenous bubbly flow region behind,
- a change in shear stress distributions and boundary friction.

Fig. III-1 - Comparison between air bubble diffusion models and experimental data

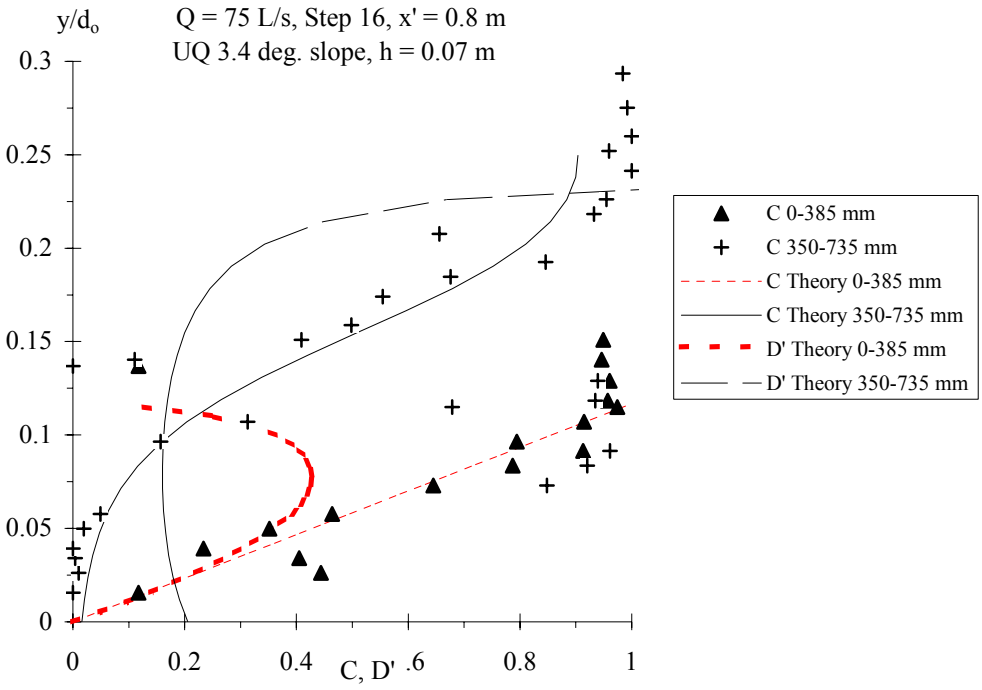

APPENDIX IV - WAVE FRONT CELERITY DATA. (1) CHANNEL DATA

IV.1 Presentation

Experiments were performed in a 25-m long 0.5-m wide flume. The channel was a flat waterway ($S_o \approx 0.065$). The flow rate was delivered by a pump controlled with an adjustable frequency AC motor drive Taian T-Verter K1/N1 (Pulse Width Modulated design), enabling an accurate discharge adjustment in a closed-circuit system. The flow was fed through a smooth convergent nozzle (1.7-m long), and the nozzle exit was 30-mm high and 0.5-m wide. The measured contraction ratio was about unity (i.e. $d_n = 30$ mm for all experiments). Earlier experiments (CHANSON 1995) showed that steady flows at the nozzle were two-dimensional and became fully-developed upstream of the first drop.

Two stepped configurations were used (Table IV-1). The first geometry was equipped with ten identical steps (0.143-m high 2.4-m long) (Fig. 2-1A). In the second configuration, the nozzle was followed by a 2.4 m long horizontal invert and by 18 steps (h = 0.0715 m, l = 1.2 m). The flow rates in steady flow conditions were measured with a Dall™ tube flowmeter, calibrated on site. The accuracy on the discharge measurement was about 2%. The surging flow was studied with two video-cameras : i.e., a VHS video-camera Panasonic™ NV-RX10A (speed: 25 frames/sec., shutter: sport mode, zoom: 1 to 14) and a digital video-camera handycam Sony™ DV-CCD DCR-TRV900 (speed: 25 frames/sec., shutter: 1/4 to 1/10,000 sec., zoom: 1 to 48). The cameras were installed above and along the axis of the channel. Studies of individual steps were further conducted by mounting the camera vertically above the step (App. V). Additional observations were obtained using a digital camera Olympus™ Camedia C-700 (shutter: 1/2 to 1/1,000 sec.).

Each step was painted with red and white stripes spaced 50 mm apart. Video-taped movies were analysed frame-by-frame. The error on the time was less than 1/250 s, and the error on the longitudinal position of the wave front was +/- 1 cm. In experiments Series 1, two video footages were taken for each experiment and subsequently analysed. The results are presented in terms of the average over the two runs. In experiments Series 2, and for each experiment, three video recordings were taken at each location and subsequently analysed. The results are presented in terms of the average over three recordings.

Further a sudden discharge release was videotaped at Brushes Clough dam spillway in 1994 (BAKER 1994). The video footage was analysed by the writer (Table IV-1) (CHANSON 2001, pp. 295-297).

Table IV-1 - Summary of unsteady flow experiments

Experiment	θ (deg.)	h m	Run	Q(t=0+) (m^3/s)	Initial channel condition	Remarks
(1)	(2)	(3)	(4)	(5)	(6)	(7)
Series 1	3.4	0.143				10 horizontal steps (l = 2.4 m). W = 0.5 m. Nozzle depth : d_n = 0030 m.
			CT15	0.019	Wet	
			CT26	0.030	Wet	
			CT37	0.040	Wet	
			CT48	0.075	Dry/Wet	
Series 2	3.4	0.0715				18 horizontal steps (l = 1.2 m). W = 0.5 m. Nozzle depth : d_n = 0030 m.

		TL1	0.040	Wet	Air-water flow measurements.
		TL2	0.0475	Wet	
		TL3	0.055	Wet	Air-water flow measurements.
		TL4	0.065	Wet	
		TL5	0.075	Wet	Air-water flow measurements.
Brushes Clough dam	18.4				Inclined downward steps, trapezoidal channel (2 m bottom width)
		BC1	0.5	Empty	

Notes : Q(t=0+) : initial flow rate; d_n : approach flow depth (nozzle depth); h : step height; l : step length.

Notation

C_s wave front celerity (m/s) : average value betwen two adjacent step edges;

d_c critical flow depth (m);

d_n nozzle depth (m) : d_n = 0.03 m;

d_o characteristic water depth (m) function of the flow rate and channel width only; $d_o = 9/4\ d_c$;

g gravity acceleration (m/s^2) : g = 9.80 m/s^2 in Brisbane;

Q water discharge (m^3/s);

s longitudinal distance (m) measured from the upstream end of the channel;

t time (s);

IV.2 Experiments Series 1

Location :	University of Queensland (Australia)
Date :	Sept. 1999
Experiments by :	H. CHANSON and L. TOOMBES
Data processing by :	H. CHANSON.
Experiment characteristics :	Flume : length: 25 m, width: 0.5 m, slope: 3.4 degrees, step height: 0.143 m, step length: 2.4 m. Inflow conditions : nozzle depth d_n = 0.03 m.
Instrumentation :	Digital video camera Sony™ DV-CCD DCR-TRV900 (speed: 25 frames/sec., shutter: 1/4 to 1/10,000 sec., zoom: 1 to 48).
Comments :	Data averaged over two identical runs.

Run CT15

$t^*\sqrt{\frac{g}{d_o}}$ (1)	$\frac{s}{d_o}$ (2)	$t^*\sqrt{\frac{g}{d_o}}$ (3)	$\frac{C_s}{\sqrt{g^*d_o}}$ (4)	Remarks (5)
15.99	20.20	7.99	1.25	s = 0 at nozzle.
30.70	40.40	23.34	1.37	s measured at step edges.
45.87	60.61	38.28	1.33	C_s averaged between step
61.22	80.81	53.54	1.32	edges.
75.75	101.01	68.48	1.39	
90.53	121.01	83.14	1.42	
106.69	142.26	98.61	1.28	
121.10	159.46	113.89	1.31	

Notes : C_S : wave front celerity averaged betweeen two adjacent step edges; s : longitudinal distance in the flow direction (measurements at step edges).

Run CT26

$t^*\sqrt{\frac{g}{d_o}}$ (1)	$\frac{s}{d_o}$ (2)	$t^*\sqrt{\frac{g}{d_o}}$ (3)	$\frac{C_s}{\sqrt{g*d_o}}$ (4)	Remarks (5)
10.61	14.90	5.30	1.41	s = 0 at nozzle.
19.97	29.80	15.29	1.59	
29.48	44.70	24.73	1.57	
39.54	59.60	34.51	1.48	
48.67	74.49	44.11	1.65	
59.59	89.39	54.13	1.38	
69.96	104.29	64.78	1.44	
82.05	119.19	76.01	1.26	

Run CT37

$t^*\sqrt{\frac{g}{d_o}}$ (1)	$\frac{s}{d_o}$ (2)	$t^*\sqrt{\frac{g}{d_o}}$ (3)	$\frac{C_s}{\sqrt{g*d_o}}$ (4)	Remarks (5)
8.36	12.30	4.18	1.52	s = 0 at nozzle.
15.87	24.60	12.12	1.64	
23.53	36.90	19.70	1.61	
31.89	48.03	27.71	1.38	
40.39	61.49	36.14	1.58	
48.90	73.79	44.65	1.47	
57.83	86.09	53.36	1.39	
66.68	98.39	62.26	1.39	

Run CT48

$t^*\sqrt{\frac{g}{d_o}}$ (1)	$\frac{s}{d_o}$ (2)	$t^*\sqrt{\frac{g}{d_o}}$ (3)	$\frac{C_s}{\sqrt{g*d_o}}$ (4)	Remarks (5)
5.98	8.09	2.99	1.37	s = 0 at nozzle.
11.26	16.18	8.62	1.54	
17.36	24.26	14.31	1.35	
22.76	32.35	20.06	1.50	
27.93	40.44	25.34	1.58	
33.45	48.53	30.69	1.49	
38.96	56.62	36.21	1.53	
43.91	64.71	41.44	1.64	

IV.3 Experiments Series 2

Location :	University of Queensland (Australia)
Date :	March-June 2002
Experiments by :	Chung Hwee "Jerry" LIM and York-wee TAN
Data processing by :	Chung Hwee "Jerry" LIM, York-wee TAN and H. CHANSON
Experiment characteristics :	Flume : length: 25 m, width: 0.5 m, slope: 3.4 degrees, step height: 0.0715 m, step length: 1.2 m. Inflow conditions : nozzle depth d_n = 0.03 m. First step : 2.4 m long, equipped with sidewall deflectors.

Instrumentation :	VHS video-camera Panasonic™ NV-RX10A (speed: 25 frames/sec., shutter: sport mode, zoom: 1 to 14).
Comments :	Data averaged over three identical runs.

Run TL1

$t^*\sqrt{\frac{g}{d_o}}$ (1)	$\frac{s}{d_o}$ (2)	$t^*\sqrt{\frac{g}{d_o}}$ (3)	$\frac{C_s}{\sqrt{g*d_o}}$ (4)	Remarks (5)
0.00	0.00	0.00	1.28	s = 0 at nozzle.
9.64	12.31	4.82	1.28	s measured at step edges.
14.45	18.47	9.64	1.28	C_S averaged between step
19.27	24.63	14.55	1.25	edges.
24.18	30.79	19.37	1.28	
29.00	36.94	24.09	1.31	
33.73	43.10	28.81	1.30	
38.45	49.26	33.44	1.33	
43.08	55.42	38.07	1.33	
47.71	61.57	42.51	1.39	
52.15	67.73	46.86	1.42	
56.49	73.89	51.30	1.39	
60.93	80.05	56.02	1.31	
65.66	86.20	60.65	1.33	
70.29	92.36	65.00	1.42	
74.63	98.52	69.15	1.48	
78.79	104.68	73.50	1.42	
83.14	110.83	77.51	1.40	
87.15	116.99	--	--	

Notes : C_S : wave front celerity averaged betweeen two adjacent step edges; s : longitudinal distance in the flow direction (measurements at step edges).

Run TL2

$t^*\sqrt{\frac{g}{d_o}}$ (1)	$\frac{s}{d_o}$ (2)	$t^*\sqrt{\frac{g}{d_o}}$ (3)	$\frac{C_s}{\sqrt{g*d_o}}$ (4)	Remarks (5)
0.00	0.00	0.00	1.17	s = 0 at nozzle.
9.37	10.98	4.64	1.18	s measured at step edges.
14.01	16.47	9.28	1.18	C_S averaged between step
18.65	21.96	13.56	1.28	edges.
22.93	27.45	17.84	1.28	
27.21	32.95	22.12	1.28	
31.49	38.44	26.05	1.40	
35.42	43.93	29.80	1.46	
39.16	49.42	33.37	1.54	
42.73	54.91	37.38	1.37	
46.75	60.40	41.31	1.40	
50.67	65.89	45.14	1.43	
54.51	71.38	48.71	1.54	
58.08	76.87	52.64	1.41	

62.00	82.36	56.47	1.43	
65.84	87.86	60.49	1.37	
69.85	93.35	64.23	1.46	
73.60	98.84	68.07	1.43	
77.44	104.33	--	--	

Run TL3

$t^*\sqrt{\frac{g}{d_o}}$	$\frac{s}{d_o}$	$t^*\sqrt{\frac{g}{d_o}}$	$\frac{C_s}{\sqrt{g^*d_o}}$	Remarks
(1)	(2)	(3)	(4)	(5)
0	0	0.00	1.18	s = 0 at nozzle.
8.41	9.96	4.33	1.15	s measured at step edges.
12.74	14.94	8.41	1.22	C_S averaged between step
16.82	19.92	12.23	1.30	edges.
20.64	24.90	15.29	1.63	
23.70	29.88	18.35	1.63	
26.76	34.86	21.49	1.58	
29.90	39.84	24.81	1.50	
33.22	44.82	28.38	1.40	
36.79	49.80	31.69	1.50	
40.10	54.78	35.00	1.50	
43.41	59.76	38.49	1.43	
46.90	64.74	41.97	1.43	
50.38	69.72	45.54	1.39	
53.95	74.70	48.94	1.46	
57.35	79.68	52.33	1.46	
60.74	84.65	55.65	1.50	
64.06	89.63	59.13	1.43	
67.54	94.61	--	--	

Run TL4

$t^*\sqrt{\frac{g}{d_o}}$	$\frac{s}{d_o}$	$t^*\sqrt{\frac{g}{d_o}}$	$\frac{C_s}{\sqrt{g^*d_o}}$	Remarks
(1)	(2)	(3)	(4)	(5)
0.00	0.00	0.00	1.15	s = 0 at nozzle.
7.71	8.91	3.86	1.15	s measured at step edges.
11.57	13.36	7.15	1.35	C_S averaged between step
14.87	17.82	9.80	1.68	edges.
17.52	22.27	12.21	1.84	
19.93	26.73	14.87	1.68	
22.58	31.18	17.68	1.58	
25.39	35.64	20.41	1.63	
28.12	40.09	23.30	1.54	
31.02	44.55	26.12	1.58	
33.83	49.00	28.93	1.58	
36.64	53.46	31.90	1.50	
39.62	57.91	34.87	1.50	
42.59	62.37	38.01	1.42	
45.72	66.82	41.06	1.46	
48.78	71.28	43.87	1.58	

51.59	75.73	46.85	1.50	
54.56	80.19	49.90	1.46	
57.62	84.64	--	--	

Run TL5

$t^*\sqrt{\frac{g}{d_o}}$ (1)	$\frac{s}{d_o}$ (2)	$t^*\sqrt{\frac{g}{d_o}}$ (3)	$\frac{C_s}{\sqrt{g*d_o}}$ (4)	Remarks (5)
0.00	0.00	0.00	1.10	s = 0 at nozzle.
7.35	8.10	2.99	1.37	s measured at step edges.
10.34	12.15	5.36	1.71	C_S averaged between step
12.72	16.20	7.58	1.82	edges.
14.94	20.25	9.73	1.89	
17.08	24.30	11.87	1.89	
19.23	28.35	14.33	1.65	
21.68	32.40	16.70	1.71	
24.06	36.45	19.23	1.60	
26.58	40.50	21.83	1.55	
29.19	44.54	24.36	1.60	
31.72	48.59	26.97	1.56	
34.32	52.64	29.65	1.51	
37.00	56.69	32.41	1.47	
39.76	60.74	34.94	1.60	
42.29	64.79	37.46	1.61	
44.82	68.84	40.37	1.39	
47.73	72.89	43.21	1.43	
50.56	76.94	--	--	

IV.4 Field tests at Brushes Clough dam spillway

Location :	Brushes Clough dam (UK)
Date :	1994
Experiments by :	Dr R. BAKER
Data processing by :	H. CHANSON
Experiment characteristics :	Full-scale flood release. Trapezoidal channel : bottom width: 2 m, bottom slope : 18.43 deg., inclined downward steps.
Instrumentation :	VHS video-camera.
Comments :	Q = 0.5 m^3/s (d_o = 0.417 m). One run.

$t^*\sqrt{\frac{g}{d_o}}$ (1)	$\frac{s}{d_o}$ (2)	Remarks (3)
0.00	0.00	s = 0 at first step.
0.40	1.44	Measurements at
0.73	2.88	step edges.
0.97	4.32	
2.27	8.09	
2.83	15.12	
3.24	16.60	
4.05	17.95	
4.85	19.79	

16.02	105.15
18.45	122.45

Note : s : longitudinal distance in the flow direction.

APPENDIX V - WAVE FRONT CELERITY DATA. (2) STUDIES OF INDIVIDUAL STEPS

V.1 Presentation

Experiments were performed in a 25-m long 0.5-m wide flume. The channel was a flat waterway ($S_o \approx 0.065$). The flow rate was delivered by a pump controlled with an adjustable frequency AC motor drive Taian T-Verter K1/N1 (Pulse Width Modulated design), enabling an accurate discharge adjustment in a closed-circuit system. The flow was fed through a smooth convergent nozzle (1.7-m long), and the nozzle exit was 30-mm high and 0.5-m wide. The measured contraction ratio was about unity (i.e. d_n = 30 mm for all experiments). Earlier experiments (CHANSON 1995) showed that steady flows at the nozzle were two-dimensional and became fully-developed upstream of the first drop.

For one stepped configuration (Table V-1), studies of individual steps were conducted by mounting the camera vertically above the step. Each step was painted with red and white stripes spaced 50 mm apart. Video-taped movies were analysed frame-by-frame. The error on the time was less than 1/250 s, and the error on the longitudinal position of the wave front was +/- 1 cm. In experiments Series 2, and for each run, three video recordings were taken at each location and subsequently analysed. The results are presented in terms of the average over three recordings.

Table V-1 - Summary of unsteady flow experiments

Experiment	θ (deg.)	h m	Run	Q(t=0+) (m^3/s)	Step locations	Remarks
(1)	(2)	(3)	(4)	(5)	(6)	(7)
Series 2	3.4	0.0715				18 horizontal steps (l = 1.2 m). W = 0.5 m. Nozzle depth : d_n = 0030 m.
			TL1	0.040	**3**, 9, **10**, 16, 17	Air-water flow measurements.
			TL2	0.0475	**3**, 9, **10**, 16, 17	
			TL3	0.055	**3**, 9, **10**, 16, 17	Air-water flow measurements.
			TL4	0.065	**3**, 9, **10**, 16, 17	
			TL5	0.075	**3**, 9, **10**, 16, 17	Air-water flow measurements.

Notes : Q(t=0+) : initial flow rate; d_n : approach flow depth (nozzle depth); h : step height; l : step length; **bold step number** : steps where both vertical and horizontal celerity were recorded.

Discussion

Most wave front celerity data on a single step were the horizontal celerity component recorded with a camera looking vertically downward onto the step. However, on the steps 3 and 10, the vertical celerity component was measured in the free-falling nappe with a camera looking horizontally onto the vertical step face. For these steps, the celerity data C_S are the magnitude of the wave celerity : $C_S = \sqrt{(C_S)_X^2 + (C_S)_Z^2}$, where the subscripts x and z refer to the horizontal and vertical celerity component respectively. Although $C_S = (C_S)_X$ downstream of nappe impact, the vertical celerity component must be accounted for in the free-falling nappe. Experiments at two steps for 5 flow rates (Table V-1, column 6) demonstrated that the vertical component of wave front celerity $(C_S)_Z$ satisfied the motion equation and hence basic trajectory equation: i.e., $(C_S)_Z \propto t' \propto$

x', where t' is the time from take-off and x' is the horizontal distance from the step vertical face. Experimental data highlighted nappe acceleration in the free-jet followed by a gradual flow deceleration downstream of nappe impact.

Notation

C_s wave front celerity (m/s);
d_c critical flow depth (m);
d_n nozzle depth (m) : d_n = 0.03 m;
d_o characteristic water depth (m) function of the flow rate and channel width only; $d_o = 9/4\ d_c$;
g gravity acceleration (m/s^2) : g = 9.80 m/s^2 in Brisbane;
h step height (m);
l step length (m);
Q water discharge (m^3/s);
x' horizontal distance (m) measured from vertical step face, positive in downstream flow direction;
t' time (s) measured from nappe take-off;

Subscript

x horizontal component;
z vertical component.

V.2 Experiments Series 2

Location :	University of Queensland (Australia)
Date :	March-June 2002
Experiments by :	Chung Hwee "Jerry" LIM and York-wee TAN
Data processing by :	Chung Hwee "Jerry" LIM, York-wee TAN and H. CHANSON
Experiment characteristics :	Flume : length: 25 m, width: 0.5 m, slope: 3.4 degrees, step height: 0.0715 m, step length: 1.2 m. Inflow conditions : nozzle depth d_n = 0.03 m. First step : 2.4 m long, equipped with sidewall deflectors.
Instrumentation :	VHS video-camera Panasonic™ NV-RX10A (speed: 25 frames/sec., shutter: sport mode, zoom: 1 to 14).
Comments :	Data averaged over three identical runs.

Run TL1

Step	t'	$(C_s)_x$	$(C_s)_z$
	s	m/s	m/s
(1)	(2)	(3)	(4)
Step 3	0.02	1.25	0.17
	0.06	1.67	0.25
	0.10	2.08	0.50
	0.14	1.83	0.54
	0.18	2.33	0.29
	0.22	2.25	n/a
	0.26	2.08	n/a
	0.30	2.08	n/a
	0.34	2.33	n/a
	0.38	1.83	n/a
	0.42	1.83	n/a
	0.46	1.67	n/a
	0.50	1.75	n/a
	0.54	1.67	n/a
	0.58	1.42	n/a
	0.62	1.50	n/a
Step 9	0.02	1.04	n/a
	0.06	1.04	n/a
	0.10	1.67	n/a
	0.14	1.33	n/a
	0.18	1.75	n/a
	0.22	1.50	n/a
	0.26	1.58	n/a
	0.30	2.75	n/a
	0.34	1.67	n/a
	0.38	2.08	n/a
	0.42	2.50	n/a
	0.46	1.50	n/a
	0.50	1.58	n/a
	0.54	1.75	n/a
	0.58	1.42	n/a
	0.62	1.67	n/a
	0.66	1.67	n/a
	0.70	1.50	n/a
Step 10	0.02	0.83	0.33
	0.06	1.25	0.53
	0.10	1.83	0.68
	0.14	2.08	0.20

	0.18	1.88	n/a
	0.22	2.04	n/a
	0.26	2.33	n/a
	0.30	1.75	n/a
	0.34	2.00	n/a
	0.38	2.08	n/a
	0.42	1.50	n/a
	0.46	1.83	n/a
	0.50	1.75	n/a
	0.54	1.42	n/a
	0.58	1.75	n/a
	0.62	2.00	n/a
	0.66	1.67	n/a
Step 16	0.02	1.25	n/a
	0.06	1.50	n/a
	0.10	1.92	n/a
	0.14	2.00	n/a
	0.18	1.83	n/a
	0.22	2.33	n/a
	0.26	2.33	n/a
	0.30	2.08	n/a
	0.34	2.00	n/a
	0.38	1.92	n/a
	0.42	1.83	n/a
	0.46	2.25	n/a
	0.50	1.92	n/a
	0.54	1.92	n/a
	0.58	2.50	n/a
Step 17	0.02	1.67	n/a
	0.06	2.50	n/a
	0.10	1.67	n/a
	0.14	2.25	n/a
	0.18	2.17	n/a
	0.22	2.58	n/a
	0.26	2.08	n/a
	0.30	2.42	n/a
	0.34	1.67	n/a
	0.38	1.42	n/a
	0.42	2.67	n/a
	0.46	2.08	n/a
	0.50	2.17	n/a
	0.54	2.25	n/a

Run TL2

Step	t'	$(C_S)_X$	$(C_S)_Z$
	s	m/s	m/s
(1)	(2)	(3)	(4)
Step 3	0.02	1.25	0.33
	0.06	2.25	0.54
	0.10	1.92	0.67
	0.14	2.67	0.21
	0.18	2.33	n/a
	0.22	2.00	n/a
	0.26	2.33	n/a
	0.30	2.08	n/a
	0.34	1.50	n/a
	0.38	1.67	n/a
	0.42	1.67	n/a
	0.46	1.75	n/a
	0.50	2.00	n/a
	0.54	1.42	n/a
	0.58	2.33	n/a
Step 9	0.02	1.88	n/a
	0.06	2.04	n/a
	0.10	2.75	n/a
	0.14	2.67	n/a
	0.18	2.33	n/a
	0.22	2.25	n/a
	0.26	1.92	n/a
	0.30	2.00	n/a
	0.34	1.75	n/a
	0.38	2.00	n/a
	0.42	1.92	n/a
	0.46	1.92	n/a
	0.50	2.50	n/a
	0.54	2.08	n/a
Step 10	0.02	1.25	0.22
	0.06	2.50	0.62
	0.10	2.50	0.72
	0.14	2.50	0.19
	0.18	2.00	n/a
	0.22	2.17	n/a
	0.26	2.25	n/a
	0.30	2.33	n/a
	0.34	2.25	n/a
	0.38	2.08	n/a
	0.42	2.50	n/a
	0.46	1.92	n/a
	0.50	2.50	n/a
Step 16	0.02	1.46	n/a
	0.06	2.29	n/a
	0.1	2.50	n/a
	0.14	2.83	n/a
	0.18	2.17	n/a
	0.22	2.67	n/a
	0.26	2.25	n/a
	0.3	1.92	n/a
	0.34	1.92	n/a
	0.38	1.58	n/a
	0.42	1.75	n/a
	0.46	1.83	n/a
	0.5	1.83	n/a
	0.54	1.75	n/a
Step 17	0.02	1.67	n/a
	0.06	2.50	n/a
	0.1	2.92	n/a
	0.14	2.08	n/a
	0.18	2.25	n/a
	0.22	2.33	n/a
	0.26	2.08	n/a
	0.3	2.08	n/a
	0.34	2.50	n/a
	0.38	2.00	n/a
	0.42	2.17	n/a
	0.46	1.75	n/a
	0.5	2.17	n/a
	0.54	1.50	n/a

Run TL3

Step	t'	$(C_S)_X$	$(C_S)_Z$
	s	m/s	m/s
(1)	(2)	(3)	(4)
Step 3	0.02	1.88	0.38
	0.06	1.88	0.63
	0.10	2.50	0.54
	0.14	2.50	0.21
	0.18	2.50	n/a
	0.22	2.50	n/a
	0.26	2.25	n/a
	0.30	1.92	n/a
	0.34	1.58	n/a
	0.38	1.92	n/a
	0.42	2.08	n/a
	0.46	1.67	n/a
	0.50	2.08	n/a
	0.54	2.08	n/a
Step 10	0.02	1.67	n/a
	0.06	2.67	n/a
	0.10	2.00	n/a
	0.14	3.25	n/a
	0.18	2.00	n/a
	0.22	1.92	n/a
	0.26	2.08	n/a
	0.30	2.33	n/a
	0.34	2.08	n/a
	0.38	2.25	n/a
	0.42	2.50	n/a
	0.46	1.92	n/a
	0.50	2.08	n/a
Step 10	0.02	1.88	0.25
	0.06	2.29	0.66
	0.10	2.42	0.77
	0.14	2.33	0.07
	0.18	2.33	n/a
	0.22	2.25	n/a
	0.26	2.75	n/a
	0.30	2.17	n/a
	0.34	2.42	n/a
	0.38	2.25	n/a
	0.42	2.33	n/a
	0.46	2.08	n/a
	0.50	2.08	n/a
Step 16	0.02	1.46	n/a
	0.06	2.29	n/a
	0.10	2.50	n/a
	0.14	2.25	n/a
	0.18	2.08	n/a
	0.22	2.33	n/a
	0.26	2.50	n/a
	0.30	1.75	n/a
	0.34	2.00	n/a
	0.38	2.25	n/a
	0.42	2.50	n/a
	0.46	2.33	n/a
	0.50	2.00	n/a
	0.54	1.75	n/a

Step 17	0.02	1.25	n/a
	0.06	1.67	n/a
	0.10	2.92	n/a
	0.14	2.50	n/a
	0.18	2.25	n/a
	0.22	2.75	n/a
	0.26	2.00	n/a
	0.30	2.92	n/a
	0.34	2.17	n/a
	0.38	2.50	n/a
	0.42	2.50	n/a
	0.46	2.08	n/a
	0.50	2.08	n/a

Run TL4

Step	t'	$(C_S)_X$	$(C_S)_Z$
	s	m/s	m/s
(1)	(2)	(3)	(4)
Step 3	0.02	1.88	0.46
	0.06	3.13	0.63
	0.10	3.08	0.58
	0.14	2.50	0.13
	0.18	2.67	n/a
	0.22	2.92	n/a
	0.26	2.50	n/a
	0.30	2.33	n/a
	0.34	2.50	n/a
	0.38	2.50	n/a
	0.42	3.17	n/a
Step 9	0.02	1.67	n/a
	0.06	2.83	n/a
	0.10	3.17	n/a
	0.14	2.50	n/a
	0.18	2.92	n/a
	0.22	2.33	n/a
	0.26	2.25	n/a
	0.30	2.75	n/a
	0.34	2.75	n/a
	0.38	2.42	n/a
	0.42	2.75	n/a
	0.46	1.67	n/a
Step 10	0.02	1.88	0.64
	0.06	2.63	0.92
	0.10	3.42	0.20
	0.14	2.50	n/a
	0.18	2.50	n/a
	0.22	2.50	n/a
	0.26	2.50	n/a
	0.30	2.33	n/a
	0.34	1.92	n/a
	0.38	2.50	n/a
	0.42	2.58	n/a
	0.46	2.33	n/a
Step 16	0.02	1.46	n/a
	0.06	2.88	n/a
	0.10	3.17	n/a
	0.14	2.83	n/a
	0.18	2.75	n/a
	0.22	2.50	n/a
	0.26	2.33	n/a
	0.30	2.50	n/a
	0.34	2.25	n/a
	0.38	2.00	n/a
	0.42	2.17	n/a
	0.46	2.33	n/a
Step 17	0.02	1.88	n/a
	0.06	2.29	n/a
	0.10	3.08	n/a
	0.14	2.83	n/a
	0.18	2.42	n/a
	0.22	2.67	n/a
	0.26	2.33	n/a
	0.30	2.25	n/a
	0.34	2.50	n/a
	0.38	2.33	n/a
	0.42	2.00	n/a
	0.46	2.33	n/a
	0.50	1.08	n/a

Run TL5

Step	t'	$(C_S)_X$	$(C_S)_Z$
	s	m/s	m/s
(1)	(2)	(3)	(4)
Step 3	0.02	1.25	0.71
	0.06	2.50	0.63
	0.10	2.92	0.42
	0.14	3.75	n/a
	0.18	2.92	n/a
	0.22	3.33	n/a
	0.26	3.33	n/a
	0.30	2.92	n/a
	0.34	3.33	n/a
	0.38	2.25	n/a
Step 9	0.02	1.46	n/a
	0.06	2.71	n/a
	0.10	2.67	n/a
	0.14	3.33	n/a
	0.18	3.33	n/a
	0.22	2.58	n/a
	0.26	2.25	n/a
	0.30	2.92	n/a
	0.34	2.67	n/a
	0.38	2.25	n/a
	0.42	2.50	n/a
Step 10	0.02	1.46	0.66
	0.06	2.88	0.94
	0.10	2.50	0.15
	0.14	2.92	n/a
	0.18	2.92	n/a
	0.22	2.50	n/a
	0.26	2.75	n/a
	0.30	3.08	n/a
	0.34	2.92	n/a
	0.38	2.75	n/a
	0.42	2.08	n/a
Step 16	0.02	1.67	n/a
	0.06	2.50	n/a
	0.10	2.75	n/a
	0.14	2.67	n/a
	0.18	2.25	n/a
	0.22	2.75	n/a
	0.26	2.67	n/a
	0.30	2.58	n/a
	0.34	2.67	n/a
	0.38	2.25	n/a
	0.42	2.33	n/a
	0.46	2.08	n/a
Step 17	0.02	2.50	n/a
	0.06	2.67	n/a
	0.10	2.50	n/a
	0.14	3.17	n/a
	0.18	2.25	n/a
	0.22	2.25	n/a
	0.26	2.33	n/a
	0.30	2.83	n/a
	0.34	2.58	n/a
	0.38	2.08	n/a
	0.42	2.92	n/a
	0.46	1.92	n/a

APPENDIX VI - UNSTEADY AIR-WATER FLOW MEASUREMENTS (1) VOID FRACTION, BUBBLE COUNT RATE, SPECIFIC INTERFACE AREA DATA

VI.1 Presentation

Unsteady air-water flow properties were recorded for three flow rates and two steps (Table VI-1). On each step, measurements were performed at distances x' = 0.2, 0.4, 0.6, 0.8 and 1.0 m from the vertical step face (Fig. 4-1A).

Air-water flow properties were measured with a series of single-tip conductivity probes (needle probe design). Each probe consisted of a sharpened rod (platinum wire ∅ = 0.35 mm) which was insulated except for its tip and set into a metal supporting tube (stainless steel surgical needle ∅ = 1.42 mm) acting as the second electrode. The probes were excited by an electronics designed with a response time less than 10 μs and calibrated with a square wave generator. Further details on the probe system and electronics were reported in CHANSON (1995) and CUMMINGS (1996). The probe output signals were scanned at 10 kHz per channel for six seconds. Data acquisition was triggered manually immediately prior to the flow arrival.

Conductivity probe measurements were taken on the centreline. At each location x', one probe (i.e. reference probe) was set on the invert, acting as a time reference, while three other probes were set at different elevations. Each experiment was repeated until sufficient data were obtained at each profile. The displacement of the three probes in the direction y normal to the invert was controlled by a fine adjustment travelling mechanism. The error in the probe position was less than 0.2 mm and 2 mm in the vertical and horizontal direction respectively.

Conductivity probe signal processing

In steady flows, the void fraction C is the proportion of time that the probe tip is in the air while the bubble count rate F is the number of bubbles impacting the probe tip (e.g. CHANSON 2002b). In unsteady gas-liquid flows, the processing technique must be adapted. Few studies considered highly unsteady gas-liquid flows : e.g., STUTZ and REBOUD (1997, 2000).

In the present study, the void fractions and bubble count rates were calculated during a short time interval τ such as $\tau = \Delta x/C_S$ where C_S is the surge front celerity measured with the video-cameras and Δx is the control volume streamwise length. A difficulty consisted in determining an optimum duration or control volume size for the moving averaging process. After preliminary tests for 10 mm $\leq \Delta x \leq$ 100 mm ([1]), the basic control volume size was set at 70 mm ([2]). Such a size would contain typically 5 to 20 bubbles, and the selection was consistent with the processing technique of STUTZ and REBOUD (2000) who set τ to encompass at least 5

[1]For $\Delta x <$ 10 mm, the control volume size was smaller than a fair proportion of detected bubbles. For $\Delta x >$ 100 mm, the averaging process did not always reflect the flow property unsteadyness, especially in the leading edge of the surging waters.

[2]Prelimary results with Δx = 50, 70 and 80 mm showed little differences between the three control volume length.

bubbles. In the present study, the voltage signal was processed using a single threshold technique. The threshold was set at about 50% of the air-water voltage range.

Bubble and water chord times were measured where the bubble chord time t_{ch} is defined as the time spent by the bubble on the probe tip. The results are presented in terms of pseudo-chord length ch defined as :

$$ch = C_s * t_{ch} \quad \text{(VI-1)}$$

where C_s is the wave front celerity. Equation (VI-1) predicts accurately chord lengths near the front where the flow velocity is about the wave front speed. Note that the chord time data analysis was independent of the selection of the integration time interval τ.

The bubble count rate measurement is sensitive to the probe tip size, bubble sizes, velocity and scanning rate, particularly when the sensor size is larger than the smallest bubble sizes (e.g. CHANSON and TOOMBES 2002b). During the present study, the bubble count rate was calculated as :

$$F = \frac{N_{ab}}{\tau} \quad \text{(VI-2)}$$

where N_{ab} is the number of bubbles detected during the time interval τ.

The measurement of air-water interface area is a function of the void fraction, velocity, bubble size and bubble count. For any bubble shape, bubble size distribution and chord length distribution, the specific air-water interface area may be estimated as:

$$a = \frac{4 * F}{C_s} \quad \text{(VI-3)}$$

Equation (VI-3) is valid in bubbly flows. In high air content regions (C > 0.3 to 0.5), the flow structure is more complex and the result is not exactly the true specific interface area. a becomes simply proportional to the number of air-water interfaces per unit length of air-water mixture : i.e., $a \propto 2*F/C_s$ (CHANSON 2002b).

Table VI-1 - Summary of unsteady air-water flow measurements in dam break wave flow

Run	θ (deg.)	h m	Q(t=0+) (m^3/s)	Air-water flow measurements	Remarks
(1)	(2)	(3)	(4)	(5)	(6)
Series 2	3.4	0.071			18 horizontal steps (l = 1.2 m, W = 0.5 m).
			0.040	Step 16	Run TL1.
			0.055	Step 16	Run TL3.
			0.075	Steps 10 & 16	Run TL5.

Notes : h : step height; l : step length; Q(t=0+) : initial flow rate; W : chute width.

Notation

a air-water specific interface area (m^{-1}): i.e., air-water interface area per unit volume of air and water;

C void fraction, or air concentration, defined as the volume of air per unit volume of air and water;

C_s wave front celerity (m/s);

ch pseudo-chord size (m);

d_c critical flow depth (m);

d_n nozzle depth (m) : d_n = 0.03 m;
d_o characteristic water depth (m) function of the flow rate and channel width only; $d_o = 9/4\ d_c$;
F bubble count rate (Hz), defined as the number of bubbles impacting a probe sensor per second;
g gravity acceleration (m/s^2) : g = 9.80 m/s^2 in Brisbane;
h step height (m);
l step length (m);
Q water discharge (m^3/s);
t time (s);
t_{ch} air/water chord time (s);
t_s time (s) of passage of the wave front at the location x';
x' horizontal distance (m) measured from vertical step face, positive in downstream flow direction;
y vertical distance (m) measured from the step invert;
Δx smallest control volume streamwise length (m); in the present study: Δx = 70 mm;
ΔX control volume streamwise length (m) : $\Delta X = I*\Delta x$ where I is an integrer equal or larger than unity.

VI.2 Experiments Series 2 - Void fraction data

Location :	University of Queensland (Australia)
Date :	June-Aug. 2002
Experiments by :	Chung Hwee "Jerry" LIM and York-wee TAN
Data processing by :	H. CHANSON
Experiment characteristics :	Flume : length: 25 m, width: 0.5 m, slope: 3.4 degrees, step height: 0.0715 m, step length: 1.2 m. Inflow conditions : nozzle depth d_n = 0.03 m. First step : 2.4 m long, equipped with sidewall deflectors.
Instrumentation :	Single-tip conductivity probe (Ø = 0.35 mm).
Comments :	Data calculated for a minimum control volume Δx of 70 mm.

Experimental results in terms of void fractions, bubble count rates and air-water specific interface areas were calculated during a short time interval ΔT such as $\Delta T = \Delta X/C_S$ where C_S is the measured surge front celerity and ΔX is the control volume streamwise length. ΔX was selected to be a multiple of Δx = 70 mm : i.e., $\Delta X = I*\Delta x$ where I is an integrer equal or larger than unity.
In turn, the data calculated along ΔX correspond to a dimensionless time $(t - t_S)$ where t_S is the time of passage of wave front. In the following paragraphs, ΔX is typically presented in the following form:

Legend	Streamwise control volume length	Corresponding time
ΔX = 210-385 mm	ΔX = 175 mm	$0.210/C_S \leq (t - t_S) \leq 0.385/C_S$

Run TL1

Q m^3/s	Step	x' m	C_S m/s	d_o m
0.040	16	0.2, 0.4, 0.6, 0.8, 1.0	1.97	0.195

x'	y	C	C	C	C	C	C	C	C	C	C

m (1)	mm (2)	(3)	(4)	(5)	(6)	(7)	(8)	(9)	(10)	(11)	(12)
$\Delta X =$	(mm)	0-70	0-210	140-210	0-385	175-385	350-735	525-595	700-1085	2100-2485	4200-4585
$t - t_s =$	(s)	0.018	0.053	0.089	0.098	0.142	0.275	0.284	0.453	1.164	2.23
$\Delta X =$	(mm)	70	210	70	385	210	385	70	385	385	385
$\frac{(t-t_s)}{\sqrt{d_o/g}}$		0.126	0.378	0.629	0.692	1.007	1.951	2.014	3.21	8.245	15.8
0.2	4.65	0.64	0.43	0.00	0.34	0.24	0.03	0.00	0.04	0.00	0.00
0.2	7.8	0.45	0.33	0.03	0.31	0.28	0.05	0.00	0.06	0.00	0.00
0.2	10.14	0.51	0.22	0.00	0.23	0.24	0.06	0.01	0.09	0.06	0.01
0.2	11.65	0.80	0.73	1.00	0.66	0.59	0.05	0.00	0.22	0.04	0.09
0.2	14.8	0.86	0.79	1.00	0.71	0.64	0.00	0.00	0.08	0.11	0.13
0.2	17.14	0.89	0.82	1.00	0.73	0.64	0.03	0.00	0.07	0.01	0.03
0.2	21.65	0.77	0.59	0.46	0.59	0.58	0.07	0.13	0.03	0.00	0.12
0.2	24.8	0.81	0.79	0.83	0.81	0.83	0.14	0.16	0.07	0.00	0.08
0.2	27.14	0.84	0.93	1.00	0.87	0.81	0.14	0.00	0.23	0.00	0.05
0.2	28.65	1.00	1.00	1.00	0.75	0.51	0.90	1.00	0.12	0.01	0.01
0.2	31.8	1.00	1.00	1.00	0.81	0.61	0.92	1.00	0.20	0.01	0.18
0.2	34.14	1.00	1.00	1.00	0.90	0.79	0.93	1.00	0.23	0.03	0.37
0.2	35.15	1.00	0.87	0.65	0.73	0.59	0.64	1.00	0.58	0.10	0.11
0.2	38.3	1.00	0.95	0.75	0.83	0.71	0.75	1.00	0.70	0.17	0.20
0.2	40.64	1.00	0.96	0.81	0.86	0.76	0.84	1.00	0.72	0.33	0.29
0.2	41.65	1.00	1.00	1.00	0.98	0.97	0.90	1.00	0.81	0.17	0.64
0.2	44.8	1.00	1.00	1.00	0.99	0.98	0.92	1.00	0.96	0.40	0.71
0.2	47.14	1.00	1.00	1.00	0.99	0.99	0.97	0.84	0.95	0.38	0.84
0.4	4.65	0.79	0.38	0.03	0.20	0.03	0.00	0.00	0.00	0.00	0.00
0.4	7.8	0.88	0.59	0.12	0.40	0.22	0.00	0.00	0.00	0.00	0.04
0.4	10.14	0.81	0.65	0.44	0.49	0.34	0.02	0.00	0.03	0.01	0.03
0.4	11.65	1.00	1.00	1.00	0.79	0.58	0.22	0.48	0.02	0.00	0.00
0.4	14.8	1.00	1.00	1.00	0.83	0.67	0.44	0.78	0.08	0.01	0.01
0.4	17.14	1.00	1.00	1.00	0.85	0.70	0.59	0.85	0.27	0.03	0.01
0.4	21.65	1.00	0.78	0.63	0.76	0.74	0.30	0.14	0.32	0.34	0.27
0.4	24.8	1.00	0.82	0.68	0.89	0.96	0.45	0.24	0.36	0.47	0.33
0.4	27.14	1.00	0.85	0.66	0.92	0.99	0.56	0.37	0.45	0.62	0.38
0.4	28.65	1.00	1.00	1.00	0.93	0.86	0.96	1.00	0.80	0.79	0.44
0.4	31.8	1.00	0.97	0.85	0.91	0.86	0.99	1.00	0.86	0.84	0.68
0.4	34.14	1.00	1.00	1.00	0.94	0.88	0.98	1.00	0.88	0.90	0.76
0.4	35.15	1.00	0.98	0.95	0.86	0.74	0.42	0.15	0.22	0.44	0.78
0.4	38.3	1.00	1.00	1.00	0.89	0.77	0.51	0.17	0.29	0.53	0.83
0.4	40.64	1.00	1.00	1.00	0.94	0.87	0.62	0.28	0.41	0.61	0.87
0.4	41.65	1.00	1.00	1.00	0.96	0.92	0.94	0.89	0.85	0.95	0.64
0.4	44.8	1.00	1.00	1.00	0.96	0.91	0.90	0.88	0.86	0.95	0.66
0.4	47.14	1.00	1.00	1.00	0.99	0.97	0.92	0.96	0.87	0.96	0.72
0.6	4.65	0.84	0.36	0.00	0.18	0.00	0.00	0.00	0.00	0.00	0.00
0.6	7.8	1.00	0.59	0.05	0.30	0.00	0.00	0.00	0.00	0.00	0.00
0.6	10.14	1.00	0.78	0.25	0.40	0.01	0.02	0.08	0.01	0.00	0.00
0.6	11.65	1.00	0.72	0.05	0.51	0.30	0.08	0.00	0.02	0.00	0.00
0.6	14.8	0.98	0.89	0.57	0.71	0.52	0.15	0.00	0.06	0.01	0.01
0.6	17.14	1.00	0.90	0.75	0.71	0.52	0.20	0.05	0.17	0.03	0.03
0.6	21.65	1.00	1.00	1.00	1.00	1.00	0.64	1.00	0.58	0.27	0.52
0.6	24.8	1.00	1.00	1.00	1.00	1.00	0.74	1.00	0.66	0.39	0.74
0.6	27.14	1.00	1.00	1.00	1.00	1.00	0.83	1.00	0.77	0.74	0.89
0.6	28.65	1.00	1.00	1.00	1.00	1.00	1.00	1.00	0.74	0.73	0.88
0.6	31.8	1.00	1.00	1.00	1.00	1.00	0.99	1.00	0.78	0.86	0.95
0.6	34.14	1.00	1.00	1.00	0.99	0.99	1.00	1.00	0.79	0.90	1.00
0.6	35.15	1.00	1.00	1.00	1.00	1.00	0.95	0.86	1.00	0.91	0.73

0.6	38.3	1.00	1.00	1.00	1.00	1.00	0.96	0.85	1.00	0.93	0.85
0.6	40.64	1.00	1.00	1.00	1.00	1.00	0.96	0.80	1.00	0.96	0.95
0.6	41.65	1.00	1.00	1.00	1.00	1.00	1.00	1.00	1.00	1.00	0.96
0.6	44.8	1.00	1.00	1.00	1.00	1.00	1.00	1.00	1.00	1.00	0.96
0.6	47.14	1.00	1.00	1.00	1.00	1.00	1.00	1.00	1.00	1.00	0.97
x' m (1)	y mm (2)	C (3)	C (4)	C (5)	C (6)	C (7)	C (8)	C (9)	C (10)	C (11)	C (12)
0.8	4.65	0.98	0.30	0.00	0.17	0.03	0.00	0.00	0.00	0.00	0.00
0.8	7.8	0.98	0.49	0.56	0.34	0.18	0.00	0.00	0.00	0.00	0.00
0.8	10.14	0.94	0.88	1.00	0.57	0.27	0.00	0.00	0.00	0.00	0.00
0.8	11.65	1.00	1.00	0.98	0.56	0.12	0.04	0.00	0.00	0.00	0.02
0.8	14.8	1.00	1.00	1.00	0.59	0.17	0.19	0.10	0.01	0.00	0.04
0.8	17.14	1.00	1.00	1.00	0.68	0.36	0.49	0.43	0.08	0.01	0.09
0.8	21.65	1.00	1.00	1.00	0.94	0.89	0.70	0.61	0.86	0.25	0.20
0.8	24.8	1.00	1.00	1.00	0.94	0.88	0.87	1.00	0.93	0.45	0.68
0.8	27.14	1.00	1.00	1.00	0.97	0.95	0.92	1.00	0.98	0.68	0.90
0.8	28.65	1.00	1.00	1.00	1.00	1.00	0.95	0.92	1.00	0.89	0.90
0.8	31.8	1.00	1.00	1.00	1.00	1.00	1.00	1.00	1.00	0.98	0.96
0.8	34.8	1.00	1.00	1.00	1.00	1.00	1.00	1.00	1.00	1.00	0.99
0.8	35.15	1.00	1.00	1.00	1.00	1.00	1.00	1.00	1.00	1.00	0.96
0.8	38.3	1.00	1.00	1.00	1.00	1.00	1.00	1.00	1.00	1.00	1.00
0.8	40.64	1.00	1.00	1.00	1.00	1.00	1.00	1.00	1.00	1.00	1.00
0.8	41.65	1.00	1.00	1.00	1.00	1.00	1.00	1.00	1.00	1.00	1.00
0.8	44.8	1.00	1.00	1.00	1.00	1.00	1.00	1.00	1.00	1.00	1.00
1	4.65	0.97	0.31	0.00	0.16	0.00	0.00	0.00	0.00	0.00	0.00
1	7.8	0.66	0.17	0.02	0.08	0.00	0.00	0.00	0.00	0.00	0.00
1	10.14	1.00	0.60	0.40	0.30	0.01	0.00	0.00	0.00	0.00	0.00
1	11.65	1.00	0.83	0.32	0.41	0.00	0.05	0.18	0.00	0.06	0.00
1	14.8	1.00	0.93	0.79	0.54	0.15	0.20	0.28	0.06	0.11	0.00
1	17.14	1.00	0.97	0.91	0.69	0.42	0.54	0.30	0.26	0.17	0.01
1	21.65	1.00	1.00	1.00	1.00	1.00	1.00	1.00	0.68	0.62	0.19
1	24.8	1.00	1.00	1.00	1.00	1.00	1.00	1.00	0.92	0.73	0.42
1	27.14	1.00	1.00	1.00	1.00	1.00	1.00	1.00	0.93	0.84	0.67
1	28.65	1.00	1.00	1.00	1.00	1.00	1.00	1.00	0.96	1.00	0.88
1	31.8	1.00	1.00	1.00	1.00	1.00	1.00	1.00	1.00	1.00	0.98
1	34.14	1.00	1.00	1.00	1.00	1.00	1.00	1.00	1.00	1.00	0.99
1	35.15	1.00	1.00	1.00	1.00	1.00	1.00	1.00	1.00	1.00	0.86
1	38.3	1.00	1.00	1.00	1.00	1.00	1.00	1.00	1.00	1.00	0.92
1	40.64	1.00	1.00	1.00	1.00	1.00	1.00	1.00	1.00	1.00	0.93
x' m (1)	y mm (2)	C (3)	C (4)	C (5)	C (6)	C (7)	C (8)	C (9)	C (10)	C (11)	C (12)

Run TL3

Q m^3/s	Step	x' m	C_s m/s	d_o m
0.055	16	0.2, 0.4, 0.6, 0.8, 1.0	2.14	0.241

x' m (1)	y mm (2)	C (3)	C (4)	C (5)	C (6)	C (7)	C (8)	C (9)	C (10)	C (11)	C (12)
ΔX =	(mm)	0-70	0-210	140-210	0-385	175-385	350-735	525-595	700-1085	2100-2485	4200-4585
$t - t_s$ =	(s)	0.016	0.049	0.082	0.09	0.131	0.254	0.262	0.417	1.071	2.053
ΔX =	(mm)	70	210	70	385	210	385	70	385	385	385

$\frac{(t-t_s)}{\sqrt{d_o/g}}$		0.104	0.313	0.521	0.573	0.834	1.615	1.667	2.657	6.826	13.08
0.2	4.65	1.00	0.44	0.02	0.23	0.01	0.08	0.00	0.06	0.06	0.00
0.2	7.80	0.87	0.25	0.00	0.16	0.07	0.00	0.00	0.00	0.01	0.00
0.2	10.14	1.00	0.64	0.43	0.53	0.42	0.01	0.06	0.03	0.10	0.04
0.2	11.65	0.83	0.84	0.57	0.64	0.45	0.31	0.51	0.18	0.08	0.00
0.2	14.80	0.72	0.53	0.35	0.47	0.42	0.29	0.54	0.48	0.16	0.00
0.2	17.14	0.35	0.17	0.00	0.12	0.08	0.34	0.71	0.47	0.33	0.05
0.2	21.65	0.72	0.86	0.76	0.63	0.40	0.32	0.20	0.47	0.67	0.30
0.2	24.80	0.55	0.61	0.56	0.40	0.18	0.25	0.00	0.31	0.43	0.38
0.2	27.14	0.54	0.48	0.46	0.24	0.00	0.10	0.03	0.02	0.16	0.28
0.2	28.65	0.00	0.17	0.19	0.22	0.27	0.12	0.00	0.17	0.36	0.10
0.2	31.80	0.00	0.25	0.30	0.31	0.36	0.06	0.00	0.08	0.16	0.07
0.2	34.14	0.18	0.48	0.42	0.43	0.38	0.06	0.00	0.01	0.07	0.05
0.2	35.15	1.00	0.92	0.74	0.75	0.58	0.43	0.61	0.19	0.03	0.00
0.2	38.30	1.00	0.94	0.84	0.80	0.66	0.65	1.00	0.39	0.06	0.00
0.2	40.64	1.00	1.00	1.00	0.87	0.75	0.73	1.00	0.52	0.11	0.04
0.2	41.65	1.00	0.99	0.93	0.87	0.75	0.59	0.33	0.32	0.03	0.02
0.2	44.80	1.00	1.00	1.00	1.00	1.00	0.67	0.46	0.60	0.09	0.09
0.2	47.14	1.00	1.00	1.00	1.00	1.00	0.81	0.94	0.65	0.24	0.29
0.2	51.65	1.00	1.00	1.00	0.95	0.90	0.82	0.74	0.76	0.66	0.50
0.2	54.80	1.00	1.00	1.00	0.95	0.89	0.84	0.78	0.78	0.74	0.67
0.2	57.14	1.00	1.00	1.00	0.96	0.92	0.88	0.81	0.82	0.80	0.83
0.4	4.65	0.84	0.51	0.05	0.26	0.00	0.00	0.00	0.00	0.00	0.00
0.4	7.80	0.71	0.42	0.06	0.23	0.04	0.00	0.00	0.00	0.01	0.01
0.4	10.14	0.91	0.69	0.36	0.53	0.37	0.15	0.06	0.00	0.00	0.02
0.4	11.65	1.00	1.00	1.00	0.80	0.60	0.08	0.00	0.00	0.00	0.00
0.4	14.80	1.00	1.00	1.00	0.82	0.64	0.14	0.08	0.01	0.00	0.01
0.4	17.14	1.00	1.00	1.00	0.86	0.73	0.18	0.13	0.03	0.00	0.01
0.4	21.65	1.00	0.83	0.78	0.77	0.71	0.20	0.28	0.15	0.05	0.06
0.4	24.80	1.00	0.87	0.80	0.82	0.77	0.23	0.27	0.16	0.09	0.13
0.4	27.14	1.00	0.86	0.79	0.82	0.79	0.33	0.31	0.19	0.19	0.18
0.4	28.65	1.00	1.00	1.00	0.98	0.96	0.41	0.29	0.33	0.28	0.14
0.4	31.80	1.00	1.00	1.00	0.98	0.96	0.55	0.46	0.41	0.41	0.22
0.4	34.14	1.00	1.00	1.00	1.00	1.00	0.56	0.34	0.44	0.42	0.29
0.4	35.15	1.00	1.00	1.00	0.94	0.87	0.51	0.75	0.59	0.33	0.29
0.4	38.30	1.00	1.00	1.00	0.99	0.98	0.52	0.73	0.66	0.47	0.33
0.4	40.64	1.00	1.00	1.00	1.00	1.00	0.55	0.78	0.78	0.54	0.34
0.4	41.65	1.00	1.00	1.00	0.98	0.95	0.73	0.49	0.63	0.76	0.76
0.4	44.80	1.00	1.00	1.00	1.00	1.00	0.78	0.57	0.78	0.83	0.76
0.4	47.14	1.00	1.00	0.98	0.99	0.99	0.82	0.60	0.83	0.84	0.76
0.4	51.65	1.00	1.00	1.00	0.96	0.92	0.82	0.58	0.79	0.91	0.74
0.4	54.80	1.00	1.00	1.00	0.96	0.92	0.92	0.80	0.83	0.95	0.85
0.4	57.14	1.00	1.00	1.00	0.97	0.95	0.95	0.85	0.86	0.99	0.90
0.6	4.65	0.69	0.17	0.00	0.09	0.00	0.00	0.00	0.00	0.00	0.00
0.6	7.80	0.84	0.27	0.03	0.14	0.00	0.00	0.00	0.00	0.00	0.00
0.6	10.14	1.00	0.66	0.18	0.45	0.25	0.00	0.00	0.00	0.00	0.00
0.6	11.65	0.85	0.26	0.00	0.13	0.00	0.00	0.00	0.00	0.00	0.00
0.6	14.80	1.00	0.44	0.19	0.22	0.00	0.00	0.00	0.00	0.00	0.00
0.6	17.14	0.99	0.63	0.55	0.35	0.07	0.00	0.00	0.00	0.00	0.01
0.6	21.65	1.00	1.00	1.00	0.85	0.71	0.09	0.00	0.05	0.01	0.00
0.6	24.80	1.00	1.00	1.00	0.87	0.74	0.11	0.08	0.06	0.01	0.02
0.6	27.14	1.00	1.00	1.00	0.89	0.78	0.15	0.08	0.10	0.04	0.04
0.6	28.65	1.00	1.00	1.00	0.85	0.70	0.30	0.03	0.25	0.10	0.22
0.6	31.80	1.00	1.00	1.00	0.91	0.82	0.45	0.05	0.37	0.13	0.46
0.6	34.14	1.00	1.00	1.00	0.93	0.86	0.52	0.02	0.48	0.17	0.60
0.6	35.15	1.00	1.00	1.00	0.89	0.78	0.12	0.02	0.09	0.17	0.10

0.6	38.30	1.00	1.00	1.00	0.91	0.81	0.19	0.04	0.37	0.24	0.22
0.6	40.64	1.00	1.00	1.00	0.95	0.90	0.21	0.15	0.59	0.28	0.34
0.6	41.65	1.00	1.00	1.00	0.98	0.95	0.73	1.00	0.86	0.36	0.64
0.6	44.80	1.00	1.00	1.00	0.99	0.98	0.77	1.00	0.91	0.51	0.70
0.6	47.14	1.00	1.00	1.00	1.00	1.00	0.80	1.00	0.94	0.68	0.74
0.6	51.65	1.00	1.00	1.00	0.78	0.55	0.75	1.00	0.90	0.95	0.64
0.6	54.80	1.00	1.00	1.00	0.84	0.67	0.79	1.00	0.95	0.97	0.73
0.6	57.14	1.00	1.00	1.00	0.86	0.73	0.80	1.00	0.98	0.99	0.81
0.8	4.65	0.97	0.58	0.06	0.29	0.00	0.00	0.00	0.00	0.00	0.00
0.8	7.80	0.93	0.77	0.29	0.39	0.01	0.00	0.00	0.00	0.00	0.00
0.8	10.14	1.00	0.72	0.10	0.36	0.00	0.00	0.00	0.00	0.00	0.00
0.8	11.65	0.97	0.47	0.00	0.24	0.00	0.00	0.00	0.00	0.00	0.00
0.8	14.80	1.00	0.56	0.05	0.28	0.00	0.00	0.00	0.00	0.00	0.00
0.8	17.14	1.00	0.81	0.31	0.45	0.09	0.00	0.00	0.00	0.00	0.01
0.8	21.65	1.00	1.00	1.00	0.88	0.77	0.06	0.00	0.20	0.01	0.00
0.8	24.80	1.00	1.00	1.00	0.94	0.87	0.17	0.00	0.31	0.05	0.00
0.8	27.14	1.00	1.00	1.00	0.95	0.90	0.31	0.00	0.46	0.12	0.06
0.8	28.65	1.00	1.00	1.00	1.00	1.00	0.15	0.00	0.76	0.10	0.84
0.8	31.80	1.00	1.00	1.00	1.00	1.00	0.29	0.17	0.86	0.24	0.97
0.8	34.14	1.00	1.00	1.00	1.00	1.00	0.68	0.25	1.00	0.43	1.00
0.8	35.15	1.00	1.00	1.00	1.00	1.00	0.69	0.61	1.00	0.81	0.38
0.8	38.30	1.00	1.00	1.00	1.00	1.00	0.83	0.87	1.00	0.94	0.53
0.8	40.64	1.00	1.00	1.00	1.00	1.00	0.86	0.87	1.00	0.96	0.57
0.8	41.65	1.00	1.00	1.00	1.00	1.00	1.00	1.00	0.91	0.76	0.87
0.8	44.80	1.00	1.00	1.00	1.00	1.00	1.00	1.00	0.96	0.85	0.91
0.8	47.14	1.00	1.00	1.00	1.00	1.00	1.00	1.00	1.00	0.91	0.92
0.8	51.65	1.00	1.00	1.00	1.00	1.00	1.00	1.00	0.79	0.98	1.00
0.8	54.80	1.00	1.00	1.00	1.00	1.00	1.00	1.00	0.89	1.00	1.00
0.8	57.14	1.00	1.00	1.00	1.00	1.00	1.00	1.00	0.91	1.00	1.00
1	4.65	1.00	0.57	0.00	0.28	0.00	0.00	0.00	0.00	0.00	0.00
1	7.80	1.00	0.77	0.36	0.41	0.05	0.00	0.00	0.00	0.00	0.00
1	10.14	1.00	0.93	0.65	0.60	0.27	0.00	0.00	0.00	0.00	0.00
1	11.65	1.00	0.76	0.15	0.38	0.00	0.06	0.00	0.00	0.00	0.00
1	14.80	1.00	0.78	0.22	0.39	0.00	0.35	0.56	0.00	0.01	0.00
1	17.14	1.00	0.91	0.57	0.47	0.03	0.51	1.00	0.00	0.04	0.00
1	21.65	1.00	0.85	0.72	0.91	0.96	0.70	1.00	0.47	0.00	0.08
1	24.80	1.00	0.92	0.85	0.95	0.97	0.79	0.99	0.64	0.09	0.22
1	27.14	1.00	0.98	0.95	0.99	0.99	0.93	1.00	0.81	0.47	0.34
1	28.65	1.00	1.00	1.00	1.00	1.00	0.95	1.00	1.00	0.74	0.58
1	31.80	1.00	1.00	1.00	1.00	1.00	0.97	1.00	1.00	0.87	0.79
1	34.14	1.00	1.00	1.00	1.00	1.00	1.00	1.00	1.00	0.92	0.92
1	35.15	1.00	1.00	1.00	1.00	1.00	1.00	1.00	1.00	0.81	0.92
1	38.30	1.00	1.00	1.00	1.00	1.00	1.00	1.00	1.00	0.88	0.94
1	40.64	1.00	1.00	1.00	1.00	1.00	1.00	1.00	1.00	0.99	0.99
x' m (1)	y mm (2)	C (3)	C (4)	C (5)	C (6)	C (7)	C (8)	C (9)	C (10)	C (11)	C (12)

Run TL5 (step 10)

Q m^3/s	Step	x' m	C_s m/s	d_o m
0.075	10	0.2, 0.4, 0.6, 0.8, 1.0	2.61	0.297

x' m	y mm	C	C	C	C	C	C	C	C	C	C

(1)	(2)	(3)	(4)	(5)	(6)	(7)	(8)	(9)	(10)	(11)	(12)
$\Delta X =$	(mm)	0-70	0-210	140-210	0-385	175-385	350-735	525-595	700-1085	2100-2485	4200-4585
$t - t_S =$	(s)	0.013	0.04	0.067	0.074	0.107	0.208	0.215	0.342	0.878	1.683
$\Delta X =$	(mm)	70	210	70	385	210	385	70	385	385	385
$(t-t_S)$		0.077	0.231	0.385	0.424	0.616	1.194	1.233	1.965	5.047	9.67
$\sqrt{d_o/g}$											
0.2	4.65	0.93	0.98	1.00	0.98	0.97	0.06	0.00	0.01	0.01	0.00
0.2	7.80	0.91	0.97	1.00	0.98	0.99	0.04	0.00	0.01	0.00	0.00
0.2	10.14	0.91	0.97	1.00	0.97	0.97	0.03	0.00	0.31	0.00	0.00
0.2	11.65	1.00	0.99	1.00	0.81	0.62	0.31	0.38	0.01	0.02	0.18
0.2	14.80	1.00	1.00	1.00	0.71	0.41	0.36	0.19	0.01	0.00	0.20
0.2	17.14	1.00	1.00	1.00	1.00	1.00	0.68	1.00	0.12	0.00	0.51
0.2	21.65	1.00	1.00	1.00	1.00	1.00	0.80	1.00	0.86	0.64	0.36
0.2	24.80	0.79	0.96	1.00	0.98	1.00	0.90	1.00	0.99	0.90	0.51
0.2	27.14	0.50	0.84	0.86	0.90	0.97	0.96	1.00	0.95	0.86	0.52
0.2	28.65	1.00	1.00	1.00	0.93	0.85	0.99	1.00	0.71	0.51	0.26
0.2	31.80	1.00	1.00	1.00	0.80	0.61	0.77	1.00	0.46	0.31	0.15
0.2	34.14	0.86	0.93	0.79	0.59	0.25	0.43	0.82	0.21	0.12	0.10
0.2	35.15	1.00	1.00	1.00	0.68	0.37	0.08	0.29	0.13	0.21	0.23
0.2	38.30	1.00	1.00	1.00	0.68	0.36	0.07	0.22	0.03	0.08	0.13
0.2	40.64	1.00	1.00	1.00	0.70	0.41	0.08	0.04	0.01	0.03	0.02
0.2	41.65	0.43	0.14	0.05	0.07	0.00	0.08	0.05	0.06	0.00	0.00
0.2	44.80	0.54	0.16	0.00	0.10	0.04	0.08	0.06	0.08	0.00	0.00
0.2	47.14	0.57	0.21	0.00	0.11	0.01	0.13	0.00	0.08	0.03	0.01
0.2	51.65	0.22	0.71	0.78	0.72	0.74	0.20	0.21	0.22	0.23	0.00
0.2	54.80	0.26	0.72	0.81	0.76	0.79	0.22	0.32	0.28	0.24	0.02
0.2	57.14	0.28	0.81	1.00	0.83	0.84	0.24	0.30	0.54	0.29	0.03
0.2	61.65	0.76	0.93	1.00	0.82	0.71	0.63	0.45	0.71	0.71	0.37
0.2	64.80	0.84	0.97	1.00	0.88	0.80	0.69	0.60	0.82	0.76	0.51
0.2	67.14	1.00	1.00	1.00	0.96	0.91	0.84	1.00	0.89	0.76	0.66
0.2	71.65	0.64	0.38	0.18	0.63	0.88	0.93	1.00	0.88	0.84	0.91
0.2	74.80	0.52	0.34	0.18	0.58	0.81	0.98	1.00	0.91	0.93	0.96
0.2	77.14	0.54	0.33	0.28	0.60	0.88	0.98	1.00	0.97	1.00	0.99
0.2	81.65	0.97	0.63	0.87	0.82	1.00	1.00	1.00	1.00	1.00	1.00
0.4	4.65	1.00	0.51	0.00	0.26	0.00	0.00	0.00	0.00	0.00	0.00
0.4	7.80	1.00	0.65	0.00	0.32	0.00	0.00	0.00	0.00	0.01	0.00
0.4	10.14	1.00	0.77	0.20	0.39	0.00	0.00	0.00	0.00	0.01	0.00
0.4	11.65	1.00	0.89	0.44	0.46	0.03	0.00	0.00	0.05	0.01	0.00
0.4	14.80	1.00	0.92	0.58	0.51	0.10	0.00	0.00	0.11	0.00	0.00
0.4	17.14	1.00	0.92	0.62	0.61	0.29	0.00	0.00	0.13	0.00	0.01
0.4	21.65	1.00	0.86	0.47	0.46	0.07	0.09	0.06	0.31	0.00	0.03
0.4	24.80	1.00	0.90	0.50	0.53	0.17	0.26	0.24	0.40	0.03	0.03
0.4	27.14	1.00	0.94	0.68	0.56	0.18	0.35	0.43	0.57	0.09	0.01
0.4	28.65	1.00	1.00	1.00	0.95	0.90	0.36	0.26	0.41	0.22	0.07
0.4	31.80	1.00	1.00	1.00	0.98	0.96	0.39	0.28	0.65	0.38	0.13
0.4	34.14	1.00	1.00	1.00	1.00	1.00	0.53	0.44	0.75	0.57	0.26
0.4	35.15	1.00	1.00	1.00	0.96	0.93	0.59	0.44	0.83	0.32	0.46
0.4	38.30	1.00	1.00	1.00	0.95	0.89	0.69	0.61	0.85	0.47	0.53
0.4	40.64	1.00	1.00	1.00	0.95	0.90	0.82	0.70	0.87	0.55	0.64
0.4	41.65	1.00	1.00	1.00	0.94	0.88	0.97	1.00	0.92	0.80	0.64
0.4	44.80	1.00	1.00	1.00	0.94	0.89	0.97	1.00	0.94	0.85	0.74
0.4	47.14	1.00	1.00	1.00	0.96	0.91	0.97	1.00	0.99	0.87	0.83
0.4	51.65	1.00	1.00	1.00	0.84	0.68	1.00	1.00	0.89	0.96	0.82
0.4	54.80	1.00	1.00	1.00	0.88	0.77	1.00	1.00	0.93	0.99	0.85
0.4	57.14	1.00	1.00	1.00	0.87	0.75	1.00	1.00	0.93	1.00	0.88
0.4	61.65	1.00	1.00	1.00	1.00	1.00	0.95	1.00	1.00	1.00	0.96
0.4	64.80	1.00	1.00	1.00	1.00	1.00	0.99	1.00	1.00	1.00	0.96

0.4	67.14	1.00	1.00	1.00	1.00	1.00	1.00	1.00	1.00	1.00	0.96
0.4	71.65	1.00	1.00	1.00	1.00	1.00	0.99	1.00	0.99	1.00	0.95
0.4	74.80	1.00	1.00	1.00	1.00	1.00	0.98	1.00	0.99	1.00	0.98
0.4	77.14	1.00	1.00	1.00	1.00	1.00	0.98	1.00	0.99	1.00	0.94
0.4	81.65	1.00	1.00	1.00	1.00	1.00	1.00	1.00	1.00	0.93	1.00
0.6	4.65	1.00	0.68	0.61	0.45	0.22	0.03	0.00	0.00	0.00	0.00
0.6	7.80	1.00	0.97	0.97	0.72	0.47	0.12	0.09	0.00	0.00	0.00
0.6	10.14	1.00	1.00	1.00	0.81	0.61	0.22	0.26	0.00	0.00	0.00
0.6	11.65	1.00	0.82	1.00	0.57	0.31	0.09	0.07	0.05	0.00	0.00
0.6	14.80	1.00	0.88	1.00	0.63	0.38	0.16	0.09	0.10	0.00	0.01
0.6	17.14	1.00	0.92	1.00	0.69	0.46	0.22	0.17	0.14	0.00	0.01
0.6	21.65	1.00	1.00	1.00	0.91	0.82	0.66	0.37	0.12	0.00	0.01
0.6	24.80	1.00	1.00	1.00	0.93	0.86	0.84	0.66	0.16	0.00	0.00
0.6	27.14	1.00	1.00	1.00	0.96	0.93	0.87	0.74	0.17	0.00	0.02
0.6	28.65	1.00	1.00	1.00	1.00	1.00	0.39	0.33	0.63	0.01	0.02
0.6	31.80	1.00	1.00	1.00	1.00	1.00	0.57	0.41	0.69	0.00	0.01
0.6	34.14	1.00	1.00	1.00	1.00	1.00	0.70	0.52	0.76	0.00	0.02
0.6	35.15	1.00	1.00	1.00	0.99	0.98	0.85	1.00	0.44	0.04	0.00
0.6	38.30	1.00	1.00	1.00	1.00	0.99	0.82	1.00	0.49	0.07	0.01
0.6	40.64	1.00	1.00	1.00	1.00	1.00	0.89	1.00	0.57	0.07	0.03
0.6	41.65	1.00	1.00	1.00	0.94	0.87	0.97	1.00	0.61	0.02	0.02
0.6	44.80	1.00	1.00	1.00	0.97	0.93	0.97	1.00	0.77	0.05	0.04
0.6	47.14	1.00	1.00	1.00	0.97	0.93	0.97	1.00	0.77	0.08	0.03
0.6	51.65	1.00	1.00	1.00	0.99	0.98	0.97	1.00	0.90	0.16	0.23
0.6	54.80	1.00	1.00	1.00	0.97	0.95	1.00	1.00	0.92	0.31	0.33
0.6	57.14	1.00	1.00	1.00	0.99	0.97	1.00	1.00	0.94	0.39	0.36
0.6	61.65	1.00	1.00	1.00	1.00	1.00	0.80	0.80	1.00	0.70	0.61
0.6	64.80	1.00	1.00	1.00	1.00	1.00	0.87	0.86	1.00	0.76	0.84
0.6	67.14	1.00	1.00	1.00	1.00	1.00	0.94	0.99	0.99	0.80	0.87
0.6	71.65	1.00	1.00	1.00	1.00	1.00	1.00	1.00	1.00	0.38	0.63
0.6	74.80	1.00	1.00	1.00	1.00	1.00	1.00	1.00	0.99	0.65	0.73
0.6	77.14	1.00	1.00	1.00	1.00	1.00	1.00	1.00	0.99	0.68	0.82
0.6	81.65	1.00	1.00	1.00	1.00	1.00	1.00	1.00	0.99	0.87	0.46
0.8	4.65	0.27	0.09	0.00	0.04	0.00	0.00	0.00	0.00	0.00	0.00
0.8	7.80	0.44	0.30	0.03	0.15	0.00	0.00	0.00	0.00	0.00	0.00
0.8	10.14	1.00	0.84	0.54	0.43	0.03	0.00	0.00	0.00	0.01	0.00
0.8	11.65	0.21	0.09	0.00	0.04	0.00	0.00	0.00	0.01	0.00	0.00
0.8	14.80	0.25	0.21	0.01	0.11	0.02	0.00	0.00	0.00	0.00	0.00
0.8	17.14	0.47	0.39	0.22	0.20	0.02	0.00	0.00	0.01	0.01	0.00
0.8	21.65	1.00	0.87	0.78	0.84	0.80	0.88	1.00	0.16	0.00	0.00
0.8	24.80	1.00	0.96	1.00	0.96	0.95	0.94	1.00	0.17	0.00	0.00
0.8	27.14	1.00	1.00	1.00	0.99	0.98	0.95	0.91	0.19	0.00	0.01
0.8	28.65	1.00	1.00	1.00	0.99	0.99	0.51	0.35	0.26	0.00	0.00
0.8	31.80	1.00	1.00	0.98	0.98	0.97	0.61	0.44	0.36	0.01	0.02
0.8	34.14	1.00	1.00	1.00	0.98	0.97	0.83	1.00	0.58	0.01	0.01
0.8	35.15	1.00	1.00	1.00	0.99	0.97	0.87	0.75	0.03	0.00	0.02
0.8	38.30	1.00	1.00	1.00	1.00	1.00	0.94	1.00	0.19	0.00	0.07
0.8	40.64	1.00	1.00	1.00	1.00	1.00	0.98	1.00	0.36	0.00	0.05
0.8	41.65	1.00	1.00	1.00	1.00	1.00	0.76	0.92	0.07	0.00	0.01
0.8	44.80	1.00	1.00	1.00	1.00	1.00	0.79	0.90	0.20	0.00	0.01
0.8	47.14	1.00	1.00	1.00	1.00	1.00	0.84	0.89	0.27	0.00	0.01
0.8	51.65	1.00	1.00	1.00	1.00	1.00	0.81	1.00	0.32	0.04	0.02
0.8	54.80	1.00	1.00	1.00	1.00	1.00	0.84	1.00	0.48	0.07	0.02
0.8	57.14	1.00	1.00	1.00	1.00	1.00	0.86	1.00	0.52	0.05	0.03
0.8	61.65	1.00	1.00	1.00	1.00	1.00	0.96	1.00	0.85	0.67	0.16
0.8	64.80	1.00	1.00	1.00	1.00	1.00	0.98	1.00	0.90	0.66	0.22
0.8	67.14	1.00	1.00	1.00	1.00	1.00	0.99	1.00	0.93	0.75	0.19
0.8	71.65	1.00	1.00	1.00	1.00	1.00	1.00	1.00	0.94	0.51	0.18
0.8	74.80	1.00	1.00	1.00	1.00	1.00	1.00	1.00	0.95	0.63	0.22

0.8	77.14	1.00	1.00	1.00	1.00	1.00	1.00	1.00	0.96	0.67	0.31
0.8	81.65	1.00	1.00	1.00	1.00	1.00	1.00	1.00	0.97	0.72	0.82
0.8	84.80	1.00	1.00	1.00	1.00	1.00	1.00	1.00	0.98	0.73	0.83
0.8	87.14	1.00	1.00	1.00	1.00	1.00	1.00	1.00	0.98	0.73	0.79
0.8	91.65	1.00	1.00	1.00	1.00	1.00	1.00	1.00	1.00	0.98	0.94
0.8	94.80	1.00	1.00	1.00	1.00	1.00	1.00	1.00	1.00	0.98	0.94
0.8	97.14	1.00	1.00	1.00	1.00	1.00	1.00	1.00	0.99	0.99	0.93
1	4.65	1.00	0.21	0.00	0.10	0.00	0.00	0.00	0.00	0.00	0.00
1	7.80	1.00	0.33	0.00	0.17	0.00	0.00	0.00	0.00	0.00	0.00
1	10.14	1.00	0.21	0.00	0.13	0.05	0.02	0.00	0.00	0.00	0.00
1	11.65	1.00	0.75	0.15	0.38	0.00	0.01	0.03	0.00	0.00	0.00
1	14.80	1.00	0.88	0.38	0.48	0.08	0.01	0.00	0.00	0.00	0.00
1	17.14	1.00	1.00	1.00	0.63	0.25	0.04	0.06	0.00	0.00	0.00
1	21.65	1.00	0.79	0.64	0.86	0.94	0.09	0.00	0.01	0.00	0.01
1	24.80	1.00	0.88	0.79	0.94	1.00	0.13	0.00	0.00	0.01	0.02
1	27.14	1.00	0.93	0.85	0.97	1.00	0.14	0.00	0.01	0.00	0.01
1	28.65	1.00	1.00	1.00	0.78	0.55	0.08	0.15	0.07	0.01	0.01
1	31.80	1.00	1.00	1.00	0.81	0.61	0.23	0.44	0.16	0.01	0.00
1	34.14	1.00	1.00	1.00	0.84	0.69	0.42	0.51	0.24	0.01	0.01
1	35.15	1.00	1.00	1.00	1.00	1.00	0.17	0.40	0.17	0.00	0.01
1	38.30	1.00	1.00	1.00	1.00	1.00	0.28	0.54	0.28	0.00	0.02
1	40.64	1.00	1.00	1.00	1.00	1.00	0.46	0.83	0.38	0.00	0.02
1	41.65	1.00	1.00	1.00	1.00	1.00	0.66	0.54	0.23	0.10	0.01
1	44.80	1.00	1.00	1.00	0.99	0.97	0.77	1.00	0.36	0.21	0.02
1	47.14	1.00	1.00	1.00	0.98	0.97	0.86	1.00	0.39	0.24	0.01
1	51.65	1.00	1.00	1.00	1.00	1.00	0.95	1.00	0.59	0.21	0.60
1	54.80	1.00	1.00	1.00	1.00	1.00	0.93	0.69	0.64	0.30	0.70
1	57.14	1.00	1.00	1.00	1.00	1.00	0.95	0.80	0.65	0.61	0.75
1	61.65	1.00	1.00	1.00	1.00	1.00	1.00	1.00	0.85	0.76	0.40
1	64.80	1.00	1.00	1.00	1.00	1.00	1.00	1.00	0.92	0.84	0.47
1	67.14	1.00	1.00	1.00	1.00	1.00	1.00	1.00	0.94	0.90	0.55
1	71.65	1.00	1.00	1.00	1.00	1.00	1.00	1.00	1.00	0.97	0.93
1	71.65	1.00	1.00	1.00	1.00	1.00	1.00	1.00	1.00	0.97	0.93
1	74.80	1.00	1.00	1.00	1.00	1.00	1.00	1.00	1.00	1.00	0.94
1	77.14	1.00	1.00	1.00	1.00	1.00	1.00	1.00	1.00	1.00	0.94
1	81.65	1.00	1.00	1.00	1.00	1.00	1.00	1.00	1.00	0.93	0.90
x' m (1)	y mm (2)	C (3)	C (4)	C (5)	C (6)	C (7)	C (8)	C (9)	C (10)	C (11)	C (12)

Run TL5 (step 16)

Q m^3/s	Step	x' m	C_s m/s	d_o m
0.075	16	0.2, 0.4, 0.6, 0.8, 1.0	2.43	0.297

x' m (1)	y mm (2)	C (3)	C (4)	C (5)	C (6)	C (7)	C (8)	C (9)	C (10)	C (11)	C (12)
$\Delta X =$	(mm)	0-70	0-210	140-210	0-385	175-385	350-735	525-595	700-1085	2100-2485	4200-4585
$t - t_s =$	(s)	0.0144	0.0432	0.072	0.0792	0.1152	0.2233	0.2305	0.3673	0.9434	1.8076
$\Delta X =$	(mm)	70	210	70	385	210	385	70	385	385	385
$\frac{(t-t_s)}{\sqrt{d_o/g}}$		0.0828	0.2483	0.4138	0.4552	0.6621	1.2828	1.3242	2.1104	5.4208	10.386

0.2	4.65	1.00	0.80	0.51	0.44	0.08	0.00	0.00	0.00	0.00	0.03
0.2	7.80	0.60	0.64	0.91	0.36	0.08	0.08	0.01	0.00	0.00	0.00
0.2	10.14	1.00	1.00	1.00	0.76	0.51	0.22	0.00	0.13	0.11	0.04
0.2	11.65	1.00	0.72	0.04	0.38	0.04	0.02	0.06	0.00	0.01	0.04
0.2	14.80	1.00	0.90	0.52	0.46	0.02	0.06	0.27	0.05	0.06	0.01
0.2	17.14	0.64	0.85	0.78	0.46	0.07	0.36	1.00	0.01	0.25	0.17
0.2	21.65	1.00	1.00	1.00	0.95	0.90	0.95	1.00	0.82	0.63	0.24
0.2	24.80	0.90	0.95	0.98	0.94	0.93	0.95	1.00	0.87	0.73	0.35
0.2	27.14	0.67	0.88	1.00	0.89	0.89	0.72	0.62	0.39	0.61	0.56
0.2	28.65	0.80	0.53	0.07	0.38	0.23	0.50	0.33	0.35	0.48	0.19
0.2	31.80	0.81	0.40	0.09	0.29	0.18	0.35	0.21	0.23	0.21	0.11
0.2	34.14	0.75	0.36	0.28	0.22	0.07	0.13	0.00	0.06	0.09	0.08
0.2	35.15	0.00	0.00	0.00	0.00	0.00	0.00	0.00	0.06	0.00	0.17
0.2	38.30	0.00	0.01	0.00	0.01	0.02	0.04	0.19	0.06	0.00	0.18
0.2	40.64	0.07	0.02	0.00	0.05	0.09	0.07	0.34	0.06	0.03	0.18
0.2	41.65	0.00	0.13	0.32	0.11	0.09	0.01	0.00	0.05	0.01	0.07
0.2	44.80	0.00	0.36	0.51	0.25	0.13	0.05	0.00	0.10	0.00	0.09
0.2	47.14	0.00	0.43	0.52	0.30	0.17	0.07	0.00	0.18	0.07	0.13
0.2	51.65	1.00	0.90	0.74	0.57	0.25	0.21	0.00	0.57	0.07	0.39
0.2	54.80	1.00	0.94	0.84	0.62	0.31	0.36	0.02	0.62	0.12	0.47
0.2	57.14	1.00	0.95	0.88	0.63	0.31	0.43	0.10	0.71	0.20	0.56
0.2	61.65	0.01	0.21	0.76	0.51	0.82	0.82	0.65	0.81	0.70	0.72
0.2	64.80	0.04	0.24	0.79	0.56	0.87	0.86	0.67	0.90	0.81	0.81
0.2	67.14	0.06	0.26	0.82	0.62	0.98	0.87	0.73	1.00	0.93	0.88
0.2	71.65	1.00	1.00	1.00	0.94	0.89	0.70	0.72	1.00	0.86	0.98
0.2	74.80	1.00	1.00	1.00	0.94	0.88	0.74	0.87	1.00	0.90	1.00
0.2	77.14	1.00	1.00	1.00	0.94	0.88	0.81	1.00	1.00	1.00	1.00
0.2	81.65	0.91	0.90	1.00	0.95	1.00	0.99	1.00	0.99	1.00	0.94
0.4	4.65	0.93	0.71	0.16	0.37	0.03	0.02	0.06	0.00	0.02	0.02
0.4	7.80	1.00	0.80	0.27	0.45	0.09	0.02	0.03	0.00	0.05	0.02
0.4	10.14	1.00	0.86	0.46	0.57	0.27	0.04	0.01	0.01	0.13	0.02
0.4	11.65	0.91	0.82	0.70	0.47	0.12	0.18	0.11	0.01	0.04	0.01
0.4	14.80	0.99	0.88	0.78	0.55	0.23	0.34	0.27	0.11	0.07	0.01
0.4	17.14	1.00	0.94	0.81	0.66	0.38	0.53	0.55	0.16	0.06	0.01
0.4	21.65	1.00	0.92	0.90	0.61	0.30	0.04	0.03	0.31	0.21	0.11
0.4	24.80	1.00	0.97	0.99	0.72	0.48	0.08	0.02	0.40	0.25	0.17
0.4	27.14	1.00	1.00	0.99	0.82	0.64	0.18	0.15	0.51	0.28	0.19
0.4	28.65	1.00	1.00	1.00	0.95	0.91	0.39	0.03	0.71	0.13	0.20
0.4	31.80	1.00	1.00	1.00	0.95	0.90	0.54	0.19	0.87	0.16	0.24
0.4	34.14	1.00	1.00	0.98	0.98	0.97	0.59	0.32	0.92	0.28	0.33
0.4	35.15	1.00	1.00	1.00	0.94	0.88	0.77	1.00	0.77	0.30	0.49
0.4	38.30	1.00	1.00	1.00	0.94	0.88	0.75	1.00	0.88	0.36	0.62
0.4	40.64	1.00	1.00	1.00	0.96	0.92	0.80	1.00	0.92	0.45	0.64
0.4	41.65	1.00	1.00	1.00	0.97	0.94	0.77	0.80	0.85	0.58	0.51
0.4	44.80	1.00	1.00	1.00	0.97	0.94	0.82	0.87	0.89	0.73	0.65
0.4	47.14	1.00	1.00	1.00	0.99	0.98	0.82	0.89	0.83	0.81	0.68
0.4	51.65	1.00	1.00	1.00	1.00	1.00	0.83	0.62	0.87	0.84	0.51
0.4	54.80	1.00	1.00	1.00	1.00	1.00	0.86	0.68	0.92	0.93	0.66
0.4	57.14	1.00	1.00	1.00	1.00	0.99	0.92	0.86	0.94	0.94	0.70
0.4	61.65	1.00	1.00	1.00	1.00	1.00	0.95	1.00	0.89	0.92	0.84
0.4	64.80	1.00	1.00	1.00	1.00	1.00	0.98	1.00	0.93	0.95	0.90
0.4	67.14	1.00	1.00	1.00	1.00	1.00	0.98	1.00	0.94	0.96	0.92
0.4	71.65	1.00	1.00	1.00	1.00	1.00	1.00	1.00	1.00	0.91	0.96
0.4	74.80	1.00	1.00	1.00	1.00	1.00	1.00	1.00	1.00	0.94	0.98
0.4	77.14	1.00	1.00	1.00	1.00	1.00	1.00	1.00	1.00	0.98	0.94
0.4	81.65	1.00	1.00	1.00	1.00	1.00	1.00	1.00	1.00	1.00	0.97
0.4	84.80	1.00	1.00	1.00	1.00	1.00	1.00	1.00	1.00	1.00	0.98
0.4	87.14	1.00	1.00	1.00	1.00	1.00	1.00	1.00	1.00	1.00	1.00
0.6	4.65	0.68	0.53	0.16	0.26	0.00	0.00	0.00	0.00	0.00	0.00

0.6	7.80	0.87	0.80	0.43	0.41	0.01	0.00	0.00	0.00	0.00	0.00
0.6	10.14	1.00	0.91	0.60	0.54	0.17	0.01	0.00	0.00	0.00	0.00
0.6	11.65	0.88	0.39	0.24	0.36	0.32	0.00	0.00	0.00	0.00	0.00
0.6	14.80	0.90	0.56	0.54	0.52	0.48	0.05	0.02	0.00	0.00	0.02
0.6	17.14	0.90	0.61	0.58	0.65	0.68	0.27	0.52	0.01	0.00	0.00
0.6	21.65	1.00	0.96	0.81	0.72	0.48	0.09	0.00	0.01	0.01	0.01
0.6	24.80	1.00	0.98	0.91	0.78	0.58	0.12	0.00	0.01	0.01	0.02
0.6	27.14	1.00	1.00	1.00	0.86	0.71	0.15	0.04	0.02	0.00	0.00
0.6	28.65	1.00	0.97	1.00	0.94	0.91	0.35	0.27	0.06	0.05	0.09
0.6	31.80	1.00	0.96	1.00	0.94	0.92	0.38	0.42	0.10	0.06	0.13
0.6	34.14	1.00	0.96	1.00	0.94	0.93	0.42	0.55	0.11	0.09	0.10
0.6	35.15	1.00	1.00	1.00	0.95	0.90	0.56	0.80	0.05	0.04	0.05
0.6	38.30	1.00	1.00	1.00	0.95	0.90	0.64	0.79	0.07	0.03	0.07
0.6	40.64	1.00	1.00	1.00	0.98	0.96	0.75	0.75	0.13	0.11	0.04
0.6	41.65	1.00	1.00	1.00	1.00	1.00	0.88	0.92	0.18	0.00	0.12
0.6	44.80	1.00	1.00	1.00	1.00	1.00	0.92	0.88	0.21	0.02	0.17
0.6	47.14	1.00	1.00	1.00	1.00	1.00	0.94	0.89	0.19	0.03	0.21
0.6	51.65	1.00	1.00	1.00	1.00	1.00	0.96	1.00	0.18	0.17	0.25
0.6	54.80	1.00	1.00	1.00	1.00	1.00	0.96	1.00	0.43	0.23	0.27
0.6	57.14	1.00	1.00	1.00	1.00	1.00	0.99	1.00	0.45	0.26	0.33
0.6	61.65	1.00	1.00	1.00	0.95	0.90	0.90	1.00	0.57	0.33	0.37
0.6	64.80	1.00	0.95	0.85	0.94	0.92	0.95	1.00	0.63	0.43	0.51
0.6	67.14	1.00	0.96	0.88	0.95	0.95	0.94	1.00	0.66	0.46	0.56
0.6	71.65	1.00	1.00	1.00	1.00	1.00	0.83	0.59	0.77	0.66	0.51
0.6	74.80	1.00	1.00	1.00	1.00	1.00	0.92	0.73	0.87	0.78	0.67
0.6	77.14	1.00	1.00	1.00	1.00	1.00	0.94	0.74	0.92	0.72	0.77
0.6	81.65	1.00	1.00	1.00	1.00	1.00	0.96	1.00	1.00	0.81	0.88
0.6	84.80	1.00	1.00	1.00	1.00	1.00	0.99	1.00	1.00	0.92	0.94
0.6	87.14	1.00	1.00	1.00	1.00	1.00	1.00	1.00	1.00	0.93	0.93
0.6	91.65	1.00	1.00	1.00	1.00	1.00	1.00	1.00	0.93	0.92	0.93
0.8	4.65	0.73	0.23	0.03	0.12	0.00	0.00	0.00	0.00	0.00	0.00
0.8	7.80	0.98	0.83	0.56	0.44	0.06	0.01	0.00	0.00	0.00	0.00
0.8	10.14	1.00	0.96	0.78	0.55	0.15	0.06	0.01	0.00	0.00	0.00
0.8	11.65	0.79	0.47	0.13	0.23	0.00	0.00	0.00	0.00	0.00	0.01
0.8	14.80	1.00	0.75	0.42	0.43	0.10	0.04	0.00	0.00	0.01	0.01
0.8	17.14	1.00	0.86	0.63	0.52	0.18	0.09	0.04	0.00	0.00	0.00
0.8	21.65	1.00	1.00	1.00	0.81	0.62	0.68	0.74	0.43	0.00	0.00
0.8	24.80	1.00	1.00	1.00	0.89	0.77	0.82	0.87	0.51	0.00	0.00
0.8	27.14	1.00	1.00	1.00	0.94	0.88	0.93	0.94	0.53	0.00	0.00
0.8	28.65	1.00	1.00	1.00	1.00	1.00	0.45	0.84	0.00	0.02	0.01
0.8	31.80	1.00	1.00	1.00	1.00	1.00	0.71	1.00	0.05	0.02	0.00
0.8	34.14	1.00	1.00	1.00	1.00	0.99	0.88	1.00	0.20	0.03	0.01
0.8	35.15	1.00	1.00	1.00	0.96	0.91	1.00	1.00	0.24	0.00	0.01
0.8	38.30	1.00	1.00	1.00	0.96	0.92	1.00	1.00	0.24	0.02	0.00
0.8	40.64	1.00	1.00	1.00	0.96	0.92	1.00	1.00	0.26	0.02	0.00
0.8	41.65	1.00	1.00	1.00	1.00	1.00	0.72	0.84	0.08	0.07	0.04
0.8	44.80	1.00	1.00	1.00	1.00	1.00	0.84	0.82	0.30	0.09	0.10
0.8	47.14	1.00	1.00	1.00	1.00	1.00	0.87	0.84	0.41	0.10	0.11
0.8	51.65	1.00	1.00	1.00	1.00	1.00	0.97	0.95	0.32	0.30	0.21
0.8	54.80	1.00	1.00	1.00	1.00	1.00	0.98	1.00	0.53	0.40	0.26
0.8	57.14	1.00	1.00	1.00	1.00	1.00	0.98	1.00	0.73	0.45	0.32
0.8	61.65	1.00	1.00	1.00	1.00	1.00	0.93	1.00	0.60	0.76	0.60
0.8	64.80	1.00	1.00	1.00	1.00	1.00	0.98	1.00	0.75	0.85	0.77
0.8	67.14	1.00	1.00	1.00	1.00	1.00	0.99	1.00	0.78	0.85	0.79
0.8	71.65	1.00	1.00	1.00	1.00	1.00	0.99	1.00	0.95	0.78	0.79
0.8	74.80	1.00	1.00	1.00	1.00	1.00	1.00	1.00	0.98	0.86	0.85
0.8	77.14	1.00	1.00	1.00	1.00	1.00	1.00	1.00	1.00	0.94	0.90
0.8	81.65	1.00	1.00	1.00	1.00	1.00	1.00	1.00	1.00	0.94	0.96
0.8	84.80	1.00	1.00	1.00	1.00	1.00	1.00	1.00	1.00	0.99	1.00

1	4.65	0.83	0.43	0.00	0.22	0.00	0.00	0.00	0.00	0.00	0.00
1	7.80	0.91	0.51	0.00	0.26	0.02	0.00	0.00	0.00	0.00	0.00
1	10.14	0.89	0.49	0.00	0.34	0.19	0.00	0.00	0.00	0.00	0.00
1	11.65	0.94	0.75	1.00	0.50	0.25	0.00	0.00	0.00	0.00	0.00
1	14.80	0.77	0.90	0.94	0.49	0.09	0.00	0.02	0.00	0.00	0.00
1	17.14	0.90	0.96	1.00	0.55	0.15	0.00	0.00	0.00	0.00	0.00
1	21.65	1.00	0.95	0.77	0.81	0.67	0.18	0.00	0.00	0.00	0.00
1	24.80	1.00	1.00	0.98	0.92	0.85	0.31	0.03	0.00	0.00	0.02
1	27.14	1.00	0.98	0.92	0.98	0.98	0.25	0.14	0.00	0.02	0.08
1	28.65	1.00	1.00	1.00	0.98	0.96	0.22	0.02	0.02	0.02	0.28
1	31.80	1.00	1.00	1.00	0.96	0.92	0.35	0.11	0.15	0.01	0.36
1	34.14	1.00	1.00	1.00	0.99	0.97	0.51	0.23	0.47	0.03	0.46
1	35.15	1.00	1.00	1.00	1.00	1.00	1.00	1.00	0.53	0.77	0.91
1	38.30	1.00	1.00	1.00	1.00	1.00	1.00	1.00	0.61	0.93	0.99
1	40.64	1.00	1.00	1.00	1.00	1.00	1.00	1.00	0.70	0.97	1.00
1	41.65	1.00	0.99	0.95	0.94	0.90	0.96	1.00	0.73	0.22	0.45
1	44.80	1.00	0.98	0.91	0.98	0.98	0.95	1.00	0.86	0.38	0.75
1	47.14	1.00	0.98	0.90	0.98	0.98	0.96	1.00	0.89	0.50	0.96
1	51.65	1.00	1.00	1.00	1.00	1.00	1.00	1.00	0.95	1.00	0.99
1	54.80	1.00	1.00	1.00	1.00	1.00	1.00	1.00	0.96	1.00	1.00
1	57.14	1.00	1.00	1.00	1.00	1.00	1.00	1.00	1.00	1.00	1.00
1	61.65	1.00	1.00	1.00	1.00	1.00	1.00	1.00	0.98	0.95	0.97
1	64.80	1.00	1.00	1.00	1.00	1.00	1.00	1.00	0.99	0.97	1.00
1	67.14	1.00	1.00	1.00	1.00	1.00	1.00	1.00	0.99	1.00	1.00
1	71.65	1.00	1.00	1.00	1.00	1.00	1.00	1.00	1.00	1.00	1.00
x' m (1)	y mm (2)	C (3)	C (4)	C (5)	C (6)	C (7)	C (8)	C (9)	C (10)	C (11)	C (12)

VI.3 Experiments Series 2 - Bubble count rate data

Location :	University of Queensland (Australia)
Date :	June-Aug. 2002
Experiments by :	Chung Hwee "Jerry" LIM and York-wee TAN
Data processing by :	H. CHANSON
Experiment characteristics :	Flume : length: 25 m, width: 0.5 m, slope: 3.4 degrees, step height: 0.0715 m, step length: 1.2 m. Inflow conditions : nozzle depth d_n = 0.03 m. First step : 2.4 m long, equipped with sidewall deflectors.
Instrumentation :	Single-tip conductivity probe (Ø = 0.35 mm).
Comments :	Data calculated for a minimum control volume Δx of 70 mm.

Experimental results in terms of bubble count rates were calculated during a short time interval ΔT such as $\Delta T = \Delta X/C_S$ where C_S is the measured surge front celerity and ΔX is the control volume streamwise length. ΔX was selected to be a multiple of Δx = 70 mm : i.e., ΔX = I*Δx where I is an integrer equal or larger than unity.

In turn, the data calculated along ΔX correspond to a dimensionless time $(t - t_S)$ where t_S is the time of passage of wave front. In the following paragraphs, the data are typically presented in the following form:

Legend	Streamwise control volume length	Corresponding time
ΔX = 210-385 mm	ΔX = 175 mm	$0.210/C_S \leq (t - t_S) \leq 0.385/C_S$

Run TL1

Q m^3/s	Step	x' m	C_S m/s	d_o m
0.040	16	0.2, 0.4, 0.6, 0.8, 1.0	1.97	0.195

x' m (1)	y mm (2)	F Hz (3)	F Hz (4)	F Hz (5)	F Hz (6)	F Hz (7)	F Hz (8)	F Hz (9)	F Hz (10)	F Hz (11)	F Hz (12)
$\Delta X =$	(mm)	0-70	0-210	140-210	0-385	175-385	350-735	525-595	700-1085	2100-2485	4200-4585
$t - t_S =$	(s)	0.018	0.053	0.089	0.098	0.142	0.275	0.284	0.453	1.164	2.23
$\Delta X =$	(mm)	70	210	70	385	210	385	70	385	385	385
$\frac{(t-t_S)}{\sqrt{d_o/g}}$		0.126	0.378	0.629	0.692	1.007	1.951	2.014	3.21	8.245	15.8
0.2	4.65	0.0	93.8	0.0	25.7	0.3	41.1	0.0	10.3	0.0	0.0
0.2	7.8	56.3	215.8	28.1	59.2	0.4	18.0	0.0	18.0	0.0	0.0
0.2	10.14	84.4	206.4	0.0	56.6	0.5	23.1	28.1	10.3	15.4	5.1
0.2	11.65	0.0	56.3	0.0	15.4	0.5	10.3	0.0	36.0	15.4	30.7
0.2	14.8	28.1	75.0	0.0	20.6	0.0	0.0	0.0	25.7	28.1	25.6
0.2	17.14	56.3	56.3	0.0	15.4	0.3	10.3	0.0	18.0	5.1	15.4
0.2	21.65	0.0	93.8	28.1	25.7	0.7	20.6	0.0	12.9	0.0	38.4
0.2	24.8	28.1	84.4	0.0	23.1	1.3	41.1	0.0	12.9	0.0	10.2
0.2	27.14	0.0	28.1	0.0	7.7	1.3	25.7	0.0	28.3	5.1	17.9
0.2	28.65	0.0	75.0	0.0	20.6	8.4	7.7	0.0	7.7	5.1	5.1
0.2	31.8	0.0	75.0	0.0	20.6	8.6	10.3	0.0	28.3	5.1	38.4
0.2	34.14	0.0	65.7	0.0	18.0	8.7	5.1	0.0	30.9	17.9	53.7
0.2	35.15	0.0	93.8	28.1	25.7	6.0	23.1	0.0	28.3	5.1	20.5
0.2	38.3	0.0	75.0	56.3	20.6	7.0	15.4	0.0	41.1	30.7	35.8
0.2	40.64	0.0	93.8	84.4	25.7	7.9	10.3	0.0	36.0	46.1	48.6
0.2	41.65	0.0	9.4	0.0	2.6	8.5	18.0	0.0	25.7	30.7	56.3
0.2	44.8	0.0	9.4	0.0	2.6	8.7	18.0	0.0	10.3	33.3	28.1
0.2	47.14	0.0	18.8	0.0	5.1	9.1	10.3	56.3	5.1	38.4	28.1
0.4	4.65	28.1	112.6	0.0	30.9	0.0	0.0	0.0	0.0	0.0	7.7
0.4	7.8	84.4	206.4	0.0	56.6	0.0	0.0	0.0	5.1	0.0	25.6
0.4	10.14	28.1	178.2	56.3	48.9	0.2	10.3	0.0	12.9	5.1	25.6
0.4	11.65	0.0	28.1	0.0	7.7	2.1	30.9	56.3	23.1	2.6	7.7
0.4	14.8	0.0	28.1	0.0	7.7	4.1	59.2	28.1	30.9	15.4	5.1
0.4	17.14	0.0	37.5	0.0	10.3	5.6	43.7	56.3	43.7	20.5	10.2
0.4	21.65	0.0	140.7	56.3	38.6	2.8	43.7	84.4	15.4	43.5	35.8
0.4	24.8	0.0	122.0	56.3	33.4	4.3	79.7	28.1	41.1	66.5	51.2
0.4	27.14	0.0	46.9	28.1	12.9	5.2	72.0	84.4	64.3	38.4	51.2
0.4	28.65	0.0	37.5	0.0	10.3	9.0	10.3	0.0	51.4	87.0	104.9
0.4	31.8	0.0	37.5	28.1	10.3	9.3	5.1	0.0	30.9	61.4	74.2
0.4	34.14	0.0	28.1	0.0	7.7	9.2	2.6	0.0	25.7	43.5	35.8
0.4	35.15	0.0	37.5	28.1	10.3	3.9	30.9	28.1	30.9	53.7	46.1
0.4	38.3	0.0	37.5	0.0	10.3	4.8	46.3	28.1	33.4	71.6	40.9
0.4	40.64	0.0	37.5	0.0	10.3	5.8	43.7	56.3	48.9	84.4	40.9
0.4	41.65	0.0	37.5	0.0	10.3	8.8	30.9	56.3	30.9	10.2	40.9
0.4	44.8	0.0	18.8	0.0	5.1	8.5	30.9	28.1	30.9	10.2	43.5
0.4	47.14	0.0	18.8	0.0	5.1	8.6	30.9	56.3	30.9	15.4	51.2
0.6	4.65	56.3	75.0	0.0	20.6	0.0	0.0	0.0	0.0	0.0	0.0
0.6	7.8	0.0	56.3	84.4	15.4	0.0	0.0	0.0	0.0	0.0	0.0
0.6	10.14	0.0	56.3	28.1	15.4	0.1	10.3	56.3	5.1	0.0	5.1
0.6	11.65	0.0	112.6	28.1	30.9	0.7	20.6	0.0	18.0	0.0	0.0
0.6	14.8	28.1	75.0	0.0	20.6	1.4	41.1	28.1	23.1	10.2	10.2
0.6	17.14	0.0	103.2	112.6	28.3	1.9	30.9	56.3	38.6	15.4	23.0
0.6	21.65	0.0	0.0	0.0	0.0	6.0	36.0	0.0	18.0	89.5	74.2

0.6	24.8	0.0	0.0	0.0	0.0	7.0	51.4	0.0	43.7	97.2	84.4
0.6	27.14	0.0	0.0	0.0	0.0	7.8	51.4	0.0	36.0	69.1	46.1
0.6	28.65	0.0	0.0	0.0	0.0	9.4	0.0	0.0	15.4	81.9	40.9
0.6	31.8	0.0	0.0	0.0	0.0	9.3	5.1	0.0	15.4	58.8	20.5
0.6	34.14	0.0	18.8	0.0	5.1	9.4	0.0	0.0	15.4	56.3	0.0
0.6	35.15	0.0	0.0	0.0	0.0	8.9	5.1	0.0	0.0	10.2	69.1
0.6	38.3	0.0	0.0	0.0	0.0	9.0	5.1	0.0	0.0	10.2	51.2
0.6	40.64	0.0	0.0	0.0	0.0	9.0	5.1	0.0	0.0	15.4	30.7
0.6	41.65	0.0	0.0	0.0	0.0	9.4	0.0	0.0	0.0	0.0	15.4
0.6	44.8	0.0	0.0	0.0	0.0	9.4	0.0	0.0	0.0	0.0	5.1
0.6	47.14	0.0	0.0	0.0	0.0	9.4	0.0	0.0	0.0	0.0	5.1
x'	y	F	F	F	F	F	F	F	F	F	F
m	mm	Hz	Hz	Hz	Hz	Hz	Hz	Hz	Hz	Hz	Hz
(1)	(2)	(3)	(4)	(5)	(6)	(7)	(8)	(9)	(10)	(11)	(12)
0.8	4.65	0.0	37.5	0.0	10.3	0.0	0.0	0.0	0.0	0.0	0.0
0.8	7.8	28.1	131.3	56.3	36.0	0.0	0.0	0.0	0.0	0.0	0.0
0.8	10.14	84.4	187.6	0.0	51.4	0.0	0.0	0.0	0.0	0.0	0.0
0.8	11.65	0.0	37.5	28.1	10.3	0.4	20.6	28.1	0.0	0.0	5.1
0.8	14.8	0.0	56.3	0.0	15.4	1.8	25.7	56.3	10.3	0.0	10.2
0.8	17.14	0.0	140.7	0.0	38.6	4.6	12.9	28.1	20.6	10.2	20.5
0.8	21.65	0.0	37.5	0.0	10.3	6.6	20.6	84.4	48.9	51.2	53.7
0.8	24.8	0.0	75.0	0.0	20.6	8.1	25.7	0.0	41.1	69.1	58.8
0.8	27.14	0.0	28.1	0.0	7.7	8.7	23.1	0.0	20.6	61.4	25.6
0.8	28.65	0.0	0.0	0.0	0.0	8.9	15.4	0.0	0.0	20.5	5.1
0.8	31.8	0.0	0.0	0.0	0.0	9.4	0.0	0.0	0.0	15.4	23.0
0.8	34.8	0.0	0.0	0.0	0.0	9.4	0.0	0.0	0.0	0.0	10.2
0.8	35.15	0.0	0.0	0.0	0.0	9.4	0.0	0.0	0.0	0.0	15.4
0.8	38.3	0.0	0.0	0.0	0.0	9.4	0.0	0.0	0.0	0.0	0.0
0.8	40.64	0.0	0.0	0.0	0.0	9.4	0.0	0.0	0.0	0.0	0.0
0.8	41.65	0.0	0.0	0.0	0.0	9.4	0.0	0.0	0.0	0.0	0.0
0.8	44.8	0.0	0.0	0.0	0.0	9.4	0.0	0.0	0.0	0.0	0.0
1	4.65	0.0	37.5	0.0	10.3	0.0	0.0	0.0	0.0	0.0	0.0
1	7.8	0.0	18.8	28.1	5.1	0.0	0.0	0.0	0.0	0.0	0.0
1	10.14	0.0	56.3	28.1	15.4	0.0	0.0	0.0	0.0	0.0	0.0
1	11.65	0.0	0.0	0.0	0.0	0.5	5.1	0.0	0.0	10.2	0.0
1	14.8	0.0	112.6	84.4	30.9	1.9	38.6	28.1	25.7	15.4	0.0
1	17.14	0.0	122.0	56.3	33.4	5.0	82.3	28.1	69.4	33.3	2.6
1	21.65	0.0	0.0	0.0	0.0	9.4	0.0	0.0	61.7	30.7	56.3
1	24.8	0.0	0.0	0.0	0.0	9.4	0.0	0.0	56.6	15.4	107.5
1	27.14	0.0	0.0	0.0	0.0	9.4	0.0	0.0	20.6	46.1	87.0
1	28.65	0.0	0.0	0.0	0.0	9.4	0.0	0.0	36.0	0.0	43.5
1	31.8	0.0	0.0	0.0	0.0	9.4	0.0	0.0	0.0	0.0	23.0
1	34.14	0.0	0.0	0.0	0.0	9.4	0.0	0.0	0.0	0.0	10.2
1	35.15	0.0	0.0	0.0	0.0	9.4	0.0	0.0	0.0	0.0	61.4
1	38.3	0.0	0.0	0.0	0.0	9.4	0.0	0.0	0.0	0.0	25.6
1	40.64	0.0	0.0	0.0	0.0	9.4	0.0	0.0	0.0	0.0	15.4
x'	y	F	F	F	F	F	F	F	F	F	F
m	mm	Hz	Hz	Hz	Hz	Hz	Hz	Hz	Hz	Hz	Hz
(1)	(2)	(3)	(4)	(5)	(6)	(7)	(8)	(9)	(10)	(11)	(12)

Run TL3

Q m^3/s	Step	x' m	C_S m/s	d_o m
0.055	16	0.2, 0.4, 0.6, 0.8, 1.0	2.14	0.241

x'	y	F	F	F	F	F	F	F	F	F	F

m (1)	mm (2)	Hz (3)	Hz (4)	Hz (5)	Hz (6)	Hz (7)	Hz (8)	Hz (9)	Hz (10)	Hz (11)	Hz (12)
$\Delta X =$	(mm)	0-70	0-210	140-210	0-385	175-385	350-735	525-595	700-1085	2100-2485	4200-4585
$t - t_S =$	(s)	0.016	0.049	0.082	0.09	0.131	0.254	0.262	0.417	1.071	2.053
$\Delta X =$	(mm)	70	210	70	385	210	385	70	385	385	385
$\frac{(t-t_S)}{\sqrt{d_o/g}}$		0.104	0.313	0.521	0.573	0.834	1.615	1.667	2.657	6.826	13.08
0.2	4.65	30.6	142.7	30.6	39.1	0.8	27.9	0.0	5.6	16.7	0.0
0.2	7.80	30.6	81.5	0.0	22.3	0.0	0.0	0.0	0.0	5.6	5.6
0.2	10.14	0.0	163.0	30.6	44.7	0.1	5.6	30.6	11.2	19.5	16.7
0.2	11.65	30.6	81.5	61.1	22.3	3.2	30.7	30.6	27.9	13.9	5.6
0.2	14.80	61.1	132.5	61.1	36.3	2.9	39.1	30.6	27.9	8.3	0.0
0.2	17.14	152.9	132.5	0.0	36.3	3.4	36.3	61.1	27.9	47.2	11.1
0.2	21.65	152.9	173.2	30.6	47.5	3.3	61.5	61.1	41.9	33.4	86.2
0.2	24.80	91.7	163.0	30.6	44.7	2.6	25.1	0.0	39.1	50.0	72.3
0.2	27.14	91.7	101.9	0.0	27.9	1.0	44.7	30.6	11.2	27.8	19.5
0.2	28.65	0.0	173.2	91.7	47.5	1.2	39.1	0.0	14.0	36.1	33.4
0.2	31.80	0.0	152.9	30.6	41.9	0.6	11.2	0.0	19.6	27.8	22.2
0.2	34.14	122.3	173.2	30.6	47.5	0.6	16.8	0.0	8.4	22.2	8.3
0.2	35.15	0.0	91.7	61.1	25.1	4.4	33.5	30.6	19.6	16.7	0.0
0.2	38.30	0.0	71.3	30.6	19.6	6.6	39.1	0.0	30.7	44.5	2.8
0.2	40.64	0.0	30.6	0.0	8.4	7.5	33.5	0.0	19.6	33.4	11.1
0.2	41.65	0.0	122.3	30.6	33.5	6.0	25.1	61.1	33.5	11.1	5.6
0.2	44.80	0.0	0.0	0.0	0.0	6.8	41.9	61.1	44.7	27.8	25.0
0.2	47.14	0.0	0.0	0.0	0.0	8.2	19.6	30.6	36.3	38.9	55.6
0.2	51.65	0.0	30.6	0.0	8.4	8.3	25.1	30.6	11.2	50.0	47.2
0.2	54.80	0.0	30.6	0.0	8.4	8.5	25.1	30.6	30.7	44.5	52.8
0.2	57.14	0.0	30.6	0.0	8.4	8.9	25.1	30.6	30.7	27.8	58.4
0.4	4.65	30.6	142.7	61.1	39.1	0.0	5.6	0.0	0.0	2.8	5.6
0.4	7.80	122.3	265.0	30.6	72.6	0.0	5.6	0.0	5.6	5.6	13.9
0.4	10.14	0.0	265.0	152.9	72.6	1.5	25.1	0.0	2.8	0.0	22.2
0.4	11.65	0.0	173.2	0.0	47.5	0.8	14.0	0.0	0.0	2.8	11.1
0.4	14.80	0.0	142.7	0.0	39.1	1.4	27.9	30.6	8.4	0.0	16.7
0.4	17.14	0.0	71.3	0.0	19.6	1.9	41.9	61.1	11.2	0.0	16.7
0.4	21.65	0.0	101.9	30.6	27.9	2.0	53.1	91.7	53.1	30.6	22.2
0.4	24.80	0.0	152.9	61.1	41.9	2.3	36.3	30.6	67.0	55.6	61.1
0.4	27.14	0.0	132.5	30.6	36.3	3.3	47.5	0.0	95.0	58.4	58.4
0.4	28.65	0.0	40.8	0.0	11.2	4.2	33.5	61.1	47.5	72.3	25.0
0.4	31.80	0.0	20.4	0.0	5.6	5.6	47.5	91.7	67.0	88.9	86.2
0.4	34.14	0.0	0.0	0.0	0.0	5.7	67.0	122.3	67.0	83.4	75.0
0.4	35.15	0.0	40.8	0.0	11.2	5.2	81.0	183.4	67.0	61.1	50.0
0.4	38.30	0.0	30.6	0.0	8.4	5.3	61.5	91.7	64.3	50.0	55.6
0.4	40.64	0.0	0.0	0.0	0.0	5.6	33.5	61.1	64.3	61.1	61.1
0.4	41.65	0.0	30.6	0.0	8.4	7.4	44.7	30.6	50.3	52.8	66.7
0.4	44.80	0.0	10.2	0.0	2.8	8.0	55.9	91.7	75.4	58.4	55.6
0.4	47.14	0.0	51.0	61.1	14.0	8.4	53.1	30.6	39.1	44.5	36.1
0.4	51.65	0.0	61.1	0.0	16.8	8.3	69.8	152.9	67.0	25.0	61.1
0.4	54.80	0.0	40.8	0.0	11.2	9.4	50.3	122.3	41.9	27.8	69.5
0.4	57.14	0.0	40.8	0.0	11.2	9.7	27.9	61.1	39.1	11.1	33.4
0.6	4.65	61.1	40.8	0.0	11.2	0.0	0.0	0.0	5.6	0.0	0.0
0.6	7.80	61.1	203.8	122.3	55.9	0.0	0.0	0.0	5.6	0.0	0.0
0.6	10.14	0.0	305.7	183.4	83.8	0.0	0.0	0.0	0.0	0.0	0.0
0.6	11.65	122.3	101.9	30.6	27.9	0.0	0.0	0.0	0.0	0.0	0.0
0.6	14.80	0.0	142.7	91.7	39.1	0.0	0.0	0.0	0.0	0.0	0.0
0.6	17.14	30.6	244.6	122.3	67.0	0.0	0.0	0.0	0.0	0.0	8.3
0.6	21.65	0.0	0.0	0.0	0.0	0.9	14.0	0.0	8.4	8.3	0.0

0.6	24.80	0.0	81.5	0.0	22.3	1.2	41.9	122.3	8.4	8.3	22.2
0.6	27.14	0.0	40.8	0.0	11.2	1.5	55.9	61.1	22.3	25.0	38.9
0.6	28.65	0.0	101.9	0.0	27.9	3.1	16.8	30.6	27.9	22.2	66.7
0.6	31.80	0.0	61.1	0.0	16.8	4.6	22.3	30.6	58.7	25.0	111.2
0.6	34.14	0.0	20.4	0.0	5.6	5.3	33.5	30.6	86.6	44.5	86.2
0.6	35.15	0.0	30.6	0.0	8.4	1.2	36.3	30.6	39.1	5.6	38.9
0.6	38.30	0.0	40.8	0.0	11.2	1.9	67.0	30.6	120.1	27.8	72.3
0.6	40.64	0.0	40.8	0.0	11.2	2.2	50.3	91.7	72.6	27.8	61.1
0.6	41.65	0.0	51.0	0.0	14.0	7.4	50.3	0.0	41.9	61.1	61.1
0.6	44.80	0.0	20.4	0.0	5.6	7.9	69.8	0.0	19.6	61.1	80.6
0.6	47.14	0.0	0.0	0.0	0.0	8.1	47.5	0.0	25.1	61.1	63.9
0.6	51.65	0.0	132.5	0.0	36.3	7.7	19.6	0.0	27.9	30.6	50.0
0.6	54.80	0.0	173.2	0.0	47.5	8.0	19.6	0.0	11.2	33.4	75.0
0.6	57.14	0.0	91.7	0.0	25.1	8.2	14.0	0.0	5.6	11.1	44.5
0.8	4.65	30.6	193.6	61.1	53.1	0.0	0.0	0.0	0.0	0.0	0.0
0.8	7.80	91.7	224.2	214.0	61.5	0.0	0.0	0.0	0.0	0.0	0.0
0.8	10.14	0.0	61.1	61.1	16.8	0.0	0.0	0.0	0.0	0.0	5.6
0.8	11.65	0.0	101.9	0.0	27.9	0.0	0.0	0.0	0.0	0.0	0.0
0.8	14.80	0.0	183.4	122.3	50.3	0.0	0.0	0.0	0.0	0.0	2.8
0.8	17.14	0.0	173.2	152.9	47.5	0.0	2.8	0.0	0.0	0.0	16.7
0.8	21.65	0.0	20.4	0.0	5.6	0.6	11.2	0.0	27.9	16.7	0.0
0.8	24.80	0.0	0.0	0.0	0.0	1.7	22.3	0.0	44.7	16.7	2.8
0.8	27.14	0.0	10.2	0.0	2.8	3.1	25.1	30.6	27.9	63.9	22.2
0.8	28.65	0.0	0.0	0.0	0.0	1.5	33.5	0.0	55.9	33.4	83.4
0.8	31.80	0.0	0.0	0.0	0.0	2.9	72.6	91.7	19.6	77.8	16.7
0.8	34.14	0.0	0.0	0.0	0.0	7.0	50.3	30.6	5.6	58.4	0.0
0.8	35.15	0.0	0.0	0.0	0.0	7.0	95.0	183.4	0.0	58.4	41.7
0.8	38.30	0.0	0.0	0.0	0.0	8.5	89.4	122.3	0.0	30.6	19.5
0.8	40.64	0.0	0.0	0.0	0.0	8.8	44.7	61.1	0.0	13.9	22.2
0.8	41.65	0.0	0.0	0.0	0.0	10.2	0.0	0.0	27.9	33.4	16.7
0.8	44.80	0.0	0.0	0.0	0.0	10.2	0.0	0.0	19.6	22.2	22.2
0.8	47.14	0.0	0.0	0.0	0.0	10.2	0.0	0.0	0.0	11.1	13.9
0.8	51.65	0.0	0.0	0.0	0.0	10.2	0.0	0.0	27.9	2.8	0.0
0.8	54.80	0.0	0.0	0.0	0.0	10.2	0.0	0.0	33.5	0.0	0.0
0.8	57.14	0.0	0.0	0.0	0.0	10.2	0.0	0.0	22.3	0.0	0.0
1	4.65	0.0	101.9	0.0	27.9	0.0	0.0	0.0	0.0	0.0	5.6
1	7.80	0.0	183.4	30.6	50.3	0.0	0.0	0.0	0.0	0.0	5.6
1	10.14	0.0	101.9	30.6	27.9	0.0	0.0	0.0	0.0	0.0	0.0
1	11.65	0.0	0.0	0.0	0.0	0.6	22.3	0.0	0.0	0.0	0.0
1	14.80	0.0	61.1	91.7	16.8	3.6	44.7	91.7	0.0	11.1	0.0
1	17.14	0.0	173.2	183.4	47.5	5.2	30.7	0.0	2.8	16.7	0.0
1	21.65	0.0	81.5	122.3	22.3	7.1	27.9	0.0	30.7	0.0	25.0
1	24.80	0.0	81.5	122.3	22.3	8.0	39.1	0.0	36.3	33.4	36.1
1	27.14	0.0	40.8	61.1	11.2	9.5	33.5	0.0	19.6	44.5	66.7
1	28.65	0.0	0.0	0.0	0.0	9.7	5.6	0.0	0.0	33.4	88.9
1	31.80	0.0	0.0	0.0	0.0	9.9	5.6	0.0	0.0	38.9	88.9
1	34.14	0.0	0.0	0.0	0.0	10.2	0.0	0.0	0.0	16.7	36.1
1	35.15	0.0	0.0	0.0	0.0	10.2	0.0	0.0	0.0	38.9	5.6
1	38.30	0.0	0.0	0.0	0.0	10.2	0.0	0.0	0.0	16.7	5.6
1	40.64	0.0	0.0	0.0	0.0	10.2	0.0	0.0	0.0	11.1	11.1
x'	y	F	F	F	F	F	F	F	F	F	F
m	mm	Hz	Hz	Hz	Hz	Hz	Hz	Hz	Hz	Hz	Hz
(1)	(2)	(3)	(4)	(5)	(6)	(7)	(8)	(9)	(10)	(11)	(12)

Run TL5 (step 10)

Q	Step	x'	C_s	d_o

m^3/s		m	m/s	m
0.075	10	0.2, 0.4, 0.6, 0.8, 1.0	2.61	0.297

x' m (1)	y mm (2)	F Hz (3)	F Hz (4)	F Hz (5)	F Hz (6)	F Hz (7)	F Hz (8)	F Hz (9)	F Hz (10)	F Hz (11)	F Hz (12)
ΔX =	(mm)	0-70	0-210	140-210	0-385	175-385	350-735	525-595	700-1085	2100-2485	4200-4585
$t - t_S$ =	(s)	0.013	0.04	0.067	0.074	0.107	0.208	0.215	0.342	0.878	1.683
ΔX =	(mm)	70	210	70	385	210	385	70	385	385	385
$\frac{(t-t_S)}{\sqrt{d_o/g}}$		0.077	0.231	0.385	0.424	0.616	1.194	1.233	1.965	5.047	9.67
0.2	4.65	37.3	24.9	0.0	6.8	0.7	20.4	0.0	6.8	3.4	0.0
0.2	7.80	37.3	24.9	0.0	6.8	0.5	0.0	0.0	6.8	0.0	0.0
0.2	10.14	74.6	37.3	0.0	10.2	0.4	0.0	0.0	27.3	0.0	0.0
0.2	11.65	0.0	49.7	0.0	13.6	3.9	44.3	111.9	6.8	13.6	30.5
0.2	14.80	0.0	24.9	0.0	6.8	4.5	17.0	37.3	3.4	6.8	20.3
0.2	17.14	0.0	0.0	0.0	0.0	8.4	17.0	0.0	34.1	0.0	33.9
0.2	21.65	0.0	0.0	0.0	0.0	9.9	13.6	0.0	6.8	37.3	91.5
0.2	24.80	74.6	37.3	0.0	10.2	11.2	6.8	0.0	6.8	30.5	54.2
0.2	27.14	74.6	62.1	37.3	17.0	11.9	17.0	0.0	6.8	30.5	67.8
0.2	28.65	0.0	74.6	0.0	20.4	12.4	6.8	0.0	47.7	61.0	54.2
0.2	31.80	0.0	111.9	0.0	30.7	9.5	54.5	0.0	54.5	71.2	40.7
0.2	34.14	74.6	136.7	74.6	37.5	5.3	57.9	74.6	68.1	50.8	20.3
0.2	35.15	0.0	223.7	0.0	61.3	1.0	20.4	37.3	34.1	33.9	13.6
0.2	38.30	0.0	186.4	0.0	51.1	0.9	40.9	74.6	13.6	23.7	6.8
0.2	40.64	0.0	174.0	0.0	47.7	1.0	51.1	37.3	6.8	10.2	16.9
0.2	41.65	74.6	62.1	37.3	17.0	1.0	40.9	37.3	27.3	0.0	0.0
0.2	44.80	111.9	136.7	0.0	37.5	1.0	40.9	37.3	27.3	0.0	0.0
0.2	47.14	74.6	87.0	0.0	23.9	1.6	34.1	0.0	20.4	16.9	3.4
0.2	51.65	37.3	161.6	111.9	44.3	2.5	40.9	111.9	51.1	44.1	0.0
0.2	54.80	74.6	124.3	37.3	34.1	2.8	44.3	149.1	51.1	23.7	13.6
0.2	57.14	74.6	87.0	0.0	23.9	3.0	34.1	74.6	81.8	33.9	13.6
0.2	61.65	37.3	161.6	0.0	44.3	7.9	27.3	74.6	27.3	47.5	27.1
0.2	64.80	37.3	186.4	0.0	51.1	8.6	34.1	37.3	34.1	40.7	47.5
0.2	67.14	0.0	99.4	0.0	27.3	10.4	34.1	0.0	34.1	20.3	50.8
0.2	71.65	186.4	198.9	111.9	54.5	11.6	20.4	0.0	20.4	47.5	10.2
0.2	74.80	261.0	372.9	74.6	102.2	12.2	13.6	0.0	20.4	40.7	20.3
0.2	77.14	261.0	335.6	74.6	92.0	12.2	13.6	0.0	13.6	0.0	10.2
0.2	81.65	0.0	99.4	37.3	27.3	12.4	0.0	0.0	0.0	0.0	0.0
0.4	4.65	0.0	62.1	0.0	17.0	0.0	0.0	0.0	0.0	0.0	0.0
0.4	7.80	0.0	24.9	0.0	6.8	0.0	3.4	0.0	3.4	13.6	0.0
0.4	10.14	0.0	62.1	74.6	17.0	0.0	0.0	0.0	17.0	23.7	13.6
0.4	11.65	0.0	87.0	186.4	23.9	0.0	0.0	0.0	13.6	13.6	0.0
0.4	14.80	0.0	62.1	111.9	17.0	0.0	0.0	0.0	27.3	6.8	6.8
0.4	17.14	0.0	174.0	111.9	47.7	0.0	0.0	0.0	10.2	6.8	20.3
0.4	21.65	0.0	174.0	186.4	47.7	1.1	27.3	74.6	61.3	0.0	20.3
0.4	24.80	0.0	285.9	298.3	78.4	3.2	88.6	111.9	109.0	16.9	44.1
0.4	27.14	0.0	161.6	186.4	44.3	4.3	143.1	186.4	54.5	30.5	16.9
0.4	28.65	0.0	99.4	0.0	27.3	4.5	64.7	37.3	47.7	67.8	20.3
0.4	31.80	0.0	99.4	0.0	27.3	4.8	68.1	37.3	81.8	135.6	37.3
0.4	34.14	0.0	0.0	0.0	0.0	6.6	75.0	74.6	68.1	128.8	84.7
0.4	35.15	0.0	12.4	0.0	3.4	7.3	85.2	223.7	57.9	78.0	44.1
0.4	38.30	0.0	87.0	0.0	23.9	8.6	71.6	37.3	71.6	98.3	50.8
0.4	40.64	0.0	87.0	0.0	23.9	10.2	51.1	74.6	71.6	71.2	84.7
0.4	41.65	0.0	62.1	0.0	17.0	12.1	13.6	0.0	37.5	30.5	44.1
0.4	44.80	0.0	24.9	0.0	6.8	12.1	6.8	0.0	37.5	37.3	91.5

0.4	47.14	0.0	37.3	0.0	10.2	12.0	13.6	0.0	13.6	33.9	50.8
0.4	51.65	0.0	124.3	0.0	34.1	12.4	0.0	0.0	34.1	10.2	27.1
0.4	54.80	0.0	62.1	0.0	17.0	12.4	0.0	0.0	47.7	3.4	50.8
0.4	57.14	0.0	99.4	0.0	27.3	12.4	0.0	0.0	27.3	0.0	27.1
0.4	61.65	0.0	0.0	0.0	0.0	11.7	10.2	0.0	0.0	0.0	10.2
0.4	64.80	0.0	0.0	0.0	0.0	12.3	3.4	0.0	0.0	0.0	10.2
0.4	67.14	0.0	0.0	0.0	0.0	12.4	0.0	0.0	0.0	0.0	16.9
0.4	71.65	0.0	0.0	0.0	0.0	12.3	10.2	0.0	13.6	0.0	27.1
0.4	74.80	0.0	0.0	0.0	0.0	12.2	6.8	0.0	13.6	0.0	27.1
0.4	77.14	0.0	0.0	0.0	0.0	12.1	10.2	0.0	6.8	0.0	54.2
0.4	81.65	0.0	0.0	0.0	0.0	12.4	0.0	0.0	0.0	27.1	0.0
0.6	4.65	0.0	236.1	111.9	64.7	0.4	20.4	0.0	0.0	0.0	6.8
0.6	7.80	0.0	248.6	74.6	68.1	1.5	64.7	74.6	13.6	6.8	6.8
0.6	10.14	0.0	62.1	0.0	17.0	2.8	81.8	111.9	6.8	3.4	6.8
0.6	11.65	0.0	149.1	0.0	40.9	1.2	34.1	37.3	17.0	0.0	6.8
0.6	14.80	0.0	161.6	0.0	44.3	2.0	44.3	37.3	61.3	6.8	13.6
0.6	17.14	0.0	211.3	0.0	57.9	2.8	61.3	37.3	51.1	0.0	13.6
0.6	21.65	0.0	62.1	0.0	17.0	8.2	47.7	37.3	20.4	0.0	13.6
0.6	24.80	0.0	62.1	0.0	17.0	10.5	37.5	37.3	23.9	0.0	10.2
0.6	27.14	0.0	24.9	0.0	6.8	10.8	34.1	37.3	10.2	3.4	37.3
0.6	28.65	0.0	0.0	0.0	0.0	4.8	122.7	74.6	98.8	13.6	20.3
0.6	31.80	0.0	0.0	0.0	0.0	7.1	139.7	111.9	88.6	0.0	13.6
0.6	34.14	0.0	0.0	0.0	0.0	8.7	95.4	186.4	85.2	6.8	27.1
0.6	35.15	0.0	24.9	0.0	6.8	10.6	10.2	0.0	71.6	20.3	0.0
0.6	38.30	0.0	12.4	0.0	3.4	10.2	20.4	0.0	75.0	37.3	27.1
0.6	40.64	0.0	0.0	0.0	0.0	11.0	10.2	0.0	54.5	33.9	54.2
0.6	41.65	0.0	62.1	0.0	17.0	12.0	13.6	0.0	75.0	30.5	33.9
0.6	44.80	0.0	24.9	0.0	6.8	12.1	3.4	0.0	88.6	47.5	40.7
0.6	47.14	0.0	12.4	0.0	3.4	12.0	3.4	0.0	61.3	61.0	33.9
0.6	51.65	0.0	12.4	0.0	3.4	12.1	6.8	0.0	23.9	64.4	91.5
0.6	54.80	0.0	37.3	0.0	10.2	12.4	6.8	0.0	27.3	64.4	162.7
0.6	57.14	0.0	24.9	0.0	6.8	12.4	0.0	0.0	13.6	67.8	128.8
0.6	61.65	0.0	0.0	0.0	0.0	10.0	51.1	37.3	0.0	67.8	67.8
0.6	64.80	0.0	0.0	0.0	0.0	10.8	51.1	74.6	0.0	57.6	71.2
0.6	67.14	0.0	0.0	0.0	0.0	11.7	27.3	37.3	6.8	61.0	47.5
0.6	71.65	0.0	0.0	0.0	0.0	12.4	3.4	0.0	0.0	74.6	81.4
0.6	74.80	0.0	0.0	0.0	0.0	12.4	0.0	0.0	3.4	88.1	115.2
0.6	77.14	0.0	0.0	0.0	0.0	12.4	0.0	0.0	3.4	71.2	71.2
0.6	81.65	0.0	0.0	0.0	0.0	12.4	0.0	0.0	3.4	47.5	94.9
0.8	4.65	37.3	37.3	0.0	10.2	0.0	0.0	0.0	0.0	0.0	0.0
0.8	7.80	298.3	323.1	74.6	88.6	0.0	6.8	0.0	0.0	0.0	0.0
0.8	10.14	0.0	186.4	111.9	51.1	0.0	0.0	0.0	0.0	6.8	0.0
0.8	11.65	0.0	49.7	0.0	13.6	0.0	0.0	0.0	6.8	6.8	0.0
0.8	14.80	111.9	298.3	37.3	81.8	0.0	0.0	0.0	0.0	6.8	0.0
0.8	17.14	186.4	248.6	111.9	68.1	0.0	0.0	0.0	6.8	23.7	0.0
0.8	21.65	0.0	174.0	74.6	47.7	11.0	47.7	0.0	0.0	6.8	6.8
0.8	24.80	0.0	149.1	0.0	40.9	11.7	44.3	0.0	13.6	6.8	6.8
0.8	27.14	0.0	24.9	0.0	6.8	11.8	40.9	37.3	6.8	0.0	16.9
0.8	28.65	0.0	12.4	0.0	3.4	6.4	20.4	0.0	61.3	0.0	6.8
0.8	31.80	0.0	62.1	37.3	17.0	7.6	61.3	37.3	64.7	16.9	13.6
0.8	34.14	0.0	24.9	0.0	6.8	10.3	17.0	0.0	64.7	13.6	27.1
0.8	35.15	0.0	12.4	0.0	3.4	10.9	34.1	111.9	40.9	13.6	27.1
0.8	38.30	0.0	0.0	0.0	0.0	11.7	34.1	0.0	75.0	6.8	61.0
0.8	40.64	0.0	0.0	0.0	0.0	12.2	10.2	0.0	78.4	10.2	10.2
0.8	41.65	0.0	0.0	0.0	0.0	9.4	6.8	37.3	37.5	0.0	27.1
0.8	44.80	0.0	0.0	0.0	0.0	9.8	27.3	37.3	71.6	13.6	13.6
0.8	47.14	0.0	0.0	0.0	0.0	10.4	17.0	74.6	64.7	13.6	20.3
0.8	51.65	0.0	0.0	0.0	0.0	10.1	0.0	0.0	47.7	13.6	20.3
0.8	54.80	0.0	0.0	0.0	0.0	10.5	34.1	0.0	105.6	30.5	27.1

0.8	57.14	0.0	0.0	0.0	0.0	10.7	27.3	0.0	78.4	44.1	40.7
0.8	61.65	0.0	0.0	0.0	0.0	11.9	10.2	0.0	40.9	61.0	67.8
0.8	64.80	0.0	0.0	0.0	0.0	12.2	10.2	0.0	34.1	47.5	111.9
0.8	67.14	0.0	0.0	0.0	0.0	12.3	6.8	0.0	13.6	54.2	88.1
0.8	71.65	0.0	0.0	0.0	0.0	12.4	0.0	0.0	20.4	44.1	74.6
0.8	74.80	0.0	0.0	0.0	0.0	12.4	0.0	0.0	23.9	57.6	101.7
0.8	77.14	0.0	0.0	0.0	0.0	12.4	0.0	0.0	20.4	50.8	105.1
0.8	81.65	0.0	0.0	0.0	0.0	12.4	0.0	0.0	20.4	67.8	57.6
0.8	84.80	0.0	0.0	0.0	0.0	12.4	0.0	0.0	17.0	84.7	37.3
0.8	87.14	0.0	0.0	0.0	0.0	12.4	0.0	0.0	10.2	40.7	54.2
0.8	91.65	0.0	0.0	0.0	0.0	12.4	0.0	0.0	0.0	6.8	6.8
0.8	94.80	0.0	0.0	0.0	0.0	12.4	0.0	0.0	3.4	6.8	6.8
0.8	97.14	0.0	0.0	0.0	0.0	12.4	0.0	0.0	3.4	6.8	20.3
1	4.65	0.0	0.0	0.0	0.0	0.0	0.0	0.0	0.0	0.0	0.0
1	7.80	0.0	186.4	0.0	51.1	0.0	0.0	0.0	0.0	0.0	0.0
1	10.14	0.0	74.6	0.0	20.4	0.2	10.2	0.0	0.0	0.0	0.0
1	11.65	0.0	99.4	111.9	27.3	0.1	6.8	37.3	6.8	0.0	0.0
1	14.80	0.0	99.4	111.9	27.3	0.1	13.6	0.0	6.8	10.2	0.0
1	17.14	0.0	174.0	0.0	47.7	0.5	34.1	74.6	6.8	0.0	6.8
1	21.65	0.0	111.9	37.3	30.7	1.2	34.1	0.0	6.8	0.0	13.6
1	24.80	0.0	87.0	74.6	23.9	1.6	27.3	0.0	0.0	13.6	20.3
1	27.14	0.0	87.0	111.9	23.9	1.8	54.5	0.0	13.6	3.4	6.8
1	28.65	0.0	87.0	0.0	23.9	1.0	54.5	223.7	47.7	13.6	13.6
1	31.80	0.0	161.6	0.0	44.3	2.9	129.5	335.6	64.7	20.3	6.8
1	34.14	0.0	99.4	0.0	27.3	5.2	85.2	37.3	51.1	13.6	3.4
1	35.15	0.0	0.0	0.0	0.0	2.1	47.7	37.3	27.3	0.0	6.8
1	38.30	0.0	0.0	0.0	0.0	3.4	61.3	74.6	47.7	6.8	23.7
1	40.64	0.0	0.0	0.0	0.0	5.7	78.4	37.3	30.7	6.8	23.7
1	41.65	0.0	0.0	0.0	0.0	8.1	64.7	0.0	64.7	54.2	13.6
1	44.80	0.0	24.9	0.0	6.8	9.6	47.7	0.0	64.7	33.9	20.3
1	47.14	0.0	12.4	0.0	3.4	10.7	47.7	0.0	51.1	27.1	16.9
1	51.65	0.0	0.0	0.0	0.0	11.8	47.7	0.0	34.1	101.7	37.3
1	54.80	0.0	0.0	0.0	0.0	11.6	92.0	410.1	61.3	64.4	33.9
1	57.14	0.0	0.0	0.0	0.0	11.9	57.9	298.3	30.7	122.0	40.7
1	61.65	0.0	0.0	0.0	0.0	12.4	0.0	0.0	13.6	47.5	67.8
1	64.80	0.0	0.0	0.0	0.0	12.4	0.0	0.0	13.6	64.4	64.4
1	67.14	0.0	0.0	0.0	0.0	12.4	0.0	0.0	13.6	47.5	50.8
1	71.65	0.0	0.0	0.0	0.0	12.4	0.0	0.0	0.0	6.8	20.3
1	71.65	0.0	0.0	0.0	0.0	12.4	0.0	0.0	0.0	6.8	20.3
1	74.80	0.0	0.0	0.0	0.0	12.4	0.0	0.0	0.0	0.0	23.7
1	77.14	0.0	0.0	0.0	0.0	12.4	0.0	0.0	0.0	0.0	16.9
1	81.65	0.0	0.0	0.0	0.0	12.4	0.0	0.0	0.0	47.5	20.3
x'	y	F	F	F	F	F	F	F	F	F	F
m	mm	Hz	Hz	Hz	Hz	Hz	Hz	Hz	Hz	Hz	Hz
(1)	(2)	(3)	(4)	(5)	(6)	(7)	(8)	(9)	(10)	(11)	(12)

Run TL5 (step 16)

Q m^3/s	Step	x' m	C_S m/s	d_o m
0.075	16	0.2, 0.4, 0.6, 0.8, 1.0	2.43	0.297

x'	y	F	F	F	F	F	F	F	F	F	F
m	mm	Hz	Hz	Hz	Hz	Hz	Hz	Hz	Hz	Hz	Hz
(1)	(2)	(3)	(4)	(5)	(6)	(7)	(8)	(9)	(10)	(11)	(12)
ΔX =	(mm)	0-70	0-210	140-210	0-385	175-385	350-735	525-595	700-1085	2100-2485	4200-4585

$t - t_S =$	(s)	0.0144	0.0432	0.072	0.0792	0.1152	0.2233	0.2305	0.3673	0.9434	1.8076
$\Delta X =$	(mm)	70	210	70	385	210	385	70	385	385	385
$\frac{(t-t_S)}{\sqrt{d_o/g}}$		0.0828	0.2483	0.4138	0.4552	0.6621	1.2828	1.3242	2.1104	5.4208	10.386
0.2	4.65	0.0	92.6	104.1	25.4	0.0	0.0	0.0	6.3	0.0	12.6
0.2	7.80	0.0	23.1	0.0	6.3	0.9	12.7	0.0	0.0	0.0	0.0
0.2	10.14	0.0	69.4	0.0	19.0	2.5	25.4	0.0	12.7	9.5	12.6
0.2	11.65	0.0	23.1	0.0	6.3	0.3	12.7	0.0	6.3	6.3	18.9
0.2	14.80	0.0	23.1	0.0	6.3	0.7	22.2	104.1	19.0	25.2	9.5
0.2	17.14	34.7	69.4	0.0	19.0	4.2	22.2	0.0	6.3	37.9	34.7
0.2	21.65	0.0	23.1	0.0	6.3	11.0	12.7	0.0	28.6	53.6	18.9
0.2	24.80	69.4	69.4	34.7	19.0	10.9	12.7	0.0	31.7	60.0	28.4
0.2	27.14	34.7	115.7	0.0	31.7	8.4	50.8	104.1	73.0	66.3	63.1
0.2	28.65	34.7	150.4	104.1	41.2	5.7	44.4	0.0	28.6	53.6	50.5
0.2	31.80	69.4	266.1	34.7	73.0	4.1	69.8	69.4	28.6	53.6	44.2
0.2	34.14	104.1	266.1	34.7	73.0	1.4	38.1	0.0	15.9	28.4	41.0
0.2	35.15	0.0	0.0	0.0	0.0	0.0	0.0	0.0	25.4	0.0	25.2
0.2	38.30	0.0	46.3	0.0	12.7	0.5	6.3	0.0	22.2	0.0	12.6
0.2	40.64	69.4	57.9	0.0	15.9	0.8	6.3	34.7	31.7	18.9	12.6
0.2	41.65	0.0	69.4	69.4	19.0	0.1	12.7	0.0	6.3	9.5	28.4
0.2	44.80	0.0	69.4	34.7	19.0	0.6	15.9	0.0	22.2	0.0	18.9
0.2	47.14	0.0	92.6	0.0	25.4	0.8	6.3	0.0	25.4	6.3	28.4
0.2	51.65	0.0	34.7	34.7	9.5	2.4	28.6	34.7	25.4	12.6	31.6
0.2	54.80	0.0	196.7	104.1	53.9	4.1	34.9	34.7	25.4	41.0	34.7
0.2	57.14	0.0	81.0	34.7	22.2	5.0	34.9	69.4	50.8	25.2	44.2
0.2	61.65	34.7	81.0	34.7	22.2	9.5	19.0	0.0	22.2	28.4	41.0
0.2	64.80	69.4	138.9	34.7	38.1	9.9	12.7	0.0	19.0	37.9	56.8
0.2	67.14	34.7	92.6	34.7	25.4	10.1	12.7	0.0	0.0	12.6	63.1
0.2	71.65	0.0	46.3	0.0	12.7	8.1	57.1	69.4	0.0	25.2	6.3
0.2	74.80	0.0	23.1	0.0	6.3	8.6	50.8	34.7	0.0	25.2	0.0
0.2	77.14	0.0	23.1	0.0	6.3	9.4	31.7	0.0	0.0	0.0	0.0
0.2	81.65	34.7	81.0	0.0	22.2	11.5	0.0	0.0	6.3	0.0	12.6
0.4	4.65	104.1	150.4	69.4	41.2	0.2	15.9	69.4	0.0	15.8	12.6
0.4	7.80	0.0	231.4	69.4	63.4	0.2	19.0	34.7	6.3	31.6	34.7
0.4	10.14	0.0	312.4	138.9	85.7	0.4	34.9	34.7	12.7	69.4	25.2
0.4	11.65	34.7	312.4	208.3	85.7	2.1	73.0	69.4	12.7	22.1	12.6
0.4	14.80	0.0	254.6	104.1	69.8	3.9	92.0	104.1	47.6	44.2	9.5
0.4	17.14	0.0	173.6	34.7	47.6	6.1	63.4	69.4	53.9	47.3	15.8
0.4	21.65	0.0	138.9	69.4	38.1	0.5	22.2	34.7	69.8	34.7	50.5
0.4	24.80	0.0	324.0	34.7	88.8	0.9	34.9	34.7	82.5	37.9	69.4
0.4	27.14	0.0	173.6	34.7	47.6	2.1	69.8	138.9	136.4	63.1	75.7
0.4	28.65	0.0	57.9	0.0	15.9	4.5	79.3	34.7	57.1	44.2	41.0
0.4	31.80	0.0	46.3	0.0	12.7	6.2	88.8	138.9	38.1	37.9	56.8
0.4	34.14	0.0	92.6	34.7	25.4	6.9	123.7	243.0	22.2	82.1	63.1
0.4	35.15	0.0	46.3	0.0	12.7	8.9	34.9	0.0	66.6	56.8	107.3
0.4	38.30	0.0	69.4	0.0	19.0	8.7	19.0	0.0	57.1	53.6	126.2
0.4	40.64	0.0	69.4	0.0	19.0	9.2	50.8	0.0	50.8	75.7	88.4
0.4	41.65	0.0	23.1	0.0	6.3	8.9	57.1	69.4	25.4	66.3	82.1
0.4	44.80	0.0	23.1	0.0	6.3	9.5	50.8	69.4	47.6	53.6	88.4
0.4	47.14	0.0	34.7	0.0	9.5	9.5	44.4	34.7	57.1	50.5	78.9
0.4	51.65	0.0	0.0	0.0	0.0	9.6	66.6	173.6	25.4	22.1	97.8
0.4	54.80	0.0	23.1	0.0	6.3	10.0	60.3	104.1	34.9	53.6	85.2
0.4	57.14	0.0	23.1	0.0	6.3	10.6	22.2	69.4	22.2	28.4	78.9
0.4	61.65	0.0	0.0	0.0	0.0	11.0	6.3	0.0	31.7	37.9	47.3
0.4	64.80	0.0	0.0	0.0	0.0	11.4	6.3	0.0	25.4	44.2	60.0
0.4	67.14	0.0	11.6	0.0	3.2	11.4	9.5	0.0	25.4	44.2	31.6
0.4	71.65	0.0	0.0	0.0	0.0	11.6	0.0	0.0	0.0	31.6	18.9
0.4	74.80	0.0	0.0	0.0	0.0	11.6	0.0	0.0	0.0	47.3	25.2

0.4	77.14	0.0	0.0	0.0	0.0	11.6	0.0	0.0	0.0	18.9	6.3
0.4	81.65	0.0	0.0	0.0	0.0	11.6	0.0	0.0	0.0	0.0	9.5
0.4	84.80	0.0	0.0	0.0	0.0	11.6	0.0	0.0	0.0	0.0	9.5
0.4	87.14	0.0	0.0	0.0	0.0	11.6	0.0	0.0	0.0	0.0	3.2
0.6	4.65	34.7	69.4	0.0	19.0	0.0	0.0	0.0	0.0	0.0	0.0
0.6	7.80	104.1	185.1	104.1	50.8	0.0	6.3	0.0	6.3	0.0	0.0
0.6	10.14	34.7	185.1	104.1	50.8	0.1	15.9	0.0	3.2	6.3	0.0
0.6	11.65	0.0	497.6	173.6	136.4	0.0	3.2	0.0	6.3	0.0	0.0
0.6	14.80	0.0	497.6	208.3	136.4	0.6	41.2	34.7	0.0	6.3	12.6
0.6	17.14	0.0	277.7	69.4	76.1	3.1	31.7	34.7	19.0	0.0	3.2
0.6	21.65	0.0	185.1	69.4	50.8	1.0	25.4	0.0	19.0	12.6	6.3
0.6	24.80	0.0	196.7	34.7	53.9	1.3	34.9	0.0	12.7	18.9	12.6
0.6	27.14	0.0	81.0	0.0	22.2	1.7	53.9	104.1	12.7	0.0	0.0
0.6	28.65	0.0	34.7	0.0	9.5	4.1	53.9	34.7	38.1	44.2	9.5
0.6	31.80	0.0	92.6	0.0	25.4	4.4	63.4	69.4	69.8	47.3	63.1
0.6	34.14	0.0	23.1	0.0	6.3	4.8	63.4	69.4	38.1	41.0	37.9
0.6	35.15	0.0	81.0	0.0	22.2	6.5	79.3	138.9	41.2	18.9	12.6
0.6	38.30	0.0	57.9	0.0	15.9	7.4	66.6	69.4	69.8	37.9	37.9
0.6	40.64	0.0	34.7	0.0	9.5	8.7	57.1	34.7	82.5	56.8	15.8
0.6	41.65	0.0	0.0	0.0	0.0	10.2	28.6	34.7	47.6	3.2	44.2
0.6	44.80	0.0	0.0	0.0	0.0	10.6	15.9	34.7	60.3	28.4	50.5
0.6	47.14	0.0	0.0	0.0	0.0	10.8	19.0	34.7	66.6	34.7	69.4
0.6	51.65	0.0	0.0	0.0	0.0	11.1	0.0	0.0	44.4	75.7	66.3
0.6	54.80	0.0	0.0	0.0	0.0	11.1	0.0	0.0	88.8	123.1	82.1
0.6	57.14	0.0	0.0	0.0	0.0	11.4	6.3	0.0	73.0	88.4	85.2
0.6	61.65	0.0	23.1	0.0	6.3	10.4	28.6	0.0	53.9	72.6	50.5
0.6	64.80	0.0	46.3	34.7	12.7	10.9	28.6	0.0	73.0	91.5	91.5
0.6	67.14	0.0	46.3	34.7	12.7	10.9	34.9	0.0	85.7	107.3	88.4
0.6	71.65	0.0	0.0	0.0	0.0	9.6	19.0	0.0	57.1	91.5	88.4
0.6	74.80	0.0	0.0	0.0	0.0	10.7	25.4	0.0	41.2	91.5	116.8
0.6	77.14	0.0	0.0	0.0	0.0	10.8	6.3	0.0	44.4	69.4	85.2
0.6	81.65	0.0	0.0	0.0	0.0	11.2	12.7	0.0	0.0	47.3	44.2
0.6	84.80	0.0	0.0	0.0	0.0	11.4	6.3	0.0	0.0	37.9	15.8
0.6	87.14	0.0	0.0	0.0	0.0	11.6	0.0	0.0	0.0	28.4	12.6
0.6	91.65	0.0	0.0	0.0	0.0	11.6	0.0	0.0	25.4	31.6	12.6
0.8	4.65	69.4	162.0	34.7	44.4	0.0	0.0	0.0	0.0	6.3	0.0
0.8	7.80	34.7	231.4	69.4	63.4	0.1	12.7	0.0	0.0	6.3	0.0
0.8	10.14	0.0	115.7	0.0	31.7	0.6	31.7	34.7	0.0	0.0	0.0
0.8	11.65	208.3	254.6	69.4	69.8	0.0	0.0	0.0	0.0	0.0	6.3
0.8	14.80	0.0	173.6	138.9	47.6	0.5	9.5	0.0	6.3	9.5	12.6
0.8	17.14	0.0	335.6	173.6	92.0	1.1	15.9	34.7	0.0	3.2	6.3
0.8	21.65	0.0	115.7	0.0	31.7	7.9	76.1	104.1	25.4	6.3	0.0
0.8	24.80	0.0	104.1	0.0	28.6	9.5	53.9	69.4	25.4	0.0	3.2
0.8	27.14	0.0	57.9	0.0	15.9	10.8	53.9	104.1	25.4	0.0	3.2
0.8	28.65	0.0	0.0	0.0	0.0	5.2	50.8	69.4	9.5	12.6	25.2
0.8	31.80	0.0	0.0	0.0	0.0	8.2	57.1	0.0	38.1	15.8	6.3
0.8	34.14	0.0	23.1	0.0	6.3	10.2	50.8	34.7	44.4	12.6	12.6
0.8	35.15	0.0	162.0	0.0	44.4	11.6	0.0	0.0	6.3	6.3	12.6
0.8	38.30	0.0	92.6	0.0	25.4	11.6	0.0	0.0	0.0	37.9	0.0
0.8	40.64	0.0	115.7	0.0	31.7	11.6	0.0	0.0	19.0	37.9	0.0
0.8	41.65	0.0	0.0	0.0	0.0	8.4	44.4	0.0	22.2	12.6	34.7
0.8	44.80	0.0	0.0	0.0	0.0	9.7	34.9	34.7	41.2	63.1	72.6
0.8	47.14	0.0	0.0	0.0	0.0	10.0	34.9	69.4	34.9	50.5	63.1
0.8	51.65	0.0	0.0	0.0	0.0	11.2	12.7	34.7	73.0	41.0	18.9
0.8	54.80	0.0	0.0	0.0	0.0	11.4	9.5	0.0	98.3	69.4	44.2
0.8	57.14	0.0	0.0	0.0	0.0	11.3	6.3	0.0	50.8	88.4	72.6
0.8	61.65	0.0	0.0	0.0	0.0	10.8	25.4	0.0	73.0	37.9	82.1
0.8	64.80	0.0	0.0	0.0	0.0	11.3	12.7	0.0	85.7	25.2	50.5
0.8	67.14	0.0	0.0	0.0	0.0	11.5	6.3	0.0	82.5	25.2	22.1

0.8	71.65	0.0	0.0	0.0	0.0	11.4	6.3	0.0	25.4	44.2	25.2
0.8	74.80	0.0	0.0	0.0	0.0	11.6	0.0	0.0	6.3	44.2	44.2
0.8	77.14	0.0	0.0	0.0	0.0	11.6	0.0	0.0	0.0	37.9	18.9
0.8	81.65	0.0	0.0	0.0	0.0	11.6	0.0	0.0	0.0	12.6	18.9
0.8	84.80	0.0	0.0	0.0	0.0	11.6	0.0	0.0	0.0	6.3	12.6
1	4.65	0.0	23.1	0.0	6.3	0.0	0.0	0.0	0.0	0.0	0.0
1	7.80	69.4	300.9	0.0	82.5	0.0	0.0	0.0	0.0	0.0	0.0
1	10.14	173.6	277.7	0.0	76.1	0.0	0.0	0.0	6.3	0.0	0.0
1	11.65	34.7	138.9	0.0	38.1	0.0	0.0	0.0	0.0	3.2	0.0
1	14.80	104.1	69.4	0.0	19.0	0.0	6.3	34.7	0.0	0.0	0.0
1	17.14	69.4	69.4	0.0	19.0	0.0	0.0	0.0	6.3	0.0	0.0
1	21.65	0.0	92.6	34.7	25.4	2.1	0.0	0.0	0.0	0.0	0.0
1	24.80	0.0	46.3	0.0	12.7	3.6	12.7	34.7	0.0	0.0	0.0
1	27.14	0.0	23.1	34.7	6.3	2.9	38.1	69.4	3.2	0.0	0.0
1	28.65	0.0	46.3	0.0	12.7	2.5	25.4	34.7	34.9	34.7	41.0
1	31.80	0.0	92.6	0.0	25.4	4.0	63.4	34.7	79.3	25.2	28.4
1	34.14	0.0	69.4	0.0	19.0	5.9	79.3	34.7	193.5	28.4	37.9
1	35.15	0.0	0.0	0.0	0.0	11.6	0.0	0.0	25.4	56.8	31.6
1	38.30	0.0	0.0	0.0	0.0	11.6	0.0	0.0	57.1	31.6	6.3
1	40.64	0.0	0.0	0.0	0.0	11.6	0.0	0.0	50.8	18.9	0.0
1	41.65	0.0	23.1	0.0	6.3	11.1	12.7	0.0	38.1	41.0	97.8
1	44.80	0.0	46.3	69.4	12.7	11.0	19.0	0.0	22.2	94.7	75.7
1	47.14	0.0	46.3	69.4	12.7	11.1	19.0	0.0	31.7	126.2	44.2
1	51.65	0.0	0.0	0.0	0.0	11.6	0.0	0.0	6.3	0.0	9.5
1	54.80	0.0	0.0	0.0	0.0	11.6	0.0	0.0	6.3	0.0	6.3
1	57.14	0.0	0.0	0.0	0.0	11.6	0.0	0.0	0.0	0.0	0.0
1	61.65	0.0	0.0	0.0	0.0	11.6	0.0	0.0	19.0	6.3	9.5
1	64.80	0.0	0.0	0.0	0.0	11.6	0.0	0.0	12.7	6.3	0.0
1	67.14	0.0	0.0	0.0	0.0	11.6	0.0	0.0	6.3	0.0	0.0
1	71.65	0.0	0.0	0.0	0.0	11.6	0.0	0.0	0.0	0.0	0.0
x'	y	F	F	F	F	F	F	F	F	F	F
m	mm	Hz	Hz	Hz	Hz	Hz	Hz	Hz	Hz	Hz	Hz
(1)	(2)	(3)	(4)	(5)	(6)	(7)	(8)	(9)	(10)	(11)	(12)

VI.4 Experiments Series 2 - Air-water specific interface data

Location :	University of Queensland (Australia)
Date :	June-Aug. 2002
Experiments by :	Chung Hwee "Jerry" LIM and York-wee TAN
Data processing by :	H. CHANSON
Experiment characteristics :	Flume : length: 25 m, width: 0.5 m, slope: 3.4 degrees, step height: 0.0715 m, step length: 1.2 m. Inflow conditions : nozzle depth d_n = 0.03 m. First step : 2.4 m long, equipped with sidewall deflectors.
Instrumentation :	Single-tip conductivity probe (Ø = 0.35 mm).
Comments :	Data calculated for a minimum control volume Δx of 70 mm.

Experimental results in terms of air-water specific interface areas were calculated during a short time interval ΔT such as $\Delta T = \Delta X/C_S$ where C_S is the measured surge front celerity and ΔX is the control volume streamwise length. ΔX was selected to be a multiple of Δx = 70 mm : i.e., $\Delta X = I*\Delta x$ where I is an integrer equal or larger than unity.

In turn, the data calculated along ΔX correspond to a dimensionless time $(t - t_S)$ where t_S is the time of passage of wave front. In the following paragraphs, the data are typically presented in the following form:

Legend	Streamwise control volume length	Corresponding time

ΔX = 210-385 mm	ΔX = 175 mm	$0.210/C_S \le (t - t_S) \le 0.385/C_S$

Run TL1

Q m^3/s	Step	x' m	C_S m/s	d_o m
0.040	16	0.2, 0.4, 0.6, 0.8, 1.0	1.97	0.195

x' m (1)	y mm (2)	a 1/m (3)	a 1/m (4)	a 1/m (5)	a 1/m (6)	a 1/m (7)	a 1/m (8)	a 1/m (9)	a 1/m (10)	a 1/m (11)	a 1/m (12)
ΔX =	(mm)	0-70	0-210	140-210	0-385	175-385	350-735	525-595	700-1085	2100-2485	4200-4585
$t - t_S$ =	(s)	0.018	0.053	0.089	0.098	0.142	0.275	0.284	0.453	1.164	2.23
ΔX =	(mm)	70	210	70	385	210	385	70	385	385	385
$\frac{(t-t_S)}{\sqrt{d_o/g}}$		0.126	0.378	0.629	0.692	1.007	1.951	2.014	3.21	8.245	15.8
0.2	0.0	190.5	0.0	52.2	0.6	83.6	0.0	20.9	0.0	0.0	0.0
0.2	114.3	438.1	57.1	120.1	0.9	36.6	0.0	36.6	0.0	0.0	0.0
0.2	171.4	419.0	0.0	114.9	1.1	47.0	57.1	20.9	31.2	10.4	10.4
0.2	0.0	114.3	0.0	31.3	0.9	20.9	0.0	73.1	31.2	62.3	62.3
0.2	57.1	152.4	0.0	41.8	0.0	0.0	0.0	52.2	57.1	51.9	51.9
0.2	114.3	114.3	0.0	31.3	0.5	20.9	0.0	36.6	10.4	31.2	31.2
0.2	0.0	190.5	57.1	52.2	1.3	41.8	0.0	26.1	0.0	77.9	77.9
0.2	57.1	171.4	0.0	47.0	2.6	83.6	0.0	26.1	0.0	20.8	20.8
0.2	0.0	57.1	0.0	15.7	2.6	52.2	0.0	57.4	10.4	36.4	36.4
0.2	0.0	152.4	0.0	41.8	17.1	15.7	0.0	15.7	10.4	10.4	10.4
0.2	0.0	152.4	0.0	41.8	17.5	20.9	0.0	57.4	10.4	77.9	77.9
0.2	0.0	133.3	0.0	36.6	17.6	10.4	0.0	62.7	36.4	109.1	109.1
0.2	0.0	190.5	57.1	52.2	12.3	47.0	0.0	57.4	10.4	41.6	41.6
0.2	0.0	152.4	114.3	41.8	14.3	31.3	0.0	83.6	62.3	72.7	72.7
0.2	0.0	190.5	171.4	52.2	16.0	20.9	0.0	73.1	93.5	98.7	98.7
0.2	0.0	19.0	0.0	5.2	17.2	36.6	0.0	52.2	62.3	114.3	114.3
0.2	0.0	19.0	0.0	5.2	17.6	36.6	0.0	20.9	67.5	57.1	57.1
0.2	0.0	38.1	0.0	10.4	18.4	20.9	114.3	10.4	77.9	57.1	57.1
0.4	57.1	228.6	0.0	62.7	0.0	0.0	0.0	0.0	0.0	15.6	15.6
0.4	171.4	419.0	0.0	114.9	0.0	0.0	0.0	10.4	0.0	51.9	51.9
0.4	57.1	361.9	114.3	99.2	0.3	20.9	0.0	26.1	10.4	51.9	51.9
0.4	0.0	57.1	0.0	15.7	4.2	62.7	114.3	47.0	5.2	15.6	15.6
0.4	0.0	57.1	0.0	15.7	8.3	120.1	57.1	62.7	31.2	10.4	10.4
0.4	0.0	76.2	0.0	20.9	11.3	88.8	114.3	88.8	41.6	20.8	20.8
0.4	0.0	285.7	114.3	78.3	5.7	88.8	171.4	31.3	88.3	72.7	72.7
0.4	0.0	247.6	114.3	67.9	8.7	161.9	57.1	83.6	135.1	103.9	103.9
0.4	0.0	95.2	57.1	26.1	10.6	146.2	171.4	130.5	77.9	103.9	103.9
0.4	0.0	76.2	0.0	20.9	18.4	20.9	0.0	104.4	176.6	213.0	213.0
0.4	0.0	76.2	57.1	20.9	18.8	10.4	0.0	62.7	124.7	150.6	150.6
0.4	0.0	57.1	0.0	15.7	18.7	5.2	0.0	52.2	88.3	72.7	72.7
0.4	0.0	76.2	57.1	20.9	7.9	62.7	57.1	62.7	109.1	93.5	93.5
0.4	0.0	76.2	0.0	20.9	9.7	94.0	57.1	67.9	145.5	83.1	83.1
0.4	0.0	76.2	0.0	20.9	11.7	88.8	114.3	99.2	171.4	83.1	83.1
0.4	0.0	76.2	0.0	20.9	17.9	62.7	114.3	62.7	20.8	83.1	83.1
0.4	0.0	38.1	0.0	10.4	17.2	62.7	57.1	62.7	20.8	88.3	88.3
0.4	0.0	38.1	0.0	10.4	17.5	62.7	114.3	62.7	31.2	103.9	103.9
0.6	114.3	152.4	0.0	41.8	0.0	0.0	0.0	0.0	0.0	0.0	0.0

0.6	0.0	114.3	171.4	31.3	0.0	0.0	0.0	0.0	0.0	0.0	0.0
0.6	0.0	114.3	57.1	31.3	0.3	20.9	114.3	10.4	0.0	10.4	10.4
0.6	0.0	228.6	57.1	62.7	1.5	41.8	0.0	36.6	0.0	0.0	0.0
0.6	57.1	152.4	0.0	41.8	2.8	83.6	57.1	47.0	20.8	20.8	20.8
0.6	0.0	209.5	228.6	57.4	3.9	62.7	114.3	78.3	31.2	46.8	46.8
0.6	0.0	0.0	0.0	0.0	12.1	73.1	0.0	36.6	181.8	150.6	150.6
0.6	0.0	0.0	0.0	0.0	14.2	104.4	0.0	88.8	197.4	171.4	171.4
0.6	0.0	0.0	0.0	0.0	15.8	104.4	0.0	73.1	140.3	93.5	93.5
0.6	0.0	0.0	0.0	0.0	19.0	0.0	0.0	31.3	166.2	83.1	83.1
0.6	0.0	0.0	0.0	0.0	18.8	10.4	0.0	31.3	119.5	41.6	41.6
0.6	0.0	38.1	0.0	10.4	19.0	0.0	0.0	31.3	114.3	0.0	0.0
0.6	0.0	0.0	0.0	0.0	18.1	10.4	0.0	0.0	20.8	140.3	140.3
0.6	0.0	0.0	0.0	0.0	18.3	10.4	0.0	0.0	20.8	103.9	103.9
0.6	0.0	0.0	0.0	0.0	18.2	10.4	0.0	0.0	31.2	62.3	62.3
0.6	0.0	0.0	0.0	0.0	19.0	0.0	0.0	0.0	0.0	31.2	31.2
0.6	0.0	0.0	0.0	0.0	19.0	0.0	0.0	0.0	0.0	10.4	10.4
0.6	0.0	0.0	0.0	0.0	19.0	0.0	0.0	0.0	0.0	10.4	10.4

x'	y	a	a	a	a	a	a	a	a	a	a
m	mm	1/m	1/m	1/m	1/m	1/m	1/m	1/m	1/m	1/m	1/m
(1)	(2)	(3)	(4)	(5)	(6)	(7)	(8)	(9)	(10)	(11)	(12)
0.8	4.65	0.0	76.2	0.0	20.9	0.0	0.0	0.0	0.0	0.0	0.0
0.8	7.8	57.1	266.7	114.3	73.1	0.0	0.0	0.0	0.0	0.0	0.0
0.8	10.14	171.4	381.0	0.0	104.4	0.0	0.0	0.0	0.0	0.0	0.0
0.8	11.65	0.0	76.2	57.1	20.9	0.9	41.8	57.1	0.0	0.0	10.4
0.8	14.8	0.0	114.3	0.0	31.3	3.7	52.2	114.3	20.9	0.0	20.8
0.8	17.14	0.0	285.7	0.0	78.3	9.3	26.1	57.1	41.8	20.8	41.6
0.8	21.65	0.0	76.2	0.0	20.9	13.4	41.8	171.4	99.2	103.9	109.1
0.8	24.8	0.0	152.4	0.0	41.8	16.5	52.2	0.0	83.6	140.3	119.5
0.8	27.14	0.0	57.1	0.0	15.7	17.6	47.0	0.0	41.8	124.7	51.9
0.8	28.65	0.0	0.0	0.0	0.0	18.0	31.3	0.0	0.0	41.6	10.4
0.8	31.8	0.0	0.0	0.0	0.0	19.0	0.0	0.0	0.0	31.2	46.8
0.8	34.8	0.0	0.0	0.0	0.0	19.0	0.0	0.0	0.0	0.0	20.8
0.8	35.15	0.0	0.0	0.0	0.0	19.0	0.0	0.0	0.0	0.0	31.2
0.8	38.3	0.0	0.0	0.0	0.0	19.0	0.0	0.0	0.0	0.0	0.0
0.8	40.64	0.0	0.0	0.0	0.0	19.0	0.0	0.0	0.0	0.0	0.0
0.8	41.65	0.0	0.0	0.0	0.0	19.0	0.0	0.0	0.0	0.0	0.0
0.8	44.8	0.0	0.0	0.0	0.0	19.0	0.0	0.0	0.0	0.0	0.0
1	4.65	0.0	76.2	0.0	20.9	0.0	0.0	0.0	0.0	0.0	0.0
1	7.8	0.0	38.1	57.1	10.4	0.0	0.0	0.0	0.0	0.0	0.0
1	10.14	0.0	114.3	57.1	31.3	0.0	0.0	0.0	0.0	0.0	0.0
1	11.65	0.0	0.0	0.0	0.0	0.9	10.4	0.0	0.0	20.8	0.0
1	14.8	0.0	228.6	171.4	62.7	3.8	78.3	57.1	52.2	31.2	0.0
1	17.14	0.0	247.6	114.3	67.9	10.2	167.1	57.1	141.0	67.5	5.2
1	21.65	0.0	0.0	0.0	0.0	19.0	0.0	0.0	125.3	62.3	114.3
1	24.8	0.0	0.0	0.0	0.0	19.0	0.0	0.0	114.9	31.2	218.2
1	27.14	0.0	0.0	0.0	0.0	19.0	0.0	0.0	41.8	93.5	176.6
1	28.65	0.0	0.0	0.0	0.0	19.0	0.0	0.0	73.1	0.0	88.3
1	31.8	0.0	0.0	0.0	0.0	19.0	0.0	0.0	0.0	0.0	46.8
1	34.14	0.0	0.0	0.0	0.0	19.0	0.0	0.0	0.0	0.0	20.8
1	35.15	0.0	0.0	0.0	0.0	19.0	0.0	0.0	0.0	0.0	124.7
1	38.3	0.0	0.0	0.0	0.0	19.0	0.0	0.0	0.0	0.0	51.9
1	40.64	0.0	0.0	0.0	0.0	19.0	0.0	0.0	0.0	0.0	31.2

x'	y	a	a	a	a	a	a	a	a	a	a
m	mm	1/m	1/m	1/m	1/m	1/m	1/m	1/m	1/m	1/m	1/m
(1)	(2)	(3)	(4)	(5)	(6)	(7)	(8)	(9)	(10)	(11)	(12)

Run TL3

Q m^3/s	Step	x' m	C_S m/s	d_o m
0.055	16	0.2, 0.4, 0.6, 0.8, 1.0	2.14	0.241

x' m (1)	y mm (2)	a 1/m (3)	a 1/m (4)	a 1/m (5)	a 1/m (6)	a 1/m (7)	a 1/m (8)	a 1/m (9)	a 1/m (10)	a 1/m (11)	a 1/m (12)
$\Delta X =$	(mm)	0-70	0-210	140-210	0-385	175-385	350-735	525-595	700-1085	2100-2485	4200-4585
$t - t_S =$	(s)	0.016	0.049	0.082	0.09	0.131	0.254	0.262	0.417	1.071	2.053
$\Delta X =$	(mm)	70	210	70	385	210	385	70	385	385	385
$\frac{(t-t_S)}{\sqrt{d_o/g}}$		0.104	0.313	0.521	0.573	0.834	1.615	1.667	2.657	6.826	13.08
0.2	4.65	57.1	266.7	57.1	73.1	1.5	52.2	0.0	10.4	31.2	0.0
0.2	7.80	57.1	152.4	0.0	41.8	0.0	0.0	0.0	0.0	10.4	10.4
0.2	10.14	0.0	304.8	57.1	83.6	0.2	10.4	57.1	20.9	36.4	31.2
0.2	11.65	57.1	152.4	114.3	41.8	5.9	57.4	57.1	52.2	26.0	10.4
0.2	14.80	114.3	247.6	114.3	67.9	5.5	73.1	57.1	52.2	15.6	0.0
0.2	17.14	285.7	247.6	0.0	67.9	6.4	67.9	114.3	52.2	88.3	20.8
0.2	21.65	285.7	323.8	57.1	88.8	6.2	114.9	114.3	78.3	62.3	161.0
0.2	24.80	171.4	304.8	57.1	83.6	4.8	47.0	0.0	73.1	93.5	135.1
0.2	27.14	171.4	190.5	0.0	52.2	1.9	83.6	57.1	20.9	51.9	36.4
0.2	28.65	0.0	323.8	171.4	88.8	2.3	73.1	0.0	26.1	67.5	62.3
0.2	31.80	0.0	285.7	57.1	78.3	1.1	20.9	0.0	36.6	51.9	41.6
0.2	34.14	228.6	323.8	57.1	88.8	1.1	31.3	0.0	15.7	41.6	15.6
0.2	35.15	0.0	171.4	114.3	47.0	8.2	62.7	57.1	36.6	31.2	0.0
0.2	38.30	0.0	133.3	57.1	36.6	12.4	73.1	0.0	57.4	83.1	5.2
0.2	40.64	0.0	57.1	0.0	15.7	14.0	62.7	0.0	36.6	62.3	20.8
0.2	41.65	0.0	228.6	57.1	62.7	11.1	47.0	114.3	62.7	20.8	10.4
0.2	44.80	0.0	0.0	0.0	0.0	12.7	78.3	114.3	83.6	51.9	46.8
0.2	47.14	0.0	0.0	0.0	0.0	15.4	36.6	57.1	67.9	72.7	103.9
0.2	51.65	0.0	57.1	0.0	15.7	15.5	47.0	57.1	20.9	93.5	88.3
0.2	54.80	0.0	57.1	0.0	15.7	15.9	47.0	57.1	57.4	83.1	98.7
0.2	57.14	0.0	57.1	0.0	15.7	16.7	47.0	57.1	57.4	51.9	109.1
0.4	4.65	57.1	266.7	114.3	73.1	0.0	10.4	0.0	0.0	5.2	10.4
0.4	7.80	228.6	495.2	57.1	135.8	0.1	10.4	0.0	10.4	10.4	26.0
0.4	10.14	0.0	495.2	285.7	135.8	2.8	47.0	0.0	5.2	0.0	41.6
0.4	11.65	0.0	323.8	0.0	88.8	1.6	26.1	0.0	0.0	5.2	20.8
0.4	14.80	0.0	266.7	0.0	73.1	2.7	52.2	57.1	15.7	0.0	31.2
0.4	17.14	0.0	133.3	0.0	36.6	3.5	78.3	114.3	20.9	0.0	31.2
0.4	21.65	0.0	190.5	57.1	52.2	3.8	99.2	171.4	99.2	57.1	41.6
0.4	24.80	0.0	285.7	114.3	78.3	4.4	67.9	57.1	125.3	103.9	114.3
0.4	27.14	0.0	247.6	57.1	67.9	6.2	88.8	0.0	177.5	109.1	109.1
0.4	28.65	0.0	76.2	0.0	20.9	7.8	62.7	114.3	88.8	135.1	46.8
0.4	31.80	0.0	38.1	0.0	10.4	10.4	88.8	171.4	125.3	166.2	161.0
0.4	34.14	0.0	0.0	0.0	0.0	10.7	125.3	228.6	125.3	155.8	140.3
0.4	35.15	0.0	76.2	0.0	20.9	9.7	151.4	342.9	125.3	114.3	93.5
0.4	38.30	0.0	57.1	0.0	15.7	9.8	114.9	171.4	120.1	93.5	103.9
0.4	40.64	0.0	0.0	0.0	0.0	10.5	62.7	114.3	120.1	114.3	114.3
0.4	41.65	0.0	57.1	0.0	15.7	13.9	83.6	57.1	94.0	98.7	124.7
0.4	44.80	0.0	19.0	0.0	5.2	14.9	104.4	171.4	141.0	109.1	103.9
0.4	47.14	0.0	95.2	114.3	26.1	15.6	99.2	57.1	73.1	83.1	67.5
0.4	51.65	0.0	114.3	0.0	31.3	15.6	130.5	285.7	125.3	46.8	114.3
0.4	54.80	0.0	76.2	0.0	20.9	17.5	94.0	228.6	78.3	51.9	129.9
0.4	57.14	0.0	76.2	0.0	20.9	18.2	52.2	114.3	73.1	20.8	62.3
0.6	4.65	114.3	76.2	0.0	20.9	0.0	0.0	0.0	10.4	0.0	0.0

0.6	7.80	114.3	381.0	228.6	104.4	0.0	0.0	0.0	10.4	0.0	0.0
0.6	10.14	0.0	571.4	342.9	156.7	0.0	0.0	0.0	0.0	0.0	0.0
0.6	11.65	228.6	190.5	57.1	52.2	0.0	0.0	0.0	0.0	0.0	0.0
0.6	14.80	0.0	266.7	171.4	73.1	0.0	0.0	0.0	0.0	0.0	0.0
0.6	17.14	57.1	457.1	228.6	125.3	0.0	0.0	0.0	0.0	0.0	15.6
0.6	21.65	0.0	0.0	0.0	0.0	1.6	26.1	0.0	15.7	15.6	0.0
0.6	24.80	0.0	152.4	0.0	41.8	2.2	78.3	228.6	15.7	15.6	41.6
0.6	27.14	0.0	76.2	0.0	20.9	2.8	104.4	114.3	41.8	46.8	72.7
0.6	28.65	0.0	190.5	0.0	52.2	5.8	31.3	57.1	52.2	41.6	124.7
0.6	31.80	0.0	114.3	0.0	31.3	8.6	41.8	57.1	109.7	46.8	207.8
0.6	34.14	0.0	38.1	0.0	10.4	9.9	62.7	57.1	161.9	83.1	161.0
0.6	35.15	0.0	57.1	0.0	15.7	2.3	67.9	57.1	73.1	10.4	72.7
0.6	38.30	0.0	76.2	0.0	20.9	3.6	125.3	57.1	224.5	51.9	135.1
0.6	40.64	0.0	76.2	0.0	20.9	4.1	94.0	171.4	135.8	51.9	114.3
0.6	41.65	0.0	95.2	0.0	26.1	13.9	94.0	0.0	78.3	114.3	114.3
0.6	44.80	0.0	38.1	0.0	10.4	14.7	130.5	0.0	36.6	114.3	150.6
0.6	47.14	0.0	0.0	0.0	0.0	15.2	88.8	0.0	47.0	114.3	119.5
0.6	51.65	0.0	247.6	0.0	67.9	14.4	36.6	0.0	52.2	57.1	93.5
0.6	54.80	0.0	323.8	0.0	88.8	15.0	36.6	0.0	20.9	62.3	140.3
0.6	57.14	0.0	171.4	0.0	47.0	15.3	26.1	0.0	10.4	20.8	83.1
0.8	4.65	57.1	361.9	114.3	99.2	0.0	0.0	0.0	0.0	0.0	0.0
0.8	7.80	171.4	419.0	400.0	114.9	0.0	0.0	0.0	0.0	0.0	0.0
0.8	10.14	0.0	114.3	114.3	31.3	0.0	0.0	0.0	0.0	0.0	10.4
0.8	11.65	0.0	190.5	0.0	52.2	0.0	0.0	0.0	0.0	0.0	0.0
0.8	14.80	0.0	342.9	228.6	94.0	0.0	0.0	0.0	0.0	0.0	5.2
0.8	17.14	0.0	323.8	285.7	88.8	0.1	5.2	0.0	0.0	0.0	31.2
0.8	21.65	0.0	38.1	0.0	10.4	1.2	20.9	0.0	52.2	31.2	0.0
0.8	24.80	0.0	0.0	0.0	0.0	3.2	41.8	0.0	83.6	31.2	5.2
0.8	27.14	0.0	19.0	0.0	5.2	5.9	47.0	57.1	52.2	119.5	41.6
0.8	28.65	0.0	0.0	0.0	0.0	2.9	62.7	0.0	104.4	62.3	155.8
0.8	31.80	0.0	0.0	0.0	0.0	5.5	135.8	171.4	36.6	145.5	31.2
0.8	34.14	0.0	0.0	0.0	0.0	13.0	94.0	57.1	10.4	109.1	0.0
0.8	35.15	0.0	0.0	0.0	0.0	13.1	177.5	342.9	0.0	109.1	77.9
0.8	38.30	0.0	0.0	0.0	0.0	15.8	167.1	228.6	0.0	57.1	36.4
0.8	40.64	0.0	0.0	0.0	0.0	16.4	83.6	114.3	0.0	26.0	41.6
0.8	41.65	0.0	0.0	0.0	0.0	19.0	0.0	0.0	52.2	62.3	31.2
0.8	44.80	0.0	0.0	0.0	0.0	19.0	0.0	0.0	36.6	41.6	41.6
0.8	47.14	0.0	0.0	0.0	0.0	19.0	0.0	0.0	0.0	20.8	26.0
0.8	51.65	0.0	0.0	0.0	0.0	19.0	0.0	0.0	52.2	5.2	0.0
0.8	54.80	0.0	0.0	0.0	0.0	19.0	0.0	0.0	62.7	0.0	0.0
0.8	57.14	0.0	0.0	0.0	0.0	19.0	0.0	0.0	41.8	0.0	0.0
1	4.65	0.0	190.5	0.0	52.2	0.0	0.0	0.0	0.0	0.0	10.4
1	7.80	0.0	342.9	57.1	94.0	0.0	0.0	0.0	0.0	0.0	10.4
1	10.14	0.0	190.5	57.1	52.2	0.0	0.0	0.0	0.0	0.0	0.0
1	11.65	0.0	0.0	0.0	0.0	1.1	41.8	0.0	0.0	0.0	0.0
1	14.80	0.0	114.3	171.4	31.3	6.6	83.6	171.4	0.0	20.8	0.0
1	17.14	0.0	323.8	342.9	88.8	9.7	57.4	0.0	5.2	31.2	0.0
1	21.65	0.0	152.4	228.6	41.8	13.3	52.2	0.0	57.4	0.0	46.8
1	24.80	0.0	152.4	228.6	41.8	15.0	73.1	0.0	67.9	62.3	67.5
1	27.14	0.0	76.2	114.3	20.9	17.7	62.7	0.0	36.6	83.1	124.7
1	28.65	0.0	0.0	0.0	0.0	18.1	10.4	0.0	0.0	62.3	166.2
1	31.80	0.0	0.0	0.0	0.0	18.5	10.4	0.0	0.0	72.7	166.2
1	34.14	0.0	0.0	0.0	0.0	19.0	0.0	0.0	0.0	31.2	67.5
1	35.15	0.0	0.0	0.0	0.0	19.0	0.0	0.0	0.0	72.7	10.4
1	38.30	0.0	0.0	0.0	0.0	19.0	0.0	0.0	0.0	31.2	10.4
1	40.64	0.0	0.0	0.0	0.0	19.0	0.0	0.0	0.0	20.8	20.8
x'	y	a	a	a	a	a	a	a	a	a	a
m	mm	1/m	1/m	1/m	1/m	1/m	1/m	1/m	1/m	1/m	1/m
(1)	(2)	(3)	(4)	(5)	(6)	(7)	(8)	(9)	(10)	(11)	(12)

Run TL5 (step 10)

Q m^3/s	Step	x' m	C_S m/s	d_o m
0.075	10	0.2, 0.4, 0.6, 0.8, 1.0	2.61	0.297

x' m (1)	y mm (2)	a 1/m (3)	a 1/m (4)	a 1/m (5)	a 1/m (6)	a 1/m (7)	a 1/m (8)	a 1/m (9)	a 1/m (10)	a 1/m (11)	a 1/m (12)
ΔX =	(mm)	0-70	0-210	140-210	0-385	175-385	350-735	525-595	700-1085	2100-2485	4200-4585
$t - t_S$ =	(s)	0.013	0.04	0.067	0.074	0.107	0.208	0.215	0.342	0.878	1.683
ΔX =	(mm)	70	210	70	385	210	385	70	385	385	385
$\frac{(t-t_S)}{\sqrt{d_o/g}}$		0.077	0.231	0.385	0.424	0.616	1.194	1.233	1.965	5.047	9.67
0.2	4.65	57.1	38.1	0.0	10.4	1.1	31.3	0.0	10.4	5.2	0.0
0.2	7.80	57.1	38.1	0.0	10.4	0.8	0.0	0.0	10.4	0.0	0.0
0.2	10.14	114.3	57.1	0.0	15.7	0.6	0.0	0.0	41.8	0.0	0.0
0.2	11.65	0.0	76.2	0.0	20.9	5.9	67.9	171.4	10.4	20.8	46.8
0.2	14.80	0.0	38.1	0.0	10.4	6.9	26.1	57.1	5.2	10.4	31.2
0.2	17.14	0.0	0.0	0.0	0.0	12.9	26.1	0.0	52.2	0.0	51.9
0.2	21.65	0.0	0.0	0.0	0.0	15.2	20.9	0.0	10.4	57.1	140.3
0.2	24.80	114.3	57.1	0.0	15.7	17.1	10.4	0.0	10.4	46.8	83.1
0.2	27.14	114.3	95.2	57.1	26.1	18.2	26.1	0.0	10.4	46.8	103.9
0.2	28.65	0.0	114.3	0.0	31.3	18.9	10.4	0.0	73.1	93.5	83.1
0.2	31.80	0.0	171.4	0.0	47.0	14.6	83.6	0.0	83.6	109.1	62.3
0.2	34.14	114.3	209.5	114.3	57.4	8.1	88.8	114.3	104.4	77.9	31.2
0.2	35.15	0.0	342.9	0.0	94.0	1.5	31.3	57.1	52.2	51.9	20.8
0.2	38.30	0.0	285.7	0.0	78.3	1.3	62.7	114.3	20.9	36.4	10.4
0.2	40.64	0.0	266.7	0.0	73.1	1.5	78.3	57.1	10.4	15.6	26.0
0.2	41.65	114.3	95.2	57.1	26.1	1.5	62.7	57.1	41.8	0.0	0.0
0.2	44.80	171.4	209.5	0.0	57.4	1.5	62.7	57.1	41.8	0.0	0.0
0.2	47.14	114.3	133.3	0.0	36.6	2.4	52.2	0.0	31.3	26.0	5.2
0.2	51.65	57.1	247.6	171.4	67.9	3.8	62.7	171.4	78.3	67.5	0.0
0.2	54.80	114.3	190.5	57.1	52.2	4.2	67.9	228.6	78.3	36.4	20.8
0.2	57.14	114.3	133.3	0.0	36.6	4.6	52.2	114.3	125.3	51.9	20.8
0.2	61.65	57.1	247.6	0.0	67.9	12.0	41.8	114.3	41.8	72.7	41.6
0.2	64.80	57.1	285.7	0.0	78.3	13.2	52.2	57.1	52.2	62.3	72.7
0.2	67.14	0.0	152.4	0.0	41.8	15.9	52.2	0.0	52.2	31.2	77.9
0.2	71.65	285.7	304.8	171.4	83.6	17.8	31.3	0.0	31.3	72.7	15.6
0.2	74.80	400.0	571.4	114.3	156.7	18.7	20.9	0.0	31.3	62.3	31.2
0.2	77.14	400.0	514.3	114.3	141.0	18.7	20.9	0.0	20.9	0.0	15.6
0.2	81.65	0.0	152.4	57.1	41.8	19.0	0.0	0.0	0.0	0.0	0.0
0.4	4.65	0.0	95.2	0.0	26.1	0.0	0.0	0.0	0.0	0.0	0.0
0.4	7.80	0.0	38.1	0.0	10.4	0.0	5.2	0.0	5.2	20.8	0.0
0.4	10.14	0.0	95.2	114.3	26.1	0.0	0.0	0.0	26.1	36.4	20.8
0.4	11.65	0.0	133.3	285.7	36.6	0.0	0.0	0.0	20.9	20.8	0.0
0.4	14.80	0.0	95.2	171.4	26.1	0.0	0.0	0.0	41.8	10.4	10.4
0.4	17.14	0.0	266.7	171.4	73.1	0.0	0.0	0.0	15.7	10.4	31.2
0.4	21.65	0.0	266.7	285.7	73.1	1.7	41.8	114.3	94.0	0.0	31.2
0.4	24.80	0.0	438.1	457.1	120.1	5.0	135.8	171.4	167.1	26.0	67.5
0.4	27.14	0.0	247.6	285.7	67.9	6.6	219.3	285.7	83.6	46.8	26.0
0.4	28.65	0.0	152.4	0.0	41.8	6.8	99.2	57.1	73.1	103.9	31.2
0.4	31.80	0.0	152.4	0.0	41.8	7.4	104.4	57.1	125.3	207.8	57.1

0.4	34.14	0.0	0.0	0.0	0.0	10.1	114.9	114.3	104.4	197.4	129.9
0.4	35.15	0.0	19.0	0.0	5.2	11.2	130.5	342.9	88.8	119.5	67.5
0.4	38.30	0.0	133.3	0.0	36.6	13.1	109.7	57.1	109.7	150.6	77.9
0.4	40.64	0.0	133.3	0.0	36.6	15.6	78.3	114.3	109.7	109.1	129.9
0.4	41.65	0.0	95.2	0.0	26.1	18.6	20.9	0.0	57.4	46.8	67.5
0.4	44.80	0.0	38.1	0.0	10.4	18.6	10.4	0.0	57.4	57.1	140.3
0.4	47.14	0.0	57.1	0.0	15.7	18.4	20.9	0.0	20.9	51.9	77.9
0.4	51.65	0.0	190.5	0.0	52.2	19.0	0.0	0.0	52.2	15.6	41.6
0.4	54.80	0.0	95.2	0.0	26.1	19.0	0.0	0.0	73.1	5.2	77.9
0.4	57.14	0.0	152.4	0.0	41.8	19.0	0.0	0.0	41.8	0.0	41.6
0.4	61.65	0.0	0.0	0.0	0.0	18.0	15.7	0.0	0.0	0.0	15.6
0.4	64.80	0.0	0.0	0.0	0.0	18.8	5.2	0.0	0.0	0.0	15.6
0.4	67.14	0.0	0.0	0.0	0.0	19.0	0.0	0.0	0.0	0.0	26.0
0.4	71.65	0.0	0.0	0.0	0.0	18.9	15.7	0.0	20.9	0.0	41.6
0.4	74.80	0.0	0.0	0.0	0.0	18.7	10.4	0.0	20.9	0.0	41.6
0.4	77.14	0.0	0.0	0.0	0.0	18.6	15.7	0.0	10.4	0.0	83.1
0.4	81.65	0.0	0.0	0.0	0.0	19.0	0.0	0.0	0.0	41.6	0.0
0.6	4.65	0.0	361.9	171.4	99.2	0.6	31.3	0.0	0.0	0.0	10.4
0.6	7.80	0.0	381.0	114.3	104.4	2.3	99.2	114.3	20.9	10.4	10.4
0.6	10.14	0.0	95.2	0.0	26.1	4.3	125.3	171.4	10.4	5.2	10.4
0.6	11.65	0.0	228.6	0.0	62.7	1.8	52.2	57.1	26.1	0.0	10.4
0.6	14.80	0.0	247.6	0.0	67.9	3.0	67.9	57.1	94.0	10.4	20.8
0.6	17.14	0.0	323.8	0.0	88.8	4.2	94.0	57.1	78.3	0.0	20.8
0.6	21.65	0.0	95.2	0.0	26.1	12.5	73.1	57.1	31.3	0.0	20.8
0.6	24.80	0.0	95.2	0.0	26.1	16.0	57.4	57.1	36.6	0.0	15.6
0.6	27.14	0.0	38.1	0.0	10.4	16.6	52.2	57.1	15.7	5.2	57.1
0.6	28.65	0.0	0.0	0.0	0.0	7.4	188.0	114.3	151.4	20.8	31.2
0.6	31.80	0.0	0.0	0.0	0.0	10.8	214.1	171.4	135.8	0.0	20.8
0.6	34.14	0.0	0.0	0.0	0.0	13.4	146.2	285.7	130.5	10.4	41.6
0.6	35.15	0.0	38.1	0.0	10.4	16.2	15.7	0.0	109.7	31.2	0.0
0.6	38.30	0.0	19.0	0.0	5.2	15.7	31.3	0.0	114.9	57.1	41.6
0.6	40.64	0.0	0.0	0.0	0.0	16.9	15.7	0.0	83.6	51.9	83.1
0.6	41.65	0.0	95.2	0.0	26.1	18.4	20.9	0.0	114.9	46.8	51.9
0.6	44.80	0.0	38.1	0.0	10.4	18.5	5.2	0.0	135.8	72.7	62.3
0.6	47.14	0.0	19.0	0.0	5.2	18.5	5.2	0.0	94.0	93.5	51.9
0.6	51.65	0.0	19.0	0.0	5.2	18.6	10.4	0.0	36.6	98.7	140.3
0.6	54.80	0.0	57.1	0.0	15.7	19.0	10.4	0.0	41.8	98.7	249.4
0.6	57.14	0.0	38.1	0.0	10.4	19.0	0.0	0.0	20.9	103.9	197.4
0.6	61.65	0.0	0.0	0.0	0.0	15.3	78.3	57.1	0.0	103.9	103.9
0.6	64.80	0.0	0.0	0.0	0.0	16.6	78.3	114.3	0.0	88.3	109.1
0.6	67.14	0.0	0.0	0.0	0.0	17.9	41.8	57.1	10.4	93.5	72.7
0.6	71.65	0.0	0.0	0.0	0.0	19.0	5.2	0.0	0.0	114.3	124.7
0.6	74.80	0.0	0.0	0.0	0.0	19.0	0.0	0.0	5.2	135.1	176.6
0.6	77.14	0.0	0.0	0.0	0.0	19.0	0.0	0.0	5.2	109.1	109.1
0.6	81.65	0.0	0.0	0.0	0.0	19.0	0.0	0.0	5.2	72.7	145.5
0.8	4.65	57.1	57.1	0.0	15.7	0.0	0.0	0.0	0.0	0.0	0.0
0.8	7.80	457.1	495.2	114.3	135.8	0.1	10.4	0.0	0.0	0.0	0.0
0.8	10.14	0.0	285.7	171.4	78.3	0.0	0.0	0.0	0.0	10.4	0.0
0.8	11.65	0.0	76.2	0.0	20.9	0.0	0.0	0.0	10.4	10.4	0.0
0.8	14.80	171.4	457.1	57.1	125.3	0.0	0.0	0.0	0.0	10.4	0.0
0.8	17.14	285.7	381.0	171.4	104.4	0.0	0.0	0.0	10.4	36.4	0.0
0.8	21.65	0.0	266.7	114.3	73.1	16.8	73.1	0.0	0.0	10.4	10.4
0.8	24.80	0.0	228.6	0.0	62.7	18.0	67.9	0.0	20.9	10.4	10.4
0.8	27.14	0.0	38.1	0.0	10.4	18.1	62.7	57.1	10.4	0.0	26.0
0.8	28.65	0.0	19.0	0.0	5.2	9.8	31.3	0.0	94.0	0.0	10.4
0.8	31.80	0.0	95.2	57.1	26.1	11.7	94.0	57.1	99.2	26.0	20.8
0.8	34.14	0.0	38.1	0.0	10.4	15.8	26.1	0.0	99.2	20.8	41.6
0.8	35.15	0.0	19.0	0.0	5.2	16.7	52.2	171.4	62.7	20.8	41.6
0.8	38.30	0.0	0.0	0.0	0.0	17.9	52.2	0.0	114.9	10.4	93.5

0.8	40.64	0.0	0.0	0.0	0.0	18.6	15.7	0.0	120.1	15.6	15.6
0.8	41.65	0.0	0.0	0.0	0.0	14.4	10.4	57.1	57.4	0.0	41.6
0.8	44.80	0.0	0.0	0.0	0.0	15.1	41.8	57.1	109.7	20.8	20.8
0.8	47.14	0.0	0.0	0.0	0.0	16.0	26.1	114.3	99.2	20.8	31.2
0.8	51.65	0.0	0.0	0.0	0.0	15.4	0.0	0.0	73.1	20.8	31.2
0.8	54.80	0.0	0.0	0.0	0.0	16.0	52.2	0.0	161.9	46.8	41.6
0.8	57.14	0.0	0.0	0.0	0.0	16.4	41.8	0.0	120.1	67.5	62.3
0.8	61.65	0.0	0.0	0.0	0.0	18.3	15.7	0.0	62.7	93.5	103.9
0.8	64.80	0.0	0.0	0.0	0.0	18.7	15.7	0.0	52.2	72.7	171.4
0.8	67.14	0.0	0.0	0.0	0.0	18.8	10.4	0.0	20.9	83.1	135.1
0.8	71.65	0.0	0.0	0.0	0.0	19.0	0.0	0.0	31.3	67.5	114.3
0.8	74.80	0.0	0.0	0.0	0.0	19.0	0.0	0.0	36.6	88.3	155.8
0.8	77.14	0.0	0.0	0.0	0.0	19.0	0.0	0.0	31.3	77.9	161.0
0.8	81.65	0.0	0.0	0.0	0.0	19.0	0.0	0.0	31.3	103.9	88.3
0.8	84.80	0.0	0.0	0.0	0.0	19.0	0.0	0.0	26.1	129.9	57.1
0.8	87.14	0.0	0.0	0.0	0.0	19.0	0.0	0.0	15.7	62.3	83.1
0.8	91.65	0.0	0.0	0.0	0.0	19.0	0.0	0.0	0.0	10.4	10.4
0.8	94.80	0.0	0.0	0.0	0.0	19.0	0.0	0.0	5.2	10.4	10.4
0.8	97.14	0.0	0.0	0.0	0.0	19.0	0.0	0.0	5.2	10.4	31.2
1	4.65	0.0	0.0	0.0	0.0	0.0	0.0	0.0	0.0	0.0	0.0
1	7.80	0.0	285.7	0.0	78.3	0.0	0.0	0.0	0.0	0.0	0.0
1	10.14	0.0	114.3	0.0	31.3	0.3	15.7	0.0	0.0	0.0	0.0
1	11.65	0.0	152.4	171.4	41.8	0.1	10.4	57.1	10.4	0.0	0.0
1	14.80	0.0	152.4	171.4	41.8	0.1	20.9	0.0	10.4	15.6	0.0
1	17.14	0.0	266.7	0.0	73.1	0.7	52.2	114.3	10.4	0.0	10.4
1	21.65	0.0	171.4	57.1	47.0	1.8	52.2	0.0	10.4	0.0	20.8
1	24.80	0.0	133.3	114.3	36.6	2.4	41.8	0.0	0.0	20.8	31.2
1	27.14	0.0	133.3	171.4	36.6	2.7	83.6	0.0	20.9	5.2	10.4
1	28.65	0.0	133.3	0.0	36.6	1.5	83.6	342.9	73.1	20.8	20.8
1	31.80	0.0	247.6	0.0	67.9	4.4	198.4	514.3	99.2	31.2	10.4
1	34.14	0.0	152.4	0.0	41.8	8.0	130.5	57.1	78.3	20.8	5.2
1	35.15	0.0	0.0	0.0	0.0	3.2	73.1	57.1	41.8	0.0	10.4
1	38.30	0.0	0.0	0.0	0.0	5.3	94.0	114.3	73.1	10.4	36.4
1	40.64	0.0	0.0	0.0	0.0	8.7	120.1	57.1	47.0	10.4	36.4
1	41.65	0.0	0.0	0.0	0.0	12.5	99.2	0.0	99.2	83.1	20.8
1	44.80	0.0	38.1	0.0	10.4	14.7	73.1	0.0	99.2	51.9	31.2
1	47.14	0.0	19.0	0.0	5.2	16.4	73.1	0.0	78.3	41.6	26.0
1	51.65	0.0	0.0	0.0	0.0	18.1	73.1	0.0	52.2	155.8	57.1
1	54.80	0.0	0.0	0.0	0.0	17.7	141.0	628.6	94.0	98.7	51.9
1	57.14	0.0	0.0	0.0	0.0	18.2	88.8	457.1	47.0	187.0	62.3
1	61.65	0.0	0.0	0.0	0.0	19.0	0.0	0.0	20.9	72.7	103.9
1	64.80	0.0	0.0	0.0	0.0	19.0	0.0	0.0	20.9	98.7	98.7
1	67.14	0.0	0.0	0.0	0.0	19.0	0.0	0.0	20.9	72.7	77.9
1	71.65	0.0	0.0	0.0	0.0	19.0	0.0	0.0	0.0	10.4	31.2
1	71.65	0.0	0.0	0.0	0.0	19.0	0.0	0.0	0.0	10.4	31.2
1	74.80	0.0	0.0	0.0	0.0	19.0	0.0	0.0	0.0	0.0	36.4
1	77.14	0.0	0.0	0.0	0.0	19.0	0.0	0.0	0.0	0.0	26.0
1	81.65	0.0	0.0	0.0	0.0	19.0	0.0	0.0	0.0	72.7	31.2
x'	y	a	a	a	a	a	a	a	a	a	a
m	mm	1/m	1/m	1/m	1/m	1/m	1/m	1/m	1/m	1/m	1/m
(1)	(2)	(3)	(4)	(5)	(6)	(7)	(8)	(9)	(10)	(11)	(12)

Run TL5 (step 16)

Q m^3/s	Step	x' m	C_s m/s	d_o m
0.075	16	0.2, 0.4, 0.6, 0.8, 1.0	2.43	0.297

x' m (1)	y mm (2)	a 1/m (3)	a 1/m (4)	a 1/m (5)	a 1/m (6)	a 1/m (7)	a 1/m (8)	a 1/m (9)	a 1/m (10)	a 1/m (11)	a 1/m (12)
ΔX =	(mm)	0-70	0-210	140-210	0-385	175-385	350-735	525-595	700-1085	2100-2485	4200-4585
$t - t_S$ =	(s)	0.0144	0.0432	0.072	0.0792	0.1152	0.2233	0.2305	0.3673	0.9434	1.8076
ΔX =	(mm)	70	210	70	385	210	385	70	385	385	385
$\frac{(t-t_S)}{\sqrt{d_o/g}}$		0.0828	0.2483	0.4138	0.4552	0.6621	1.2828	1.3242	2.1104	5.4208	10.386
0.2	4.65	0.0	152.4	171.4	41.8	0.0	0.0	0.0	10.4	0.0	20.8
0.2	7.80	0.0	38.1	0.0	10.4	1.5	20.9	0.0	0.0	0.0	0.0
0.2	10.14	0.0	114.3	0.0	31.3	4.1	41.8	0.0	20.9	15.6	20.8
0.2	11.65	0.0	38.1	0.0	10.4	0.5	20.9	0.0	10.4	10.4	31.2
0.2	14.80	0.0	38.1	0.0	10.4	1.1	36.6	171.4	31.3	41.6	15.6
0.2	17.14	57.1	114.3	0.0	31.3	6.9	36.6	0.0	10.4	62.3	57.1
0.2	21.65	0.0	38.1	0.0	10.4	18.1	20.9	0.0	47.0	88.3	31.2
0.2	24.80	114.3	114.3	57.1	31.3	18.0	20.9	0.0	52.2	98.7	46.8
0.2	27.14	57.1	190.5	0.0	52.2	13.8	83.6	171.4	120.1	109.1	103.9
0.2	28.65	57.1	247.6	171.4	67.9	9.4	73.1	0.0	47.0	88.3	83.1
0.2	31.80	114.3	438.1	57.1	120.1	6.7	114.9	114.3	47.0	88.3	72.7
0.2	34.14	171.4	438.1	57.1	120.1	2.4	62.7	0.0	26.1	46.8	67.5
0.2	35.15	0.0	0.0	0.0	0.0	0.0	0.0	0.0	41.8	0.0	41.6
0.2	38.30	0.0	76.2	0.0	20.9	0.8	10.4	0.0	36.6	0.0	20.8
0.2	40.64	114.3	95.2	0.0	26.1	1.4	10.4	57.1	52.2	31.2	20.8
0.2	41.65	0.0	114.3	114.3	31.3	0.2	20.9	0.0	10.4	15.6	46.8
0.2	44.80	0.0	114.3	57.1	31.3	0.9	26.1	0.0	36.6	0.0	31.2
0.2	47.14	0.0	152.4	0.0	41.8	1.3	10.4	0.0	41.8	10.4	46.8
0.2	51.65	0.0	57.1	57.1	15.7	4.0	47.0	57.1	41.8	20.8	51.9
0.2	54.80	0.0	323.8	171.4	88.8	6.8	57.4	57.1	41.8	67.5	57.1
0.2	57.14	0.0	133.3	57.1	36.6	8.2	57.4	114.3	83.6	41.6	72.7
0.2	61.65	57.1	133.3	57.1	36.6	15.6	31.3	0.0	36.6	46.8	67.5
0.2	64.80	114.3	228.6	57.1	62.7	16.3	20.9	0.0	31.3	62.3	93.5
0.2	67.14	57.1	152.4	57.1	41.8	16.6	20.9	0.0	0.0	20.8	103.9
0.2	71.65	0.0	76.2	0.0	20.9	13.4	94.0	114.3	0.0	41.6	10.4
0.2	74.80	0.0	38.1	0.0	10.4	14.1	83.6	57.1	0.0	41.6	0.0
0.2	77.14	0.0	38.1	0.0	10.4	15.5	52.2	0.0	0.0	0.0	0.0
0.2	81.65	57.1	133.3	0.0	36.6	18.9	0.0	0.0	10.4	0.0	20.8
0.4	4.65	171.4	247.6	114.3	67.9	0.4	26.1	114.3	0.0	26.0	20.8
0.4	7.80	0.0	381.0	114.3	104.4	0.4	31.3	57.1	10.4	51.9	57.1
0.4	10.14	0.0	514.3	228.6	141.0	0.7	57.4	57.1	20.9	114.3	41.6
0.4	11.65	57.1	514.3	342.9	141.0	3.5	120.1	114.3	20.9	36.4	20.8
0.4	14.80	0.0	419.0	171.4	114.9	6.5	151.4	171.4	78.3	72.7	15.6
0.4	17.14	0.0	285.7	57.1	78.3	10.0	104.4	114.3	88.8	77.9	26.0
0.4	21.65	0.0	228.6	114.3	62.7	0.8	36.6	57.1	114.9	57.1	83.1
0.4	24.80	0.0	533.3	57.1	146.2	1.5	57.4	57.1	135.8	62.3	114.3
0.4	27.14	0.0	285.7	57.1	78.3	3.5	114.9	228.6	224.5	103.9	124.7
0.4	28.65	0.0	95.2	0.0	26.1	7.3	130.5	57.1	94.0	72.7	67.5
0.4	31.80	0.0	76.2	0.0	20.9	10.2	146.2	228.6	62.7	62.3	93.5
0.4	34.14	0.0	152.4	57.1	41.8	11.3	203.7	400.0	36.6	135.1	103.9
0.4	35.15	0.0	76.2	0.0	20.9	14.6	57.4	0.0	109.7	93.5	176.6
0.4	38.30	0.0	114.3	0.0	31.3	14.4	31.3	0.0	94.0	88.3	207.8
0.4	40.64	0.0	114.3	0.0	31.3	15.2	83.6	0.0	83.6	124.7	145.5
0.4	41.65	0.0	38.1	0.0	10.4	14.6	94.0	114.3	41.8	109.1	135.1
0.4	44.80	0.0	38.1	0.0	10.4	15.7	83.6	114.3	78.3	88.3	145.5
0.4	47.14	0.0	57.1	0.0	15.7	15.7	73.1	57.1	94.0	83.1	129.9
0.4	51.65	0.0	0.0	0.0	0.0	15.9	109.7	285.7	41.8	36.4	161.0
0.4	54.80	0.0	38.1	0.0	10.4	16.4	99.2	171.4	57.4	88.3	140.3

0.4	57.14	0.0	38.1	0.0	10.4	17.5	36.6	114.3	36.6	46.8	129.9
0.4	61.65	0.0	0.0	0.0	0.0	18.2	10.4	0.0	52.2	62.3	77.9
0.4	64.80	0.0	0.0	0.0	0.0	18.7	10.4	0.0	41.8	72.7	98.7
0.4	67.14	0.0	19.0	0.0	5.2	18.7	15.7	0.0	41.8	72.7	51.9
0.4	71.65	0.0	0.0	0.0	0.0	19.0	0.0	0.0	0.0	51.9	31.2
0.4	74.80	0.0	0.0	0.0	0.0	19.0	0.0	0.0	0.0	77.9	41.6
0.4	77.14	0.0	0.0	0.0	0.0	19.0	0.0	0.0	0.0	31.2	10.4
0.4	81.65	0.0	0.0	0.0	0.0	19.0	0.0	0.0	0.0	0.0	15.6
0.4	84.80	0.0	0.0	0.0	0.0	19.0	0.0	0.0	0.0	0.0	15.6
0.4	87.14	0.0	0.0	0.0	0.0	19.0	0.0	0.0	0.0	0.0	5.2
0.6	4.65	57.1	114.3	0.0	31.3	0.0	0.0	0.0	0.0	0.0	0.0
0.6	7.80	171.4	304.8	171.4	83.6	0.1	10.4	0.0	10.4	0.0	0.0
0.6	10.14	57.1	304.8	171.4	83.6	0.2	26.1	0.0	5.2	10.4	0.0
0.6	11.65	0.0	819.0	285.7	224.5	0.0	5.2	0.0	10.4	0.0	0.0
0.6	14.80	0.0	819.0	342.9	224.5	0.9	67.9	57.1	0.0	10.4	20.8
0.6	17.14	0.0	457.1	114.3	125.3	5.0	52.2	57.1	31.3	0.0	5.2
0.6	21.65	0.0	304.8	114.3	83.6	1.7	41.8	0.0	31.3	20.8	10.4
0.6	24.80	0.0	323.8	57.1	88.8	2.2	57.4	0.0	20.9	31.2	20.8
0.6	27.14	0.0	133.3	0.0	36.6	2.8	88.8	171.4	20.9	0.0	0.0
0.6	28.65	0.0	57.1	0.0	15.7	6.7	88.8	57.1	62.7	72.7	15.6
0.6	31.80	0.0	152.4	0.0	41.8	7.2	104.4	114.3	114.9	77.9	103.9
0.6	34.14	0.0	38.1	0.0	10.4	8.0	104.4	114.3	62.7	67.5	62.3
0.6	35.15	0.0	133.3	0.0	36.6	10.7	130.5	228.6	67.9	31.2	20.8
0.6	38.30	0.0	95.2	0.0	26.1	12.2	109.7	114.3	114.9	62.3	62.3
0.6	40.64	0.0	57.1	0.0	15.7	14.3	94.0	57.1	135.8	93.5	26.0
0.6	41.65	0.0	0.0	0.0	0.0	16.7	47.0	57.1	78.3	5.2	72.7
0.6	44.80	0.0	0.0	0.0	0.0	17.5	26.1	57.1	99.2	46.8	83.1
0.6	47.14	0.0	0.0	0.0	0.0	17.8	31.3	57.1	109.7	57.1	114.3
0.6	51.65	0.0	0.0	0.0	0.0	18.2	0.0	0.0	73.1	124.7	109.1
0.6	54.80	0.0	0.0	0.0	0.0	18.2	0.0	0.0	146.2	202.6	135.1
0.6	57.14	0.0	0.0	0.0	0.0	18.8	10.4	0.0	120.1	145.5	140.3
0.6	61.65	0.0	38.1	0.0	10.4	17.1	47.0	0.0	88.8	119.5	83.1
0.6	64.80	0.0	76.2	57.1	20.9	18.0	47.0	0.0	120.1	150.6	150.6
0.6	67.14	0.0	76.2	57.1	20.9	17.9	57.4	0.0	141.0	176.6	145.5
0.6	71.65	0.0	0.0	0.0	0.0	15.8	31.3	0.0	94.0	150.6	145.5
0.6	74.80	0.0	0.0	0.0	0.0	17.5	41.8	0.0	67.9	150.6	192.2
0.6	77.14	0.0	0.0	0.0	0.0	17.8	10.4	0.0	73.1	114.3	140.3
0.6	81.65	0.0	0.0	0.0	0.0	18.4	20.9	0.0	0.0	77.9	72.7
0.6	84.80	0.0	0.0	0.0	0.0	18.8	10.4	0.0	0.0	62.3	26.0
0.6	87.14	0.0	0.0	0.0	0.0	19.0	0.0	0.0	0.0	46.8	20.8
0.6	91.65	0.0	0.0	0.0	0.0	19.0	0.0	0.0	41.8	51.9	20.8
0.8	4.65	114.3	266.7	57.1	73.1	0.0	0.0	0.0	0.0	10.4	0.0
0.8	7.80	57.1	381.0	114.3	104.4	0.2	20.9	0.0	0.0	10.4	0.0
0.8	10.14	0.0	190.5	0.0	52.2	1.1	52.2	57.1	0.0	0.0	0.0
0.8	11.65	342.9	419.0	114.3	114.9	0.0	0.0	0.0	0.0	0.0	10.4
0.8	14.80	0.0	285.7	228.6	78.3	0.8	15.7	0.0	10.4	15.6	20.8
0.8	17.14	0.0	552.4	285.7	151.4	1.7	26.1	57.1	0.0	5.2	10.4
0.8	21.65	0.0	190.5	0.0	52.2	13.0	125.3	171.4	41.8	10.4	0.0
0.8	24.80	0.0	171.4	0.0	47.0	15.7	88.8	114.3	41.8	0.0	5.2
0.8	27.14	0.0	95.2	0.0	26.1	17.8	88.8	171.4	41.8	0.0	5.2
0.8	28.65	0.0	0.0	0.0	0.0	8.6	83.6	114.3	15.7	20.8	41.6
0.8	31.80	0.0	0.0	0.0	0.0	13.6	94.0	0.0	62.7	26.0	10.4
0.8	34.14	0.0	38.1	0.0	10.4	16.8	83.6	57.1	73.1	20.8	20.8
0.8	35.15	0.0	266.7	0.0	73.1	19.0	0.0	0.0	10.4	10.4	20.8
0.8	38.30	0.0	152.4	0.0	41.8	19.0	0.0	0.0	0.0	62.3	0.0
0.8	40.64	0.0	190.5	0.0	52.2	19.0	0.0	0.0	31.3	62.3	0.0
0.8	41.65	0.0	0.0	0.0	0.0	13.8	73.1	0.0	36.6	20.8	57.1
0.8	44.80	0.0	0.0	0.0	0.0	15.9	57.4	57.1	67.9	103.9	119.5
0.8	47.14	0.0	0.0	0.0	0.0	16.5	57.4	114.3	57.4	83.1	103.9

0.8	51.65	0.0	0.0	0.0	0.0	18.5	20.9	57.1	120.1	67.5	31.2
0.8	54.80	0.0	0.0	0.0	0.0	18.7	15.7	0.0	161.9	114.3	72.7
0.8	57.14	0.0	0.0	0.0	0.0	18.7	10.4	0.0	83.6	145.5	119.5
0.8	61.65	0.0	0.0	0.0	0.0	17.8	41.8	0.0	120.1	62.3	135.1
0.8	64.80	0.0	0.0	0.0	0.0	18.7	20.9	0.0	141.0	41.6	83.1
0.8	67.14	0.0	0.0	0.0	0.0	18.8	10.4	0.0	135.8	41.6	36.4
0.8	71.65	0.0	0.0	0.0	0.0	18.8	10.4	0.0	41.8	72.7	41.6
0.8	74.80	0.0	0.0	0.0	0.0	19.0	0.0	0.0	10.4	72.7	72.7
0.8	77.14	0.0	0.0	0.0	0.0	19.0	0.0	0.0	0.0	62.3	31.2
0.8	81.65	0.0	0.0	0.0	0.0	19.0	0.0	0.0	0.0	20.8	31.2
0.8	84.80	0.0	0.0	0.0	0.0	19.0	0.0	0.0	0.0	10.4	20.8
1	4.65	0.0	38.1	0.0	10.4	0.0	0.0	0.0	0.0	0.0	0.0
1	7.80	114.3	495.2	0.0	135.8	0.0	0.0	0.0	0.0	0.0	0.0
1	10.14	285.7	457.1	0.0	125.3	0.0	0.0	0.0	10.4	0.0	0.0
1	11.65	57.1	228.6	0.0	62.7	0.0	0.0	0.0	0.0	5.2	0.0
1	14.80	171.4	114.3	0.0	31.3	0.1	10.4	57.1	0.0	0.0	0.0
1	17.14	114.3	114.3	0.0	31.3	0.0	0.0	0.0	10.4	0.0	0.0
1	21.65	0.0	152.4	57.1	41.8	3.4	0.0	0.0	0.0	0.0	0.0
1	24.80	0.0	76.2	0.0	20.9	5.9	20.9	57.1	0.0	0.0	0.0
1	27.14	0.0	38.1	57.1	10.4	4.8	62.7	114.3	5.2	0.0	0.0
1	28.65	0.0	76.2	0.0	20.9	4.1	41.8	57.1	57.4	57.1	67.5
1	31.80	0.0	152.4	0.0	41.8	6.6	104.4	57.1	130.5	41.6	46.8
1	34.14	0.0	114.3	0.0	31.3	9.7	130.5	57.1	318.5	46.8	62.3
1	35.15	0.0	0.0	0.0	0.0	19.0	0.0	0.0	41.8	93.5	51.9
1	38.30	0.0	0.0	0.0	0.0	19.0	0.0	0.0	94.0	51.9	10.4
1	40.64	0.0	0.0	0.0	0.0	19.0	0.0	0.0	83.6	31.2	0.0
1	41.65	0.0	38.1	0.0	10.4	18.3	20.9	0.0	62.7	67.5	161.0
1	44.80	0.0	76.2	114.3	20.9	18.1	31.3	0.0	36.6	155.8	124.7
1	47.14	0.0	76.2	114.3	20.9	18.3	31.3	0.0	52.2	207.8	72.7
1	51.65	0.0	0.0	0.0	0.0	19.0	0.0	0.0	10.4	0.0	15.6
1	54.80	0.0	0.0	0.0	0.0	19.0	0.0	0.0	10.4	0.0	10.4
1	57.14	0.0	0.0	0.0	0.0	19.0	0.0	0.0	0.0	0.0	0.0
1	61.65	0.0	0.0	0.0	0.0	19.0	0.0	0.0	31.3	10.4	15.6
1	64.80	0.0	0.0	0.0	0.0	19.0	0.0	0.0	20.9	10.4	0.0
1	67.14	0.0	0.0	0.0	0.0	19.0	0.0	0.0	10.4	0.0	0.0
1	71.65	0.0	0.0	0.0	0.0	19.0	0.0	0.0	0.0	0.0	0.0
x'	y	a	a	a	a	a	a	a	a	a	a
m	mm	1/m	1/m	1/m	1/m	1/m	1/m	1/m	1/m	1/m	1/m
(1)	(2)	(3)	(4)	(5)	(6)	(7)	(8)	(9)	(10)	(11)	(12)

APPENDIX VII - STEADY AIR-WATER FLOW MEASUREMENTS. VOID FRACTION AND BUBBLE COUNT RATE

VII.1 Presentation

Air-water flow properties were recorded in steady flow conditions by CHANSON and TOOMBES (1997,2002a). Measurements were performed with a single-tip conductivity probe (needle probe design) identical to the present study. The probe consisted of a sharpened rod (platinum wire ∅ = 0.35 mm) which was insulated except for its tip and set into a metal supporting tube (stainless steel surgical needle ∅ = 1.42 mm) acting as the second electrode. The probe was excited by an electronics designed with a response time less than 10 μs and calibrated with a square wave generator. Further details on the probe system and electronics were reported in CHANSON (1995) and CUMMINGS (1996). The probe output signals were scanned at 5 kHz per channel for 180 seconds (CHANSON and TOOMBES 2002a). Conductivity probe measurements were taken on the centreline. At each location x', the vertical displacement of the probe was controlled by a fine adjustment travelling mechanism. The error in the probe position was less than 0.2 mm and 2 mm in the vertical and horizontal direction respectively.

Notation

C void fraction, or air concentration, defined as the volume of air per unit volume of air and water;
d_c critical flow depth (m);
d_n nozzle depth (m) : d_n = 0.03 m;
d_o characteristic water depth (m) function of the flow rate and channel width only; $d_o = 9/4\ d_c$;
F bubble count rate (Hz), defined as the number of bubbles impacting a probe sensor per second;
g gravity acceleration (m/s^2) : g = 9.80 m/s^2 in Brisbane;
h step height (m);
l step length (m);
Q water discharge (m^3/s);
x' horizontal distance (m) measured from vertical step face, positive in downstream flow direction;
y vertical distance (m) measured from the step invert;

VII.2 Experimental data (steady flow conditions)

Location :	University of Queensland (Australia)
Date :	March-June 2000
Experiments by :	Matt EASTMAN and Nic VAN SCHAGEN
Data processing by :	H. CHANSON
Experiment characteristics :	Flume : length: 25 m, width: 0.5 m, slope: 3.4 degrees, step height: 0.0715 m, step length: 1.2 m. Inflow conditions : nozzle depth d_n = 0.03 m. First step : 2.4 m long, equipped with sidewall deflectors.
Instrumentation :	Single-tip conductivity probe (Ø = 0.35 mm).
Comments :	Steady flow conditions. Probe signal scanned at 5 kHz for 180 seconds.

Run Q40 (40 L/s)

Q m^3/s	Step	x' m
0.040	16	0.2, 0.4, 0.6, 0.8, 1.0

x'(m)	y (mm)	C	F (Hz)
1	1.65	0	0
	21.65	0.002	0.883
	28.65	0.065	10.8
	31.65	0.163	20.07
	33.65	0.257	27.62
	35.15	0.35	33.21
	36.65	0.439	33.61
	39.65	0.617	33.82
	41.65	0.706	31.66
	43.65	0.796	26.17
	46.65	0.883	18.66
	48.65	0.925	14.07
	51.65	0.963	8.222
0.8	1.65	0	0.017
	21.65	0.016	3.906
	26.65	0.085	14.81
	28.65	0.155	21.79
	31.65	0.27	30.46
	34.65	0.428	37.19
	36.65	0.517	39.56
	38.65	0.637	36.89
	41.65	0.741	31.86
	43.65	0.828	25.64
	46.65	0.882	19.56
	51.65	0.954	10.03
0.6	1.65	0	0.011
	16.65	0.007	2.567
	21.65	0.042	9.372
	24.65	0.103	17.38
	26.65	0.164	23.75
	29.65	0.296	32.29
	31.65	0.379	38.08
	33.65	0.486	38.44
	36.65	0.635	36.41
	38.65	0.714	33.85
	41.65	0.812	27.31
	46.65	0.917	15.59
	51.65	0.963	8.694
0.4	1.65	0	0.011
	21.65	0.018	4.889
	25.15	0.059	11.09
	26.65	0.084	13.77
	31.65	0.224	27.51
	36.65	0.449	37.42
	39.15	0.552	38.37
	41.65	0.645	37.09
	46.65	0.786	29.27
	51.65	0.873	22.38
	56.65	0.917	17.17
	61.65	0.951	11.68
	66.65	0.967	8.639
0.2	1.65	0	0.039
	21.65	7E-04	0.422
	26.65	0.003	1.056
	31.65	0.018	4.111
	36.65	0.079	11.95
	41.65	0.208	23.35
	44.15	0.294	28.77
	46.65	0.381	32.63
	51.65	0.557	34.69
	56.65	0.7	30.97
	61.65	0.793	27.58
	66.65	0.866	20.51
	71.65	0.906	16.12
	76.65	0.945	10.99
	81.65	0.965	8.072

Run Q55 (55 L/s)

Q m^3/s	Step	x' m
0.055	16	0.2, 0.4, 0.6, 0.8, 1.0

x'(m)	y (mm)	C	F (Hz)
1	1.65	0	0
	1.65	0	0
	30.65	0.022	5.856
	34.15	0.071	11.83
	36.65	0.122	17.43
	39.15	0.2	22.78
	44.15	0.413	30.86
	49.15	0.634	29.47
	54.15	0.8	22.49
	56.65	0.86	17.52
	59.15	0.91	13.37
	64.15	0.957	7.656
0.8	1.65	0	0
	29.15	0.034	9.411
	31.65	0.057	13.96
	34.65	0.109	20.11
	37.65	0.185	26.83
	41.65	0.319	31.89
	46.65	0.508	35.86
	51.65	0.683	30.87
	56.65	0.811	22.92
	61.65	0.904	15.41
	64.15	0.93	12.14
	66.65	0.947	9.506
	69.15	0.965	7.294
0.6	1.65	0	0
	24.15	0.034	8.578
	26.65	0.058	12.13
	29.15	0.094	16.52
	31.65	0.137	21.29

	36.65	0.256	29.51
	41.65	0.425	34.94
	48.65	0.617	33.73
	55.65	0.788	25.63
	61.65	0.877	18.57
	66.65	0.929	12.86
	71.65	0.958	9.139
0.4	1.65	0	0
	34.15	0.041	10.95
	36.65	0.07	15.52
	39.15	0.112	21.9
	41.65	0.165	28.23
	46.65	0.333	41.4
	51.65	0.5	46.61
	56.65	0.667	44.88
	63.65	0.812	34.61
	70.65	0.905	22.1
	76.65	0.944	15.18
	81.65	0.964	10.67
0.2	1.65	0	0
	36.15	0.04	7.417
	37.65	0.056	9.517
	40.15	0.09	13.3
	44.15	0.185	19.96
	49.15	0.338	25.55
	54.15	0.498	27.83
	59.15	0.625	27.32
	64.15	0.735	26.38
	69.15	0.808	23.54
	74.15	0.855	21.14
	79.15	0.891	18.73
	86.65	0.932	14.06
	96.65	0.959	9.961

Run Q75 (75 L/s)

Q m^3/s	Step	x' m
0.075	10	0.2, 0.4, 0.6, 0.8, 1.0

x'(m)	y (mm)	C	F (Hz)
1	0	0	0
	35	0.028	18.11
	40	0.077	32.94
	45	0.205	57.49
	50	0.394	75.08
	55	0.615	77.47
	60	0.781	59.03
	62.5	0.844	47.38
	65	0.899	35.27
	70	0.954	20.28
0.8	1.65	0	0
	44.65	0.038	23.91
	49.65	0.076	36.37
	56.65	0.192	62.63
	61.65	0.296	74.13
	68.65	0.485	82.54
	76.65	0.672	70.02
	83.65	0.788	54.09
	91.65	0.875	38.34
	97.65	0.916	28.72
	106.65	0.954	18.64
0.6	1.65	0	0
	43.65	0.033	21.37
	48.65	0.066	33.03
	55.65	0.14	55.43
	62.65	0.24	73.79
	69.65	0.365	88.83
	77.65	0.519	86.87
	85.65	0.637	84.61
	93.65	0.751	71.84
	101.65	0.84	52.69
	109.65	0.9	38.65
	117.65	0.94	25.46
	121.65	0.954	20.41
0.4	1.65	0	0
	41.65	0.042	20.82
	46.65	0.092	36.54
	51.65	0.174	60.25
	56.65	0.29	85.22
	63.65	0.494	110
	71.65	0.685	100.6
	76.65	0.774	84.14
	81.65	0.843	67.27
	87.65	0.901	48.27
	93.65	0.942	32.03
	98.65	0.962	21.74
0.2	1.65	0	0
	34.65	0.044	18.77
	46.65	0.211	48.76
	51.65	0.338	61.15
	56.65	0.454	68.09
	61.65	0.595	66.83
	68.65	0.723	62.74
	74.65	0.818	53.07
	81.65	0.885	42.41
	86.65	0.915	35.37
	96.65	0.957	23.36

Q m^3/s	Step	x' m
0.075	16	0.2, 0.4, 0.6, 0.8, 1.0

x'(m)	y (mm)	C	F (Hz)
1	1.65	0	0
	38.65	0.039	10.772
	41.65	0.0782	16.389
	43.65	0.1195	20.633
	46.65	0.197	27.767
	53.65	0.4599	39.233

	60.65	0.7294	32.133
	63.65	0.8038	26.617
	66.65	0.8787	19.9
	71.65	0.9409	12.133
	76.65	0.9723	6.6778
0.8	1.65	0	0
	36.65	0.0324	9.45
	41.65	0.0741	15.872
	46.65	0.1517	24.478
	51.65	0.274	33.506
	59.65	0.5173	38.65
	66.65	0.7158	32.956
	71.65	0.8167	25.45
	76.65	0.892	18.128
	81.65	0.9332	13.072
	86.65	0.9601	8.7111
0.6	1.65	0	0
	39.65	0.0372	9.7778
	43.65	0.0817	16.739
	48.65	0.1489	24.244
	54.65	0.2802	32.261
	61.65	0.4397	38.922
	66.65	0.561	38.756
	71.65	0.653	37.367
	76.65	0.7474	33.244
	81.65	0.8111	28.678
	89.65	0.8873	21.356
	96.65	0.9289	15.744
	101.65	0.9518	12.011
0.4	1.65	0	0
	46.65	0.0362	10.683
	49.15	0.0579	14.194
	51.65	0.0929	20.4
	56.65	0.1862	33.961
	61.65	0.3209	48.856
	66.65	0.4947	56.172
	71.65	0.6381	56.256
	76.65	0.7605	49.189
	81.65	0.8384	40.328
	86.65	0.8988	29.294
	91.65	0.9368	21.094
	96.65	0.9586	15.128
0.2	1.65	0	0
	43.65	0.0316	8.05
	47.65	0.0613	11.978
	53.65	0.1475	20.783
	59.65	0.2909	30.078
	66.65	0.4854	33.761
	71.65	0.6091	33.306
	76.65	0.7105	31.478
	81.65	0.7885	28.156
	86.65	0.848	24.483
	96.65	0.9206	17.189
	103.65	0.9461	13.75
	111.65	0.9677	9.9611

APPENDIX VIII - UNSTEADY AIR-WATER FLOW MEASUREMENTS (2) DEPTH-AVERAGED VOID FRACTION, BUBBLE COUNT RATE, SPECIFIC INTERFACE AREA DATA

VIII.1 Presentation

For the experiments described in Appendices VI (Table VIII-1) and VII, depth-averaged flow properties were calculated from time-averaged data calculated during a short time interval ΔT such as $\Delta T = \Delta X/C_S$ where C_S is the measured surge front celerity and ΔX is the control volume streamwise length. ΔX was selected to be a multiple of Δx = 70 mm : i.e., $\Delta X = I*\Delta x$ where I is an integrer equal or larger than unity and Δx is the smallest control volume streamwise length (in the present study: Δx = 70 mm). Data calculated along ΔX correspond to a dimensionless time $(t - t_S)$ where t_S is the time of passage of wave front.

Table VIII-1 - Summary of unsteady air-water flow measurements in dam break wave flow

Run	θ (deg.)	h m	Q(t=0+) (m^3/s)	Air-water flow measurements	Remarks
(1)	(2)	(3)	(4)	(5)	(6)
Series 2	3.4	0.071			18 horizontal steps (l = 1.2 m, W = 0.5 m).
			0.040	Step 16	Run TL1.
			0.055	Step 16	Run TL3.
			0.075	Steps 10 & 16	Run TL5.

Notes : h : step height; l : step length; Q(t=0+) : initial flow rate; W : chute width.

The basic results include the depth-averaged void fraction C_{mean}, the maximum bubble count rate F_{max} and the depth-averaged air-water specific interface area a_{mean}, where :

$$C_{mean} = \frac{1}{Y_{90}} * \int_{y=0}^{Y_{90}} C * dy \quad \text{(VIII-1)}$$

$$F_{max} = Max(F, \text{ for } 0 \leq y \leq Y_{90}) \quad \text{(VIII-2)}$$

$$a_{mean} = \frac{1}{Y_{90}} * \int_{y=0}^{Y_{90}} a * dy \quad \text{(VIII-3)}$$

where C is the void fraction, F is the bubble count rate, a is the air-water specific interface area, y is the distance normal to the invert and Y_{90} is the distance where C = 0.9.

Discussion

For all investigated unsteady flow conditions (Table VIII-1), a free-falling nappe was observed at x' = 0.2 m. For such a free-jet flow, Equations (VIII-1) to (VIII-3) are not valid. In experimental studies of free-jets above spillway aeration devices and at a drop structure, alternative definitions were introduced (CHANSON 1989,1997, TOOMBES 2002).

The reader must note that results presented in paragraph VIII.2 were calculated for streamwise control volume lengths ΔX ranging from 70 to 385 mm. Data obtained with different streamwise lengths ΔX are not strictly comparable.

Notation

a air-water specific interface area (m^{-1}): i.e., air-water interface area per unit volume of air and water;
a_{mean} depth-averaged specific interface area defined between 0 and Y_{90};
C void fraction, or air concentration, defined as the volume of air per unit volume of air and water;
C_{mean} depth-averaged void fraction defined between 0 and Y_{90};
C_s wave front celerity (m/s);
d_c critical flow depth (m);
d_n nozzle depth (m) : d_n = 0.03 m;
d_o characteristic water depth (m) function of the flow rate and channel width only; $d_o = 9/4\ d_c$;
F bubble count rate (Hz), defined as the number of bubbles impacting a probe sensor per second;
F_{max} maximum bubble count rate (Hz) for $0 \leq y \leq Y_{90}$;
g gravity acceleration (m/s^2) : g = 9.80 m/s^2 in Brisbane;
h step height (m);
l step length (m);
Q water discharge (m^3/s);
t time (s);
t_s time (s) of passage of the wave front at the location x';
x' horizontal distance (m) measured from vertical step face, positive in downstream flow direction;
Y_{90} characteristic distance (m) where C = 0.90;
y vertical distance (m) measured from the step invert;
Δx smallest control volume streamwise length (m); in the present study: Δx = 70 mm;
ΔX control volume streamwise length (m) : ΔX = I*Δx where I is an integrer equal or larger than unity.

All data are expressed in dimensionless units (see above) unless indicated.

VIII.2 Experiments Series 2. Depth-averaged air-water flow characteristics

Location :	University of Queensland (Australia)
Date :	June-Aug. 2002
Experiments by :	Chung Hwee "Jerry" LIM and York-wee TAN
Data processing and analysis by :	H. CHANSON
Experiment characteristics :	Flume : length: 25 m, width: 0.5 m, slope: 3.4 degrees, step height: 0.0715 m, step length: 1.2 m. Inflow conditions : nozzle depth d_n = 0.03 m. First step : 2.4 m long, equipped with sidewall deflectors.
Instrumentation :	Single-tip conductivity probe (Ø = 0.35 mm).
Comments :	Data calculated for a minimum control volume Δx of 70 mm.

Legend	Streamwise control volume length	Corresponding time

ΔX = 210-385 mm	ΔX = 175 mm	$0.210/C_S \leq (t - t_S) \leq 0.385/C_S$

Run TL1

Q m^3/s	Step	x' m	C_S m/s	d_o m
0.040	16	0.2, 0.4, 0.6, 0.8, 1.0	1.97	0.195

x' m (1)	Y_{90}, C_{mean}, F_{max}, a_{mean} SI units (2)	Y_{90}, C_{mean}, F_{max}, a_{mean} SI units (3)	Y_{90}, C_{mean}, F_{max}, a_{mean} SI units (4)	Y_{90}, C_{mean}, F_{max}, a_{mean} SI units (5)	Y_{90}, C_{mean}, F_{max}, a_{mean} SI units (6)	Y_{90}, C_{mean}, F_{max}, a_{mean} SI units (7)	Y_{90}, C_{mean}, F_{max}, a_{mean} SI units (8)	Y_{90}, C_{mean}, F_{max}, a_{mean} SI units (9)	Y_{90}, C_{mean}, F_{max}, a_{mean} SI units (10)	Y_{90}, C_{mean}, F_{max}, a_{mean} SI units (11)	Y_{90}, C_{mean}, F_{max}, a_{mean} SI units (12)
ΔX (mm) =	0-70	0-210	140-210	0-385	175-385	350-735	525-595	700-1085	2100-2485	4200-4585	
$t - t_S$ (s) =	0.018	0.053	0.089	0.098	0.142	0.275	0.284	0.453	1.164	2.23	Steady flow
ΔX (mm) =	70	210	70	385	210	385	70	385	385	385	
$\frac{(t-t_S)}{\sqrt{d_o/g}}$	0.126	0.378	0.629	0.692	1.007	1.951	2.014	3.21	8.245	15.8	
0.2	Free-jet	Free-jet	Free-jet	Free-jet	Free-jet	Free-jet	Free-jet	Free-jet	Free-jet	Free-jet	0.071 0.28 34.7 35.1
0.4	0.0 0.82 84.4 85.1	*0.0* *0.70* *206.4* *203.4*	*0.0* *0.48* *56.3* *13.0*	0.0 0.60 56.6 58.7	0.0 0.44 9.0 4.2	0.0 0.27 79.7 66.7	*0.0* *0.30* *84.4* *68.8*	0.1 0.41 64.3 56.3	*0.0* *0.27* *87.0* *57.9*	*0.0* *0.30* *104.9* *68.7*	0.055 0.29 38.4 32.1
0.6	0.006 0.8 56.3 110.1	0.017 0.607 113 155.0	0.020 0.272 113 71.2	0.020 0.449 31 42.2	0.021 0.256 8 2.0	0.028 0.263 51 47.6	*0.021* *0.100* *56* *36.1*	0.035 0.335 44 35.6	0.034 0.260 97 74.0	0.030 0.249 84 54.1	0.046 0.29 38.4 25.78
0.8	*N/A* *N/A* *84.4* *0.0*	0.010 0.433 188 168.2	0.010 *0.229* *56* *31.9*	0.021 0.467 51 46.1	0.026 0.340 9 5.2	0.026 0.289 26 24.5	0.024 0.203 84 53.4	0.024 0.169 49 25.9	0.029 0.153 69 39.3	0.029 0.193 59 37.6	0.048 0.25 39.6 26.7
1.0	*N/A* *0.967* *0.0* *0.0*	0.014 0.440 122 70.4	0.017 *0.273* *84* *50.1*	0.020 0.370 33 30.1	0.021 0.162 9 3.7	0.021 0.186 82 38.4	0.021 0.183 28 16.7	0.025 0.199 69 51.3	0.028 0.248 46 30.4	0.029 0.149 107 51.6	0.047 0.2 33.7 21.7

Notes : *Italic data* = suspicious data; All data are expressed in dimensionless units unless indicated.

Run TL3

Q m^3/s	Step	x' m	C_S m/s	d_o m
0.055	16	0.2, 0.4, 0.6, 0.8, 1.0	2.14	0.241

x' m (1)	Y_{90}, C_{mean}, F_{max}, a_{mean} SI units (2)	Y_{90}, C_{mean}, F_{max}, a_{mean} SI units (3)	Y_{90}, C_{mean}, F_{max}, a_{mean} SI units (4)	Y_{90}, C_{mean}, F_{max}, a_{mean} SI units (5)	Y_{90}, C_{mean}, F_{max}, a_{mean} SI units (6)	Y_{90}, C_{mean}, F_{max}, a_{mean} SI units (7)	Y_{90}, C_{mean}, F_{max}, a_{mean} SI units (8)	Y_{90}, C_{mean}, F_{max}, a_{mean} SI units (9)	Y_{90}, C_{mean}, F_{max}, a_{mean} SI units (10)	Y_{90}, C_{mean}, F_{max}, a_{mean} SI units (11)	Y_{90}, C_{mean}, F_{max}, a_{mean} SI units (12)
ΔX (mm) =	0-70	0-210	140-210	0-385	175-385	350-735	525-595	700-1085	2100-2485	4200-4585	
$t - t_S$ (s) =	0.016	0.049	0.082	0.09	0.131	0.254	0.262	0.417	1.071	2.053	Steady
ΔX (mm) =	70	210	70	385	210	385	70	385	385	385	flow
$\frac{(t-t_S)}{\sqrt{d_O/g}}$	0.104	0.313	0.521	0.573	0.834	1.615	1.667	2.657	6.826	13.08	
0.2	Free-jet	Free-jet	Free-jet	Free-jet	Free-jet	Free-jet	Free-jet	Free-jet	Free-jet	Free-jet	0.081 0.309 27.8 28.2
0.4	0.010 0.815 122.3 97.5	*0.011* *0.534* *265.0* *362.5*	*0.019* *0.487* *152.9* *75.4*	0.028 0.613 72.6 77.4	0.028 0.462 5.7 2.5	0.054 0.384 81.0 76.0	*0.060* *0.388* *183.4* *113.9*	0.060 0.394 95.0 76.7	0.051 0.282 88.9 66.0	*0.057* *0.301* *86.2* *74.1*	0.070 0.26 46.6 37.8
0.6	0.011 0.78 122.3 99.0	*0.020* *0.40* *305.7* *258.8*	*0.021* *0.20* *183.4* *128.3*	0.031 0.45 83.8 56.9	0.041 0.42 8.1 2.2	0.056 0.30 69.8 39.7	*0.042* *0.03* *122.3* *43.2*	0.044 0.17 120.1 48.9	0.051 0.17 61.1 36.0	*0.060* *0.30* *111.2* *70.2*	0.064 0.30 34.9 28.3
0.8	N/A N/A 92 0.0	0.019 0.650 224 308.0	0.021 0.201 214 172.5	0.023 0.412 61 75.6	0.027 0.244 *3* *0.7*	0.041 0.209 95 47.0	0.041 0.141 183 53.2	0.032 0.192 56 26.3	0.037 0.115 78 37.9	*0.044* *0.279* *83* *25.4*	0.061 0.25 35.9 26.3
1.0	N/A N/A 0 0.0	0.017 0.723 183 184.4	0.026 0.396 183 130.1	0.022 0.445 50 54.0	0.021 0.124 *9* *3.7*	0.027 0.312 45 36.3	0.017 0.132 92 27.7	0.028 0.184 36 17.5	*0.033* *0.171* *44* *25.3*	0.034 0.173 89 47.1	0.059 0.22 30.9 19.9

Notes : *Italic data* = suspicious data; All data are expressed in dimensionless units unless indicated.

Run TL5 (step 10)

Q m^3/s	Step	x' m	C_s m/s	d_o m
0.075	10	0.2, 0.4, 0.6, 0.8, 1.0	2.61	0.297

x' m (1)	Y_{90}, C_{mean}, F_{max}, a_{mean} SI units (2)	Y_{90}, C_{mean}, F_{max}, a_{mean} SI units (3)	Y_{90}, C_{mean}, F_{max}, a_{mean} SI units (4)	Y_{90}, C_{mean}, F_{max}, a_{mean} SI units (5)	Y_{90}, C_{mean}, F_{max}, a_{mean} SI units (6)	Y_{90}, C_{mean}, F_{max}, a_{mean} SI units (7)	Y_{90}, C_{mean}, F_{max}, a_{mean} SI units (8)	Y_{90}, C_{mean}, F_{max}, a_{mean} SI units (9)	Y_{90}, C_{mean}, F_{max}, a_{mean} SI units (10)	Y_{90}, C_{mean}, F_{max}, a_{mean} SI units (11)	Y_{90}, C_{mean}, F_{max}, a_{mean} SI units (12)
ΔX (mm) =	0-70	0-210	140-210	0-385	175-385	350-735	525-595	700-1085	2100-2485	4200-4585	
$t - t_S$ (s) =	0.013	0.04	0.067	0.074	0.107	0.208	0.215	0.342	0.878	1.683	Steady
ΔX (mm) =	70	210	70	385	210	385	70	385	385	385	flow

$\frac{(t-t_s)}{\sqrt{d_o/g}}$	0.077	0.231	0.385	0.424	0.616	1.194	1.233	1.965	5.047	9.67	
0.2	Free-jet	Free-jet	Free-jet	Free-jet	Free-jet	Free-jet	Free-jet	Free-jet	Free-jet	Free-jet	0.084 0.30 68.1 53.5
0.4	N/A N/A N/A N/A	*0.019* *0.73* *285.9* *117.8*	0.028 0.35 298.3 171.1	0.028 0.44 92.0 49.6	*0.032* 0.19 8.6 1.9	0.041 0.22 143.1 57.7	0.041 0.19 223.7 72.5	0.041 0.34 109.0 63.6	0.049 0.25 135.6 57.0	0.058 0.32 91.5 48.1	0.088 0.27 110.0 75.8
0.6	N/A N/A N/A N/A	*0.016* *0.83* *248.6* *295.3*	*0.007* *0.66* *111.9* *163.2*	0.021 0.64 68.1 76.7	0.027 0.51 10.8 5.8	0.041 0.43 139.7 80.6	*0.035* *0.27* *186.4* *80.8*	*0.052* *0.35* *98.8* *69.0*	*0.082* *0.23* *88.1* *53.8*	*0.069* *0.16* *162.7* *60.7*	0.110 0.29 88.8 90.4
0.8	*0.021* *0.44* *298.3* *146.0*	0.023 0.35 323.1 258.9	0.023 0.22 111.9 76.5	0.023 0.26 88.6 70.9	0.025 0.19 11.8 3.7	*0.036* *0.37* 61.3 29.7	*0.037* *0.38* *111.9* *15.7*	0.065 0.24 105.6 56.5	*0.090* *0.24* *84.7* *40.0*	0.090 0.16 111.9 53.8	0.095 0.27 82.5 67.2
1.0	N/A N/A N/A N/A	*0.015* *0.40* 186.4 109.7	0.029 0.41 111.9 66.4	0.035 0.54 51.1 41.2	0.035 0.40 8.1 1.5	0.049 0.22 129.5 60.5	0.044 0.19 335.6 76.1	0.064 0.24 64.7 40.3	0.067 0.17 122.0 43.5	0.071 0.19 67.8 31.9	0.067 0.20 77.5 42.0

Notes : *Italic data* = suspicious data; All data are expressed in dimensionless units unless indicated.

Run TL5 (step 16)

Q m^3/s	Step	x' m	C_S m/s	d_o m
0.075	16	0.2, 0.4, 0.6, 0.8, 1.0	2.43	0.297

x' m (1)	Y_{90}, C_{mean}, F_{max}, a_{mean} SI units (2)	Y_{90}, C_{mean}, F_{max}, a_{mean} SI units (3)	Y_{90}, C_{mean}, F_{max}, a_{mean} SI units (4)	Y_{90}, C_{mean}, F_{max}, a_{mean} SI units (5)	Y_{90}, C_{mean}, F_{max}, a_{mean} SI units (6)	Y_{90}, C_{mean}, F_{max}, a_{mean} SI units (7)	Y_{90}, C_{mean}, F_{max}, a_{mean} SI units (8)	Y_{90}, C_{mean}, F_{max}, a_{mean} SI units (9)	Y_{90}, C_{mean}, F_{max}, a_{mean} SI units (10)	Y_{90}, C_{mean}, F_{max}, a_{mean} SI units (11)	Y_{90}, C_{mean}, F_{max}, a_{mean} SI units (12)
ΔX (mm) =	0-70	0-210	140-210	0-385	175-385	350-735	525-595	700-1085	2100-2485	4200-4585	
$t - t_s$ (s) =	0.0144	0.0432	0.072	0.0792	0.1152	0.2233	0.2305	0.3673	0.9434	1.8076	Steady flow
ΔX (mm) =	70	210	70	385	210	385	70	385	385	385	
$\frac{(t-t_s)}{\sqrt{d_o/g}}$	0.0828	0.2483	0.4138	0.4552	0.6621	1.2828	1.3242	2.1104	5.4208	10.386	
0.2	Free-jet	Free-jet	Free-jet	Free-jet	Free-jet	Free-jet	Free-jet	Free-jet	Free-jet	Free-jet	0.094 0.27 33.8 28.1
0.4	N/A 1.00 104.1 N/A	0.016 0.79 324.0 368.8	0.022 0.52 208.3 147.2	0.028 0.55 88.8 95.7	0.029 0.26 8.9 3.0	0.056 0.45 123.7 83.3	*0.047* *0.35* *243.0* *105.5*	0.039 0.35 136.4 71.3	0.054 0.30 82.1 71.2	0.065 0.36 126.2 95.9	0.087 0.23 56.3 38.4
0.6	0.010	0.021	0.024	0.028	0.029	0.043	0.045	0.076	0.084	0.083	0.092

	0.76	0.63	0.47	0.53	0.36	0.25	0.29	0.24	0.22	0.24	0.29
	104.1	497.6	208.3	136.4	6.5	79.3	138.9	88.8	123.1	116.8	38.9
	88.6	397.5	135.3	99.8	1.5	56.2	53.9	69.0	73.5	71.6	32.4
0.8	0.008	0.009	0.020	0.025	0.027	*0.035*	0.026	0.070	0.076	0.077	0.078
	0.77	0.43	0.39	0.46	0.26	*0.35*	0.20	0.31	0.24	0.22	0.24
	208.3	335.6	173.6	92.0	11.6	76.1	104.1	98.3	88.4	82.1	38.7
	102.7	295.2	122.1	84.4	4.7	50.6	48.8	53.6	43.4	40.7	25.9
1.0	0.017	0.015	*0.011*	0.024	0.026	0.035	*0.035*	0.048	*0.051*	*0.046*	0.068
	0.86	0.56	*0.05*	0.42	0.25	0.13	*0.04*	0.21	0.21	*0.27*	0.21
	173.6	300.9	*0.0*	82.5	5.9	79.3	*69.4*	57.1	126.2	*97.8*	39.2
	93.4	214.4	*0.0*	47.5	1.1	22.3	*26.2*	20.4	39.2	*26.6*	21.6

Notes : *Italic data* = suspicious data; All data are expressed in dimensionless units unless indicated.

APPENDIX IX - UNSTEADY AIR-WATER FLOW MEASUREMENTS (3) DISTRIBUTIONS OF AIR AND WATER CHORD SIZES

IX.1 Presentation

For the unsteady air-water flow experiments described in Appendix VI (Table IX-1), air and water chord times were measured where the air/water chord time t_{ch} is defined as the time spent by air (or water) on the probe tip. The results are presented in terms of pseudo-chord length ch defined as :

$$ch = C_s * t_{ch} \quad \text{(IX-1)}$$

where C_s is the wave front celerity. Equation (IX-1) predicts accurately chord lengths near the wave front where the flow velocity is about the wave front speed. Note that the chord time data analysis is independent of the selection of an integration time interval τ (App. VI & VIII).

Air and water pseudo-chord size distributions were analysed for the flow conditions described in Table IX-1. Basic statistical properties are summarised in paragraph IX.2.

Table IX-1 - Summary of unsteady air-water flow measurements in dam break wave flow

Run	θ (deg.)	h m	Q(t=0+) (m^3/s)	Air-water flow measurements	Remarks
(1)	(2)	(3)	(4)	(5)	(6)
Series 2	3.4	0.071			18 horizontal steps (l = 1.2 m, W = 0.5 m).
			0.040	Step 16	Run TL1.
			0.055	Step 16	Run TL3.
			0.075	Steps 10 & 16	Run TL5.

Notes : h : step height; l : step length; Q(t=0+) : initial flow rate; W : chute width.

Discussion

Statistical properties of air and water chord sizes were calculated from the first water detection by the probe sensor. At each location (x', y), the number of bubbles and the duration of the study are reported.

Note that, at the leading edge of the wave front, some splashing was observed. Sometimes the probe sensor was wetted by water droplets and spray although the event was followed by a significant air chord time. That is, the splashing may bias the average air chord size estimate. Therefore both the average and median ([1]) chord sizes are reported. For all air chord size distributions, the writer believes that the median chord size is a more representative indicator of typical bubble chord sizes.

For all investigated unsteady flow conditions, a free-falling nappe was observed at x' = 0.2 m. For such a free-jet flow, the probe sensor at a constant location y might not stay at the same relative position in the free-falling nappe. In turn, all the statistical results for x' = 0.2 m must be considered with great care.

[1]The median size is defined as the size for which 50% of all the data are smaller.

Notation

C_s wave front celerity (m/s);

ch pseudo-chord size (m);

d_n nozzle depth (m) : d_n = 0.03 m;

d_o characteristic water depth (m) function of the flow rate and channel width only; $d_o = 9/4\ d_c$;

g gravity acceleration (m/s^2) : g = 9.80 m/s^2 in Brisbane;

h step height (m);

Kurt Fisher kurtosis (dimensionless) (paragraph IX.3);

l step length (m);

Mean statistical mean or number mean size (m) (paragraph IX.3);

Q water discharge (m^3/s);

Skew Fisher skewness (dimensionless) (paragraph IX.3);

Std standard deviation of chord size (m) (paragraph IX.3);

t time (s);

t_{ch} air/water chord time (s);

x' horizontal distance (m) measured from vertical step face, positive in downstream flow direction;

y vertical distance (m) measured from the step invert;

IX.2 Experiments Series 2. Statistical properties of air and water chord size distributions

Location :	University of Queensland (Australia)
Date :	June-Aug. 2002
Experiments by :	Chung Hwee "Jerry" LIM and York-wee TAN
Data processing and analysis by :	Hubert CHANSON
Experiment characteristics :	Flume : length: 25 m, width: 0.5 m, slope: 3.4 degrees, step height: 0.0715 m, step length: 1.2 m. Inflow conditions : nozzle depth d_n = 0.03 m. First step : 2.4 m long, equipped with sidewall deflectors.
Instrumentation :	Single-tip conductivity probe (Ø = 0.35 mm).
Comments :	Pseudo-chord size distributions. Pseudo-chord sizes are defined as : $ch = C_s * t_{ch}$ where t_{ch} is the bubble chord time and C_s is the wave front celerity.

Run TL1

Q m^3/s	Step	x' m	C_s m/s	d_o m
0.040	16	0.2, 0.4, 0.6, 0.8, 1.0	1.97	0.195

x'	y	Study time	Nb of bubble	Air chord sizes Mean	Median	Std	Skew	Kurt	Water chord sizes Mean	Median	Std	Skew	Kurt
m	mm	s		mm	mm	mm			mm	mm	mm		
(1)	(2)	(3)	(4)	(5)	(6)	(7)	(8)	(9)	(10)	(11)	(12)	(13)	(14)
1.0	4.65	5.40	3	398.2	4.3	685.8	1.73	N/A	2.2	2.2	0.0	N/A	N/A
1.0	7.80	5.39	2	602.1	602.1	849.9	N/A	N/A	128.2	128.2	N/A	N/A	N/A

1.0	10.14	5.37	5	256.5	9.1	551.4	2.23	4.99	1679.1	26.0	3321.3	2.00	4.00
1.0	11.65	5.60	4	208.0	15.9	390.5	2.00	4.00	716.8	323.5	974.6	1.52	N/A
1.0	14.80	5.60	39	26.4	2.6	126.1	6.19	38.53	256.7	16.8	580.7	3.93	18.18
1.0	17.14	5.59	98	17.2	3.8	80.9	9.52	92.84	82.6	3.7	265.9	5.59	36.57
1.0	21.65	5.21	188	24.5	4.0	116.3	12.21	159.61	36.2	3.3	98.0	4.34	20.51
1.0	24.80	5.21	205	28.4	3.9	116.2	11.40	147.00	27.2	3.2	76.6	5.21	30.62
1.0	27.14	5.19	223	32.1	4.1	121.8	10.28	127.00	20.9	3.0	63.0	5.81	39.60
1.0	28.65	4.89	219	38.6	3.7	184.5	9.75	102.94	15.3	3.0	48.1	7.46	65.17
1.0	31.80	3.97	197	48.5	4.3	292.3	12.76	172.14	11.4	2.2	41.3	8.32	81.82
1.0	34.14	3.97	159	64.2	5.7	333.1	10.76	125.65	10.1	2.2	38.6	9.91	111.31
1.0	35.15	3.38	102	101.7	4.4	521.8	9.23	89.44	12.0	2.8	24.8	4.46	25.26
1.0	38.30	3.39	109	99.0	2.8	506.7	9.34	92.77	8.9	2.8	15.8	3.77	18.60
1.0	40.64	3.39	57	196.9	6.1	712.3	6.27	43.17	9.7	2.2	17.4	3.55	15.23
1.0	41.65	2.29	47	233.2	5.9	1064.8	6.65	45.07	10.1	3.7	21.6	4.65	25.29
1.0	44.80	2.23	28	398.9	9.1	1402.1	5.02	25.86	9.5	4.9	16.1	3.94	17.37
1.0	47.14	2.02	16	689.2	5.0	1957.7	3.68	14.06	7.9	3.4	10.8	2.48	7.05
0.2	4.65	5.62	65	16.2	1.6	92.4	7.95	63.75	124.8	34.8	204.5	2.35	5.07
0.2	7.80	5.64	87	14.5	3.5	75.5	9.16	84.90	106.5	21.9	211.3	3.43	12.86
0.2	10.14	5.65	100	13.5	3.2	69.6	9.76	96.79	90.6	28.6	136.4	2.61	8.49
0.2	11.65	5.62	121	13.7	2.6	70.6	10.03	105.16	64.4	31.2	84.9	1.80	2.71
0.2	14.80	5.62	159	11.8	3.3	62.0	11.35	135.14	47.2	18.1	69.0	2.91	12.43
0.2	17.14	5.62	138	11.9	3.0	66.5	10.58	117.15	73.2	26.8	249.5	10.36	115.50
0.2	21.65	5.60	74	17.5	2.8	92.1	8.32	70.55	127.7	37.4	254.2	3.63	14.80
0.2	24.80	5.60	80	17.3	3.1	89.4	8.49	74.16	94.0	21.1	194.6	3.50	12.24
0.2	27.14	5.58	72	21.3	3.0	101.6	7.49	58.86	107.5	35.7	150.4	2.15	4.84
0.2	28.65	5.73	34	41.7	4.0	110.5	3.54	12.96	231.5	55.8	340.3	1.75	2.05
0.2	31.80	5.73	98	22.4	4.0	70.3	5.58	34.20	89.1	17.7	156.2	3.17	11.84
0.2	34.14	5.52	130	22.8	4.7	88.3	9.20	93.31	62.0	14.0	113.4	3.62	15.94
0.2	35.15	5.51	147	22.3	4.5	82.3	10.34	117.25	55.9	17.1	93.0	3.06	11.42
0.2	38.30	5.46	195	22.6	4.3	79.8	11.50	148.34	36.3	10.0	57.8	2.37	5.51
0.2	40.64	5.46	216	26.5	4.6	80.2	10.32	129.04	26.8	10.8	41.8	3.12	11.71
0.2	41.65	5.48	188	35.6	4.8	91.6	7.21	70.72	27.3	8.7	47.3	3.35	13.51
0.2	44.80	5.48	183	43.3	5.1	104.1	5.68	44.29	21.4	8.9	28.7	2.09	4.06
0.2	47.14	5.48	160	55.7	5.5	139.3	5.80	41.17	18.2	7.3	25.3	2.22	4.92
0.4	4.65	5.51	11	91.4	3.7	290.1	3.32	11.00	532.7	98.6	856.8	1.90	3.37
0.4	7.80	5.51	45	25.1	1.6	144.1	6.68	44.70	180.1	32.4	368.8	3.64	15.62
0.4	10.14	5.50	60	20.8	1.6	128.0	7.68	59.33	133.9	26.0	234.6	2.63	7.47
0.4	11.65	5.47	47	27.1	1.8	150.9	6.81	46.55	198.3	109.0	225.6	1.26	0.65
0.4	14.80	5.44	102	15.0	2.0	109.9	10.01	100.79	83.8	32.7	124.9	2.22	4.78
0.4	17.14	5.43	119	15.7	2.8	102.6	10.63	114.68	67.9	21.1	96.8	1.96	3.70
0.4	21.65	5.60	197	14.2	3.5	57.6	12.31	163.87	46.0	15.6	105.2	7.02	65.24
0.4	24.80	5.60	285	13.0	3.5	49.0	13.79	214.18	27.2	8.9	58.9	7.60	82.11
0.4	27.14	5.60	294	15.8	4.1	50.8	12.23	179.96	23.2	8.7	48.6	7.56	77.68
0.4	28.65	5.85	295	16.6	4.7	33.0	4.98	33.90	22.6	5.9	52.0	6.42	56.10
0.4	31.80	5.85	295	19.9	4.9	38.6	5.22	39.24	19.3	5.7	34.1	3.55	16.74
0.4	34.14	5.85	271	24.1	5.3	44.3	3.99	23.41	18.6	6.7	33.2	4.54	29.90
0.4	35.15	5.57	234	29.6	7.0	69.2	8.10	88.36	20.9	7.4	32.4	2.78	8.53
0.4	38.30	5.48	238	32.7	6.9	85.2	7.83	81.33	16.8	7.5	25.1	3.16	12.56
0.4	40.64	5.48	222	38.4	8.3	89.5	7.13	70.58	14.6	6.5	20.5	3.33	16.01
0.4	41.65	5.62	226	39.6	6.4	80.8	4.54	29.62	12.8	7.1	13.8	1.88	4.29
0.4	44.80	5.62	195	48.4	8.5	89.8	3.85	21.58	12.2	7.7	13.1	1.89	4.15
0.4	47.14	5.61	182	54.0	10.8	95.7	3.60	18.58	10.8	6.7	11.9	1.98	4.02
x'	y	Study	Nb of	Air	chord	sizes			Water	chord	sizes		
		time	bubble	Mean	Median	Std	Skew	Kurt	Mean	Median	Std	Skew	Kurt

m	mm	s		mm	mm	mm			mm	mm	mm		
(1)	(2)	(3)	(4)	(5)	(6)	(7)	(8)	(9)	(10)	(11)	(12)	(13)	(14)
0.6	4.65	5.84	5	72.2	12.6	137.8	2.23	4.98	4.0	4.5	2.6	-1.19	2.31
0.6	7.80	5.80	16	26.2	1.3	99.1	4.00	16.00	553.4	155.2	928.3	2.12	3.74
0.6	10.14	5.79	37	13.7	1.8	67.4	6.06	36.79	261.7	106.0	384.7	2.47	6.78
0.6	11.65	5.77	38	15.5	1.7	73.7	6.12	37.59	273.7	87.1	479.4	3.56	15.80
0.6	14.80	5.83	86	9.6	2.2	38.8	7.79	65.65	120.5	24.6	198.3	2.56	7.55
0.6	17.14	5.76	111	10.3	2.2	45.6	9.38	93.42	87.2	11.9	162.3	4.14	24.18
0.6	21.65	5.55	221	14.3	3.2	62.2	12.97	181.84	39.2	8.1	97.5	6.35	52.89
0.6	24.80	5.55	274	15.3	3.8	58.0	12.96	192.90	27.9	5.7	73.9	6.33	49.25
0.6	27.14	5.55	273	19.8	4.1	63.4	10.22	134.37	23.1	4.7	72.1	9.53	115.58
0.6	28.65	5.23	204	34.9	4.5	117.4	10.08	122.95	23.0	6.1	55.6	6.85	60.76
0.6	31.80	5.40	212	38.0	4.9	110.1	6.53	57.37	17.8	5.1	39.2	6.85	66.20
0.6	34.14	5.48	203	43.2	4.3	136.6	5.44	32.52	15.0	5.1	27.6	3.66	16.00
0.6	35.15	5.33	188	50.4	5.3	157.6	5.93	39.32	12.4	4.5	20.3	3.61	16.26
0.6	38.30	5.33	152	66.8	5.8	182.2	4.83	26.35	10.7	3.4	21.7	5.20	36.86
0.6	40.64	5.33	102	104.0	7.3	220.6	3.63	15.05	11.5	4.4	18.9	2.93	9.57
0.6	41.65	4.66	103	106.0	8.1	310.5	6.05	45.06	8.6	4.1	13.1	2.89	8.61
0.6	44.80	4.65	72	119.2	13.6	296.8	5.04	30.99	7.9	3.4	10.7	2.97	12.23
0.6	47.14	4.56	57	200.0	11.4	539.9	4.05	17.16	7.3	3.4	11.2	3.43	13.32
0.8	4.65	5.70	3	248.8	6.1	423.9	1.73	N/A	96.2	96.2	133.0	N/A	N/A
0.8	7.80	5.70	8	100.8	4.6	257.6	2.81	7.94	19.4	3.2	26.0	1.27	0.12
0.8	10.14	5.69	11	84.1	4.4	220.6	3.22	10.52	3.1	1.5	3.0	1.23	0.01
0.8	11.65	5.44	13	108.3	1.7	378.0	3.60	13.00	826.6	189.1	998.5	0.71	-1.21
0.8	14.80	5.43	38	42.7	3.0	222.7	6.15	37.85	225.1	62.9	285.6	1.35	1.02
0.8	17.14	5.43	92	23.5	3.8	144.4	9.42	89.65	132.4	11.7	300.8	4.08	20.21
0.8	21.65	5.36	202	26.0	4.9	116.2	11.76	151.97	39.1	5.6	121.1	7.81	78.69
0.8	24.80	5.36	208	25.3	3.9	96.2	10.60	131.41	28.7	3.5	64.6	3.58	14.98
0.8	27.14	5.36	231	27.1	3.3	102.8	8.80	95.27	23.3	4.3	52.1	3.84	16.39
0.8	28.65	5.10	225	33.9	3.7	136.6	10.00	121.50	18.5	5.3	41.3	4.34	20.81
0.8	31.80	4.72	217	39.9	3.7	183.3	11.83	157.77	14.4	3.7	32.3	4.31	20.82
0.8	34.80	4.72	141	67.9	4.5	254.2	7.44	65.36	15.8	3.9	34.0	3.86	17.10
0.8	35.15	4.58	142	68.7	4.4	262.0	8.55	84.73	14.4	3.5	28.7	3.56	13.97
0.8	38.30	4.48	116	89.3	4.5	319.5	7.14	60.61	12.5	3.9	21.0	3.51	16.42
0.8	40.64	3.75	92	117.6	4.6	484.4	8.06	71.28	10.9	3.9	17.9	4.11	23.53
0.8	41.65	2.99	96	111.1	5.1	623.5	8.84	82.33	11.1	4.4	15.4	2.30	5.28
0.8	44.80	3.56	73	151.1	5.5	625.1	6.40	44.69	9.5	3.7	16.6	3.71	15.49
0.8	47.14	1.83	51	220.7	6.1	1147.4	7.03	49.88	9.0	4.3	10.3	1.62	2.22
x'	y	Study	Nb of	Air	chord	sizes			Water	chord	sizes		
		time	bubble	Mean	Median	Std	Skew	Kurt	Mean	Median	Std	Skew	Kurt
m	mm	s		mm	mm	mm			mm	mm	mm		
(1)	(2)	(3)	(4)	(5)	(6)	(7)	(8)	(9)	(10)	(11)	(12)	(13)	(14)

Run TL3

Q	Step	x'	C_s	d_o
m^3/s		m	m/s	m
0.055	16	0.2, 0.4, 0.6, 0.8, 1.0	2.14	0.241

x'	y	Study	Nb of	Air	chord	sizes			Water	chord	sizes		
		time	bubble	Mean	Median	Std	Skew	Kurt	Mean	Median	Std	Skew	Kurt
m	mm	s		mm	mm	mm			mm	mm	mm		
(1)	(2)	(3)	(4)	(5)	(6)	(7)	(8)	(9)	(10)	(11)	(12)	(13)	(14)

1.0	4.65	5.95	7	15.6	2.6	36.3	2.64	6.97	650.5	4.7	1584.1	2.45	6.00
1.0	7.80	5.95	11	13.6	2.4	30.2	3.05	9.58	386.4	2.6	1184.1	3.16	9.99
1.0	10.14	5.91	9	24.3	1.6	55.9	2.82	8.10	283.2	30.8	377.2	0.86	-1.31
1.0	11.65	5.27	9	162.0	2.2	476.0	3.00	9.00	287.1	24.6	656.0	2.73	7.56
1.0	14.80	5.27	24	66.2	2.5	291.4	4.89	23.92	276.4	10.8	557.4	2.44	5.79
1.0	17.14	5.26	35	50.9	2.2	245.4	5.80	34.04	284.9	16.7	840.2	4.68	23.91
1.0	21.65	5.20	152	22.8	3.2	129.5	11.49	137.57	50.6	5.7	153.8	7.69	73.75
1.0	24.80	5.20	225	20.6	3.3	108.9	13.19	187.52	26.3	3.4	72.3	6.10	49.28
1.0	27.14	5.18	237	25.3	3.9	111.0	12.72	180.84	21.6	2.4	73.3	8.83	98.91
1.0	28.65	5.05	231	29.4	3.5	132.6	12.07	164.41	21.8	3.3	101.1	11.47	149.51
1.0	31.80	5.05	242	32.1	3.5	133.3	11.40	152.96	15.8	2.4	61.1	6.51	44.50
1.0	34.14	4.64	145	59.8	4.1	235.3	9.77	107.33	20.2	2.6	67.5	5.53	33.34
1.0	35.15	4.55	165	51.1	3.7	240.8	10.08	114.66	24.1	4.2	57.5	4.32	22.05
1.0	38.30	4.55	177	51.4	3.9	236.4	9.94	114.07	14.9	2.2	44.7	6.16	43.78
1.0	40.64	4.28	138	72.1	4.2	320.0	8.74	86.67	12.9	3.3	23.5	3.31	12.31
0.6	4.65	5.72	4	140.6	2.9	277.2	2.00	4.00	211.8	9.1	357.6	1.73	N/A
0.6	7.80	5.72	17	34.3	0.6	134.1	4.12	16.97	516.9	16.9	1077.5	2.26	4.49
0.6	10.14	5.70	24	28.7	1.7	118.1	4.88	23.85	461.2	5.5	1037.2	2.68	7.05
0.6	11.65	5.23	19	82.3	1.6	347.8	4.36	19.00	402.4	160.5	590.6	2.20	5.13
0.6	14.80	5.21	46	35.5	1.2	229.2	6.78	45.99	180.0	58.5	376.8	4.25	21.00
0.6	17.14	5.22	61	27.7	1.4	196.2	7.80	60.94	139.9	57.6	183.9	1.67	2.45
0.6	21.65	5.41	78	19.8	2.0	131.5	8.78	77.36	121.1	37.0	239.9	3.44	13.53
0.6	24.80	5.41	168	11.1	1.9	90.0	12.73	163.85	58.1	14.4	121.7	4.67	28.49
0.6	27.14	5.40	214	11.2	2.4	80.7	14.14	204.01	43.2	8.3	93.2	4.55	26.55
0.6	28.65	5.28	217	16.4	2.8	97.0	14.01	202.61	36.5	7.7	65.2	2.94	9.90
0.6	31.80	5.28	290	15.8	3.0	85.9	15.51	254.65	24.2	5.5	41.8	3.01	10.85
0.6	34.14	5.26	294	18.1	3.1	88.3	14.82	239.79	21.9	6.5	38.4	3.00	10.00
0.6	35.15	5.36	255	18.8	3.2	83.1	13.53	202.14	27.6	6.7	49.6	3.93	21.25
0.6	38.30	5.36	299	20.1	3.5	79.9	13.11	201.36	19.4	5.1	33.7	3.08	11.32
0.6	40.64	5.35	269	24.9	3.3	87.9	11.32	157.56	18.8	5.7	31.6	3.27	14.13
0.6	41.65	5.48	241	31.7	3.7	82.9	7.86	86.71	16.5	4.9	30.4	3.27	11.31
0.6	44.80	5.48	244	35.1	3.9	92.6	6.16	55.19	12.7	3.7	22.3	3.80	18.55
0.6	47.14	5.37	220	41.1	4.0	115.4	6.49	56.82	12.6	4.5	20.7	3.43	14.84
0.6	51.65	5.68	137	73.3	6.5	144.7	3.00	10.63	10.9	5.9	14.5	4.29	28.07
0.6	54.80	5.68	137	77.2	4.7	172.9	3.18	10.94	7.0	3.9	8.9	3.20	13.33
0.6	57.14	5.68	98	110.2	10.4	232.7	3.26	11.99	7.4	3.9	9.6	2.78	9.88
0.2	4.65	5.43	66	21.3	2.4	138.6	8.11	65.79	157.0	46.3	298.1	4.23	22.76
0.2	7.80	5.43	64	22.9	3.4	140.9	7.97	63.72	121.0	38.6	208.2	3.10	11.06
0.2	10.14	5.39	90	20.2	4.0	126.4	9.41	88.95	109.1	42.9	178.2	3.01	10.06
0.2	11.65	5.65	103	14.9	3.2	69.2	9.34	91.32	89.6	31.6	198.8	5.93	43.52
0.2	14.80	5.65	128	15.7	4.5	62.4	10.09	108.68	66.1	20.1	156.8	5.59	35.65
0.2	17.14	5.65	143	15.4	5.7	58.2	11.07	128.52	57.9	21.6	149.9	8.03	77.42
0.2	21.65	5.65	167	16.2	4.3	56.5	10.72	127.71	52.0	14.8	223.7	11.70	145.03
0.2	24.80	5.65	171	14.4	4.5	54.3	11.84	148.94	52.5	15.3	157.2	8.21	81.88
0.2	27.14	5.65	129	13.5	4.1	61.7	10.87	121.50	75.4	22.3	146.8	3.46	13.07
0.2	28.65	5.59	102	15.9	5.3	79.1	9.95	99.91	87.3	28.4	154.2	3.33	12.89
0.2	31.80	5.59	80	17.5	4.2	89.2	8.82	78.54	126.8	39.6	192.3	2.14	4.40
0.2	34.14	5.57	61	22.3	3.9	107.5	7.65	59.21	172.5	49.7	310.4	3.39	13.22
0.2	35.15	5.45	88	21.7	2.8	115.8	9.03	83.45	108.3	22.3	164.4	1.64	1.39
0.2	38.30	5.46	120	20.4	3.7	97.7	10.34	110.70	74.7	16.2	118.0	2.13	4.32
0.2	40.64	5.40	139	23.0	4.1	101.4	10.96	125.54	62.0	13.4	93.6	2.48	8.30
0.2	41.65	5.38	175	22.2	4.3	94.4	11.95	151.97	45.3	9.9	89.9	3.64	15.13
0.2	44.80	5.27	210	23.9	4.1	101.4	12.87	178.11	32.3	8.1	60.6	3.70	17.28
0.2	47.14	5.25	154	33.5	4.3	124.3	10.47	121.20	23.0	9.8	40.7	4.93	33.59

0.2	51.65	5.29	220	35.8	5.1	106.0	10.14	126.00	18.0	7.3	29.1	3.69	17.41
0.2	54.80	5.29	236	36.5	3.9	108.3	9.14	107.24	13.5	5.6	22.9	3.48	13.59
0.2	57.14	5.29	205	45.1	4.1	123.1	7.40	72.75	12.5	5.5	22.5	5.22	36.35
x'	y	Study	Nb of	Air	chord	sizes			Water	chord	sizes		
		time	bubble	Mean	Median	Std	Skew	Kurt	Mean	Median	Std	Skew	Kurt
m	mm	s		mm	mm	mm			mm	mm	mm		
(1)	(2)	(3)	(4)	(5)	(6)	(7)	(8)	(9)	(10)	(11)	(12)	(13)	(14)
0.4	4.65	5.67	20	36.4	1.2	145.2	4.46	19.93	372.5	155.6	539.6	1.76	2.60
0.4	7.80	5.66	45	17.4	1.4	100.9	6.70	44.89	248.2	141.1	299.1	1.58	2.13
0.4	10.14	5.66	56	16.0	1.2	89.9	7.34	54.47	174.5	56.7	289.7	2.51	6.48
0.4	11.65	5.42	44	29.3	1.2	171.2	6.61	43.76	180.3	52.2	267.6	2.16	5.28
0.4	14.80	5.43	80	17.2	1.5	126.4	8.89	79.39	114.7	32.1	229.5	4.19	21.69
0.4	17.14	5.43	81	17.4	1.4	125.7	8.94	80.24	93.7	27.7	130.0	1.83	3.19
0.4	21.65	5.25	135	16.5	2.2	126.8	11.48	132.85	60.6	17.2	96.8	2.57	8.02
0.4	24.80	5.25	194	13.4	2.4	105.7	13.70	189.70	45.4	12.2	96.1	5.70	45.21
0.4	27.14	5.25	221	13.7	3.0	99.4	14.51	213.82	37.8	10.8	96.8	7.68	76.93
0.4	28.65	5.47	163	13.2	2.8	81.7	12.40	156.60	50.0	12.6	119.5	6.20	49.63
0.4	31.80	5.47	268	10.8	2.5	64.3	15.45	247.52	31.9	9.9	58.5	3.35	12.93
0.4	34.14	5.41	274	12.4	3.0	71.3	15.66	254.05	30.1	9.3	61.6	5.89	51.88
0.4	35.15	5.58	281	13.0	3.5	51.6	13.82	213.47	26.4	6.7	73.6	8.79	96.97
0.4	38.30	5.57	330	13.6	3.3	50.1	14.16	231.15	21.8	4.5	58.0	7.00	60.48
0.4	40.64	5.49	312	16.3	3.0	60.9	14.09	226.95	19.1	5.5	46.4	8.08	84.18
0.4	41.65	5.56	352	17.1	4.1	51.8	13.29	216.21	16.2	5.7	25.2	2.87	10.05
0.4	44.80	5.54	385	18.6	3.9	53.2	12.48	201.78	12.0	3.9	18.9	3.14	12.74
0.4	47.14	5.61	340	23.0	4.1	53.5	8.60	110.60	11.6	4.3	18.6	3.50	16.50
0.4	51.65	5.50	328	26.7	4.6	68.4	8.96	115.26	9.3	4.3	14.9	4.36	26.64
0.4	54.80	5.50	288	33.3	5.3	77.5	7.19	78.11	7.8	3.3	11.5	3.31	14.44
0.4	57.14	5.50	204	48.0	10.8	96.4	5.45	45.24	9.0	4.7	11.7	2.72	8.50
0.8	4.65	5.33	11	124.6	2.2	396.7	3.32	10.99	5.2	2.9	8.2	2.99	9.16
0.8	7.80	5.33	14	100.4	2.2	350.5	3.73	13.92	650.9	2.8	2048.4	3.49	12.36
0.8	10.14	5.28	7	204.0	2.4	534.7	2.65	7.00	1591.1	1045.9	1844.8	0.38	-2.45
0.8	11.65	5.67	13	52.4	1.6	177.9	3.60	12.98	909.4	4.0	1519.2	1.36	0.13
0.8	14.80	5.67	28	25.4	1.3	121.7	5.27	27.87	398.1	19.1	644.4	1.97	3.84
0.8	17.14	5.64	43	18.6	1.4	108.6	6.56	42.98	257.3	58.3	379.3	1.82	2.60
0.8	21.65	5.39	87	19.9	2.0	129.2	9.19	85.28	110.8	22.7	165.7	2.01	4.07
0.8	24.80	5.38	173	13.4	2.6	93.4	12.79	166.54	53.9	6.5	118.2	4.18	21.49
0.8	27.14	5.38	246	13.0	2.6	79.9	14.47	219.57	33.9	4.5	66.3	3.18	12.47
0.8	28.65	5.34	241	16.5	3.2	86.6	14.00	208.46	29.5	4.1	68.3	4.04	18.69
0.8	31.80	5.34	302	16.7	3.2	80.4	14.19	224.45	21.3	3.9	50.2	4.47	22.47
0.8	34.14	5.33	267	23.6	3.5	94.7	10.68	138.07	20.1	3.2	43.6	3.77	15.68
0.8	35.15	5.29	273	24.1	3.7	94.9	11.79	164.80	19.0	4.1	59.6	7.31	68.35
0.8	38.30	5.29	235	33.2	4.1	108.1	9.33	110.87	17.1	3.0	54.4	8.05	80.23
0.8	40.64	5.28	171	50.8	4.3	144.2	6.26	50.37	18.4	3.9	56.2	7.63	70.18
0.8	41.65	4.93	173	56.2	4.3	179.3	8.94	98.81	10.2	3.2	19.7	4.87	32.03
0.8	44.80	4.94	148	70.1	4.5	203.0	7.22	68.02	8.6	2.6	17.9	5.27	35.11
0.8	47.14	4.75	100	107.9	4.1	293.8	5.70	41.67	9.0	3.0	17.6	5.07	34.43
0.8	51.65	5.26	53	205.1	34.7	517.7	4.42	22.47	12.5	8.1	15.2	2.06	4.19
0.8	54.80	5.24	52	213.1	4.7	560.2	3.96	17.30	8.7	4.6	12.4	2.61	6.75
0.8	57.14	5.24	45	246.9	5.3	599.2	3.59	14.26	7.5	4.1	11.0	2.65	7.82
x'	y	Study	Nb of	Air	chord	sizes			Water	chord	sizes		
		time	bubble	Mean	Median	Std	Skew	Kurt	Mean	Median	Std	Skew	Kurt
m	mm	s		mm	mm	mm			mm	mm	mm		
(1)	(2)	(3)	(4)	(5)	(6)	(7)	(8)	(9)	(10)	(11)	(12)	(13)	(14)

Run TL5 (step 10)

Q m^3/s	Step	x' m	C_s m/s	d_o m
0.075	10	0.2, 0.4, 0.6, 0.8, 1.0	2.61	0.297

x'	y	Study time	Nb of bubble	Air chord sizes					Water chord sizes				
				Mean	Median	Std	Skew	Kurt	Mean	Median	Std	Skew	Kurt
m	mm	s		mm	mm	mm			mm	mm	mm		
(1)	(2)	(3)	(4)	(5)	(6)	(7)	(8)	(9)	(10)	(11)	(12)	(13)	(14)
1.0	4.65	0.73	1	0.3	0.3	N/A	N/A	N/A	11927	11927	N/A	N/A	N/A
1.0	7.80	5.30	10	2.4	1.6	2.8	2.49	6.64	1255.9	4.7	2868.0	2.18	3.86
1.0	10.14	5.26	7	2.3	0.8	2.7	1.25	-0.05	1718.9	153.1	2823.5	1.81	2.83
1.0	11.65	5.33	17	2.3	1.6	2.7	3.43	12.98	609.1	332.0	774.5	1.46	1.36
1.0	14.80	5.32	27	2.1	1.6	2.3	2.89	10.83	494.1	188.6	752.1	2.32	6.03
1.0	17.14	5.31	34	2.9	1.7	4.8	4.88	26.30	393.5	212.5	431.8	0.85	-0.46
1.0	21.65	6.00	52	5.6	1.4	24.4	6.79	47.37	274.9	71.8	501.8	2.68	7.27
1.0	24.80	6.00	43	7.3	1.6	36.5	6.55	42.91	333.9	91.2	447.4	1.90	4.41
1.0	27.14	5.75	48	7.0	1.6	35.1	6.90	47.70	299.3	53.2	486.9	2.28	5.45
1.0	28.65	5.63	63	2.3	1.6	2.7	3.84	16.32	223.3	44.1	413.9	3.19	11.49
1.0	31.80	5.62	112	2.8	1.8	3.5	3.21	13.09	127.1	32.6	217.4	2.63	7.07
1.0	34.14	5.62	100	5.1	1.8	8.6	2.90	8.35	140.3	27.4	211.9	1.76	2.51
1.0	35.15	5.48	62	4.8	2.3	7.7	3.28	12.15	211.3	69.3	406.7	4.34	22.99
1.0	38.30	5.48	137	4.3	2.1	10.0	6.13	41.43	99.9	22.2	169.0	2.64	7.49
1.0	40.64	5.50	149	6.4	2.1	14.8	5.29	31.53	89.5	17.0	160.5	2.87	9.62
1.0	41.65	5.53	150	10.4	2.3	23.4	3.62	13.69	84.0	15.9	193.9	5.80	44.59
1.0	44.80	5.58	215	11.0	2.6	25.0	3.79	15.48	56.4	10.2	123.1	5.38	40.00
1.0	47.14	5.58	240	12.7	2.9	28.0	3.57	13.99	47.8	8.6	91.2	3.56	16.05
1.0	51.65	5.34	332	18.7	3.3	48.0	5.15	32.50	23.3	5.5	43.6	4.20	26.78
1.0	54.80	5.34	315	23.1	3.4	56.8	4.34	21.79	21.1	5.4	36.6	3.07	12.73
1.0	57.14	5.34	318	27.1	3.7	63.0	4.10	19.99	16.7	5.2	30.8	4.71	32.18
1.0	61.65	5.27	218	46.8	4.2	111.3	4.77	29.83	16.3	7.0	26.0	4.06	23.45
1.0	64.80	5.27	234	47.7	4.3	117.8	4.35	23.74	10.7	3.9	16.6	2.77	8.60
1.0	67.14	5.27	166	71.5	6.3	164.9	4.21	21.24	10.7	4.2	16.7	3.19	11.97
1.0	71.65	5.12	93	134.5	16.7	312.5	4.38	24.13	9.3	6.3	8.7	1.72	2.75
1.0	74.80	5.11	87	132.5	14.4	305.2	4.59	27.27	6.8	4.8	6.3	1.65	2.86
1.0	77.14	5.12	66	176.9	8.5	361.8	3.53	16.17	6.3	4.4	6.0	1.61	2.57
1.0	81.65	4.89	60	205.4	15.1	580.7	6.08	42.03	7.6	5.4	7.0	1.31	0.95
1.0	84.80	5.36	44	276.3	27.0	683.6	4.93	28.06	7.8	5.5	7.1	1.71	3.55
1.0	87.14	5.36	37	317.7	45.7	737.2	4.57	23.93	7.9	5.7	6.7	2.33	7.78
0.2	4.65	5.38	22	19.2	3.3	71.3	4.67	21.87	584.4	355.6	931.1	2.38	5.24
0.2	7.80	5.38	23	19.6	4.4	70.1	4.77	22.85	566.8	312.2	843.2	3.05	11.39
0.2	10.14	5.38	50	14.6	4.4	47.8	6.44	43.43	261.3	48.8	410.8	2.08	3.83
0.2	11.65	5.48	107	13.0	4.4	26.9	5.97	45.59	97.2	23.2	180.2	4.13	23.78
0.2	14.80	5.37	99	14.2	4.4	26.5	3.96	19.33	127.3	40.5	261.2	3.90	16.33
0.2	17.14	5.25	142	15.5	5.2	33.8	6.31	52.45	80.9	18.8	251.9	7.45	64.41
0.2	21.65	5.14	182	18.5	5.0	42.2	4.21	20.30	32.1	14.1	47.0	3.08	12.49
0.2	24.80	5.52	193	27.8	7.3	59.9	5.34	39.47	46.5	13.1	173.8	9.46	102.65
0.2	27.14	5.54	207	23.7	8.1	40.9	3.13	11.10	45.9	11.1	158.9	9.26	97.15
0.2	28.65	5.16	189	19.6	8.1	37.3	4.54	25.05	45.5	15.4	115.4	6.76	56.57
0.2	31.80	5.17	225	12.6	6.0	21.6	6.40	60.98	47.2	17.2	96.0	5.62	45.07
0.2	34.14	5.16	149	10.5	6.8	15.0	6.01	50.86	79.5	27.0	206.3	8.79	92.73
0.2	35.15	5.82	106	9.3	5.5	10.3	2.07	5.64	125.6	39.3	218.7	2.79	7.82

0.2	38.80	5.82	113	6.5	3.4	8.0	2.48	6.87	127.0	39.4	207.6	2.75	8.64
0.2	40.64	5.82	102	6.3	3.1	8.1	2.33	5.37	141.3	47.5	218.2	2.66	8.68
0.2	41.65	5.42	95	9.4	4.4	12.6	2.30	5.73	139.6	56.1	203.3	2.61	8.12
0.2	44.80	5.42	128	11.0	4.4	17.0	3.00	11.50	98.7	32.9	156.7	3.22	13.28
0.2	47.14	5.42	157	12.8	4.2	19.9	3.15	14.44	76.8	28.3	107.8	2.29	6.07
0.2	51.65	5.35	161	18.3	6.5	27.9	2.91	11.11	67.6	28.4	110.0	4.16	24.43
0.2	54.80	5.35	245	15.5	3.9	27.3	4.14	24.90	41.3	17.2	68.9	4.92	36.22
0.2	57.14	5.35	241	19.6	4.7	35.4	4.52	28.09	38.2	21.5	55.8	3.95	21.78
0.2	61.65	5.36	199	34.8	18.8	45.7	2.53	8.83	35.5	20.1	43.5	2.46	7.02
0.2	64.80	5.34	244	33.5	11.2	59.0	5.34	46.11	23.4	12.5	29.4	2.84	10.55
0.2	67.14	5.22	213	42.1	12.5	80.1	6.55	64.52	21.6	12.3	27.3	3.07	13.43
0.2	71.65	5.69	123	102.5	30.3	204.8	4.80	28.93	18.2	10.4	24.6	3.53	15.22
0.2	74.80	5.69	121	108.0	13.3	224.2	4.47	26.01	14.5	7.4	21.2	3.83	18.83
0.2	77.14	5.70	102	131.1	13.4	290.0	3.78	15.75	14.5	8.4	21.1	3.80	18.37
0.2	81.65	5.58	75	179.9	15.7	433.8	4.51	22.21	14.6	9.9	15.7	2.86	9.69
0.2	84.80	5.60	98	141.3	5.0	443.1	5.58	34.54	7.9	5.2	9.9	3.45	16.50
0.2	87.14	5.60	67	207.4	6.5	542.8	4.29	20.30	8.8	4.8	11.0	3.14	12.94
0.4	4.65	5.41	12	6.6	1.7	16.5	3.43	11.82	793.8	242.2	1215.4	1.69	1.62
0.4	7.80	5.38	43	1.7	1.3	1.8	2.71	9.48	317.5	219.0	308.2	1.07	0.22
0.4	10.14	5.37	50	1.6	0.8	2.5	5.08	30.35	273.4	108.3	403.7	2.62	7.81
0.4	11.65	5.78	54	2.3	1.3	3.0	3.38	13.22	268.5	101.4	563.0	5.30	33.06
0.4	14.80	5.78	128	2.3	1.0	4.4	5.89	38.67	114.7	28.4	278.9	6.53	54.37
0.4	17.14	5.78	122	3.2	1.7	5.4	4.88	28.69	119.5	22.7	288.0	6.03	45.75
0.4	21.65	5.54	123	5.8	2.9	8.0	2.93	10.18	105.4	28.4	208.2	3.64	14.74
0.4	24.80	5.53	217	5.1	2.3	7.8	3.95	21.07	61.2	16.3	194.9	8.39	85.19
0.4	27.14	5.53	212	7.2	2.6	10.9	3.45	15.87	60.7	12.5	235.5	11.27	145.17
0.4	28.65	5.48	165	10.0	5.0	12.9	2.32	6.26	47.5	13.8	106.4	6.42	54.57
0.4	31.80	5.48	269	9.5	3.1	14.0	2.47	6.83	43.6	8.1	177.3	9.95	108.78
0.4	34.14	5.43	260	12.2	3.7	18.2	2.18	4.73	42.2	9.9	171.3	11.24	147.14
0.4	35.15	5.47	223	15.8	4.2	29.7	4.97	37.84	44.6	8.9	186.8	9.50	101.98
0.4	38.30	5.50	299	14.5	3.1	25.0	2.72	8.14	33.4	7.0	119.5	8.14	79.72
0.4	40.64	5.50	271	17.6	4.4	28.7	2.36	5.42	35.2	6.8	130.5	7.71	69.25
0.4	41.65	5.79	223	25.1	7.8	38.9	2.81	9.97	37.5	8.1	168.7	10.50	125.38
0.4	44.80	5.78	258	25.2	5.2	48.1	4.25	26.88	33.2	6.3	129.0	7.38	58.72
0.4	47.14	5.79	239	29.2	5.5	53.1	3.76	20.70	33.9	5.7	108.5	5.65	33.80
0.4	51.65	5.71	187	39.5	5.5	74.6	3.57	17.83	37.4	7.0	102.7	4.50	21.80
0.4	54.80	5.70	230	35.7	5.0	77.0	3.73	17.54	28.9	5.5	63.2	4.17	21.79
0.4	57.14	5.70	215	40.0	5.2	83.3	3.37	13.79	29.2	6.7	66.6	3.95	16.94
0.4	61.65	5.31	157	58.3	10.4	123.8	3.85	17.57	30.0	7.0	55.1	2.89	8.60
0.4	64.80	5.31	209	47.6	4.7	133.1	4.90	26.68	18.5	4.4	34.7	3.28	12.55
0.4	67.14	4.96	195	47.9	5.5	119.4	4.48	22.91	18.3	4.7	34.2	3.29	11.68
0.4	71.65	5.56	191	59.7	7.0	142.1	4.27	22.28	16.2	7.8	23.7	2.75	7.98
0.4	74.80	5.56	206	59.7	6.0	174.0	5.66	37.82	10.8	4.4	15.6	2.61	7.53
0.4	77.14	5.56	176	71.9	6.3	186.0	4.61	24.93	10.5	5.0	14.8	2.88	9.87
0.4	81.65	5.18	147	82.1	11.2	199.9	5.58	38.86	9.9	5.0	14.1	3.41	14.32
0.4	84.80	5.24	134	93.6	6.7	239.1	4.80	26.99	8.2	3.9	13.2	3.71	16.92
0.4	87.14	5.23	118	107.9	8.0	272.9	4.49	22.80	7.6	2.9	11.9	3.59	16.40
x'	y	Study	Nb of	Air	chord	sizes			Water	chord	sizes		
		time	bubble	Mean	Median	Std	Skew	Kurt	Mean	Median	Std	Skew	Kurt
m	mm	s		mm	mm	mm			mm	mm	mm		
(1)	(2)	(3)	(4)	(5)	(6)	(7)	(8)	(9)	(10)	(11)	(12)	(13)	(14)
0.6	4.65	5.52	20	4.9	1.4	8.9	3.22	11.11	580.2	10.3	1328.8	2.64	6.15
0.6	7.80	5.51	45	5.0	1.8	12.0	4.26	18.63	307.7	30.0	571.3	2.93	10.92
0.6	10.14	5.45	50	3.2	1.7	4.6	3.47	14.19	275.9	35.2	523.4	2.91	10.04
0.6	11.65	5.63	30	6.4	1.8	19.3	5.12	27.09	338.3	152.6	425.8	1.40	1.41

0.6	14.80	5.63	76	4.3	1.8	13.8	7.77	64.07	187.1	51.9	377.7	4.27	20.96
0.6	17.14	5.64	74	5.0	1.6	16.3	7.23	56.66	191.4	47.8	320.2	3.08	12.56
0.6	21.65	5.68	50	8.3	1.8	20.1	4.11	18.29	268.3	28.1	694.0	5.55	34.90
0.6	24.80	5.67	99	6.2	1.6	20.0	6.28	44.18	142.1	36.3	250.5	3.25	13.91
0.6	27.14	5.67	97	7.1	1.6	23.2	5.33	30.82	144.1	42.2	281.6	3.82	16.93
0.6	28.65	5.71	82	7.2	2.1	14.5	3.73	15.88	135.4	18.9	253.3	2.72	7.84
0.6	31.80	5.71	118	6.4	1.8	14.6	3.78	16.04	119.0	18.8	332.6	5.44	33.12
0.6	34.14	5.71	109	8.1	2.3	17.2	3.33	11.00	127.6	26.0	374.9	7.51	65.94
0.6	35.15	5.59	100	9.7	1.8	36.4	8.32	75.48	98.6	19.8	196.9	3.18	10.92
0.6	38.30	5.59	189	6.9	2.1	26.1	10.66	128.78	69.9	18.8	195.3	9.87	117.22
0.6	40.64	5.44	181	5.9	1.8	13.4	4.80	30.18	72.3	13.1	179.5	7.87	80.74
0.6	41.65	5.55	125	12.6	2.6	29.4	4.01	18.03	98.4	16.4	189.1	3.35	13.66
0.6	44.80	5.54	221	8.9	2.1	30.9	9.64	114.07	56.3	9.4	140.0	6.70	62.34
0.6	47.14	5.52	223	10.2	2.1	32.8	8.60	94.29	54.3	12.4	110.0	4.56	26.84
0.6	51.65	5.19	255	10.8	2.3	33.2	6.19	42.26	42.1	10.4	81.3	3.83	17.30
0.6	54.80	5.23	340	10.3	2.3	30.8	6.37	46.56	29.7	7.6	54.0	2.92	9.00
0.6	57.14	5.19	315	11.9	2.9	39.4	9.61	118.21	31.0	9.3	50.3	2.54	6.49
0.6	61.65	5.67	310	17.9	3.8	46.9	8.05	93.01	29.4	8.4	53.9	3.63	17.55
0.6	64.80	5.65	400	16.2	3.3	43.7	8.26	101.16	20.7	6.3	39.5	4.66	33.68
0.6	67.14	5.66	358	19.9	3.9	42.6	4.44	28.84	21.2	5.7	37.9	3.28	12.54
0.6	71.65	5.55	262	27.2	8.2	58.7	6.33	60.02	28.0	12.3	43.2	3.24	13.35
0.6	74.80	5.41	384	21.1	4.0	45.3	4.04	19.54	15.5	6.3	26.2	5.26	44.19
0.6	77.14	5.41	331	26.0	5.0	54.4	3.72	15.97	16.4	6.0	25.6	3.30	14.31
0.6	81.65	5.43	288	33.9	6.7	75.3	5.71	46.09	15.4	7.4	23.3	3.30	12.55
0.6	84.80	5.44	332	32.4	5.2	78.3	5.64	42.48	10.4	4.7	16.9	3.67	15.50
0.6	87.14	5.44	265	41.7	4.7	93.0	4.58	28.23	11.8	5.6	18.5	3.75	17.61
0.8	4.65	3.88	6	925.5	3.5	2258.2	2.45	6.00	1532.4	593.8	2360.5	1.98	4.02
0.8	7.80	3.88	22	3.1	1.7	5.6	3.28	10.67	437.4	6.8	937.1	2.33	4.58
0.8	10.14	3.87	18	5.6	2.0	9.0	2.07	3.29	526.0	5.2	1072.0	1.97	3.00
0.8	11.65	5.57	15	2.1	1.6	1.8	1.92	4.58	850.7	573.4	810.8	0.91	-0.05
0.8	14.80	5.59	30	1.8	0.9	3.1	4.36	21.33	469.1	163.9	656.2	1.53	1.44
0.8	17.14	5.59	35	2.6	1.3	6.3	5.19	28.73	402.9	79.7	606.2	1.92	2.87
0.8	21.65	5.76	32	18.0	2.5	37.8	2.60	5.65	319.6	14.1	753.9	3.58	14.85
0.8	24.80	5.76	85	8.6	1.6	39.8	7.01	51.64	166.5	53.8	265.1	2.58	7.68
0.8	27.14	5.69	64	8.4	1.6	36.4	6.97	51.38	220.2	50.1	307.6	1.76	3.12
0.8	28.65	5.73	37	10.8	1.3	39.9	5.68	33.41	376.3	93.2	600.3	2.03	3.61
0.8	31.80	5.77	107	6.6	1.8	26.0	7.77	67.42	133.0	32.9	266.6	4.85	28.92
0.8	34.14	5.77	77	9.7	2.1	33.0	5.72	37.29	183.7	37.7	300.7	2.31	5.99
0.8	35.15	5.42	63	8.9	1.6	33.0	5.51	32.27	175.0	61.6	256.4	1.86	2.92
0.8	38.30	5.33	128	4.7	2.0	14.3	7.70	66.27	103.1	31.6	165.7	2.90	10.86
0.8	40.64	5.33	119	6.9	2.1	17.6	5.48	35.12	109.1	29.9	185.0	3.22	14.03
0.8	41.65	5.26	98	4.9	1.6	13.3	6.36	46.46	133.3	40.1	223.9	3.59	17.13
0.8	44.80	5.26	176	5.4	2.1	12.2	5.76	40.44	72.3	28.4	113.0	3.35	15.59
0.8	47.14	5.26	170	6.8	1.8	17.4	4.83	26.90	73.6	20.9	123.2	2.94	10.01
0.8	51.65	5.39	179	7.1	2.6	11.9	3.20	11.95	67.3	19.3	100.7	2.75	11.55
0.8	54.80	5.43	299	6.7	2.3	13.4	4.51	24.28	40.7	13.6	76.0	5.52	48.41
0.8	57.14	5.44	342	8.2	2.3	18.7	5.25	35.16	33.3	10.4	56.2	3.39	15.10
0.8	61.65	5.38	283	16.9	3.7	37.9	4.33	22.46	32.4	8.9	51.9	2.38	5.42
0.8	64.80	5.38	342	16.9	3.1	40.2	4.33	22.79	24.1	8.6	36.2	2.71	8.66
0.8	67.14	5.49	321	21.4	3.4	52.9	4.74	30.03	23.2	8.9	33.9	3.05	12.22
0.8	71.65	5.30	288	26.4	4.4	58.6	3.83	17.02	21.7	9.9	29.3	2.51	7.74
0.8	74.80	5.30	337	25.7	3.9	60.0	3.99	18.02	15.3	7.3	21.0	2.73	9.25
0.8	77.14	5.28	317	29.4	4.2	65.8	3.68	14.97	14.0	6.8	18.1	2.46	6.81
0.8	81.65	5.41	246	44.8	6.5	84.6	3.34	14.38	12.6	7.0	15.7	2.93	11.25
0.8	84.80	5.42	241	45.4	5.5	90.4	3.31	12.67	10.2	6.8	10.5	1.90	4.33

0.8	87.14	5.42	202	56.1	8.1	108.7	3.50	16.02	10.2	6.3	10.9	2.57	9.30
0.8	91.65	5.13	165	71.2	13.1	141.1	3.53	15.34	10.0	5.7	10.5	2.10	5.03
0.8	94.80	5.33	155	79.7	11.7	162.1	3.43	14.11	8.0	5.2	8.3	2.07	4.84
0.8	97.14	5.33	129	97.3	12.3	190.5	2.88	8.92	8.1	5.0	8.8	2.76	9.84
x'	y	Study	Nb of	Air	chord	sizes			Water	chord	sizes		
		time	bubble	Mean	Median	Std	Skew	Kurt	Mean	Median	Std	Skew	Kurt
m	mm	s		mm	mm	mm			mm	mm	mm		
(1)	(2)	(3)	(4)	(5)	(6)	(7)	(8)	(9)	(10)	(11)	(12)	(13)	(14)

Run TL5 (step 16)

Q	Step	x'	C_s	d_o
m^3/s		m	m/s	m
0.075	16	0.2, 0.4, 0.6, 0.8, 1.0	2.43	0.297

x'	y	Study	Nb of	Air	chord	sizes			Water	chord	sizes		
		time	bubble	Mean	Median	Std	Skew	Kurt	Mean	Median	Std	Skew	Kurt
m	mm	s		mm	mm	mm			mm	mm	mm		
(1)	(2)	(3)	(4)	(5)	(6)	(7)	(8)	(9)	(10)	(11)	(12)	(13)	(14)
1.0	4.65	4.98	2	1009.2	1009.2	1423.9	N/A	N/A	3.0	3.0	N/A	N/A	N/A
1.0	7.80	4.98	19	108.6	1.4	462.8	4.36	19.00	495.0	4.1	1195.4	3.04	9.76
1.0	10.14	4.96	16	132.1	2.9	508.7	4.00	15.99	479.1	2.6	1354.2	3.51	12.77
1.0	11.65	5.14	11	165.1	1.0	509.0	3.30	10.91	601.3	11.2	867.6	1.13	-0.32
1.0	14.80	5.13	14	132.0	1.1	456.6	3.71	13.84	669.6	336.7	811.2	1.50	1.23
1.0	17.14	5.13	15	124.8	1.2	442.6	3.83	14.77	707.3	360.0	797.9	0.76	-1.10
1.0	21.65	5.23	25	69.3	1.6	302.0	4.94	24.56	375.4	117.6	445.6	0.89	-0.86
1.0	24.80	5.23	57	32.9	1.6	200.7	7.42	55.60	118.6	39.7	174.2	2.01	3.84
1.0	27.14	5.21	77	26.4	2.0	177.9	8.62	75.06	123.6	32.5	232.5	4.69	28.88
1.0	28.65	5.04	155	19.2	1.8	152.5	12.29	152.32	49.3	9.2	97.0	4.07	21.56
1.0	31.80	5.04	225	16.0	2.6	126.5	14.56	216.00	34.9	6.3	77.4	5.07	33.84
1.0	34.14	5.04	268	16.5	2.4	117.1	15.51	248.74	25.3	4.1	62.7	5.55	37.78
1.0	35.15	4.95	199	41.2	3.2	171.3	9.46	103.94	16.8	4.5	35.8	4.94	30.49
1.0	38.30	4.95	183	50.1	3.5	190.8	7.80	73.12	14.3	3.2	36.0	5.18	32.74
1.0	40.64	4.95	144	67.6	3.6	225.7	6.30	47.46	14.5	3.0	31.5	5.06	33.49
1.0	41.65	5.41	233	25.6	2.6	89.5	9.65	116.14	22.1	4.5	61.3	5.87	40.06
1.0	44.80	5.40	237	30.9	3.5	108.8	7.89	73.29	12.6	2.9	29.1	5.31	36.48
1.0	47.14	5.40	200	40.3	3.5	149.8	7.76	69.61	18.6	3.0	73.1	8.76	88.33
1.0	51.65	5.10	160	67.7	2.0	200.2	5.28	35.47	6.2	1.3	11.9	3.18	11.20
1.0	54.80	5.10	115	89.6	4.7	264.2	4.85	26.22	13.0	2.9	37.2	6.83	53.60
1.0	57.14	5.10	88	120.3	4.9	338.1	4.09	17.77	13.9	4.1	29.7	4.22	19.72
1.0	61.65	5.04	67	158.1	4.5	445.7	3.85	15.35	14.3	4.5	33.6	6.02	41.76
1.0	64.80	5.03	61	178.0	4.3	633.5	5.55	34.33	11.1	3.5	25.9	5.46	34.95
1.0	67.14	5.02	46	240.2	5.0	877.3	5.52	32.86	9.6	4.0	14.5	2.67	6.78
1.0	71.65	3.98	27	424.2	36.1	962.4	3.06	9.05	11.5	7.9	11.1	2.26	6.20
1.0	74.80	3.98	24	482.3	33.1	949.7	2.66	7.67	7.7	4.1	9.3	2.34	5.81
1.0	77.14	3.42	16	709.9	64.3	1344.9	2.66	7.72	6.5	3.8	8.7	2.14	3.74
0.8	4.65	5.40	9	132.3	1.0	391.9	3.00	9.00	225.4	9.3	602.2	2.83	7.99
0.8	7.80	5.40	15	85.9	2.2	303.9	3.86	14.95	374.3	3.1	995.0	2.97	8.94
0.8	10.14	5.34	26	51.9	1.2	254.8	5.10	26.00	413.5	27.4	1011.2	3.92	16.84
0.8	11.65	5.27	19	78.3	1.2	328.2	4.36	18.99	505.8	12.5	985.2	2.37	5.64
0.8	14.80	5.24	33	47.8	1.6	260.2	5.74	32.99	308.4	205.3	401.3	1.83	2.88
0.8	17.14	5.24	39	41.4	1.4	239.7	6.24	38.96	185.5	10.9	361.3	2.62	6.81
0.8	21.65	5.23	47	40.7	1.6	222.1	6.79	46.33	188.4	16.1	311.7	2.00	3.50

0.8	24.80	5.22	81	25.3	1.6	172.5	8.80	78.41	120.8	61.3	183.8	2.87	9.72
0.8	27.14	5.22	77	27.4	1.4	176.8	8.56	74.27	125.6	27.0	202.5	2.15	4.20
0.8	28.65	5.31	51	30.3	1.4	190.8	7.12	50.80	198.3	39.3	336.5	2.69	8.04
0.8	31.80	5.31	87	20.1	1.2	146.9	9.20	85.34	113.0	19.2	187.5	2.19	4.21
0.8	34.14	5.38	89	21.3	1.8	130.5	9.05	83.80	111.0	19.5	190.9	2.43	6.27
0.8	35.15	5.11	116	23.0	1.8	166.2	10.10	105.19	78.9	16.0	111.4	2.16	6.97
0.8	38.30	5.11	176	17.0	2.0	135.4	12.35	158.01	48.4	12.2	88.0	4.28	26.57
0.8	40.64	5.11	183	17.9	2.2	132.8	12.56	163.56	46.7	9.0	86.4	3.26	13.24
0.8	41.65	5.19	173	18.4	2.2	122.0	12.59	162.64	49.6	8.7	103.6	5.27	40.34
0.8	44.80	5.20	255	14.7	2.0	100.8	15.04	234.51	30.9	7.7	53.4	3.09	11.82
0.8	47.14	5.19	259	16.6	2.6	101.1	14.73	228.44	28.4	6.9	72.7	9.02	108.85
0.8	51.65	5.12	275	18.0	2.8	107.5	15.11	241.12	24.6	7.1	49.0	3.85	16.92
0.8	54.80	5.11	340	17.2	2.6	98.9	16.40	288.40	17.0	5.5	32.5	5.37	43.94
0.8	57.14	5.11	284	23.2	3.0	110.4	14.10	220.08	18.5	6.3	37.2	4.66	26.48
0.8	61.65	5.18	247	33.2	3.3	123.0	9.46	112.06	14.4	5.1	29.5	6.15	49.62
0.8	64.80	5.28	216	41.4	3.5	130.2	6.95	61.94	13.1	5.5	21.8	3.60	16.15
0.8	67.14	5.28	187	50.3	4.3	143.1	6.05	47.77	12.6	6.9	17.3	2.75	9.26
0.8	71.65	5.62	152	66.1	5.7	139.9	3.21	11.10	10.6	5.6	15.0	3.86	19.05
0.8	74.80	5.36	151	69.3	4.1	163.1	4.21	22.71	7.8	4.1	10.9	3.46	15.84
0.8	77.14	5.16	118	90.6	5.2	206.4	4.59	28.46	8.2	4.3	10.7	3.40	15.73
0.8	81.65	5.13	60	184.8	39.0	370.3	3.45	13.14	8.9	4.6	12.6	3.85	16.97
0.8	84.80	5.13	58	194.1	11.1	460.6	4.67	25.23	6.2	3.6	8.2	3.84	19.09
0.8	87.14	5.13	48	236.1	23.9	515.4	3.95	17.99	5.6	3.8	7.1	4.23	20.84
0.6	4.65	5.33	7	196.7	1.0	497.4	2.64	6.97	1185.8	19.1	1832.7	1.03	-1.51
0.6	7.80	5.33	21	68.0	1.4	287.9	4.56	20.88	433.9	18.1	982.9	3.17	10.75
0.6	10.14	5.32	29	51.0	1.4	247.8	5.35	28.74	258.0	13.1	456.7	1.95	3.07
0.6	11.65	5.44	48	25.0	1.4	159.5	6.93	47.98	185.1	13.6	299.4	1.72	1.95
0.6	14.80	5.44	63	20.3	1.6	139.3	7.93	62.90	123.7	26.2	176.8	1.34	0.35
0.6	17.14	5.44	63	22.0	1.4	139.4	7.87	62.28	124.1	18.5	223.4	2.31	4.60
0.6	21.65	5.83	51	10.2	1.4	45.9	6.79	47.38	205.7	74.7	325.1	2.63	8.55
0.6	24.80	5.81	101	6.1	1.2	37.0	9.48	92.53	107.0	46.9	243.5	6.87	56.48
0.6	27.14	5.81	76	8.3	1.3	44.4	8.23	69.78	112.8	55.9	151.4	1.86	2.89
0.6	28.65	5.37	105	17.5	1.6	123.4	9.82	98.58	83.4	18.5	136.1	2.53	6.83
0.6	31.80	5.37	158	12.7	1.4	100.4	12.00	147.70	61.7	17.5	120.8	4.48	25.36
0.6	34.14	5.37	133	15.9	1.8	109.7	10.97	123.62	70.7	17.9	135.9	3.85	18.10
0.6	35.15	5.62	118	13.3	1.6	71.0	9.99	104.49	86.2	16.0	175.4	3.44	12.62
0.6	38.30	5.62	175	10.6	1.6	59.1	11.68	146.17	54.5	13.5	133.1	6.95	62.68
0.6	40.64	5.62	174	11.9	2.2	59.9	11.24	137.76	54.0	15.2	118.0	4.55	24.73
0.6	41.65	5.20	141	18.2	2.2	132.9	11.65	137.36	65.7	17.9	114.9	2.98	10.54
0.6	44.80	5.17	246	12.4	2.0	105.2	15.28	237.36	35.6	11.8	59.4	3.39	16.72
0.6	47.14	5.17	250	13.8	2.0	104.9	15.22	237.28	33.4	9.1	62.1	5.81	54.15
0.6	51.65	5.09	241	16.1	2.6	117.7	14.72	223.72	32.1	8.9	51.0	2.83	10.71
0.6	54.80	5.08	336	13.3	2.4	100.0	17.30	309.92	21.2	6.9	33.6	2.75	8.83
0.6	57.14	5.08	322	14.9	2.4	102.6	16.73	291.85	21.6	7.7	34.0	2.78	8.77
0.6	61.65	5.35	272	20.3	2.8	87.5	12.10	167.77	22.5	10.4	32.0	2.71	8.94
0.6	64.80	5.38	383	16.6	2.6	73.3	12.95	199.64	13.9	5.5	20.4	2.61	8.01
0.6	67.14	5.38	373	18.4	2.8	75.4	12.31	183.28	12.9	5.9	18.5	2.92	10.59
0.6	71.65	5.56	342	23.8	4.2	59.5	9.01	116.87	10.8	5.3	15.9	3.73	18.11
0.6	74.80	5.56	341	26.0	4.1	64.2	7.87	91.00	8.6	4.1	11.3	2.64	8.35
0.6	77.14	5.55	297	28.0	5.1	54.0	3.64	17.32	8.8	4.3	12.0	3.00	10.36
0.6	81.65	5.53	193	50.7	7.3	102.8	4.53	29.93	10.0	6.3	11.6	2.72	9.83
0.6	84.80	5.44	209	48.9	4.9	110.9	5.35	41.55	7.1	4.1	9.1	3.44	17.17
0.6	87.14	5.22	172	60.7	7.1	146.1	6.75	61.62	7.3	4.1	8.8	2.74	10.30
0.6	91.65	5.45	124	88.1	18.9	163.6	3.35	14.03	7.2	5.1	7.6	2.97	12.54
x'	y	Study	Nb of	Air	chord	sizes			Water	chord	sizes		

m	mm	time s	bubble	Mean mm	Median mm	Std mm	Skew	Kurt	Mean mm	Median mm	Std mm	Skew	Kurt
(1)	(2)	(3)	(4)	(5)	(6)	(7)	(8)	(9)	(10)	(11)	(12)	(13)	(14)
0.4	4.65	5.56	42	23.6	1.0	134.3	6.44	41.61	195.1	93.8	248.5	1.88	3.09
0.4	7.80	5.52	74	14.1	1.0	109.3	8.60	73.95	143.9	57.3	340.7	6.35	46.70
0.4	10.14	5.52	103	11.3	1.4	92.7	10.13	102.78	86.9	17.1	225.0	7.56	67.23
0.4	11.65	5.52	68	17.1	1.6	113.5	8.18	67.23	156.5	19.3	338.5	3.78	15.92
0.4	14.80	5.52	121	11.3	1.4	85.6	10.88	119.20	74.4	17.4	152.1	4.24	22.52
0.4	17.14	5.48	111	13.3	1.4	96.8	10.45	109.77	93.4	16.0	280.7	7.22	58.64
0.4	21.65	5.49	97	15.7	2.6	100.9	9.75	95.71	100.8	31.4	230.3	6.50	51.24
0.4	24.80	5.50	193	9.7	1.8	71.8	13.60	187.46	48.5	15.3	105.6	5.71	43.03
0.4	27.14	5.45	222	9.8	2.0	72.6	14.63	216.45	41.6	8.5	178.7	12.59	173.57
0.4	28.65	5.45	181	12.8	2.2	80.8	13.08	174.04	44.3	13.0	172.1	12.24	158.60
0.4	31.80	5.45	250	13.7	2.7	85.6	15.06	233.70	40.6	11.9	121.1	10.54	135.66
0.4	34.14	5.50	265	14.7	2.9	77.7	14.53	225.38	36.2	10.3	97.8	6.56	48.41
0.4	35.15	5.42	254	17.7	3.5	91.3	14.34	218.91	39.4	10.2	114.6	6.54	52.55
0.4	38.30	5.42	338	15.8	3.4	80.4	15.83	273.87	27.1	6.8	70.9	6.09	47.13
0.4	40.64	5.41	284	20.1	4.4	88.7	14.47	229.25	31.2	7.3	82.2	5.94	40.80
0.4	41.65	5.42	302	19.3	5.0	83.4	15.26	252.07	24.2	7.0	60.1	5.74	39.29
0.4	44.80	5.42	349	19.5	4.4	78.6	15.78	275.79	19.3	6.1	45.6	5.54	37.86
0.4	47.14	5.42	330	22.0	5.1	81.9	14.80	247.65	20.0	5.8	50.3	6.00	44.28
0.4	51.65	5.33	319	23.3	4.4	95.9	14.73	243.20	22.1	7.0	52.0	4.74	24.41
0.4	54.80	5.45	354	24.6	5.3	80.3	12.75	201.05	16.5	4.1	36.4	4.89	31.21
0.4	57.14	5.45	316	29.6	5.6	87.0	11.22	161.86	16.4	4.9	33.2	4.70	27.29
0.4	61.65	5.45	260	40.7	9.1	102.4	8.54	99.15	15.1	5.8	31.4	6.77	60.10
0.4	64.80	5.45	267	43.2	6.8	103.5	8.12	92.42	11.2	3.9	29.2	8.91	98.89
0.4	67.14	5.46	237	50.0	6.3	115.7	6.50	60.41	11.3	4.5	20.6	5.22	38.63
0.4	71.65	5.40	220	57.2	8.4	126.4	7.00	71.38	8.8	4.4	11.4	3.29	15.42
0.4	74.80	5.42	211	61.9	12.9	127.4	6.26	59.09	6.9	3.6	9.2	3.69	19.54
0.4	77.14	5.40	170	78.3	16.0	153.9	5.16	39.85	7.0	4.1	7.8	2.71	9.59
0.4	81.65	5.06	86	159.4	74.2	292.1	5.00	33.62	9.8	6.1	10.2	2.30	5.88
0.4	84.80	5.25	82	170.1	66.7	286.1	3.30	14.26	7.2	5.3	8.7	3.19	12.29
0.4	87.14	5.25	72	194.3	58.8	332.2	2.84	9.23	6.6	4.1	7.9	2.87	9.55
0.2	4.65	5.77	26	27.8	3.2	108.2	5.02	25.40	481.1	56.4	796.3	2.44	6.29
0.2	7.80	5.81	32	22.8	2.7	82.8	5.24	28.42	334.7	150.9	427.7	1.41	0.81
0.2	10.14	5.73	64	18.6	4.5	80.8	7.80	61.83	208.7	45.0	361.4	2.79	8.21
0.2	11.65	5.29	88	26.6	3.4	184.1	9.32	87.18	101.7	31.6	143.6	2.60	9.23
0.2	14.80	5.48	84	30.6	4.1	146.5	7.83	64.93	93.3	36.0	156.2	3.32	12.85
0.2	17.14	5.48	121	28.8	9.0	117.4	10.08	107.02	78.3	25.6	247.2	9.19	93.20
0.2	21.65	5.42	174	30.4	7.5	112.8	10.73	128.83	43.2	11.4	167.7	10.55	123.60
0.2	24.80	5.55	169	29.9	8.5	91.0	10.03	115.33	42.2	13.5	99.7	5.59	38.54
0.2	27.14	5.61	189	21.6	9.5	71.2	11.61	148.64	47.9	13.5	162.4	9.54	104.38
0.2	28.65	5.72	168	17.9	8.1	55.3	10.95	131.50	54.5	19.7	155.7	7.55	66.30
0.2	31.80	5.72	165	14.3	6.1	54.2	11.69	144.43	69.8	22.4	134.9	4.52	26.49
0.2	34.14	5.72	100	15.8	4.5	68.3	9.57	94.09	113.4	32.3	219.8	4.40	24.09
0.2	35.15	5.38	66	30.1	2.8	185.0	8.07	65.34	172.7	43.5	297.4	3.09	11.88
0.2	38.30	5.38	68	29.2	2.8	183.3	8.19	67.40	168.7	70.7	277.6	3.41	13.56
0.2	40.64	5.38	91	23.0	2.2	159.0	9.47	90.03	135.2	64.5	185.5	2.51	7.46
0.2	41.65	5.68	101	15.2	3.2	77.8	9.47	92.68	129.9	54.3	205.3	3.07	11.55
0.2	44.80	5.68	153	13.5	3.2	64.1	11.13	131.12	82.1	20.0	156.3	4.12	23.29
0.2	47.14	5.68	175	15.1	3.4	60.5	11.47	142.57	68.4	21.7	119.1	3.19	12.01
0.2	51.65	5.55	172	32.4	9.7	91.9	9.48	106.36	51.1	21.6	79.2	3.85	20.41
0.2	54.80	5.55	247	28.0	5.3	81.8	9.80	120.21	31.0	11.4	56.7	5.03	34.20
0.2	57.14	5.55	232	34.2	5.8	88.5	8.39	92.47	28.6	10.6	55.7	5.44	40.06
0.2	61.65	5.45	185	47.3	20.2	68.1	2.63	9.41	24.1	10.9	39.1	4.37	25.18

0.2	64.80	5.46	197	56.0	11.2	118.0	6.66	63.94	17.7	8.1	31.2	4.74	31.18
0.2	67.14	5.46	164	71.0	22.5	136.9	5.34	41.22	17.5	6.8	31.1	5.06	36.52
0.2	71.65	5.57	133	88.6	14.1	172.9	3.74	16.48	21.1	9.1	33.8	3.62	16.26
0.2	74.80	5.57	138	89.3	9.2	183.6	3.57	14.46	16.4	9.2	24.3	3.71	16.21
0.2	77.14	5.57	102	125.2	5.8	273.7	3.21	10.99	17.7	8.9	28.4	4.63	27.38
0.2	81.65	5.55	80	166.3	29.3	272.8	2.14	4.12	15.6	7.0	34.2	6.64	50.85
x'	y	Study time	Nb of bubble	Air chord sizes Mean	Median	Std	Skew	Kurt	Water chord sizes Mean	Median	Std	Skew	Kurt
m	mm	s		mm	mm	mm			mm	mm	mm		
(1)	(2)	(3)	(4)	(5)	(6)	(7)	(8)	(9)	(10)	(11)	(12)	(13)	(14)

IX.3 Remarks

The mean chord size is the number mean or arithmetic mean :

$$\text{Mean} = \frac{1}{N} * \sum_{i=1}^{N} ch_i \qquad \text{(IX-2)}$$

where N is the number of data.

The standard deviation of the chord sizes is calculated using the "nonbiased" or "n-1" method :

$$\text{Std} = \sqrt{\frac{1}{(N-1)} * \left(\sum_{i=1}^{N} (ch_i - \text{Mean})^2 \right)} \qquad \text{(IX-3)}$$

The skewness characterizes the degree of asymmetry of a distribution around its mean. Positive skewness indicates a distribution with an asymmetric tail extending toward more positive values, and a chord size mode ([2]) smaller than the mean. Negative skewness indicates a distribution with an asymmetric tail extending toward more negative values. The Fisher skewness is defined as :

$$\text{Skew} = \frac{N}{(N-1)*(N-2)} * \left(\sum_{i=1}^{N} \left(\frac{ch_i - \text{Mean}}{\text{Std}} \right)^3 \right) \qquad \text{(IX-4)}$$

The kurtosis characterizes the relative peakedness or flatness of a distribution compared with the normal (Gaussian) distribution. Positive kurtosis indicates a relatively peaked distribution (i.e. more peaked than a normal distribution). Negative kurtosis indicates a relatively flatter distribution. The Fisher kurtosis equals :

$$\text{Kurt} = \frac{N*(N+1)}{(N-1)*(N-2)*(N-3)} * \left(\sum_{i=1}^{N} \left(\frac{ch_i - \text{Mean}}{\text{Std}} \right)^4 \right) - \frac{3*(N-1)^2}{(N-2)*(N-3)} \qquad \text{(IX-5)}$$

Note that, if there are fewer than four data points, the Fisher kurtosis cannot be defined.

[2]The mode is the chord size for which the probability distribution function is the largest. It is the most frequent value of the set of data.

REFERENCES

ANCEY, C. (2000). "Debris Flows and Related Phenomena." *Lecture notes*, Gran Combin Summer School, Aosta, Italy, June. (also in "Geomorphological Fluid Mechanics", *Springer*, Berlin, N.J. BALMFORTH and A. PROVENZALE Ed., 2001, pp. 528-547.)

BAKER, R. (1994). "Brushes Clough Wedge Block Spillway - Progress Report No. 3." *SCEL Project Report No. SJ542-4*, University of Salford, UK, Nov., 47 pages.

BAKER, R. (2000). "Field Testing of Brushes Clough Stepped Block Spillway." *Intl Workshop on Hydraulics of Stepped Spillways*, Zürich, Switzerland, H.E. MINOR & W.H. HAGER Editors, Balkema Publ., pp. 13-20.

CAPART, H., and YOUNG, D.L. (1998). "Formation of a jump by the dam-break wave over a granular bed." *Jl of Fluid Mech.*, Vol. 372, pp. 165-187.

CHANSON, H. (1995). "Air Bubble Entrainment in Free-surface Turbulent Flows. Experimental Investigations." *Report CH46/95*, Dept. of Civil Engineering, University of Queensland, Australia, June, 368 pages (ISBN 0 86776 611 5).

CHANSON, H. (1997a). "Air Bubble Entrainment in Free-Surface Turbulent Shear Flows." *Academic Press*, London, UK, 401 pages (ISBN 0-12-168110-6).
{http://www.uq.edu.au/~e2hchans/reprints/book2.htm}

CHANSON, H. (1997b). "Air Bubble Entrainment in Open Channels. Flow Structure and Bubble Size Distributions." *Intl Jl of Multiphase Flow*, Vol. 23, No. 1, pp. 193-203 (ISSN 0301-9322).

CHANSON, H. (1999). "The Hydraulics of Open Channel Flows : An Introduction." *Butterworth-Heinemann*, Oxford, UK, 512 pages (ISBN 0 340 74067 1). (Reprinted in 2001)
{http://www.uq.edu.au/~e2hchans/reprints/errata.htm}

CHANSON, H. (2000). "A Review of Accidents and Failures of Stepped Spillways and Weirs." *Proc. Instn Civ. Engrs Water and Maritime Engrg*, UK, Vol. 142, Dec., pp. 177-188 (ISSN 0965-0946).

CHANSON, H. (2001). "The Hydraulics of Stepped Chutes and Spillways." *Balkema*, Lisse, The Netherlands, 418 pages (ISBN 90 5809 352 2).
{http://www.uq.edu.au/~e2hchans/reprints/book4.htm}

CHANSON, H. (2002a). "Hydraulic Modelling of Unsteady Open Channel Flows." *Lecture Notes*, Subject CIVL4120, Dept. of Civil Engrg., Univ. of Queensland, Australia, 132 pages.

CHANSON, H. (2002b). "Air-Water Flow Measurements with Intrusive Phase-Detection Probes. Can we Improve their Interpretation ?." *Jl of Hyd. Engrg.*, ASCE, Vol. 128, No. 3, pp. 252-255.

CHANSON, H. (2002c). "Hidraulica Del Flujo De Canales Abiertos." *McGraw Hill Interamericana*, División Universidad, Columbia (ISBN: 958-410-256-7).

CHANSON, H., and TOOMBES, L. (1997). "Energy Dissipation in Stepped Waterway." *Proc. 27th IAHR Congress*, San Francisco, USA, Vol. D, F.M. HOLLY Jr. and A. ALSAFFAR Ed., pp. 595-600 (ISBN 0 7844 0274 4).

CHANSON, H., and TOOMBES, L. (2002a). "Energy Dissipation and Air Entrainment in a Stepped Storm Waterway: an Experimental Study." *Jl of Irrigation and Drainage Engrg.*, ASCE, Vol. 128, No. 5, pp. 305-315 (ISSN 0733-9437).

CHANSON, H., and TOOMBES, L. (2002b). "Experimental Study of Gas-Liquid Interfacial Properties in a Stepped Cascade Flow." *Environmental Fluid Mechanics*, Vol. 2, No. 3, pp. 241-263 (ISSN 1567-7419).

CHANSON, H., and TOOMBES, L. (2002c). "Air-Water Flows down Stepped chutes : Turbulence and Flow Structure Observations." *Intl Jl of Multiphase Flow*, Vol. 27, No. 11, pp. 1737-1761 (ISSN 0301-9322).

CHANSON, H., and TOOMBES, L. (2002d). "Experimental Investigations of Air Entrainment in Transition and Skimming Flows down a Stepped Chute." *Can. Jl of Civil Eng.*, Vol. 29, No. 1, pp. 145-156. (ISSN 0315-1468).

CHANSON, H., AOKI, S., and MARUYAMA, M. (2000). "Experimental Investigations of Wave Runup Downstream of Nappe Impact. Applications to Flood Wave Resulting from Dam Overtopping and Tsunami Wave Runup." *Coastal/Ocean Engineering Report*, No. COE00-2, Dept. of Architecture and Civil Eng., Toyohashi University of Technology, Japan, 38 pages.

CHANSON, H., YASUDA, Y., and OHTSU, I. (2002). "Flow Resistance in Skimming Flows and its Modelling." *Can Jl of Civ. Eng.*, Vol. 29, No. 6, pp. 809-819 (ISSN 0315-1468).

CROWE, C., SOMMERFIELD, M., and TSUJI, Y. (1998). "Multiphase Flows with Droplets and Particles." *CRC Press*, Boca Raton, USA, 471 pages.

CUMMINGS, P.D. (1996). "Aeration due to Breaking Waves." *Ph.D. thesis*, Dept. of Civil Engrg., University of Queensland, Australia.

DRESSLER, R.F. (1952). "Hydraulic Resistance Effect upon the Dam-Break Functions." *Jl of Research, Natl. Bureau of Standards*, Vol. 49, No. 3, pp. 217-225.

DRESSLER, R. (1954). "Comparison of Theories and Experiments for the Hydraulic Dam-Break Wave." *Proc. Intl Assoc. of Scientific Hydrology Assemblée Générale*, Rome, Italy, Vol. 3, No. 38, pp. 319-328.

ESCANDE, L., NOUGARO, J., CASTEX, L., and BARTHET, H. (1961). "Influence de Quelques Paramètres sur une Onde de Crue Subite à l'Aval d'un Barrage." ('The Influence of certain Parameters on a Sudden Flood Wave Downstream from a Dam.') *Jl La Houille Blanche*, No. 5, pp. 565-575.

FAURE, J., and NAHAS, N. (1961). "Etude Numérique et Expérimentale d'Intumescences à Forte Courbure du Front." ('A Numerical and Experimental Study of Steep-Fronted Solitary Waves.') *Jl La Houille Blanche*, No. 5, pp. 576-586. Discussion: No. 5, p. 587.

FAURE, J., and NAHAS, N. (1965). "Comparaison entre Observations Réelles, Calcul, Etudes sur Modèles Distordu ou Non, de la Propagation d'une Onde de Submersion." ('Comparison between Field Observations, Calculations, Distorted and Undistorted Model Studies of a Dam Break Wave.') *Proc. 11th IAHR Biennial Congress*, Leningrad, Russia, Vol. III, Paper 3.5, pp. 1-7 (in French).

GALAY, V. (1987). "Erosion and Sedimentation in the Nepal Himalaya. An Assessment of River Processes." *CIDA, ICIMOD, IDRC & Kefford Press*, Singapore (also *Report No. 4/3/010587/1/1 Seq. 259*, Govt. of Nepal).

GULLIVER, J.S. (1990). "Introduction to Air-Water Mass Transfer." *Proceedings of the 2nd International Symposium on Gas Transfer at Water Surfaces*, Air-Water Mass Transfer, ASCE Publ., S.C. WILHELMS and J.S. GULLIVER Ed., Minneapolis MN, USA, pp. 1-7.

HENDERSON, F.M. (1966). "Open Channel Flow." *MacMillan Company*, New York, USA.

HOQUE, A. (2002). "Air Bubble Entrainment by Breaking Waves and Associated Energy Dissipation." *Ph.D. thesis*, Dept of Architecture and Civil Eng., Toyohashi Univ. of Technology, Japan, 151 pages.

HOYT, J.W., and TAYLOR, J.J. (1977). "Waves on Water Jets." *Jl of Fluid Mech.*, Vol. 83, Pt 1, pp. 119-127.

HUNT, B. (1982). "Asymptotic Solution for Dam-Break Problems." *Jl of Hyd. Div.*, Proceedings, ASCE, Vol. 108, No. HY1, pp. 115-126.

HUNT, B. (1984). "Perturbation Solution for Dam Break Floods." *Jl of Hyd. Engrg.*, ASCE, Vol. 110, No. 8, pp. 1058-1071.

HUNT, B. (1988). "An Asymptotic Solution for Dam Break Floods in Sloping Channels." in "Civil Engineering Practice", *Technomic Publ.*, Editors P.N. CHEREMISINOFF, N.P. CHEREMISINOFF and

HWANG, H.Y. (1999). "Taiwan Chi-Chi Earthquake 9.21.99. Bird's Eye View of Cher-Lung-Pu Fault." *Flying Tiger Cultural Publ.*, Taipei, Taiwan, 150 pages.

HWUNG, H.H., CHYAN, J.M., and CHUNG, Y.C. (1992). "Energy Dissipation and Air Bubbles Mixing inside Surf Zone." *Proc. 23rd Intl Conf. on Coastal Eng.*, ASCE, Venice, Italy, Vol. 1, Chap. 22, pp. 308-321.

JIRKA, G.H. (1991). "Gas Transfer Processes at the Air/Water Interface." in *Environmental Hydraulics*, J.H.E. LEE and Y.K. CHEUNG Ed., Balkema, pp. 357-370.

KAWASE, Y., and MOO-YOUNG, M. (1992). "Correlations for Liquid-Phase Mass Transfer Coefficients in Bubble Column Reactors with Newtonian and Non-Newtonian Fluids." *Can. Jl of Chem. Eng.*, Vol. 70, Feb., pp. 48-54.

KHAN, A.A., STEFFLER, P.M., and GERARD, R. (2000). "Dam-Break Surges with Floating Debris" Jl of Hyd. Engrg., ASCE, Vol. 126, No. 5, pp. 375-379.

LIGGETT, J.A. (1994). "Fluid Mechanics." *McGraw-Hill*, New York, USA.

MONTES, J.S. (1998). "Hydraulics of Open Channel Flow." *ASCE Press*, New-York, USA, 697 pages.

NSOM, B., DEBIANE, K., and PIAU, J.M. (2000). "Bed Slope Effect on the Dam Break Problem." *Jl of Hyd. Res.*, IAHR, Vol. 38, No. 6, pp. 459-464.

RÉ, R. (1946). "Etude du Lacher Instantané d'une Retenue d'Eau dans un Canal par la Méthode Graphique." ('Study of the Sudden Water Release from a Reservoir in a Channel by a Graphical Method.') *Jl La Houille Blanche*, Vol. 1, No. 3, May, pp. 181-187 & 5 plates (in French).

REIN, M. (1998). "Turbulent Open-Channel Flows : Drop-Generation and Self-Aeration." *Jl of Hyd. Engrg.*, ASCE, Vol. 124, No.1, pp. 98-102. Discussion : Vol. 125, No. 6, pp. 668-670.

SCHNITTER, N.J. (1994). "A History of Dams : the Useful Pyramids." *Balkema Publ.*, Rotterdam, The Netherlands.

SCHOKLITSCH, A. (1917). Über Dambruchwellen." *Sitzungberichten der Königliche Akademie der Wissenschaften, Vienna*, Vol. 126, Part IIa, pp. 1489-1514.

SMITH, N. (1971). "A History of Dams." *The Chaucer Press*, Peter Davies, London, UK.

STUTZ, B., and REBOUD, J.L. (1997). "Experiments in Unsteady Cavitation." *Experiments in Fluids*, Vol. 22, pp. 191-198.

STUTZ, B., and REBOUD, J.L. (2000). "Measurements within Unsteady Cavitation." *Experiments in Fluids*, Vol. 29, pp. 545-552.

TOOMBES, L. (2002). "Experimental Study of Air-Water Flow Properties on Low-Gradient Stepped Cascades." *Ph.D. thesis*, Dept of Civil Engineering, The University of Queensland.

VARDOULAKIS, I. (2000). "Catastrophic Landslides due to Frictional Heating of the Failure Plane." *Mech of Cohesive-Frictional Materials*, Vol. 5, pp. 443-467.

WALKDEN, M.J.A. (1999). "Model Wave Impulse Loads on Caisson Breakwaters: Aeration, Scale and Structural Response." *Ph.D. thesis*, University of Plymouth, UK, 250 pages.

WALTHAM, T., and SHOLJI, I. (2001). "The Demise of the Aral Sea - An Environmental Disaster." *Geology Today*, Vol. 17, No. 6, pp. 218-224.

WEGMANN, E. (1922). "The Design and Construction of Dams." *John Wiley & Sons*, New York, USA, 7th edition.

WITHAM, G.B. (1955). "The Effects of Hydraulic Resistance in the Dam-Break Problem." *Proc. Roy. Soc. of London*, Ser. A, Vol. 227, pp. 399-407.

WOOD, I.R. (1991). "Air Entrainment in Free-Surface Flows." *IAHR Hydraulic Structures Design Manual No. 4*, Hydraulic Design Considerations, Balkema Publ., Rotterdam, The Netherlands, 149 pages.

Internet references

URL	Description
{http://www.uq.edu.au/~e2hchans/reprints.html}	Reprints of research papers in hydraulic engineering
{http://www.uq.edu.au/~e2hchans/reprints/book4.htm}	CHANSON, H. (2001). "The Hydraulics of Stepped Chutes and Spillways." *Balkema*, Lisse, The Netherlands (ISBN 90 5809 352 2).
{http://www.uq.edu.au/~e2hchans/photo.html}	Gallery of photographs in water engineering and environmental fluid mechanics.

{http://www.uq.edu.au/~e2hchans/reprints/icce03c1.pdf} {http://www.uq.edu.au/~e2hchans/reprints/icce03c2.pdf}	"Hydraulic Engineering into the 21st Century: the Rediscovery of the Wheel ? A Review and Perspectives (2 Parts)." *Proc. 6th Intl Conf. on Civil Eng.*, Isfahan, Iran, May 5-7 2003, Keynote lecture.
{http://www.uq.edu.au/~e2hchans/reprints/ifems.pdf}	"The Role of Environmental Fluid Mechanics in Water System Management." *Proc. 1st Intl Conf. of International Federation for Environmental Management System IFEMS'01*, Tsurugi, Japan, Keynote lecture, Jan. 2001.

Bibliographic reference of the Report CH51/03

The Hydraulic Model research report series CH is a refereed publication published by the Department of Civil Engineering at the University of Queensland, Brisbane, Australia.

The bibliographic reference of the present report is :

CHANSON, H. (2003). "Sudden Flood Release down a Stepped Cascade. Unsteady Air-Water Flow Measurements. Applications to Wave Run-up, Flash Flood and Dam Break Wave." *Report No. CH51/03*, Dept. of Civil Engineering, The University of Queensland, Brisbane, Australia, January (ISBN 1864996552).

The Report CH51/03 is available, in the present form, as a series of .PDF files on the Internet at the following address :

http://www.uq.edu.au/~e2hchans/reprints/ch5103.zip

The .zip file contains the following files :

0_cont.pdf	Title page, table of contents, list of symbols ...
1_intro.pdf	1. Introduction. 2. experimental apparatus
3_result.pdf	3. Experimental results (1) Wave front propagation. 4. Unsteady air-water flow properties (1) Void fractions, bubble count rates and specific interface areas
5_bubl.pdf	5. Unsteady air-water flow properties (2) Air and water chord sizes. 6. Summary and discussion. Acknowledgments
a_appen.pdf	Appendix I - Basic unsteady flow equations. Appendix II - A solution of the unsteady flow equations. Appendix III - Air bubble diffusion in self-aerated flows
b_appen.pdf	Appendix IV - Wave front celerity data. (1) Channel data
c_appen.pdf	Appendix V - Wave front celerity data. (2) Studies of individual steps
d_appen.pdf	Appendix VI - Unsteady air-water flow measurements (1) Void fraction, Bubble count rate, specific interface area data
e_appen.pdf	Appendix VII - Steady air-water flow measurements. Void fraction and Bubble count rate
f_appen.pdf	Unsteady air-water flow measurements (2) Depth-averaged Void fraction, Bubble count rate, specific interface area data
g_appen.pdf	Appendix IX - Unsteady air-water flow measurements (3) Distributions of air and water chord sizes
referenc.pdf	References.